WARWICK
THE UNIVERSITY OF WARWICK

Cellular heterogeneity of the human endometrium: transcriptomic deconvolution and characterization of stem/progenitor cells

Maria José Minhoto Diniz da Costa

A thesis submitted to the University of Warwick for the degree of Doctor of Philosophy.

Division of Biomedical Sciences

Warwick Medical School

University of Warwick

November 2019

Para os meus pais,

que me ensinaram a seguir sonhos e enfrentar desafios.

Para Ana e Francisco,

que de cada um à sua maneira, olham sempre por mim.

Table of Contents

List of Figures

Chapter 1: Introduction

Chapter 3: Transcriptomic deconvolution of the human endometrium

Supplementary Information

List of Tables

Acknowledgments

First and foremost, I would like to thank my supervisor, Professor Jan Brosens, who on a leap of faith accepted my application to be his PhD student. At every goal achieved, he set the next one to a much further length than I originally thought was possible. His knowledge is immeasurable, his enthusiasm for science is contagious and his dedication, guidance, and excellence made me a better scientist. I not only thank him for challenging me but also for caring when most needed.

I also would like to thank Dr. Emma Lucas, who had an essential role in guiding my project. Her expertise in the lab was my saviour and I am grateful for the time she devoted to train me. Dr. Lucas' office also deserves a thanking note for being a place to catch one's breath when it seems that the PhD just ran us over.

Dr. Sascha Ott had a decisive role in helping me to understand the overwhelming world of transcriptomics. Together with Dr. Pavle Vrljicak, they had the eternal patience to make me understand that bioinformatics is not a seven-headed monster. I thank the lab members, Dr. Paul Brighton, Dr. Joanne Muter, Dr. Andy Blanks, Dr. Katherine Fishwick, Chow, Alex, Claudia, Tom and Komal, for their kind help and support in these last three years, but most of all for giving me an enjoyable work environment. A special acknowledgement goes to Tom and Komal, for their friendship and support in some of the most difficult moments… and for always being my 'sweet tooth' company.

I wish to express my heartfelt gratitude to all my friends and family for supporting me in this journey. I cannot thank enough my friend Jinus for being my 'partner in crime' and becoming my family in these last three years; Ana, one of the most brilliant and grounded people I know and who gave me some of the best advices; Raquel, my confidant, who knows me inside out and helps me to see the positive side in each situation; Joana, the bravest soul I know and who inspires me; Mafalda, who has been an amazing support during my thesis and MJ, who showed me that I could get to the end of this thesis. Eduardo, Matias, Vieira and Zé, thank you for always making me laugh and Maria and Gerard, for making me feel that home isn't that far away.

I am eternally grateful to my family that taught me how to be resilient and fight for my dreams… my mother, who is the true meaning of strength and courage and was the pioneer to make me passionate about the field of reproductive sciences; my father, who taught me the right balance between kindness and assertiveness and all about

work ethics; my sister, who is my everything and saw me when no one else did. I also thank Gianfranco for his support and my beautiful niece for always being a ray of sunshine.

Ultimately, I would to thank ‘Tommy’s national Centre for Miscarriage Research’ for financially supporting my research and to the women who have donated their tissues samples to this project.

Declaration

This thesis is submitted to the University of Warwick in support of my application for the degree of Doctor of Philosophy. It has been composed by myself and has not been submitted in any previous application for any degree.

The work presented (including data generated and data analysis) was carried out by the author except in the cases outlined below:

i) RNA-seq data set presented on section 3.2.2 regarding the transcriptome analysis of 36 endometrial biopsies was obtained previous to this thesis by Dr. Emma Lucas in the Brosens' lab

ii) analysis of the RNA-seq and scRNA-seq datasets in collaboration with Dr. Emma Lucas and Dr. Pavle Vrljicak

iii) analysis of immunohistochemistry of samples presented on section 4.2.3 in collaboration with Chow Kong

Parts of this thesis have been submitted in the article:

Lucas, E. S.*, Vrljicak, P.*, Muter, J., Diniz-da-Costa, M. M., Brighton, P. J., Kong, C. S., Lipecki, J., Fishwick, K., Odendaal, J., Ewington, L. J., Quenby, S., Ott, S. & Brosens, J. J. (2020) Recurrent pregnancy loss is associated with a pro-senescent decidual response during the peri-implantation window. Communications Biology, 3 (37)

*These authors contributed equally to this work.

Abstract

During a woman's reproductive years the human endometrium becomes a highly dynamic tissue that sheds and regenerates on a cyclic basis. Apart from the main cell populations (i.e. stromal, endothelial, epithelial and immune cells), the endometrium also comprises a hierarchy of stem and more committed cells that are responsible for the remarkable regenerative ability of this tissue. This heterogeneity hinders the interpretation of bulk RNA-seq data and subsequently, the identification of specific stem cell transcriptomic signatures. Hence, the aim of this thesis was to assess and interpret endometrial heterogeneity with a focus on the characterization of stem/progenitor cells. Firstly, a reference matrix with the transcriptome profile of epithelial, uNK and stromal subpopulations was generated and used in the deconvolution of whole tissue transcriptome data across the menstrual cycle. This analysis showed that the transition from early- to mid-secretory is followed by an adjustment in the stromal:epithelial ratio. Additionally, it was demonstrated that endometrial mesenchymal stem cells (eMSC) encompass a heterogeneous population, and that their microenvironment may share common stemness properties with other adult stem cells.

Secondly, single cell RNA-seq was employed to analyse endometrial cell heterogeneity. Apart from stromal, endothelial, epithelial and diverse immune cell populations, a discrete population of highly proliferative mesenchymal cells was identified and further characterized. Through several lines of evidence, I demonstrated that these cells correspond to a putative progenitor cell population and that anillin is a candidate marker for endometrial clonogenicity.

Lastly, single-nucleus transcriptomic analysis was optimized for archived endometrial samples in order to bypass the disadvantages inherent to single cell approaches that are dependent on fresh tissues. In summary, this thesis contributed to the characterization of endometrial stem cell biology and identified a progenitor cell population that might be related to the decidua remodelling during pregnancy.

List of Abbreviations

3D	Three dimensional
ABCG2	ATP-binding cassete transporter G2
AIF-1	Allograft inflammatory factor-1
ALDH1L1	Aldehyde dehydrogenase 1
ALI	Acute lung injury
ANLN	Anillin
ASC	Adult stem cells
bFGF	Basic fibroblast growth factor
BM-MSC	Bone marrow mesenchymal stem cells
BMDC	Bone marrow derived cell
cAMP	Cyclic adenosine monophosphate
CFU	Colony forming unit
CIBERSORT	Cell-type identification by estimating relative subsets of RNA transcript
Ct	Cycle threshold
DCC-FBS	Dextran and charcoal-treated fetal bovine serum
DE	Differential expression
DGE	Differential gene expression
DMD	Duchenne muscular dystrophy
DMEM	Dulbecco's Modified Eagle Medium
DMSO	Dimethyl sulfoxide
DNase I	Deoxyribonuclease I
Drop-seq	Droplet barcoding and high throughput sequencing of RNA
EC	Endothelial cells
ECM	Extracellular matrix
EDT-MSC	Endometrial decidual tissue mesenchymal stem cells
eMSC	Endometrial mesenchymal stem cells
EnSC	Endometrial stromal cells
EOC	Epithelial ovarian cancer
EpC	Epithelial cells
EpCAM	Epithelial cell adhesion molecule
ER	Estrogen receptor
ERC	Endometrial regenerative cells
ESC	Embryonic stem cells
ESE	Early-secretory
FHF	Fulminant hepatic failure
FSH	Follicle stimulating hormone
GEO	Gene Expression Omnibus
GnRH	Gonadotropin-releasing hormone
GO	Gene ontology
HSC	Hematopoietic stem cells
hTERT	Telomerase reverse transcriptase
ICM	Inner cell mass
IGFBP1	Insulin like growth factor binding protein 1
IHC	Immunohistochemistry
IkB	Inhibitor of kB
IL-8	Interleukin 8
iPSC	Induced pluripotent stem cells
ISH	*In situ* hybridization
ITGA6	Integrin α6
IUA	Intrauterine adhesions

KO	Knock out
LH	Luteinizing hormone
LSE	Late-secretory
MACS	magnetic activated cell sorting
mbMSC	Menstrual blood mesenchymal stem cells
MBPC	Menstrual blood progenitor cells
MCP-1	Monocyte chemoattractant protein 1
MDR	Multi drug resistance
MenSC	Menstrual blood derived stem cells
MMP	Matrix metalloproteinases
MSC	Mesenchymal stem cells
MSE	Mid-secretory
NF-kB	Nuclear factor kB
PC	Proliferative cells
PCA	Principal component analysis
PE	Phycoerythrin
PFN2	Profilin 2
PFO	1H,1H,2H,2H-Perfluorooctan-1-ol
PPIB	Peptidylpropyl isomerase B
PR	Progesterone receptor
PRL	Prolactin
PTGS1	Prostaglandin endoperoxidase synthase 1
RM	Recurrent miscarriage
RPL	Recurrent pregnancy loss
RXFP1	Relaxin receptor 1
SASP	Senescence associated secretory phenotype
scRNA-seq	Single-cell RNA-sequencing
SDF-1	Stromal cell derived factor 1
SDS	Sodium dodecyl sulfate
SHH	Sonic hedgehod
snRNA-seq	Single-nucleus RNA sequencing
SP	Side population
SSEA1	Stage specific embryonic antigen 1
SUSD2	Sushi domain containing 2
t-SNE	*t*-distributed stochastic neighbor embedding
T1DM	Type 1 diabetes mellitus
TA	Transit-amplifying cells
Tm	Melting temperature
TNAP	Tissue nonspecific alkaline phosphatase
TPM	Transcripts per million
TSO	Template Switch Oligo
uNK	Uterine natural killer
VEGF	Vascular endothelial growth factor
vSMC	Vascular smooth muscle cells
WOI	Window of implantation
WT	Wild type
αSMA	α smooth muscle actin

Chapter 1

Introduction

1.1 Human endometrium

The uterine corpus is composed of a specialized mucosa that lines the lumen of the uterus known as the **endometrium,** a fibromuscular wall called the **myometrium** and an outer serosal lining termed the **peritoneum**. The endometrium itself is divided into two layers, the stratum functionalis and stratum basalis. For each menstrual cycle, the upper functional layer (stratum functionalis) proliferates, vascularizes and is subsequently sloughed off during the process of menstruation, while the lower basal layer (stratum basalis) adjacent to the myometrium remains relatively constant and provides cells for generating a new functional layer (Spencer *et al*, 2012; Rendi *et al*, 2012). Throughout the female adult reproductive life, the endometrium becomes a highly dynamic structure regulated directly by the ovarian hormones, progesterone and estradiol, and indirectly by various growth factors and cytokines. The key role of the endometrium is to create a suitable environment in the right window of time (from day 20 to day 24 of menstrual cycle) to receive the embryo and establish a successful pregnancy.

1.1.2 Endometrial cellular composition

The endometrium consists of a single layer of columnar epithelium supported by a specialized connective tissue (stroma) and a rich supply of blood vessels (Jiménez-Ayala and Jiménez-Ayala, 2008). The endometrial blood vessels form a vascular bed and unlike most adult vasculature that maintains a constant structure and function throughout life, the endometrial vasculature alters dynamically responding to the cyclical fluctuations in sex steroids (Rogers, 1996). Arterial blood reaches the endometrium through the radial arteries present in the myometrium. After crossing the myometrial–endometrial junction the radial arteries split into smaller basal arteries that supply the basal layer and spiral arterioles, which extend towards the endometrial surface and supply the functional layer (Farrer-Brown *et al*, 1970; Rogers, 1996). The endometrial blood vessels are lined by a continuous single layer of endothelial cells surrounded by a specialized extracellular matrix called the basal lamina (Hickey and Fraser, 2000).

The endometrial glands consist of a pseudostratified columnar epithelium that extends from the luminal epithelium to the endometrial/myometrial junction and are considered key regulators of uterine receptivity, blastocyst implantation and stromal

cell decidualization (Filant and Spencer, 2014). In addition, their secretory products act as an important source of nutrients, growth factors and cytokines for the conceptus during the first trimester (Hempstock *et al*, 2004). The stromal compartment is comprised of a heterogeneous population of mesenchymal cells including mature fibroblast, which differentiate into decidual cells, and stem/progenitor cells such as mesenchymal stem cells (MSC) and transit amplifying (TA) cells (Jiménez-Ayala and Jiménez-Ayala, 2008; Gargett *et al*, 2015).

The endometrium also harbors resident immune populations, such as neutrophils, eosinophils, macrophages, B and T lymphocytes and uterine natural killer (uNK) cells (Salamonsen and Lathbury, 2000). Leukocytes are present in low numbers during the proliferative phase, followed by a striking influx during the secretory phase of the cycle (Kamat and Isaacson, 1987). If implantation ensues, these leukocytes continue to increase in number and are found in close contact with trophoblasts (Trundley and Moffett, 2003). Macrophages are thought to play an important role in the preparation of a receptive endometrium and subsequent differentiation of the endometrial stroma (decidualization), which is essential for successful implantation and establishment of early pregnancy (Thiruchelvam *et al*, 2012). In the human endometrium, uNK cells are phenotypically $CD56^{bright}$ $CD16^{-}$ and considered a unique subset of NK cells. $CD56^{+}$ cells are present in proliferative phase, albeit in small number, and increase substantially in the mid-secretory phase becoming the major endometrial lymphocyte population in the late secretory phase and the first trimester of pregnancy (Bulmer *et al*, 1991). Instead of predominant cytotoxic actions against virus-infected or cancerous cells the uterine subsets show mostly angiogenic and vessel remodelling activities (Rätsep *et al*, 2015). uNK cells are detected predominantly in the functional layer during the secretory phase and early pregnancy decidua, often forming aggregates around spiral arterioles/arteries and glands (Bulmer *et al*, 1991). Once trophoblast invasion is complete (around week 20 of gestation) the number of uNK cells begins to decline, rendering the lymphocyte population much less prominent compared to first trimester (Williams *et al*, 2009). Ultimately, uNK cells that have been implicated in maintaining homeostasis in cycling endometrium, remodelling of the decidua vasculature, regulating the invasion of trophoblast cells, and providing immunity (Smith *et al*, 2009; Moffett and Colucci, 2014; Brighton *et al*, 2017).

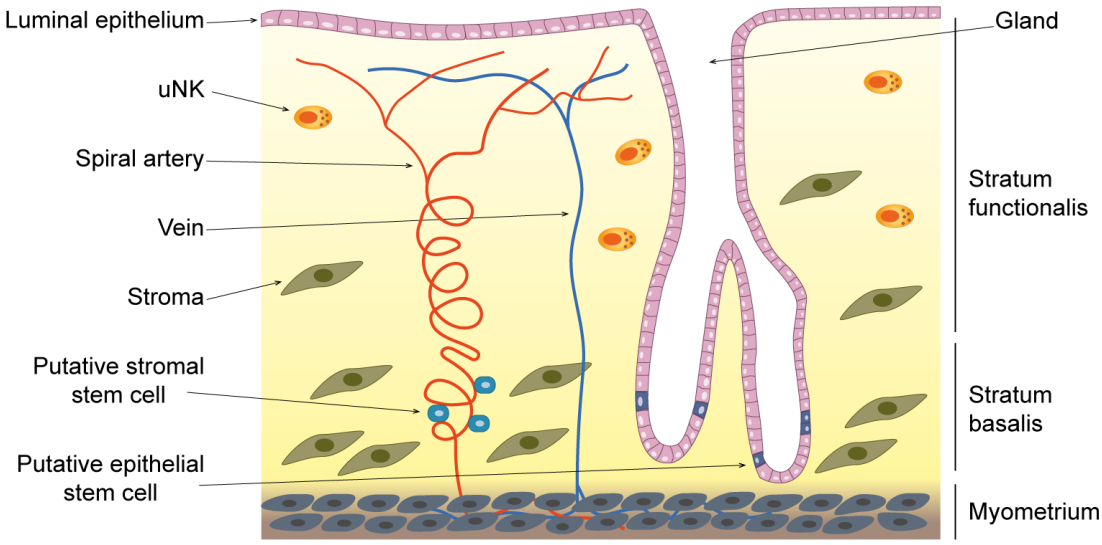

Figure 1.1. Human endometrium. The endometrium is the inner layer of the uterus and is divided into the stratum basalis and the stratum funtionalis. It is a highly complex tissue composed by a luminal and glandular epithelium surrounded by a stromal compartment that harbours immune cells and blood vessels. The stratum functionalis is regenerated each menstrual cycle upon reprogramming of stromal and epithelial stem cells.

1.2 Menstrual Cycle

The human menstrual cycle is characterized by a tightly coordinated interplay between the hypothalamus, which secretes gonadotropin-releasing hormone (GnRH); the pituitary, which secretes the glycoproteins luteinizing hormone (LH) and follicle stimulating hormone (FSH); the ovary, which secretes estrogen, progesterone and other modulators; and the endometrium, which responds to the ovarian hormones (Silberstein and Merriam, 2000) (Figure 1.2). A typical cycle lasts approximately 28 days, although there is considerable variation between individuals. Apart from menstruation, the menstrual cycle is divided into proliferative and secretory phases.

1.2.1 Proliferative phase

The proliferative phase begins from the first day of menses until ovulation and is characterized by the development of ovarian follicles upon an increase of GnRH and consequently of FSH (Messinis *et al*, 2010). The main secretory product of the follicle during this phase is estradiol, which mediates the negative feedback regulation in the hypothalamic–pituitary system (Messinis *et al*, 2014). As the proliferative phase progresses, the ovaries also produce progesterone at low concentration (Wallach *et al*, 1970; Alexandris *et al,* 1997), which ultimately slows the follicular growth (Chaffkin *et al*, 1992). Towards the end of the proliferative phase, estradiol levels increase rapidly and stimulate the hypothalamus and the anterior pituitary. This positive feedback results in a LH surge responsible for the initiation of a cascade of proteolytic events that control ovulation (Conti *et al*, 2012).

The ovaries also produce non-steroidal substances, such as inhibins (Messinis *et al*, 2014). The major form of inhibin secreted during proliferative phase is inhibin B. Its serum levels rise sharply from early follicular phase and reach a first peak in early- to mid-proliferative phase, followed by a second peak 2 days after the midcycle LH peak (Groome *et al*, 1996; Luisi *et al*, 2005). Although the data concerning the role of inhibin B is still limited, it has been suggested that this glycoprotein participates in the negative feedback effect of the ovaries on FSH secretion and that it is an important regulator of follicle development (Messinis *et al*, 2014).

1.2.3 Secretory phase

Ovulation occurs 1 to 2 days following the LH surge (Testart and Frydman, 1982) and the follicle is transformed into a corpus luteum that secretes mainly progesterone and lower concentrations of estradiol (Niswender *et al*, 2000). The ovarian control of pituitary hormone secretions during the secretory phase is mediated by a negative feedback mechanism, in which progesterone and estradiol inhibit the release of LH and FSH (Alexandris *et al* 1997; Messinis *et al*, 2014) and stimulate the formation of the secretory endometrium. In contrast to inhibin B, inhibin A concentration is low in the proliferative phase but increases to its maximal level during the mid-secretory phase (Groome *et al*, 1996). Inhibin A has been shown to negatively mediate FSH secretion (Muttukrishna *et al*, 2002), rendering it an important mediator of the negative feedback control of gonadotrophin during this phase.

The secretory phase is characterized by the inhibition of endometrial growth and subsequent morphological and biochemical endometrial changes through a process called decidualization. This reaction is characterized by modification of uterine glands, influx of specialized natural killer cells, vascular remodelling and transformation of endometrial stromal fibroblasts into decidual cells (Gellersen and Brosens, 2014).

In the absence of fertilization, the levels of ovarian hormones decline resulting in an intracycle rise of FSH 2 to 3 days before the onset of menstruation (Messinis *et al*, 2006).

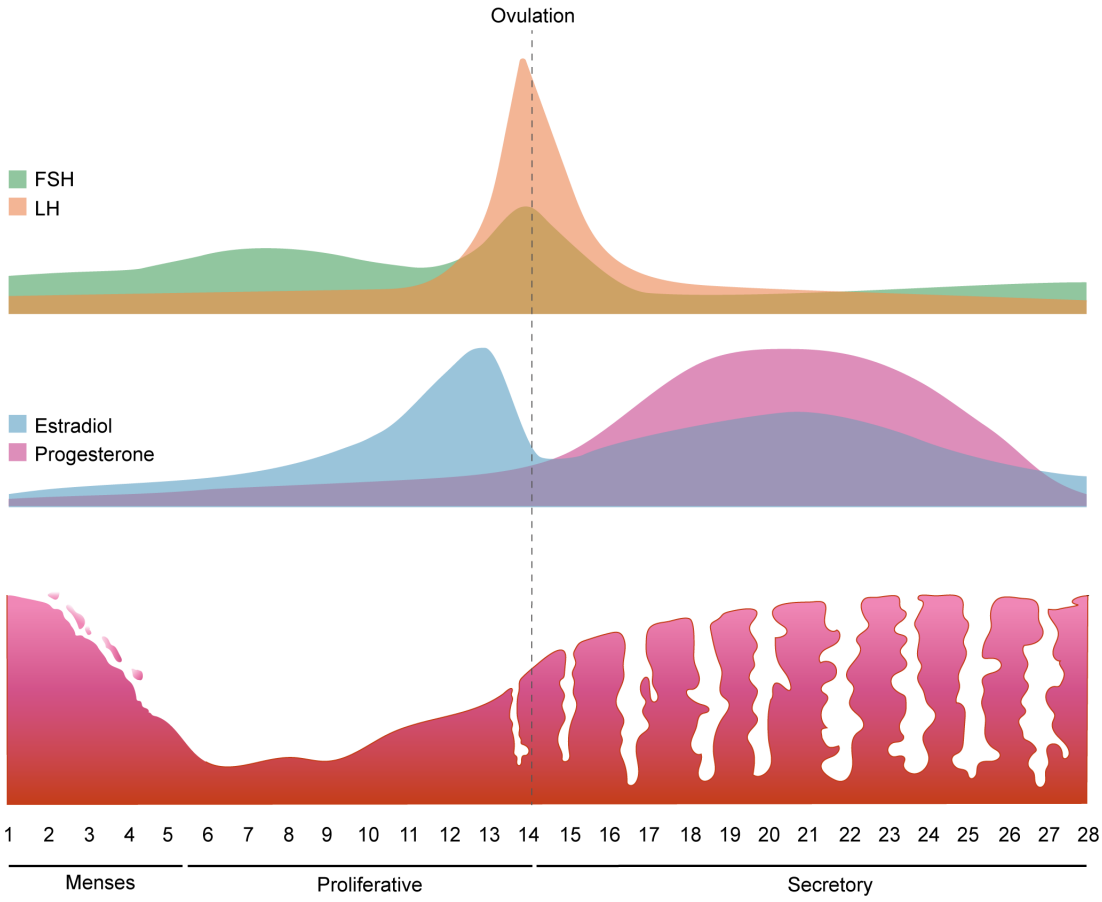

Figure 1.2 Human menstrual cycle. Coordination between gonadotropins (FSH and LH) and ovarian hormones (estradiol and progesterone) is essential to regulate cyclic endometrial modifications and divide the menstrual cycle into proliferative and secretory phases.

1.3 Endometrial remodelling

1.3.1 Menstruation

Cyclical growth and regression of the endometrium is a universal phenomenon in non-pregnant mammals, but external loss of blood is only observed in primates (Old World monkeys, apes and humans), a few bats and the elephant shrew (Rasweiler and de Bonilla, 1992; Martin, 2007). Menstruation is the reproductive process whereby the functionalis layer is shed upon withdrawal of steroid hormones at the end of each menstrual cycle (Salamonsen, 2003) (Figure 1.3). It is comparable to an inflammatory response, characterized by the recruitment of immune cells to the area and associated release of pro-inflammatory cytokines (Finn, 1986). Progesterone withdrawal releases nuclear factor kB (NF-κB) from its inhibitor (IkB) leading to inflammatory gene induction, resulting in an influx of inflammatory cells. Interactions between these and decidualized stromal cells mediate release of a wide variety of pro-inflammatory mediators including chemokines, cytokines and prostaglandins (Evans and Salamonsen, 2012). Key inflammatory mediators such as interleukin-8 (IL-8), monocyte chemoattractant protein-1 (MCP-1) and cyclooxygenase-2 (COX-2) have a perivascular location with a significant increase in the premenstrual endometrium (Jones *et al*, 1997; Milne *et al*, 1999). IL-8 and MCP-1 are potent chemoattractants and activators for neutrophils and monocytes respectively, while COX-2 is the inducible enzyme responsible for synthesis of prostaglandins. The presence of these inflammatory mediators coincide with the marked influx of leucocytes to the endometrium (Jones *et al*, 1997), which leads to activation of matrix metalloproteinases (MMP) that are important for tissue degradation during menstruation (Evans and Salamonsen, 2012).

1.3.2 Tissue repair

Although it was initially thought that endometrial repair followed menstruation, histological evidence combined with scanning electron microscopy showed that shedding and repair occur simultaneously in adjacent areas during menstruation (Garry *et al*, 2009). Endometrial tissue repair shares common features with the classic wound healing process, such as inflammation, tissue formation and tissue remodelling (Salamonsen, 2003). The inflammatory process that is the basis of

menstruation is also the initial point for the repair process. The occurrence of the apoptotic process is crucial for the resolution of inflammation, in particular by limiting the presence of inflammatory cells (Maybin and Critchley, 2012). By contrast to postnatal wound healing, but recapitulating fetal wound healing, endometrial repair is scar-free (Salamonsen, 2003) partially due to specific changes in the extracellular matrix (ECM) involving integrins, the TGFβ superfamily, MMPs, and the innate immune system (Evans *et al*, 2011). Understanding how the endometrium limits inflammation, modulates immune-cell activity, rapidly repairs and remains scar-free has implications for the development of treatments in regenerative medicine (Evan *et al*, 2016).

Endometrial regeneration starts with the re-epithelialization process, which is hormone-independent (Figure 1.3). It is still open to debate whether adult human endometrial glands originate from clonogenic epithelial or mesenchymal progenitors, or both cell types present in the basal layer (Garry et al, 2009; Nguyen et al, 2017). Once the endometrial surface is re-epithelialized, estrogen is required to stimulate glandular and stromal regeneration. As the levels of this hormone rise, estrogen receptors (ER) and progesterone receptors (PR) are induced in the epithelium and stroma and there is extensive proliferation of glandular epithelial and stromal cells in the functional layer (Gargett *et al*, 2012). Simultaneously with tissue breakdown and re-epithelization, formation of new blood vessels occurs from existing vessels. Apart from menstruation, angiogenesis also occurs during the rapid endometrial growth in the proliferative phase and during the secretory stage when spiral arterioles show significant growth and coiling (Gargett and Rogers, 2001). Numerous angiogenic factors have been identified in human endometrium at the time of endometrial repair, though the family of vascular endothelial growth factor (VEGF) genes is thought to be the most important (Smith, 2001). VEGF stimulation is triggered by progesterone withdrawal with hypoxia and prostaglandins as downstream mediators (Maybin *et al*, 2011). Additionally, stromal cell-derived factor-1 (SDF-1, also known as CXCL12) and its receptor CXCR4 have been implicated in endometrial vascular regeneration. SDF-1 is present throughout the menstrual cycle and CXCR4 expression peaks in the early proliferative phase and is present in epithelial cells and endothelial cells (Laird *et al*, 2011). Through synergistic interaction, VEGF and SDF-1 promote the functions of vascular endothelial cells such as cell migration, cell survival, and gene expression (Salcedo *et al*, 1999; Nishigaki *et al*, 2011). MMPs also play a key role in angiogenesis by degrading the extracellular matrix and permitting the migration and tube formation of endothelial cells (Smith, 2001).

The identification of rare epithelial and stromal populations of clonogenic cells in human endometrium suggests that stem/progenitor cells are responsible for the cyclic tissue regeneration (Gargett *et al*, 2016). The human endometrium is believed to hold both endogenous and exogenous sources of adult stem cell that are recruited to the perivascular niche during menstruation (Khatun *et al*, 2017). The identification and characterization of endometrial stem cells and their clinical applications will be further explored on following sections.

1.3.3 The secretory endometrium

After ovulation, the endometrium undergoes secretory changes and becomes receptive during the 'window of implantation' (WOI), which starts from day 6 to day 9 after the LH surge (Achache and Revel, 2006; Aghajanova *et al*, 2008) (Figure 1.3). Key endometrial events associated with the WOI are the increased expression of chemokines and cytokines, the onset of decidualization, and the presence of increased numbers of leukocytes, including uNK cells (King *et al*, 2012).

Epithelium

The luminal epithelium is perceived as a major mediator of uterine receptivity since it is the first point of contact for blastocysts. To facilitate embryo attachment and subsequent implantation, the plasma membrane in cells of the luminal epithelium is transformed from a non-adhesive to an adhesive surface (Murphy *et al*, 2004). The plasma membrane remodelling encompasses transformation from a microvillous into a smooth and flattened apical membrane, downregulation of the junction complexes on the lateral membrane, and increase in the thickness of the basal lamina (Murphy *et al*, 2004).

The transformation of the glandular epithelium during the secretory phase is associated with secretion of glycogen, presence of giant mitochondria and modifications in the nuclear channel system (Spornitz, 1992; Demir *et al*, 2002). The molecular mediators known to be important for the receptive phenotype include integrins, osteopontin, Notch signalling, heparin-binding EGF-like growth factor, cell-surface-associated mucins, glycodelin and ion channels (Davidson and Coward, 2016).

Decidualization

In the mid- to late-secretory phase of each menstrual cycle, endometrial stromal cells (EnSC) differentiate into larger, round, secretory and epithelioid-like decidual cells (Aplin *et al*, 1988). Characteristic secretory products include prolactin (PRL) and insulin-like growth factor binding protein-1 (IGFBP1). Decidual cell also produce ECM proteins such as type IV-collagen, laminin, decorin, fibronectin and heparan sulphate proteoglycans (Gellersen and Brosens, 2014). In humans decidualization occurs spontaneously and independent of the presence of an implanting blastocyst, whereas in nonmenstruating species, this process is initiated by the implanting conceptus (Gellersen and Brosens, 2014).

Decidualization is a progressive process, initiated around the terminal spiral arteries of the superficial endometrial layer in response to elevated progesterone levels and increased intracellular cyclic adenosine monophosphate (cAMP) production (Brosens *et al*, 2002; Gellersen and Brosens, 2014). The initial decidual response is characterized by cell cycle arrest at G0/G1 and a transient pro-inflammatory phenotype, followed by a profound anti-inflammatory response associated with the secretory phenotype (Logan et al, 2012; Gellersen and Brosens, 2014). Microarray analysis have been used to show that the decidual process is associated with the sequential reprogramming of functionally related families of genes involved in steroid hormone action and metabolism, cell cycle regulation, ECM organization, cell adhesion, cytoskeletal organization, angiogenesis, immune modulation of implantation, stress response and apoptosis modulation (Popovoci *et al*, 2000; Giudice *et al*, 2004).

In vitro studies of decidual cells with conditioned medium of individually cultured human pre-implantation embryos inferred that at the time of implantation, the decidua is responsible for sensoring embryo quality (Brosens *et al*, 2014). Thus, cyclic decidualization coupled to menstruation emerged as a strategy for early detection and active rejection of developmentally abnormal embryos that have breached the luminal epithelium. Low quality embryos elicit an endoplasmic stress response in human decidual cells, which in turn compromises secretion of decidual factors, including PRL and IGFBP1, essential for placental formation and fetal development (Brosens *et al*, 2014).

The human decidua also contains a high number of immune cells, such as macrophages, natural killer cells and regulatory T cells. Although the origin of

endometrial leukocytes is still uncertain, most likely these cells are derived from circulating immune cells that undergo tissue-specific differentiation upon recruitment (Lee *et al*, 2015). This specific endometrial environmental supports multiple physiological functions, such as immune tolerance toward implanted allogeneic embryo, surveillance against infections and neoplastic transformations, and placenta development (Oreshkova *et a*l, 2012).

Recently, it has been demonstrated that receptive phenotype is intrinsically associated with a cell fate decision between differentiation and acute senescence in an IL-8 dependent manner (Brighton *et al*, 2017). While the decidual cells are highly resistant to various stress signals and protect the embryo-maternal interface from influx of T-cells, senescent decidual cells drive the transient inflammatory response associated with endometrial receptivity (Gellersen and Brosens, 2014; Brighton *et al*, 2017). Toward the late secretory phase, the influx of uNK is responsible for clearing the senescent subpopulation and create ingresses in the tightly adherent decidual cell matrix to facilitate trophoblast invasion and anchoring of the conceptus (Brighton *et al*, 2017). Additionally, it has been suggested that a tight control of the senescence-associated secretory phenotype (SASP) is essential to stimulate regenerative signals that induce cell plasticity and stemness (Ritschka *et al*, 2017; Brighton *et al*, 2017).

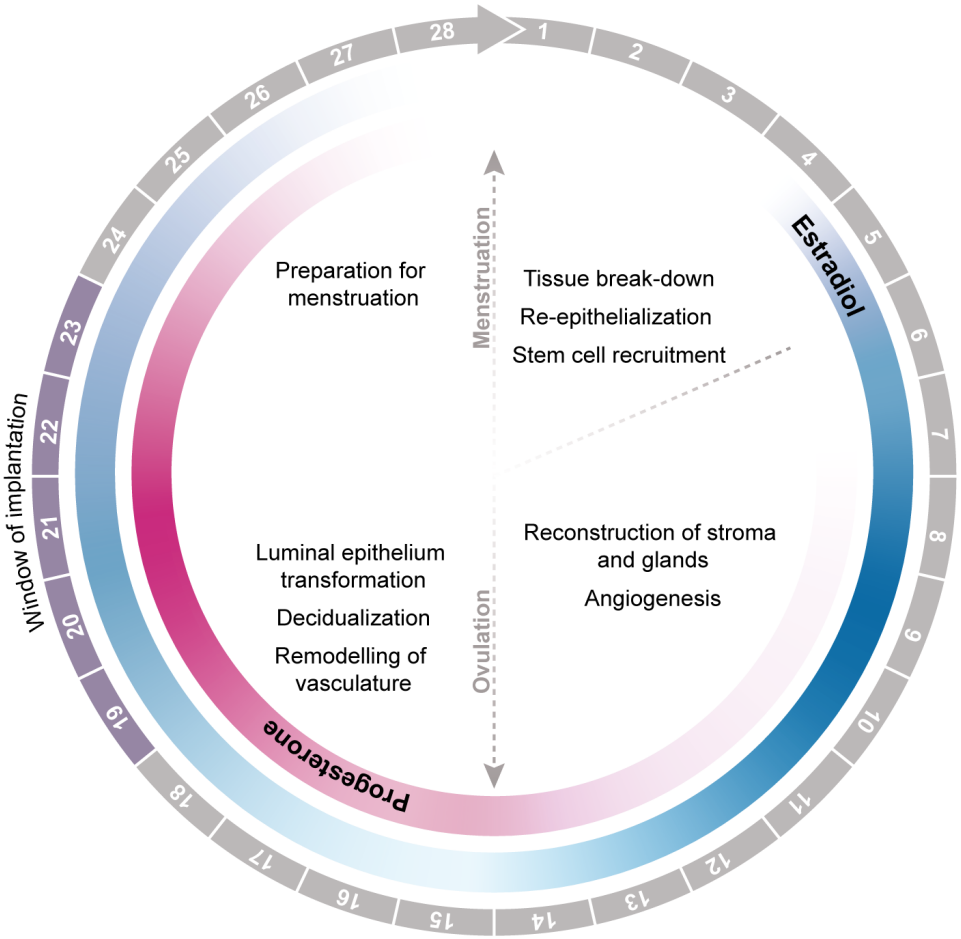

Figure 1.3 Human endometrial remodelling. Throughout the reproductive years, the endometrium demonstrates a remarkable regenerative capacity in cyclic manner. Each menstrual cycle starts with the shedding of the tissue and simultaneous regeneration, followed by induction of a receptive phenotype during the WOI. In the absence of implantation, the ovarian hormone levels decrease and the endometrium is prepared for a new cycle.

1.4 Stem cells

The concept of stem cells originated at the end of the 19th century in the works of the German biologist Ernst Haeckel, who used the term ‘‘Stammzelle’’ (German for stem cell) to describe the fertilized egg that gives rise to all cells of the organism (reviewed in Ramalho-Santos and Willenbring, 2007). However, the first experimental evidence of stem cells was only achieved in 1961, when Ernest A McCulloch and James E Till documented the self-renewing activity of transplanted mouse bone marrow cells (Till and McCulloch, 1961). Since then, stem cells research has become a prominent subject in biosciences because of its transferrable relevance to a wide range of other fields, such as neurobiology, autoimmune diseases, cardiovascular diseases and cancer, among others (Ullah *et al*, 2015).

Stem cells are defined as having the ability to both self-renew and give rise to differentiated cells. The capacity to differentiate into mature and specialized cell types is referred to as potency and can be divided in different levels (Hima Bindu and Srilatha, 2011):

- Totipotent stem cells are produced from the fusion of an egg and sperm cell and can differentiate into embryonic and extraembryonic cell types.
- Pluripotent stem cells are the descendants of totipotent cells and can differentiate into specialized cell types deriving from the three germ layers (ectoderm, endoderm, and mesoderm). These pluripotent cells are characterized by self-renewal and a differentiation potential for all cell types of the adult organism (Romito and Cobellis, 2016).
- Multipotent stem cells can only differentiate into only a closely related family of cells (e.g. hematopoietic stem cells differentiate into white blood cells, red blood cells, platelets, etc.)
- Unipotent stem cells have the property of self-renewal but only can differentiate along one cell lineage (e.g. skin cells).

While differentiating, the cell usually goes through several stages, becoming more specialized at each step through a process called asymmetric division. In a typical outcome of an asymmetric division, the cell generates a copy of itself, which retains self-renewal ability and differentiation potential, and one daughter (transit-amplifying cell/progenitor cell) that enters the path of differentiation (Figure 1.4). This process is essential to generate cellular diversity during development and maintain adult tissue homeostasis (Hima Bindu and Srilatha, 2011; Gómez-López *et al*, 2014).

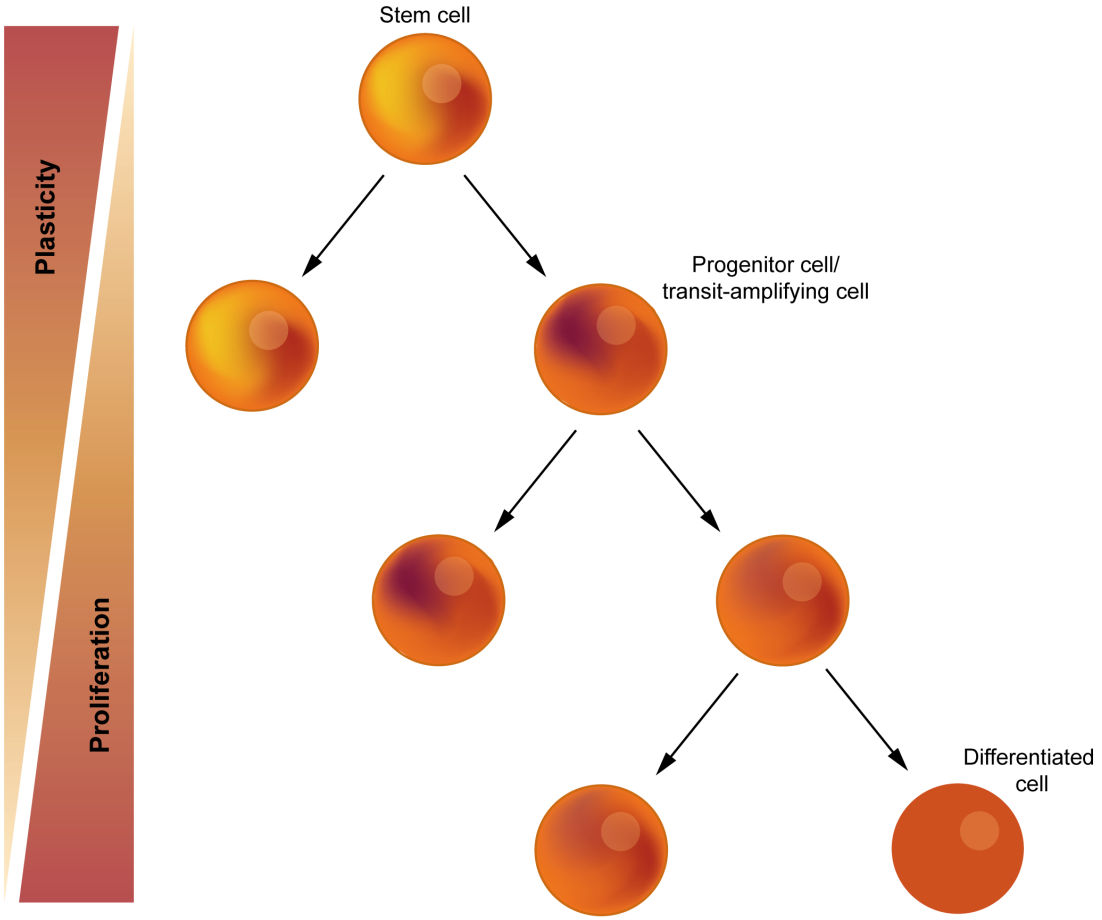

Figure 1.4 The asymmetric cell division. The asymmetric stem cell division produces one copy of itself and one daughter cell that is more committed in the lineage differentiation. Transit-amplifying cells have intermediate properties between stem cells and mature differentiated cells, with limited proliferative and self-renewal potentials. Thus, the mechanism of asymmetric stem cell division is used to balance stem cell self-renewal and differentiation.

Stem cells can be divided into different categories according to their basis of origin**.** **Embryonic stem cells** (ESC) are derived from the inner cell mass (ICM) of blastocysts and characterized by their self-renewal ability and pluripotency. Due to their unlimited proliferation and transformation capacity *in vitro* and *in vivo*, allied to CRISPR/Cas9 genetic studies, ESC have become a comprehensive cell source to study development and new therapeutic approaches for regenerative medicine (Hima Bindu and Srilatha, 2011). **Induced pluripotent stem cells** (iPSC) are generated from somatic cells and epigenetically reprogrammed to behave like embryonic stem cells. Initial iPSCs were obtained from mouse fibroblasts by introducing four transcription factors, Oct3/4, Sox2, c-Myc, and Klf4 (Takahashi and Yamanaka, 2006). Although these cells are an important tool to study normal development and disease progression, their genomic stability is still questionable (Ullah *et al*, 2015). In fact, it is still unclear whether iPSCs generated from different cell types are molecularly and functionally similar (Polo *et al*, 2011). Lastly, **adult stem cells** (ASC), also called tissue stem cells, can be isolated from several tissue sources, including the central nervous system, bone marrow, retina and skeletal muscle (Gurusamy *et al*, 2018). ASC are multipotent cells that give rise to cell types of one particular tissue to maintain and replenish the function of organs or tissues. Evidence suggests that although there are many types of ASC, they all share common core characteristics, such as (Caplan *et al*, 2015):

a) multipotency;
b) localized in a well-defined niche or in contact with blood vessels;
c) sense and respond to dynamic changes of their microenvironment;
d) paracrine activity;
e) immune-modulatory activity;
f) homing: involved in site-specific regeneration, upon the loss of cells or injury to the tissue.

ASCs include hematopoietic stem cells (HSC), which are generated in the bone marrow and differentiate into mature types of blood cells, and mesenchymal stem cells (MSC), which can be isolated from several sources (e.g. bone marrow, fat tissue and cord blood) and are considered the most promising pharmaceutical multipotent cells *(Gazit et al, 2008;* Gurusamy *et al*, 2018*).*

1.4.1 Hematopoietic stem cells (HSC)

The initial observation of adult bone marrow as a source of HSC capable of regenerating the irradiation-ablated haematopoietic system led to an extreme effort to isolate and characterize these cells (Ng and Alexander, 2017). Nowadays, HSC are commonly isolated based on the combination of markers summarized in Table 1.1. In the hematopoietic system, HSC reside at the top of the hierarchy and give rise to more than ten diverse functional cell types, including erythrocytes, platelets, myeloid cells (macrophages and granulocytes), T- and B- lymphocytes, NK and dendritic cells (Seita and Weissman, 2010). Due to their characteristically short lifespan, one million blood cells are produced per second in an adult human to replenish the hematopoietic system. The immediate progeny of HSC are multipotent progenitor cells that have a limited capacity for self-renewal yet retaining full lineage potential (Seita and Weissman, 2010). These transiently hematopoietic progenitors have a high proliferative and developmental capacity, rendering them capable of reconstituting myeloablated recipients more rapidly than HSC (Bryder *et al*, 2006). The hierarchical differentiation structure creates a low proliferative pressure on HSCs, which primarily reside in the G0 phase of the cell cycle. Thus, HSC are less subjected to potentially mutagenic hazards of DNA replication and cell division, ultimately contributing to the integrity and longevity required for these cells (Bryder *et al*, 2006; Seita and Weissman, 2010).

Research on the biology and regulation of HSC has revolutionised bone marrow transplantation and regenerative medicine (Ng and Alexander, 2017) and consequently can be applied to interpret the nature of other adult stem cells.

Table 9.1 Human HSC markers through positive and negative selection

Marker	Selection	Description	Reference
CD34	Positive	Major positive marker for human hematopoietic stem and progenitor cells	Kondo *et al*, 2003
CD90 (Thy-1)	Positive	Differentiates between HSC and multipotent hematopoietic progenitor cells	Craig *et al,* 1993 Majeti *et al*, 2007
Lin	Negative	Lineage (Lin) markers expressed on mature blood cells such as, CD3, CD4, CD8, CD19, CD20, CD56, CD11b, CD14, and CD15	Baum *et al*, 1992 Kondo *et al*, 2003
CD38	Negative	CD38 Is expressed in more differentiated hematopoietic cells	Terstappen *et al*, 1991
CD45RA	Negative	CD45RA Is expressed in more differentiated hematopoietic cells	Kondo *et al*, 2003

1.4.2 Mesenchymal stem cells (MSC)

MSC were first isolated from bone marrow and designated bone marrow-derived MSC (BM-MSC). They have osteogenic potential and are defined as clonogenic for their ability to generate colony-forming units (CFUs) of fibroblast-like cells from single cells when plated in culture (Owen and Friedenstein, 1988). Since then, MSC have been described in several other tissues including adipose tissue, umbilical cord blood (Wagner *et al*, 2005), dental tissues (Huang *et al*, 2009), endometrium (Chan *et al*, 2004) menstrual blood (Allickson *et al*, 2011), placenta (Raynaud *et al*, 2012) and skin (Bartsch *et al*, 2005).

The minimum criteria to define MSC was proposed by the Committee of the International Society for Cellular Therapy as follow (Dominici *et al*, 2006):

a) exhibit plastic adherence;
b) positive expression of CD73, CD90 and CD105;
c) negative expression of HLA-DR, CD11b, CD14, CD19, CD34, CD45 and CD79a;
d) have the ability to differentiate *in vitro* into adipocyte, chondrocyte and osteoblast.

Additionally, MSC from various human tissues exhibit different cell surface markers (summarized in Table 1.2). However, there is still no consensus on a single surface molecule to identify MSCs from various sources (Lv *et al*, 2014). Besides, the isolation process usually requires a culturing step to discriminate genuine clonogenic cells. Conversely, this process can modulate the expression of cell surface markers and underscores the necessity to characterize these cells. It has also been observed that sub-culturing MSC at higher passages induces senescence and loss of potency (Ullah *et* al, 2015).

Currently, the concept of 'mesenchymal stem cell' is wrapped up in controversy over the real *in situ* identity of these cells. The term was first coined in Caplan (1991) for stem cells isolated solely from bone marrow and with progeny exclusively committed to cartilage or bone. However, as described above, over the subsequent three decades the MSC research field has fallen into 'one size fits all' stem cell type, accepting adult stem cells isolated from different tissues that display distinct differentiation patterns and different cell surface proteins (Elahi *et al*, 2016; Laplane and Solary, 2019). In parallel, MSC have been identified *in vivo* as perivascular/mural cells, i.e., pericytes and vascular smooth muscle cells (vSMC) that express MSC markers and behave as MCS *in vitro* as well as upon heterologous transplantation (Crisan *et al*, 2008). On the other hand, a recent study published by Guimarães-Camboa and colleagues (2017) challenge this concept and use lineage tracing to demonstrate that perivascular cells do not behave as tissue-specific progenitors during aging and repair in multiple adult mice organs, despite showing MSC potential *in vitro*. Interestingly, it is important to highlight that a small percentage of perivascular cells failed to label in this study, an observation overlooked in the final conclusion. Above all, it is crucial to have a better understanding of MSC biology and improved laboratory platforms to accurately identify these cells.

Table 1.2 Summary of potential MSC sole markers

Marker	Description	MSC source	References
Stro-1	May be involved in clonogenicity and play a role in homing and angiogenesis of MSCs. It has also been detected in endothelial cells.	BM-MSC	Psaltis *et al*, 2010 Ning *et al*, 2011
CD271	CD271-selected MSC from adipose tissue enhance cartilage repair	BM-MSC Adipose tissue	Bühring *et al*, 2007 Kohli *et al*, 2019
SSEA-4	An ESC marker.	BM-MSC	Gang *et al*, 2007
CD146	Used in combination with PDGFRb to isolate endometrial MSC. CD146 expression also defines MSCs with higher multipotency.	Endometrium BM-MSC Periodontal ligament	Schwab and Gargett, 2007 Sorrentino *et al*, 2008
CD49f	Also known as ITGA6. Expression of CD49f is regulated by Oct-4 and Sox-2. Identified as a specific HSC marker	BM-MSCs Umbilical cord blood	Yu *et al*, 2012 Nystedt *et al*, 2013
CD349	Not essential for enriching MSC function	Placenta	Battula *et al*, 2008
GD2	High specificity for isolating MSCs from BM	BM-MSC Umbilical cord	Nystedt *et al*, 2013 Martinez *et al,* 2008
3G5	Pericyte marker. Hematopoietic cells also express 3G5.	BM-MSCs, Dental pulp Decidua	Shi *et al*, 2003 Castrechini *et al*, 2012
SUSD2	Perivascular marker	Endometrium	Masuda *et al*, 2012
CD200	CD200 expression is related to the osteoblastic lineage	BM-MSC	Pontikoglou *et al,* 2016
SSEA-3	Enrich cells with clonogenicity and ectodermal, endodermal, and mesodermal differentiation potency	BM-MSC Placenta	Kuroda *et al*, 2010 Nazarov *et al*, 2012
MSCA-1	Also known as tissue nonspecific alkaline phosphatase (TNAP). It is involved in a wide range of MSC features described below from cell differentiation to immunomodulatory properties	BM-MSC Endometrium	Sobiesiak et al, 2010

1.5 Endometrial stem / progenitor cells

The human endometrium is a complex multicellular tissue that undergoes dynamic remodelling through cycles of regeneration, differentiation and shedding in order to establish a microenvironment that is suitable for implantation. This remarkable regenerative potential is mediated via endogenous and exogenous stem/progenitor cells that are recruited during menstruation (Khatun *et al*, 2017). Emerging evidence also suggests that these cells are essential modulators of tissue homeostasis and subsequently, alterations in this subpopulation are associated with endometrial disorders.

1.5.1 Endometrial stromal stem / progenitor cells

The first functional evidence of endometrial stem cells was published in 2004 by Chan and colleagues that identified rare clonogenic cells from purified populations of human endometrial epithelial and stromal cells (Chan *et al*, 2004). This study identified a small population (1.25%) of EnSC with colony-forming ability. This population was composed by two types of CFUs: small (1.23 % of EnSC) and large CFUs (0.02% of EnSC). Both large and small colonies expressed fibroblast markers, with some cells expressing α smooth muscle actin (α-SMA), which is indicative of myofibroblast differentiation (Chan *et al*, 2004). Later, it was suggested that large CFUs originate from stem/progenitor cell with a greater potential for self-renewal, whereas small CFUs are derived from more differentiated TA cells (Gargett *et al*, 2009).

A sub-population of human EnSC, $CD146^{+}PDGFR\beta^{+}$, has been described to exhibit MSC properties such as, clonogenicity, multi-lineage (adipogenic, myogenic, chondrogenic and osteoblastic) differentiation and expression of typical MSC surface markers (CD29, CD44, CD73, CD90 and CD105) (Schwab and Gargett, 2007). These endometrial MSC (eMSC) are located at perivascular sites in the functional and basal layer of the human endometrium (Schwab and Gargett, 2007). Gene profiling of freshly isolated $CD146^{+}PDGFR\beta^{+}$ alongside $CD146^{-}PDGFR\beta^{+}$ (fibroblasts) and $CD146^{+}PDGFR\beta^{-}$ (endothelial) showed that $CD146^{+}PDGFR\beta^{+}$ cells express genes involved in angiogenesis/vasculogenesis, steroid hormone/hypoxia responses, inflammation, immunomodulation, cell communication, and proteolysis/inhibition, and exhibited increased Notch, TGFβ, IGF, Hedgehog, and G-protein-coupled receptor signalling pathways, characteristic of adult tissue MSC self-renewal and multipotency

(Spitzer *et al*, 2012). Nevertheless, it is important to state that equating $CD146^{+}PDGFR\beta^{+}$ to eMSC is a misconception, since the conjugation of both markers, $CD146^{+}PDGFR\beta^{+}$, labels the perivascular population (Figure 1.5) and only 7.7% of these cells exhibit clonogenic ability (Schwab and Gargett, 2007).

SUSD2 was identified as a single marker of eMSC. Purified $SUSD2^{+}$ cells exhibit self-renewal ability; differentiate into various cell lineages (adipogenic, osteogenic, chondrogenic, and myogenic) and reconstitute mesodermal tissue *in vivo* (Masuda *et al*, 2012). W5C5 antibody recognizes the sushi domain containing-2 (SUSD2) antigen and like $CD146^{+}PDGFR\beta^{+}$, SUSD2/W5C5 expressing cells surround the spiral arteries throughout the endometrium. $W5C5^{+}$ cells account for 4.2% of EnSC and express MSC markers, CD29, CD44, CD73, CD90, CD105, CD117, CD140b (PDGFRβ) and CD146. The cloning efficiency of $W5C5^{+}$ is 1.3- and 14.7-fold higher than $CD146^{+}PDGFR\beta^{+}$ and $W5C5^{-}$ (TA), respectively (Masuda *et al*, 2012). As in other endometrial stem cell- associated populations, $W5C5^{+}$ perivascular cells do not express ERα (Ulrich *et al*, 2014). Inhibition of TGFβ receptor signalling maintains $SUSD2^{+}$ eMSC stemness and promotes proliferation by blocking senescence and apoptosis in late passage cultures (Gurung *et al*, 2015). Once again, SUSD2 is considered a MSC marker, although it should be viewed as a perivascular marker (Figure 1.5). Ultimately, this leads to a misperception between EnSC, perivascular cells (PVC), eMSC and TA cells. Currently, the only way to purify eMSC is through isolation of perivascular cells followed by a CFU assay, in which cells are seeded at low density and propagated in culturing conditions that maintain their stemness.

Taken together, evidence suggests that in the endometrium, the perivascular space around spiral arterioles constitutes an important regulatory niche, likely consisting of both quiescent and active MSCs, TA cells, and neighbouring stromal cells. Simultaneously, this is also the starting point for the decidualization process. The comparison between the decidual response by cultured $W5C5^{+}$ and $W5C5^{-}$ cells demonstrated that perivascular cells establish a specific chemokine profile around the uterine vessels (Murakami *et al*, 2014). This differential molecular response at the perivascular site might be important during early pregnancy to promote endovascular trophoblast invasion and coordinate immune cell trafficking (Murakami *et al*, 2014). Furthermore, it has been demonstrated that decidualization is associated with a significant increase in CFUs driven by senescent cells implying that the decidual transformation increases tissue plasticity prior to pregnancy (Brighton *et al*, 2017).

Surprisingly, despite the fact that the extensive proliferation and remodelling of the human uterus has been explored for many years, studies on adult stem cells and their role in the uterine tissue lag far behind other areas of stem cell research (Ghobadi *et al*, 2015). This is in spite of the obvious potential application of these cells in cellular therapies and regenerative medicine.

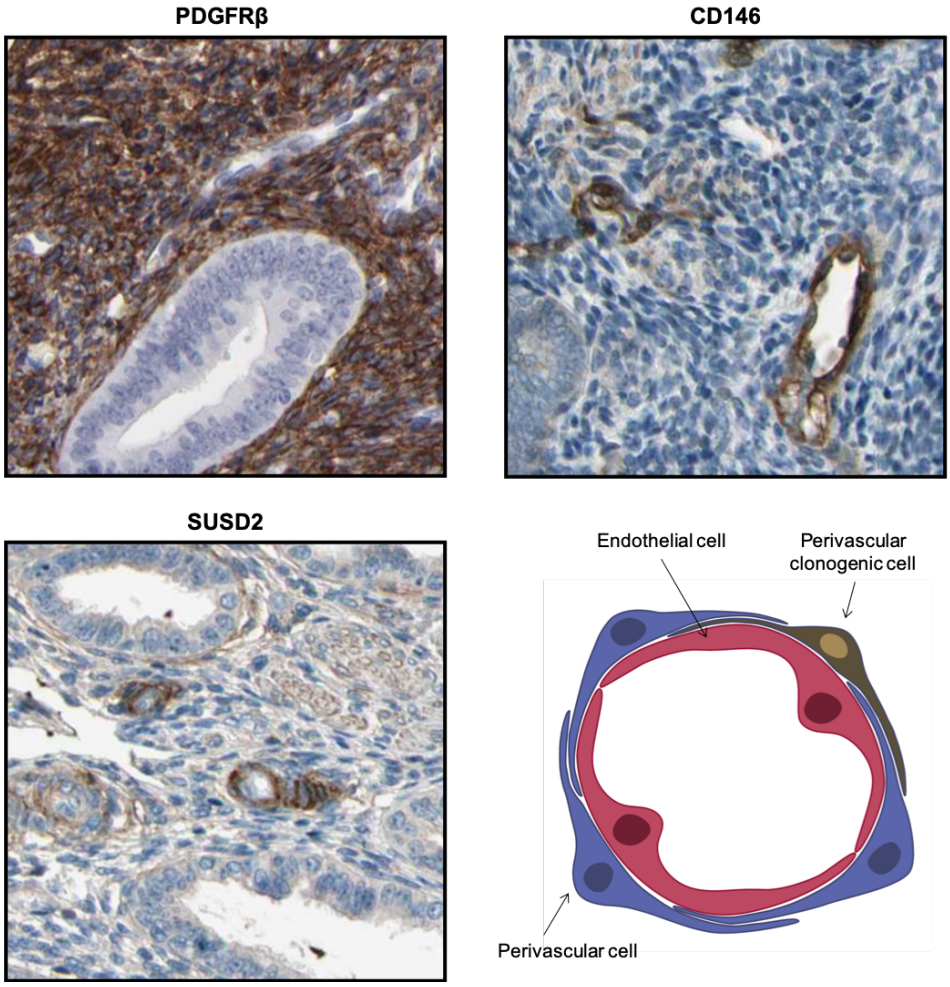

Figure 1.5 Combination of PDGFRβ and CD146 alongside SUSD2 antibodies label endometrial PVC. The micrographs were obtained from The Human Protein Atlas (http://www.proteinatlas.org/). The schematic representation shows perivascular cells surrounding the endothelial cells.

1.5.2 Side population

In addition to CFUs, a rare endometrial side population (SP) has been isolated from human endometrial stromal cell suspensions through its unique ability to efflux intracellular DNA-binding dye Hoechst 33342 via the multi drug resistance (MDR) proteins, such as the ATP-binding cassette transporter G2 (ABCG2) (Masuda et al, 2010). These cells exhibit stem-cell like properties, low clonogenic capacity in short-term cultures due to their quiescent stage, express ERβ rather than ERα, and are speculated to give rise to TA cells (Masuda *et al*, 2010; Masuda *et al*, 2015).

Endometrial SP cells show long-term repopulating properties and produce gland and stroma-like cells when cultured *in vitro* (Kato *et al*, 2007). When transplanted under the kidney capsule of severely immunodeficient mice, these cells were able to reconstitute an organized endometrial tissue with well-delineated glandular structures (Masuda *et al*, 2010). *In vivo* these cells are distributed across both the functional and basal layers, preferentially located around small capillaries rather than large vessels (Masuda *et al*, 2010). These observations suggest that SP cells are bone marrow-derived and may be closely related to eMSC as constituents of a potential endometrial stem cell hierarchy (Masuda *et al*, 2015).

1.5.3 Endometrial epithelial stem cells

Initial cell cloning studies on human endometrium showed that 0.2% of epithelial cells have CFU activity and that two types of CFUs are formed: large (0.09%) and small (0.14%) (Chan *et al*, 2004; Gargett *et al*, 2009). Additionally, it was described that different sizes of CFU present different epithelial markers. Small CFU expressed epithelial differentiation markers [i.e. cytokeratin, epithelial cell adhesion molecule (EpCAM) and integrin α6 (ITGA6/CD49f)], whereas large CFU only expressed ITGA6. The loss of differentiation molecule EpCAM in the large colonies and their high nuclear:cytoplasmic ratio suggested that these cells were associated with an undifferentiated phenotype (Chan *et al*, 2004). Later, it was described that large single-cell-derived epithelial CFUs have the ability of *in vitro* self-renewal and differentiated into gland-like structures in three-dimensional (3D) culture (Gargett *et al*, 2009). Interestingly, when a stromal feeder layer was included, these gland-like structures became larger, indicating that stromal cells provide epithelial progenitor cell

niche factors that promote differentiation and morphogenesis (Gargett *et al*, 2009; Valentijn *et al*, 2013).

Other studies hypothesized that the basalis endometrium harbours the epithelial progenitor cell population, specifically located at the remaining glands after menstruation (Gargett *et al*, 2008). Thus, stage-specific embryonic antigen 1 (SSEA-1, CD15) was used as a marker of endometrial basalis epithelium (Figure 1.6) and it was demonstrated that the SSEA-1$^+$ cells have greater telomerase activity and are more quiescent with lower proliferation rates than SSEA-1$^-$ epithelial cells. Additionally, the transcripts for ERα and PR are significantly lower in SSEA-1$^+$ epithelial cells compared with SSEA-1$^-$ epithelial cells. SSEA-1$^+$ cells also formed spheroids in 3D culture and differentiated into spheres with polarized epithelium (Valentijn *et al*, 2013). However, this study did not demonstrate stem cell activity of human endometrial SSEA-1$^+$ cells.

Only recently, N-cadherin (*CDH2*) was identified as a specific endometrial epithelial progenitor cell candidate marker (Nguyen *et al*, 2017). N-cadherin$^+$ cells were enriched for clonogenic and self-renewing epithelial cells with high proliferative potential that differentiated into cytokeratin$^+$ gland-like structures in 3D cultures. *In vivo*, these cells are quiescent, express ERα and locate predominantly in the deep basalis of endometrial glands. It was also suggested a potential hierarchy of epithelial differentiation starting adjacent to the myometrium and through the basalis toward the lumen (Nguyen *et al*, 2017).

Overall, the research regarding the epithelium and the epithelial stem cells has been a challenge due to the inaccessibility *in vivo* and the absence of *in vitro* models (Turco *et al*, 2017). In addition, cultured primary human epithelial cells (EpC) on a monolayer have limited lifespan and undergo cellular de-differentiation making them difficult to maintain in long-term (Hombach-Klonisch *et al*, 2005). Recently, Turco *et al*, (2017) established 3D endometrial gland organoid cultures, which are able to respond to hormonal signals and differentiate into ciliated luminal epithelial cells. These organoids can be cultured long-term and recapitulate the molecular signature of endometrial glands *in vivo*.

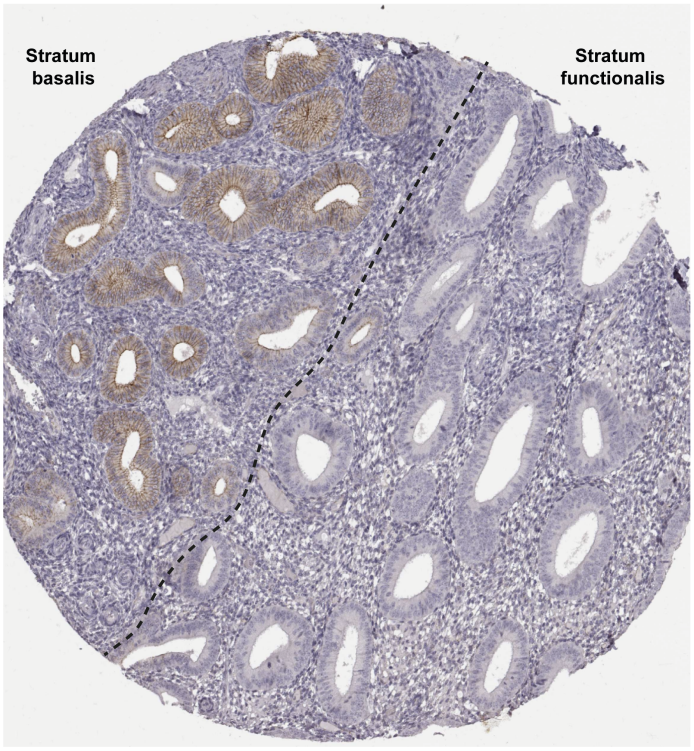

Figure 1.6 Expression of SSEA-1 in endometrial basal layer. The micrographs were obtained from The Human Protein Atlas (http://www.proteinatlas.org/).

1.5.4 Endometrial stem cells in menstrual blood

Menstrual blood- derived stem cells (MenSC) have been extensively investigated due to their advantageous non-invasive collection process (Chen *et al*, 2019). Stem cells cultured from menstrual blood have been given various names as summarized in Table 1.3. In general, epithelial cells were not observed in cultured menstrual blood, either because they were not present or had been overgrown by the stromal fibroblast populations (Musina *et al*, 2008). This observation also corroborates the theory that epithelial progenitors are more likely located in the basalis and not normally shed during menstruation (Gargett and Masuda, 2010; Gargett *et al*, 2016).

MenSC are highly proliferative, pluripotent and express telomerase reverse transcriptase (hTERT) as well as typical MSC phenotypic markers: CD29, CD73, CD90, and CD105 (Meng *et al*, 2007; Khanmohammadi *et al*, 2014; Wu *et al*, 2014). Additionally, these cells are positive for other surface molecules, such as CD9, CD29, CD44, CD59, OCT-4 and CD166 (Meng *et al*, 2007; Patel *et al*, 2008). MenSCs are

also negative for hematopoietic stem/progenitor cell markers, such as CD34, CD45, and CD133 (Meng *et al*, 2007).

Cultured MenSC double every 20 h, which is twice as fast as BM-MSCs (estimated 40–45 h) and retain a stable karyotype for 68 passages (Meng *et al*, 2007; Wu *et al*, 2014). Such a high proliferative rate and stable genetic characteristic, as well as the apparent pluripotency, are exceptional characteristics essential for regenerative medicine (Chen *et al*, 2019). MenSC also have a broad *in vitro* differentiation capacity. Under specific culturing conditions, MenSC can differentiate into adipocyte, chondrocyte, osteoblast, endothelial, neurogenic, cardiogenic, pancreatic, hepatocytes and decidual cells (Meng *et al*, 2007; Patel *et al*, 2008; Sugawara *et al*, 2014; Khoury *et al*, 2014). The therapeutic potential of MenSCs has already been recognized in pre-clinical research of several diseases and could possibly be incorporated for future clinical applications in tissue repair and regenerative medicine (Chen *et al*, 2019; Table 1.4).

Table 1.3 Nomenclatures for MenSC in different studies.

Names	Reference
Endometrial regenerative cells (ERC)	Meng *et al*, 2007
Menstrual blood stromal stem cells (MenSC)	Patel *et al*, 2008
Menstrual blood MSC (mbMSC)	Gargett and Masuda, 2010
Endometrial decidual tissue MSC (EDT-MSC)	Rossignoli *et al*, 2013
Endometrial stem cells	Jiang *et al*, 2013
Menstrual blood-derived mesenchymal stem cells	Mou *et al*, 2013
Menstrual blood progenitor cells (MBPC)	Wu *et al*, 2014
Menstrual stem cells	Alcayaga-Miranda *et al*, 2015

Table 1.4 Pre-clinical research in MenSC therapeutic potential

Disease	Application description	Reference
Fulminant hepatic failure (FHF)	MenSC-derived exosomes possess therapeutic potential by inhibiting hepatocyte apoptosis in induced FHF in mice, suggesting that exosomes may be an alternative therapeutic approach to treat FHF	Chen *et al*, 2017
Type 1 diabetes mellitus (T1DM)	T1DM is characterized by the deficiency of secreting insulin in islet β cells. Transplantation of MenSC in T1DM mice recovered islet structures and increased the β-cell number by promoting differentiation of endogenous progenitor cells	Wu *et al*, 2014
Ischemic stroke	Intracerebral/intravenous transplantation of MenSC improved the behaviour and neurostructure in ischemic stroke induced rat	Borlongan *et al*, 2010
Duchenne muscular dystrophy (DMD)	MenSC restored muscle degeneration and repaired skeletal muscle abnormalities by increasing muscle-like protein expression in immunodeficient DMD model mice	Cui *et al*, 2007
Epithelial ovarian cancer (EOC)	Transplantation of MenSCs improved the symptoms of EOC in mice model. *In vitro*, co-culture with MenSCs induced angiogenic ability and reduced EOC cells	Bu *et al*, 2016
Asherman syndrome	Autologous MenSC transplantation significantly increased endometrial thickness in Asherman syndrome women	Tan *et al*, 2016
Alzheimer's disease	Intracerebral transplantation of MenSC improved the spatial learning and memory of APP/PS1 mice	Zhao *et al*, 2018
Acute lung injury (ALI)	MenSCs promoted the repair of injured lung by inhibiting the inflammatory response in LPS-induced ALI in mice	Xiang *et al*, 2017

1.5.5 Stem cells in endometrial decidua

Human endometrial stromal cells terminally differentiate into the decidua from mid- to late-secretory phase of the menstrual cycle. It has been demonstrated that first trimester decidua also harbours multipotent MSC, which have clonogenic properties, can differentiate into different cell lineages, and express surface markers specific to mesenchymal stem cells (Dimitrov *et al*, 2010; Abomaray *et al*, 2016). Additionally, clonogenic SP cells, which are negative for CD34, CD45 and the mature decidual cell marker CD13 have also been isolated from first-trimester decidua and suggested to be part of the MSC population (Guo *et al*, 2010). Purified decidual SP cells differentiated into endothelial cells *in vitro* and induced functional revascularization following intramuscular injection in a mouse ischaemic hind limb injury model, rescuing the limb (Wang *et al*, 2013). These SP cells also have a higher proliferation and migration rate compared to the main population under estrogen and progesterone treatment (Wang *et al*, 2013). More studies are required to determine the relationship among eMSC, decidual MSC and the potential therapeutic application of the latter (Gargett *et al*, 2016).

1.5.6 Endometrial plasticity and reproductive disorders

The key role of stem cells in tissue homeostasis also implies that alterations in this population are likely associated with benign gynaecological diseases. The activation, proliferation and differentiation of stem/progenitor cells are regulated by the stem cell niche, which may also have roles in the development and progression of endometriosis, Asherman's syndrome and recurrent pregnancy loss.

Endometriosis

Endometriosis is a benign gynecologic condition defined by the presence of ectopic endometrial tissue, most commonly in the peritoneal cavity (involving the ovary, cul-de-sac, uterosacral, broad and round ligaments, fallopian tubes, colon, and appendix). Less common sites include the intestine, bladder, pelvic lymph nodes and rarely the cervix, abdominal wall, vagina, pleura, skin and brain (Dhesi and Morelli, 2015). This disease affects 6–10% of reproductive aged women, and 20% to 50% of infertile women (Eskenazi and Warner, 1997).

Endometriosis is an inflammatory process that often manifests as painful periods (dysmenorrhea) associated with intermenstrual bleeding, painful urination (dysuria), painful intercourse (dyspareunia) and infertility (Parasar *et al*, 2017). The most widely accepted theory to explain the pathogenesis of this disease is Sampson's theory of retrograde menstruation, first described in 1922 (Sampson, 1922; Dhesi and Morelli, 2015). This hypothesis was then modified upon discovery of endometrial stem/progenitor cells. Nowadays, it is proposed that endometrial stem/progenitor cells shed during menses, gain access to the peritoneal cavity by retrograde menstruation and establish ectopic implants, causing endometriosis (Gargett *et al*, 2016). Furthermore, based on the observation that this disease is also present in normal young girls before menarche, Brosens and Benagiano postulated that endometrial stem/progenitor cells may be involved in the onset of endometriosis through retrograde neonatal uterine bleeding due to maternal progesterone withdrawal at birth (Brosens and Benagiano, 2013).

Several lines of evidence contributed to support the effect of endometrial stem/progenitor cells in ectopic endometriotic lesions. Leyendecker and colleagues identified significantly more basalis fragments in the menstrual blood of endometriosis patients, suggesting that an increased number of stem cells in this layer that can result in a propensity for endometriosis (Leyendecker *et al*, 2002). Additionally, SSEA-1, a marker of basal endometrial epithelial cells, was found in endometriotic lesions (Valentijn *et al*, 2013). Cultured ectopic eMSC express *OCT4*, present MSC phenotypic surface markers and demonstrate greater ability of cell migration and invasion. Also, when transplanted in immune-deficient mice, ectopic endometrial MSC increase angiogenesis and invasion into surrounding tissue (Kao *et al*, 2011). Stemness-related genes (e.g. *SOX2, NANOG*, and *OCT4*) were significantly higher in the eutopic endometrium of endometriosis patients, thus supporting a role for stem cell origin of endometriosis (Song *et al*, 2014). Nevertheless, it is still necessary to parse the functions of endometrial stem/progenitor cells in the pathogenesis and severity of this enigmatic disease (Gargett *et al*, 2016).

Asherman's syndrome

Asherman's Syndrome or intrauterine adhesions (IUA) is an acquired gynecological condition characterized by fibrous scars (uterine synechiae), resulting in reduced menstrual flow, pelvic pain and infertility. The distinction between the functional and

basal layer of the endometrium is lost. The endometrial stroma is largely replaced by fibrous tissue, and the glands usually contain inactive epithelial cell that are nonresponsive to hormone stimulation (Yu *et al*, 2008). Consequently, uterine synechiae are associated with a considerable increase in the risk of placental abruption and preterm premature rupture of membranes (Tuuli *et al*, 2012).

The main cause of Asherman's syndrome is the occurrence of trauma to a gravid uterine cavity, which can be induced by postpartum curettage, from termination of pregnancy, spontaneous miscarriage or Caesarean section. Low estrogen levels at the time of the operation, or immediately afterwards, are one of the possible explanations why gravid uterus is susceptible to Asherman's syndrome (Yu *et al*, 2008). Although after menstruation or parturition the endometrial surface epithelium repairs without scarring in the absence of estrogen, it is considered that the deep trauma involving the basalis and underlying myometrium may explain the failure of the endometrial functional layer to regenerate in Asherman's syndrome and IUA. Additionally, it is hypothesized that resident endometrial stem/progenitor cells may be damaged or lost, particularly in basalis layer (Gargett and Ye, 2012).

Transplantation of male bone marrow cells in a mouse model of Asherman's syndrome led to reduced fibrosis and pregnancies with normal litter sizes (Alawadhi *et al*, 2014). However, only a small number (0.1%) of $Y^{+}CD45^{-}$ cells were detected in the endometrium of the transplanted mice, suggesting that either an immediate systemic cytokine effector or an indirect activation of endogenous endometrial stem/progenitor cells or their niches (Alawadhi *et al*, 2014; Gargett *et al*, 2016). A recent non-controlled pilot study also reported that autologous cell therapy using peripheral blood $CD133^{+}$ bone marrow-derived stem cells in conjunction with hormonal replacement therapy temporarily improves endometrium thickness in patients with refractory Asherman's syndrome (Santamaria *et al*, 2016).

Recurrent pregnancy loss

Miscarriage is defined as the loss of pregnancy before a fetus reaches viability and is estimated to occur in 15-25% of all clinically recognized pregnancies (Pfeifer *et al*, 2012). Consequently, recurrent pregnancy loss (RPL) is defined as the loss of two or more pregnancies. In RPL, the incidence of euploid fetal loss increases with each additional miscarriage, whereas the likelihood of a future successful pregnancy gradually decreases (Ogasawara *et al*, 2000). Additionally, the cumulative live-birth

rate for most RPL patients is high, irrespective of medical intervention. These observations suggests that there is a dynamic interaction between embryo and endometrium that progresses in order to adapt to a successful pregnancy (Ewington *et al*, 2019).

As previously described, the decidualization of endometrial stromal cells act as sensor that responds to embryonic serine proteases in a manner that either supports further development (positive selection) or ensures rapid disposal through menstruation-like shedding (negative selection) (Brosens *et al*, 2014). Decidualization is a gradual process initially characterized by an acute pro-inflammatory response that transitions into an anti-inflammatory phenotype, which limits the "window of implantation" to a restricted timing (Gellersen and Brosens, 2014). RPL is associated with a prolonged pro-inflammatory decidual response, which promotes out-of-phase implantation, and disables embryo selection (Salker *et al*, 2010; Salker *et al*, 2012).

Another key event in endometrial remodelling is the onset of menstruation and simultaneous tissue regeneration. Over the last decade the participation of stem/ progenitor cells in endometrial regeneration has been widely investigated. Recently, it was identified that RPL is associated with a marked reduction in methylation of defined CA-rich motifs, which is a hallmark of stem cells, embryos and gametes (Lucas *et al*, 2016). To explain this difference in the methylation signature, the authors compared the total number of freshly isolated SUSD2/W5C5^{+} cells, the abundance of clonogenic SUSD2/W5C5^{+} eMSC and the abundance of clonogenic SUSD2/W5C5^{-} TA cells between RPL and control subjects. The total number of SUSD2/W5C5^{+} cells did not differ between the study and control groups. However, RPL was associated with significant reduction in the abundance of clonogenic eMSC and TA cells (Lucas *et al*, 2016). Once again, these results corroborate the previous statement that SUSD2/W5C5 should be viewed as a perivascular marker and not as a specific eMSC cell surface protein.

1.6 Research Justification and Aims

The human endometrium is a highly heterogeneous tissue comprising multiple cell-types and cellular states that change in cycle-dependent manner. Apart from the main cell populations (i.e. stromal, endothelial, epithelial and immune cells), the endometrium also comprises a hierarchy of stem and more committed cells that are responsible for the remarkable regenerative ability of this tissue. Nevertheless, this endometrial cell heterogeneity is a major drawback when interpreting bulk (whole biopsy) transcriptomic data. Additionally, there is a lack of specific stem cell markers that hinders the study of these cells *in vivo.* Therefore, the main goal of my project was to assess and interpret endometrial heterogeneity with a focus on the characterization of rare stem/progenitor cells. For this, different aims were established as follow:

1) To generate a reference matrix consisting of the transcriptome profiles of epithelial, uNK and stromal subsets (EnSC, PVC, eMSC and TA) for the computational deconvolution of whole tissue transcriptome data.

2) Compare the transcriptional data of each stromal subpopulation in order to characterize cultured eMSC and identify specific cell surface proteins.

3) Use high-throughput single-cell droplet barcoding to profile the transcriptome of peri-implantation endometrial biopsies.

4) Identify rare populations from single cell transcriptomic data and further characterize them.

5) Optimize a single nucleus transcriptomic technique for archived endometrial samples in order to bypass the disadvantages inherent to single cell approaches that are dependent on fresh tissues.

Chapter 2

Material and Methods

2.1 Materials

2.1.1 Cell culture reagents

Reagent	Concentration	Manufacturer
Dulbecco's Modified Eagle Medium (DMEM)/F12 (1:1) with phenol red	1X	Thermo Fisher Scientific
Collagenase type IA	0.5 mg/ml	Sigma-Aldrich
Deoxyribonuclease I (DNAse I)	0.1 mg/ml	Roche
Insulin	2 µg/ml	Sigma-Aldrich
L-Glutamine	1%	Thermo Fisher Scientific
Penicillin (10,000 µg/ml)-Streptomycin (10,000µg/ml) solution	1%	Thermo Fisher Scientific
Dextran and charcoal-treated fetal bovine serum (DCC-FBS)	10%	Thermo Fisher Scientific
β-estradiol	1 nM	Sigma-Aldrich
Ficoll-Paque PLUS	n/a	GE Healthcare
Basic fibroblast growth factor (bFGF)	10 ng/ml	Merck Millipore
Fibronectin	1 mg/ml	Sigma-Aldrich
Dimethyl sulfoxide (DMSO)	10%	Life Technologies
RNA-later	n/a	Sigma-Aldrich
Matrigel	n/a	Corning
Cell Recovery Solution	n/a	Corning
Trypsin	n/a	

Expansion medium reagents

Reagent	Concentration	Manufacturer
Advanced DMEM/F12	1X	Life Technologies
N2 supplement	1X	Life Technologies
B27 supplement minus vitamin A	1X	Life Technologies
Antibiotic-antimycotic	1 %	Invitrogen
N-Acetyl-L-cysteine	1.25 mM	Sigma-Aldrich
L-Glutamine	2 mM	Life Technologies
Recombinant human EGF	50 ng/ml	Peprotech
Recombinant human Noggin	100 ng/ml	Peprotech
Recombinant human Rspondin-1	500 ng/ml	Peprotech
Recombinant human FGF-10	100 ng/ml	Peprotech
Recombinant human HGF	50 ng/ml	Peprotech
ALK-4, -5, -7 inhibitor, A83-01	500 nM	System Biosciences
Nicotinamide	10 nM	Sigma-Aldrich
Y-27632	10 µM	Abcam

Consumables

Consumable	Manufacturer
MS columns	Miltenyi Biotec
Luna automated cell counter slides	Logos Biosystems
Haemacytometer	VWR International Ltd
Cell scraper	Corning
Anti-PE-magnetic-activated cell sorting microbeads	Miltenyi Biotec

2.1.2 Antibodies

Primary

Antibody	Host	Dilution	Manufacturer
Anti SUSD2-PE	Mouse	1:50	Miltenyi Biotec
Anti MRP4-PE	Mouse	1:100	Santa Cruz
ANLN	Mouse & rabbit	1:100	Sigma-Aldrich
CD34	Rabbit	1:250	Abcam
CD56	Mouse	1:200	Leica Biosystems
CD163	Rabbit	1:200	Abcam

Secondary

Antibody	Manufacturer	Dilution
Alexa-Fluor™ 488 anti-rabbit secondary	Invitrogen	1:500
Alexa-Fluor™ 594 anti-mouse secondary	Invitrogen	1:500 (IHC) / 1:1000 (IC)

2.1.3 General chemical reagents

Reagent	Manufacturer
4 % Formaldehyde	VWR International Ltd
Bovine serum albumin	Sigma-Aldrich
Chloroform	VWR International Ltd
DPX coverslip mountant	Sigma-Aldrich
Haemotoxyxlin	Leica

Isopropanol	Sigma-Aldrich
Precision plus qPCR master mix SYBR Green	PrimerDesign
ProLong Gold antifade mounting medium with DAPI	Invitrogen
RNase free water	Life Technologies
RNase ZAP	Fisher Scientific
STAT-60	AMS Biotechnology
Triton X-100	Sigma-Aldrich
Trypan blue	Invitrogen
Tween 20	Sigma-Aldrich
VECTASHIELD antifade mounting medium with DAPI	Vector Laboratories

2.1.4 Kits

Kit	**Manufacturer**
AllPrep DNA/RNA Micro Kit	QIAGEN
Autofluorescence quenching kit	Vector Laboratories
QIAquick Gel Extraction Kit	QIAGEN
QuantiTECT Reverse Transcription Kit	QIAGEN
TruSeq RNA Library preparation kit V2	Illumina
Qubit RNA BR Assay kit	Invitrogen

2.1.5 General solutions

Separation buffer (for MACS separation)

1X PBS

0.5 % BSA

Sodium citrate buffer (antigen retrieval)

10 mM sodium citrate

0.05% Tween-20, pH 6

Blocking solution

1X PBS

1% BSA

2.1.6 scRNA Seq & snRNA Seq

Reagents and Consumables

Reagent	Manufacturer
0.5 M EDTA	Sigma-Aldrich
1 M Tris pH 7.5	Fisher Scientific
1 M Tris pH 8.0	Fisher Scientific
1 M DTT	Fisher Scientific
20X SSC	Fisher Scientific
1H,1H,2H,2H-Perfluorooctan-1-ol (PFO)	Sigma-Aldrich
10 mM dNTPs	Clontech
200 Proof Ethanol	Sigma-Aldrich
Ampure XP beads	Beckman Coulter

Barcoded beads SeqB	ChemGenes (Macosko *et al*, 2015)
Exonuclease I kit	NEB
Ficoll PM-400	Fisher Scientific
Kapa HiFi Hotstart PCR Kit	Roche
Maxima H RT buffer	Fisher Scientific
Maxima H RT enzyme	Fisher Scientific
Nuclease free water	Life Technologies
Nextera XT sample prep kit	Illumina
Nuclei EZ lysis buffer	Sigma-Aldrich
PBS buffer	Fisher Scientific
QX200 DG Oil for EvaGreen	Bio Rad
Qubit dsDNA HS Assay kit	Invitrogen
RNase inhibitor (RT master mix)	Lucigen
RNase inhibitor (Nuclei isolation buffer)	Clontech
Sarkosyl	Fisher Scientific
Sodium dodecyl sulfate (SDS)	Sigma-Aldrich
Trypan Blue	Invitrogen

Primer	**Sequence**
Template Switch Oligo (TSO)	AAGCAGTGGTATCAACGCAGAGTGAATrGrGrG
SMART PCR primer	AAGCAGTGGTATCAACGCAGAGT
SMART P5-PCR hybrid oligo	AATGATACGGCGACCACCGAGATCTACACGCCTGTC CGCGGAAGCAGTGGTATCAACGCAGAGT*A*C
Custom Read 1 primer	GCCTGTCCGCGGAAGCAGTGGTATCAACGCAGAGTAC

Consumable	Manufacturer
Cell strainers 35, 40 and 70 μm	Fisher Scientific
Dounce homogenizers	
C-chip Fuchs-Rosenthal hemocytometer	Labtech
scRNA seq microfluidic chip (100 μm etch depth)	Dolomite Bio
sNuc-Seq microfluidic chip (85 μm etch depth)	Dolomite Bio
BioAnalyzer High Sensitivity Chip DNA	Agilent
LoBind 1.5 tubes	Eppendorf
Illumina NextSeq 75 cycle v3 High Output	Illumina

Solutions

PBS-BSA

1X PBS

0.01% BSA

Nuclei Suspension Buffer (NSB)

1X PBS

0.01% BSA

0.1% RNAse inhibitor

Lysis buffer (1 mL)

400 μL H2O

300 μL 20 % Ficoll PM400

10 μL 20% Sarkosyl

40 μL 0.5 M EDTA

200 μL 1 M Tris pH 7.5

50 μL 1 M DTT → add this just prior to starting each experiment

TE-SDS (50 mL)

0.5 mL 1M Tris pH 8.0

0.1 mL 0.5 M EDTA

0.5 g SDS (or 25 mL of a 1% solution)

Nuclease free water

TE-TW (50 mL)

0.5 mL 1M Tris pH 8.0

0.1 mL 0.5 M EDTA

5 µL Tween-20

Nuclease free water

Reverse transcriptase mix

75 µl water

40 µl Maxima 5X RT buffer

40 µl 20 % Ficoll PM400

20 µl 10 mM dNTPs

5 µl RNase inhibitor

10 µl 50 µM TSO

10 µl Maxima H RTase

Exonuclease I mix

20 µl 10X Exo I buffer

170 µl water

10 µl Exo I

PCR mix

24.6 μl water

0.4 μl 100 μM SMART PCR primer

25 μl 2X KAPA HiFi HotStart Readymix

Tagmentation mix

15 μl Nextera PCR mix

8 μl water

1 μl 10 μM P5-SMART PCR hybrid primer

1 μl 10 μM Nextera N70X oligo

2.2 Methods

2.2.1 Human endometrial biopsies

Endometrial biopsies were obtained from women attending the Implantation Clinic, a dedicated research unit at University Hospitals Coventry and Warwickshire National Health Service Trust. Written informed consent was obtained from all participants in accordance with the guidelines in The Declaration of Helsinki 2000. Samples were obtained using a Wallach Endocell™ sampler under ultrasound guidance and immediately portioned for use in multiple applications: snap frozen in liquid nitrogen and stored at -80 ºC; placed in growth media for cell dissociation and culture; in RNA-later for RNA studies or in formalin for paraffin embedded tissue blocks.

2.2.2 Cell culture

2.2.2.1 Endometrial tissue processing

All biopsies were processed immediately and cultured as described previously (Barros et al., 2016). Samples were washed in DMEM/F12 medium, finely minced, and enzymatically digested with collagenase type IA and DNase type I for 1 hour at 37 °C. The dissociated cells were filtered through a 40-µm cell strainer. Stromal cells and blood cells, present as a single-cell suspension, passed through the cell strainer, whereas the undigested fragments, mostly comprising glandular clumps, were retained on the strainer. EnSC used in repeat biopsy experiments were cryopreserved in 10% DMSO in FBS and stored in liquid nitrogen.

2.2.2.2 Isolation of $W5C5^{+}$/$W5C5^{-}$ and $MRP4^{+}$/$MRP4^{-}$ stromal cells and primary cell culture

EnSC suspensions were layered over Ficoll-Paque PLUS and centrifuged to remove erythrocytes. The medium/Ficoll-Paque PLUS interface, containing EnSC, was carefully collected, washed with growth medium, and counted. A total of 3 x 10^{6} cells

were used for magnetic bead separation of $W5C5^{+}$/$W5C5^{-}$ and $MRP4^{+}$/$MRP4^{-}$ cells, as described previously (Barros *et al*, 2016). Remaining cells were plated into a T-25 flask for isolation of uNK cell. For W5C5 and MRP4 separation, EnSC were resuspended in separation buffer (100 µl/ 1 x 10^6 cells) containing phycoerythrin (PE) conjugated antihuman W5C5 (SUSD2) or MRP4 antibody for 20 minutes at 4 ºC. Cell suspensions were then incubated with anti-PE-magnetic-activated cell sorting microbeads (20 µl/ 1 x 10^7 cells) for 20 minutes at 4 ºC. Cell suspensions were applied onto MS columns in a magnetic field, followed by washing with 500 µl of separation buffer three times. The columns were removed from the magnetic field and magnetic labelled cells were flushed with 1 ml of separation buffer. To increase cell purity, $W5C5^{+}$ and $MRP4^{+}$ cells were separated again using a new MS column and washed as previously described. Positive and negative selected cells were cultured in growth medium: DMEM/F12 medium containing DCC-FBS, L-glutamine, antibiotic-antimycotic solution, insulin and estradiol until 90% confluence and collected for RNA extraction. Media was changed every 3 days.

2.2.2.3 *In vitro* Colony Forming Unit (CFU) assay

Freshly isolated $W5C5^{+}$ and $W5C5^{-}$ cells were seeded at a clonal density of 30 cells/cm^2 onto fibronectin-coated 6 well plates and cultured in growth medium supplemented with bFGF. The first half medium change was after the first 7 days. Subsequently, half media was changed every 3-4 days. Colonies were monitored microscopically to ensure that they were derived from single cells. Cultures were terminated at 15 days and collected for RNA extraction.

For CFU staining experiments, $W5C5^{+}$ and $MRP4^{+}$ cells were seeded at a clonal density of 50 cells/cm^2 and cultured for 10 days.

2.2.2.4 Isolation of Epithelial cells and organoid culture

To isolate epithelial cells (EpC), the 40 µm cell strainer was inverted over a 50 ml falcon and backwashed with additive-free, phenol-red free DMEM/F12 media. The glandular clumps were centrifuged and resuspended in trypsin for 10 min at 37 °C to disperse clustered cells. Cells were washed with media, centrifuged, resuspended and counted. EpC were resuspended in ice cold Matrigel (Corning, New York, USA) in order to obtain 1000 cells per 5 µl of matrigel. Matrigel-cell suspension was plated

in 96-well plates at 5 µl per well. After 1 hour, 100 µl of Expansion Medium supplemented with Y-27632 was added to each well. Media was changed every 3 days and after 10 days cells were recovered using Cell Recovery Solution. After complete release from the gel, cells were centrifuged, washed with cold PBS, pelleted and stored at -80 ºC until RNA extraction.

2.2.2.5 uNK cell isolation

Following overnight culture, the supernatant from EnSC cultures in T-25 was collected and cells were washed with PBS, which was pooled with the original supernatant. Collected medium was centrifuged to pellet suspended cells. $CD56^{+}$ cells were isolated following the same protocol used for $W5C5^{+}$ MACS separation with CD56 antibody and frozen at -80 ºC for later RNA extraction.

2.2.3 Microscopy

2.2.3.1 Immunohistochemistry

Endometrial biopsies were fixed overnight in 10% neutral buffered formalin at 4°C and wax embedded in Surgipath Formula 'R' paraffin using the Shandon Excelsior ES Tissue processor (ThermoFisher). Tissues were sliced into 3 µm sections on a microtome and adhered to coverslips by overnight incubation at 60°C. Deparaffinization, antigen retrieval, antibody staining, hematoxylin counter stain and DAB colour development were fully automated in a Leica BondMax autostainer (Leica BioSystems). Tissue sections were labelled for ANLN. Stained slides were dehydrated, cleared and cover-slipped in a Tissue-Tek Prisma Automated Slide Stainer, model 6134 (Sakura Flinetek Inc. CA, USA) using DPX coverslip mountant. A Mirax Midi slide scanner with a 20x objective lens was used to obtain bright-field images of each slide. Per sample, three randomly selected areas of interest underlying the luminal epithelium were identified and captured using Pannoramic Viewer v1.15.3 (3DHISTECH Ltd, Budapest, Hungary). Each field was divided manually into 3 compartments: stroma, glandular epithelium, and luminal epithelium. ImageJ image analysis software (Rasband, W. S., ImageJ, National Institutes of Health) was applied

for ANLN$^+$ cells quantification. Staining intensity of positive area was manually determined by background threshold (Ruifrok and Johnston, 2003). Target cell density in each sample was calculated by the percentage of ANLN$^+$ cells within the selected compartment (i.e. ANLN$^+$ cells/total cells in selected compartment x 100%) (Drury *et al*, 2011).

2.2.3.2 Immunofluorescence

CFUs and EnSC monolayers in 6-well plates were fixed in 4% paraformaldehyde for 10 min, permeabilised with 0.5% Triton X-100 for 10 min and blocked with 1% BSA/PBS for 30 min. Cells were probed with mouse anti-ANLN monoclonal primary antibody overnight at 4°C. Labelled cells were stained with Alexa-Fluor™ 594 anti-mouse secondary antibody for 1 hr at RT and counterstained with VECTASHIELD antifade mounting medium with DAPI.

Tissue sections were double-labelled with ANLN and either CD34, CD56, CD163 or cytokeratin overnight at 4°C. Labelled cells were labelled with Alexa Fluor™ 594 anti-mouse secondary antibody and Alexa Fluor™ 488 anti-rabbit secondary antibody. Tissue autofluorescence was eliminated using the Autofluorescence quenching kit according to manufacturer's instructions. Tissue sections were stained with ProLong Gold antifade mounting medium with DAPI. Imaging was performed on EVOS FL Auto fluorescence microscope (Life Technologies, Paisley, UK). For cell counting, three randomly selected fields were assessed using ImageJ image analysis software.

2.2.3.3 CFU Staining

Following 10 days of culture, colonies were washed with PBS and fixed with 4 % formaldehyde for 10 minutes at room temperature. Cells were washed again with PBS and distilled water. Staining was performed with filtered haematoxylin for 4 minutes, followed by washes with distilled water. PBS was added to colonies to intensify the staining for 4 minutes at room temperature, aspirated and dishes allowed to dry. Clusters of ≥ 50 cells were counted and cloning efficiency (CE) was determined from the formula:

$$\mathrm{CE}\ (\%) = \frac{\text{number of colonies}}{\text{number of cells seeded}} \times 100$$

2.2.4 RNA extraction

To minimize risks of RNA degradation, RNase-free plastic-ware and nuclease free water were used throughout in combination with RNase ZAP decontamination. Total RNA was extracted from cells and tissues using STAT-60 reagent, which maintains RNA integrity while disrupting other cellular components. For RNA experiments, cells were cultured in 6-well plates. At the end of the experiment, cells were washed with PBS and 400 μl of Stat-60 was added to each well for 5 minutes at room temperature. Cells were scraped thoroughly and transferred to RNase-free 1.5ml eppendorfs placed on ice. 80 μl of cold chloroform (0.2 volume of Stat-60) was added and mixed well by vortexing. Samples were snap frozen and placed at -80°C overnight. After defrosting on ice, tubes were centrifuged at 12,000 x g at 4°C for 30 minutes in order to separate the sample into three phases: upper colourless aqueous phase, white interphase and lower red phenol chloroform phase. The aqueous phase, containing the RNA, was carefully transferred into half of the original Stat-60 volume of isopropanol and incubated at room temperature for 10 minutes to precipitate the RNA. RNA was pelleted by centrifugation at 12,000 x g at 4 °C for 10 minutes, washed twice with 1 ml 75% ice cold ethanol, air-dried and dissolved in 20 μl of nuclease free water. RNA concentration and quality were assessed by Nanodrop ND 1000 and cDNA synthesis was carried out. In RNA extraction experiments from tissue samples, it was followed the same protocol with an additional homogenization step in Stat-60 with a mechanical probe.

2.2.5 Gene expression analysis

2.2.5.1 Reverse transcriptase reaction: cDNA synthesis

In order to synthesize cDNA from previously extracted RNA, the QuantiTech Reverse Transcription Kit was used according to the manufacturer instructions. 2 μl of gDNA wipeout buffer (7x) was added to 1μg of template RNA and made up to a total volume of 14 μl with RNase-free water, to remove any traces of genomic DNA. Samples were incubated at 42 °C for 2 minutes and placed immediately on ice. A master mix containing 1 μl of Quantiscript Reverse Transcriptase, 4 μl 5x Quantiscript RT Buffer and 1 μl RT Primer Mix was added to each sample. Minus RT controls were also prepared in which Quantiscript Reverse Transcriptase was replaced by 1 μl nuclease

free water. Reactions were incubated at 42 °C for 30 minutes followed by an incubation at 95 ˚C for 3 minutes. cDNA samples were diluted to 20 ng/ul and stored at -20 °C

2.2.5.1 Primer design and optimization

Primers were designed using Universal Probe Library Assay Design Center from Roche and Primer3. Primers were chosen according to the following requirements:

a) Primers are required to be exon spanning (to distinguish between cDNA and gDNA)
b) Melting temperature (Tm) between 58.0 °C and 59.9 °C and shouldn't differ between the forward and reverse primer by greater than 1˚C
c) Total amplicon length to be between 75 and 110 base pairs
d) At the 3' end of the primer, of the last five bases, 2 bases should be either G or C
e) Primer length should be between 18-24 bases
f) No more than four of the same base consecutively

Per pair of primers, standard curve PCRs were run in order to determine the primer efficiency. The amplified product was mixed with loading dye and run on a 1 % agarose gel for approximately 50 minutes at 100V. The purified product was excised from the gel using Qiagen Gel Extraction Kit and cDNA concentration measured using Nanodrop. The cDNA was serially diluted between 100 pg/µl to 10 ag/µl in 10 fold dilution providing 8 dilutions that were amplified using the appropriate primers and PrecisionPlus 2x Mastermix. The log of the concentration of cDNA was plotted against average Ct values. Primer efficiency was determined from the formula:

$$\text{Primer efficiency} = 10^{\frac{-1}{\text{Gradient of the line}}}$$

Gene	Primers	Primer efficiency
CBLN2	(F) AAGAAGAGAAGCGACCGGTG (R) AGAAGAAAGGCGCCTGTGAA	1.92
COL10A1	(F) GCCAGAAGGCATTGGAAA (R) CCCAGGGAGACCTTTTGTTC	1.97
LRRC17	(F) ACACCGCAGCAAAGAGAGAAGA (R) GGCTGAACTTGGGGAATGGA	1.96
NPWBR1	(F) GCTGGTCATCGCTATCTCCT (R) CGTAGAGGAAGGGGTTGAGG	1.98
ITGA8	(F) GGACCAAGTACCATCAGTGACA (R) GCAGAGGTCCCAGAGTTTGA	1.96
PCDH9	(F) TTAAGTTGGTGCCCCTCTCA (R) CCAGTGTCAACATCCACTGC	1.98
KRT40	(F) GCCCGGATTATCAGCGTTAC (R) GGCCAGTTTGCAGTTGTCAA	1.98
DPT	(F) GGGAACTTGTGGGGATGAGA (R) AGGTGCCAGTGACTCAAACT	2
CLDN11	(F) CCACAGAGGTGCTGTAGATGC (R) GGCAGAGGAATGGGCTTC	2
CST1	(F) ACTTGGACACCTGTGCCTTC (R) GGATTTCACCAGGGACCTTC	1.96
MRP4	(F) CTGGCGAATTGTTAGCTGTG (R) AGCACGGCACTTAACAGTGA	2
ANLN	(F) GCATCGAAGATGGTGTGTTC (R) CCTATGGGATTCTTGCGTTT	1.97
ACTA2	(F) CTGTTCCAGCCATCCTTCAT (R) TCATGATGCTGTTGTAGGTGGT	1.81
S100A4	(F) AGGGTGACAAGTTCAAGCTCAA (R) GTCCTTTTCCCCAAGAAGCTG	1.95
ABCG2	(F) GATAAATGGAGCACCGCGAC (R) CGTCAGAGTGCCCATCACAA	1.98

2.2.5.2 Real-Time polymerase chain reaction

Real Time PCR was performed using the PrecisionPlus qPCR Master Mix according to the manufacturer instructions. Primers were used at a concentration of 300 nM and at a 50:50 ratio between forward and reverse. Reactions were carried out on a 96 well plate in a total volume of 20 µl. 1 µl of cDNA template was added to the well and set up in triplicate for technical replicate. Non-template controls in which 1 µl nuclease free water replaced the cDNA were also used. The reaction plate was sealed, centrifuged briefly and placed in the Real time-PCR machine. Thermocycling conditions were as follow: 1) 95 °C for 2 mins; 2) 40 cycles of 95 °C for 10 seconds and 60 °C for 60 seconds. Analysis was carried out according to Pfaffl, 2004. The cycle threshold (Ct) values of the samples were normalised to the reference gene L19 (Lucas *et al*, 2016).

2.2.6 RNA sequencing

Total RNA was extracted from whole tissue, uNK, organoids, $W5C5^+$ CFUs, $W5C5^-$ CFUs, $W5C5^+$ standard and $W5C5^-$ standard using the AllPrep DNA/RNA Micro Kit following the manufacturer's protocol (QIAGEN). RNA concentration was assessed using the Qubit RNA BR assay and RNA quality was analysed on an Agilent 2100 Bioanalyser (Agilent Technologies) at the Genomics facility and assessed with either the Eukaryotic Total RNA Nano or Pico chip, as appropriate based on Qubit results, according to the manufacturer's instructions. Libraries were prepared using the TruSeq RNA Library preparation kit V2 and sequenced on HiSeq 4000 with 75 bp PE reads at the Wellcome Trust Centre for Human Genetics (Oxford, UK). Transcriptomic maps of single-end reads were generated using Bowtie-2.2.3, Samtools-0.1.19, and Tophat-2.0.12 against the University of California Santa Cruz (UCSC) hg19 reference transcriptome from the Illumina Genomes resource. Transcript counts were assessed by HTSeq-0.6.1 using the reverse strand setting and intersection non-empty mode and counts were assigned to gene IDs. Transcripts per million were calculated using the method described by Wagner et al. [67]. Count data from the TopHat-HTSeq pipeline were analysed using DESeq2. To characterize the relative proportions of epithelial, stromal and uNK cells, gene expression profiling was performed with the online analytical platform CIBERSORT (https://cibersort.stanford.edu/).

2.2.7 Single-molecule *in situ* hybridization.

Formalin-fixed paraffin-embedded (FFPE) samples were cut to 5 µm sections. RNA in situ hybridization was carried with RNAscope® 2.5 HD assay -RED (ACD, California, USA) with probe for ABCC (422321) according to manufacturer's guidelines. Following hybridization and amplification, slides were counterstained with 50 % haematoxylin. Images were obtained using an EVOS AUTO microscope (ThermoFisher Scientific) with a 40x objective lens.

2.2.8 Single cell RNA-Seq & single nuclei RNA-Seq

2.2.8.1 Sample preparation

Endometrial biopsies were processed as described in section 2.2.2.1 with an additional Ficoll-Paque PLUS density gradient step. Cells were then resuspended and diluted to 300 cells/µl in PBS-BSA.

2.2.8.2 Nuclei isolation

Nuclei were isolated from frozen tissues as described by Habib and colleagues (Habib et al., 2017). Snap frozen samples were homogenized with a dounce homogenizer in 1.8 ml of ice cold Nuclei EZ lysis buffer. Tissue was dounced 25 times with pestle A, followed by 25 times with pestle B. After transferring the fragmented tissue in a 15 ml conical tube, 2 ml of ice cold Nuclei EZ lysis buffer were added to the sample and incubated on ice for 5 minutes. Nuclei were collected by centrifugation at 500 x *g* for 5 minutes at 4 °C and then resuspended in ice cold Nuclei EZ lysis buffer for another 5 minutes. Nuclei were collected once more by centrifugation, resuspended in 2ml of NSB and filtered through a 35 µm cell strainer. 20 µl of the single nuclei suspension were stained with trypan blue, loaded on an Fuchs-Rosenthal (FR) hemocytometer and counted under a microscope. A final concentration of 453 nuclei/µl was used for snRNA-seq experiments.

2.2.8.3 Barcoded beads preparation

Beads were prepared according to the manufacturer's instructions. Briefly, dry resin was washed twice with 30 mL of 100% EtOH and twice with 30 mL of TE/TW. The bead pellet was resuspended in 10 mL TE/TW and passed through a 70 µm filter into a 50 ml falcon tube for long-term storage at 4 °C. For snRNA-seq, beads were filtered a second time through a 40 µm filter. For scRNA-seq and snRNA-seq, an aliquot of beads was removed from the stock tube and resuspended in appropriate volume of lysis buffer at a concentration of 280 and 420 beads/ul, respectively.

2.2.8.4 Droplet generation and cDNA library preparation

Single cell transcriptome studies were performed using a droplet based microfluidic system (scRNA, Dolomite Bio) according to the manufacturer's protocol, which integrates the Drop-seq protocol described by Macosko and colleagues (Macosko *et al*, 2015). Oil, cells and barcoded beads in suspension were loaded into each corresponding pump and connected to a microfluidic chip. Cell and bead solutions were run at a flow rate of 30 µl/ min, along with carrier oil at a flow rate of 200 µl/ min for 18 minutes. Droplets were collected into a 50 ml Falcon tube, quality checked using a C-Chip Fuchs-Rosenthal Haemocytometer and bead doublets counted. Excess oil was removed from the bottom of the collection tube and droplets were washed with 30 ml of 6X SSC. To break droplets, 1ml of Perfluoro-1-octanol was added and the tube was shaken vigorously. After centrifugation for 1 minute at 1000 x g and 4 °C, supernatant was removed, and beads were washed with additional 30 ml of 6X SSC. The aqueous layer with beads in suspension was transferred to a new tube and centrifuged again. The supernatant was removed, and the bead pellet transferred to a LoBind 1.5 mL microcentrifuge tubes. The pellet was then washed twice with 1 mL 6X SSC, and once with 300 µl of 5x Maxima H RT buffer. Reverse transcription was performed for 30 minutes at room temperature, followed by 90 minutes at 42 ºC. Beads were then washed once with 1ml TE-SDS, twice with 1 ml TE/TW and once with 1 ml 10 mM Tris pH 7.5. The bead pellet was then resuspended in Exonuclease I mix and incubated at 37 ºC for 45 minutes. The beads were then washed once with 1 mL TE-SDS, twice with 1 mL TE-TW, once with 1 mL water, and resuspended in water. Bead concentration was determined using a Fuchs-Rosenthal cell counter.

PCR was performed on 8000 beads per reaction, with two reactions per sample, to give ~800 single-cell transcriptomes attached to microparticles (STAMPS). Aliquots were resuspended in PCR mix and thermocycled as follow: 95 ºC 3 min; four cycles of: 98 ºC for 20 sec, 65 ºC for 45 sec, 72 ºCfor 3 min; 9 cycles of: 98 ºC for 20 sec, 67 ºC for 20 sec, 72 ºC for 3 min; then a final extension step of 5 min.

Ampure XP clean-up was performed according to standard Illumina RNAseq protocols with a 0.6X beads to sample ratio. cDNA concentration was determined by Qubit High Sensitivity DNA assay, while quality and size were assessed using an Agilent Bioanalyzer High Sensitivity DNA chip.

Tagmentation was performed using Illumina Nextera XT DNA Sample Kit and Indexing Kit. 600 pg cDNA was diluted in water to the final volume of 5 μl. 10 μl Nextera TD buffer and 5 μl Amplicon Tagment were added to each sample and incubated at 55 ºC for 5 minutes. After addition of 5 μl neutralization buffer, samples were incubated at room temperature for 5 min and reagents of tagmentation mix were added to the tube. The samples were then amplified as follows: 95 ºC for 30 sec; 12 cycles of 95 ºC for 10 sec, 55 ºC for 30 sec, 72 ºC for 30 sec; then a final extension step of 72 ºC for 5 min. Tagmented libraries were cleaned up using AMPure XP beads with a 0.6× beads ratio followed by a repeat clean-up using 1× beads. Eluted libraries were analysed using Qubit High Sensitivity DNA assay and Agilent Bioanalyzer High Sensitivity DNA chip. Library dilution and denaturation was performed as per standard Illumina protocols and sequenced using NextSeq High Output 75 cycle V2 kit to sequence paired-end reads as follows: 20 bp (Read 1), 50 bp (Read 2), and 8 bp for Index 1 with Custom Read1 primer.

For single nuclei transcriptome studies, the same protocol was used as previously described, with small modifications. The sample loop from Dolomite bio used for snRNA-seq is 6 meters long instead of the 10 meters scRNA-seq system. In order to accommodate the lower amount of RNA in nuclei compared to whole cells, the chips used for snRNA-seq (85 μm Etch Depth) are smaller than the chips used in scRNA-seq (100 μm Etch Depth). Running flow rates were: 20 μl/min for beads and nuclei lines and 120 μl/min for carrier oil. PCR was performed on 5000 beads per reaction, with four or eight reactions per sample. Any additional optimizations are described separately in Chapter 5.

2.2.8.5 Computational data analysis

Computational data analysis was performed as described in Lucas *et al*, 2020. Initial data processing was done using Drop-seq_tools-1.0.1 following the protocol described by Nemesh (seqAlignmentCookbook_v1.2Jan2016.pdf, http://mccarrolllab.com/dropseq). Reads with low-quality bases in either cell or molecular barcode were filtered and trimmed for contaminating primer or poly-A sequence. Sequencing errors in barcodes were inferred and corrected, as implemented by Drop-seq_tools-1.0.1. Reads were aligned to the reference genome human hg19 (Human) using STAR-2.5.3a (Dobin et al., 2013). Uniquely mapped reads, with ≤ 1 insertion or deletion, were used in quantification. Cell numbers were selected computationally from the inflection point in a cumulative distribution of reads plotted against the cell barcodes ordered by descending number of reads. Cell barcodes beyond the inflection point are believed to represent 'ambient RNA' (e.g. contaminating RNA from damaged cells), not cellular transcriptomes, and therefore excluded from further analysis.

The expression count (or number of transcripts) for a given gene in a given cell was determined by counting unique UMIs, and compiled into a digital gene expression matrix. Analysis of DGE data was performed with Seurat (Satija *et al*, 2015). To select high quality data for analysis, cells were included when at least 200 genes were detected, while genes were included if they were detected in at least 3 cells. Cells which had more than 4500 genes were excluded from the analysis as were cells with more than 5% mitochondrial gene transcripts to minimize doublets and low-quality (broken or damaged) cells, respectively. After scaling and normalization of the raw counts in the digital gene expression matrix, cell-cycle regression was applied.

For cell aggregation, a set of highly variable genes was first identified, with an average expression mean between 0.0125 and 3 and a Log Variant to Mean Ratio of at least 0.5, which were used to perform principal component (PC) analysis. Judged by their statistical significance and the robustness of the results, the first 10 PCs were subsequently used as inputs for clustering via shared nearest neighbour (SNN) and subsequent *t*-distributed stochastic neighbour embedding (*t*-SNE) representation. The Seurat function 'FindAllMarkers' employing the Wilcox test was used to identify marker genes for each cell state cluster in the *t*-SNE representation.

2.2.9 Statistical Analysis

Data was analysed using the statistical package GraphPad Prism (GraphPad Software, CA, USA). Data were checked for normal distribution using Kolmogorov-Smirnov test. Where appropriate, a Mann-Whitney *U* test, t-test, one-way analysis of variance (ANOVA) or Kruskal-Wallis test was applied. ANOVA and Kruskal-Willis test were followed up by multiple comparisons, in which the mean or mean rank of each group was compared to the mean or mean rank of every other column. Spearman's' rank or Pearson test was used for correlative analysis. Values of $P<0.05$ were considered statistically significant.

In the Tukey box plots, the line within the box marks the median, the boundary of the box closest to zero indicates the 25 th percentile, and the boundary of the box farthest from zero indicates the 75 th percentile. Individual dots represent outliers.

For RNA-seq data analysis, statistical significance was assessed on a large number of variables (i.e. genes). Benjamin-Hochberg post-hoc test was applied to control the false discovery rate. Adjusted *P* values < 0.05 were considered statistically significant.

Chapter 3

Transcriptomic Deconvolution of the Human Endometrium

3.1 Introduction

In recent decades, transcriptome profiling has become indispensable to define and investigate pathological mechanisms associated with human disease. Specially, with the advent of next generation sequencing, a technology that enables sequencing of millions of small fragments of DNA in parallel, RNA-Seq has emerged as a powerful methodology to study the transcriptome (Herzyk *et al*, 2014). Bulk RNA-Seq is the most revolutionary and widely used tool for transcriptomic studies but when applied to tissues it assumes and represents all the cells as a homogeneous material and loses sight of specific cell subset variance (Li and Xie, 2013). Since most genes are expressed to varying degrees across multiple cell subsets in a tissue, when the genome-wide transcriptional profile of heterogeneous samples is measured under different physiological states, any observed differences are strongly confounded by differences in cell type compositions between samples (Shen-Orr and Gaujoux, 2013; Zhong *et al*, 2013). Therefore, it is critical to be able to measure and interpret phenotypic changes at the cellular context between specific conditions in order to understand the role of each cell subset.

As for most biological samples, the endometrium has a heterogeneous and varying cellular composition comprising multiple cell types and subsets. In general, the total measured abundance of a gene in a biological sample is dependent on characteristic condition (e.g. disease type), individual variation and cell subsets variation (Shen-Orr and Gaujoux, 2013). In addition, when dealing with endometrial samples, it is important to consider one more component as the basis of gene expression variation. Due to its cyclic and dynamic regeneration, the day of the cycle on which the sample is obtained has an impact on gene expression and therefore the temporal variation should also be taken into account in the analysis. In fact, a previous study using laser microdissection microscopy to separate the two dominant endometrial cell types, epithelial and stromal cells, during the WOI has shown that each compartment has a distinct transcriptomic signature, which varies depending on the day of the cycle (Evans *et al*, 2012).

Until recently, when facing the problem of sample heterogeneity, researchers had to choose between one of two approaches. One method involves cell isolation and focusing on a single cell type, which entails a loss of a systems perspective. On the other hand, whole tissue transcriptome analysis may lead to misinterpretation of the results (Shen-Orr and Gaujoux, 2013). To overcome this hurdle, it is possible, through

the development of alternative in silico approaches, to deconvolve the transcriptome of heterogeneous samples and estimate the proportion and/or gene expression profile of different cell subsets.

One of the available computational methods is the cell-type identification by estimating relative subsets of RNA transcript (CIBERSORT) that accurately resolves relative fractions of diverse cell subsets in gene expression profiles from complex tissues (Newman *et al*, 2015). CIBERSORT requires the gene expression profiles of isolated cell populations as an input to create a custom gene expression signature matrix, which is then applied to deconvolve the transcriptome profile of whole tissue (Figure 3.1). CIBERSORT is based on a machine learning approach with a novel application of linear support vector regression that unlike previous methods, performs a feature selection, in which genes from the signature matrix are adaptively selected to deconvolve a given mixture. Consequently, this method is highly effective for mixtures with unknown content and noise and for discriminating closely related cell types (Newman *et al*, 2015).

CIBERSORT has been widely used to infer the proportion of immune cell types in cancer tissues (Gentles *et al*, 2015; Chen *et al*, 2019; Deng *et al*, 2020; Zhang *et al*, 2020). Tumor infiltrating leukocytes are an essential component of the tumor microenvironment and have been found to correlate with prognosis and response to therapy (Chen *et al*, 2019). Therefore, the analysis of the leukocyte population is an important tool to identify candidates for immunotherapy. Nevertheless, CIBERSORT algorithm has the potential to be applied to other signature matrices of tissues with complex compositions (Newman *et al*, 2015).

The most significant limitation of CIBERSORT, as well as all signature gene–based methods, is the fidelity of reference profiles, which could deviate in cells undergoing phenotypic plasticity. Additionally, CIBERSORT systematically over- or underestimates some cell types, even though it shows a considerably lower estimation bias than other (Newman *et al*, 2015).

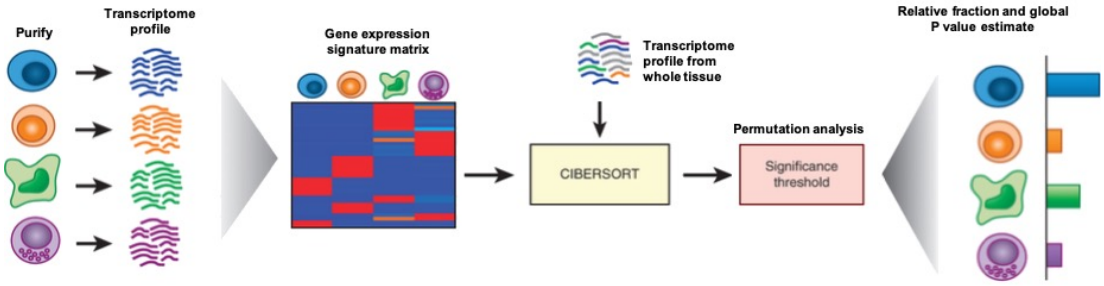

Figure 3.1. Schematic of the CIBERSORT. This computational approach requires as an input the gene expression matrix of isolated cell populations to resolve relative fractions of diverse cell subsets from complex tissues (Newman *et al*, 2015).

The first aim of this work was to deconvolve the whole endometrial tissue transcriptomics using CIBERSORT by assigning a specific gene expression profile to stromal, epithelial and uNK cells. Furthermore, as the stroma compartment is represented by an intricate cell hierarchy, an additional aim was to identify a specific transcriptome signature of cell subsets present at low proportion and apply them in the deconvolution. Hence, RNA-seq analysis was performed on four isolated stromal cell populations [W5C5$^+$ perivascular stromal cells (PVC), endometrial stromal cells (EnSC), W5C5$^+$ clonal cells (eMSC), and clonal transit amplifying cells (TA)], glandular epithelial cells, uNK cells, and matched whole tissue.

As described in Chapter 1, one of the challenges to be overcome is the lack of consensus on a single surface molecule to identify endometrial stem/progenitor cells. Thus, the second aim was to use the previous data to identify specific cell surface markers and key transcription factors of adult stem/progenitor cells that can then be used to determine stem cell deficiency in clinical samples.

3.2 Results

3.2.1 Endometrial cell types isolation

The first goal for this project was to generate a reference matrix consisting of the transcriptome profiles of epithelial, uNK and stromal subsets for the deconvolution of whole tissue transcriptome data. In parallel, differential gene expression (DGE) analysis was performed between the stromal subtypes in order to characterize de eMSC population (Figure 3.2).

Three independent midluteal biopsies were used to isolate, culture and sequence different endometrial cell types and stromal subsets. Following enzymatic digestion, EpC were separated from the stromal cell fraction as described (Barros *et al*, 2016) PVC and EnSC were then subjected to magnetic activated cell sorting (MACS) using the W5C5 antibody that recognises SUSD2, a cell surface protein selectively expressed on PVC (Masuda *et al*, 2012). PVC and EnSC were maintained in standard cultures (Figure 3.3 A, C) as well as subjected to colony forming unit (CFU) assays. Briefly, freshly isolated PVC and EnSC were seeded at low density (30 cells/cm^2) and cultured in the presence of bFGF. Total RNA was then extracted from the resulted clones, designated eMSC and TA, respectively (Figure 3.3 B, D). The standard PVC and EnSC cultures were propagated until 90% confluence and then subjected to total RNA extractions.

EpC isolated from midluteal biopsies undergo rapid cellular senescence when cultured as a monolayer (Barros, 2017), precluding further expansion in culture. To resolve this problem, primary EpC were subjected to gland organoid formation using a recently described protocol (Turco *et al*, 2017). Briefly, primary EpC were first seeded in Matrigel and cultured in a chemically defined medium. After 10 days in culture, the gland-like structures were harvested and total RNA extracted (Figure 3.3E).

uNK cells were also isolated although not cultured. After overnight incubation, the supernatant of the stromal cell fraction was subjected to MACS to isolate uNK cells using a PE-conjugated anti-human CD56 monoclonal antibody. As shown in Figure 3.3F, this method yields highly purified uNK cells as described previously (Brighton *et al*, 2017). Cells were isolated from 3 biopsies and subjected to RNA extraction.

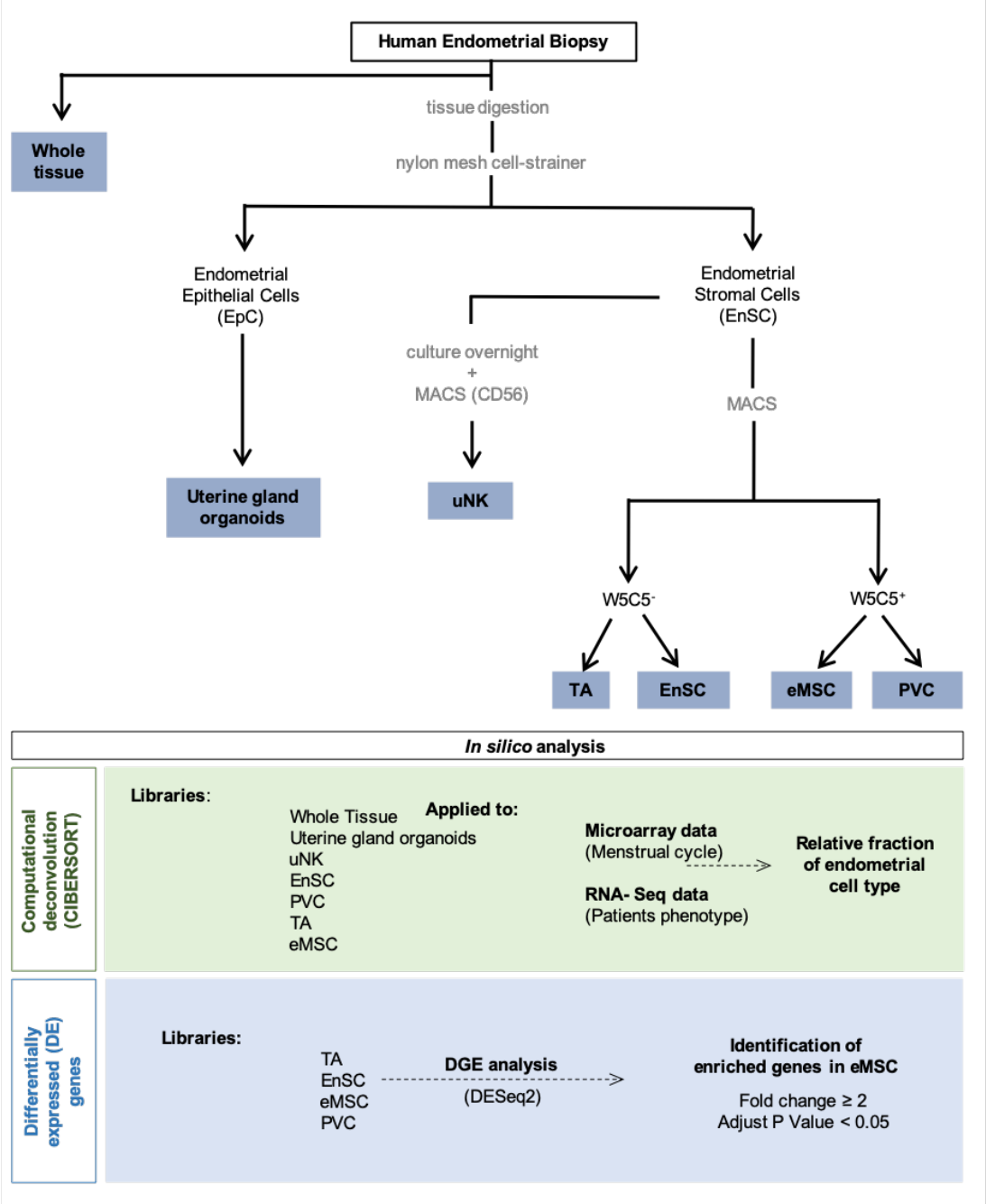

Figure 3.2. Schematic workflow of different endometrial cell types isolation and further *in silico* analysis. From the top: the total RNA from whole tissue, uterine gland organoids, uterine natural killer (uNK) cells, perivascular cells (PVC), endometrial mesenchymal stem cells (eMSC), endometrial stromal cells (EnSC) and transit-amplifying cells (TA) was extracted and sent for RNA-seq. Libraries were used for two different *in silico* analysis: Computational deconvolution of whole transcriptome profiles 1) throughout the menstrual cycle and 2) associated with different patients phenotype. Differential gene expression (DGE) analysis using DESeq2 to identify genes enriched in eMSC using as selection criteria fold change ≥ 2 and adjust P value < 0.05.

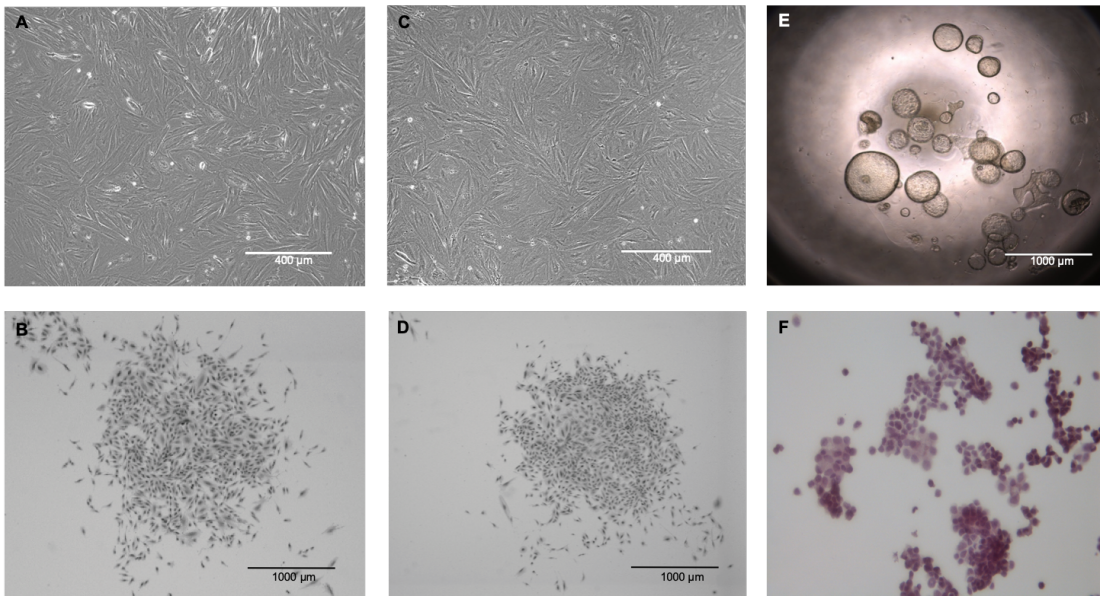

Figure 3.3. Representative pictures of cultured endometrial cell types. A) Perivascular cells (PVC) cultured until 90% confluence B) Close up of a colony from endometrial mesencgymal stem cells (eMSC) C) Endometrial stromal cells (EnSC) cultured until 90% confluence D) Close up of a colony from transit-amplifying cells (TA) E) Gland organoids cultured for 10 days in matrigel and expansion media F) Hematoxylin-eosin staining of uNK cells sorted using a PE-conjugated anti-human CD56 monoclonal antibody.

Total RNA from 6 different cell types/subsets and the corresponding whole tissue sample was subjected to RNA-seq analysis. As aforementioned, this analysis was performed on 3 separate mid-luteal biopsies. Principal component analysis (PCA) was then performed on the 21 libraries. PCA is a statistical procedure used for exploratory analysis of multidimensional data. It is based on DESeq2 regularized logarithm transformation (rlog) that stabilizes the variance across the data and avoids that the analysis becomes dominated by highly variable genes (Love *et al*, 2015). Whole tissue, uNK, gland organoids and stromal subsets (PVC, EnSC, eMSC, and TA) showed distinct spatial distribution in the two-dimensional space constructed by the first and second principal components (PC1 and PC2, respectively). Within each cell type, the three biological replicates clustered together, demonstrating that different cell types exhibit similar transcription profiles across biopsies (Figure 3.4 A).

When restricting the PCA to the stromal subsets, standard cultures (EnSC and PVC) were distinctly separated from clonogenic cells (eMSC and TA) in PC1 (Figure 3.4 B). Notably, all six libraries from clonal cells clustered tightly together. On the other hand, PVC and EnSC clustered together depending on the sample of origin. This observation suggests marked inter-patient variability in the transcriptome of committed endometrial stromal cells, which appears less pronounced in their progenitor cells.

The kinship between various cell types and subsets was further investigated using unsupervised hierarchical clustering based on Euclidean distance. As shown in Figure 3.4 C, the first bifurcation in the dendogram separated the stromal subsets from whole tissue, uNK cells and gland organoids. It was surprising that the whole tissue transcriptome was closer to that of uNK than stromal subsets, which probably reflects transcriptional drift induced upon culturing of cells in monolayers. The hierarchical cluster analysis further revealed that eMSC and TA also clustered by sample of origin.

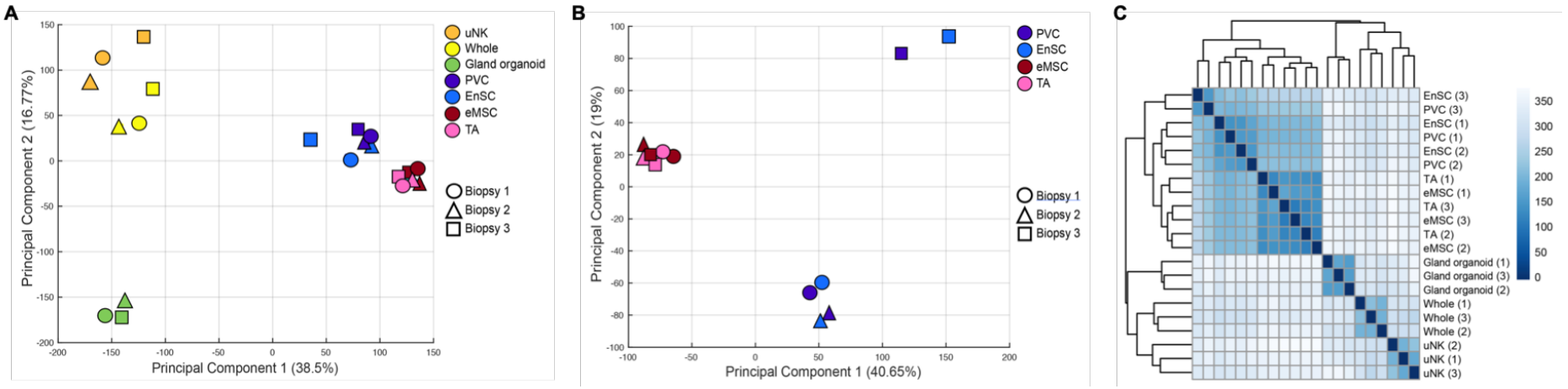

Figure 3.4. Principal component analysis and hierarchical clustering of endometrial cell populations RNA-seq. Different cell types from three independent endometrial biopsies were isolated and cultured. Each cell type or subtype was subjected to RNA-Seq analysis. (A) Principal-component analysis of RNA-seq data of six cell types plus whole tissue. Principal-component scores of RNA-seq are plotted on components 1 and 2. Patient samples and cell subtypes are distinguished by different symbols and colours, respectively. (B) Principal-component analysis of RNA-seq data of stromal subtypes. Principal-component scores of RNA-seq are plotted on components 1 and 2. (C) Heatmap representing the Euclidean distance on Log2 transformed counts from stromal (EnSCs, PVCs, eMSCs and TAs), epithelial and uNK cell populations and whole tissue libraries.

3.2.2 Computational deconvolution of whole endometrial gene expression profiles

The transcriptomic profiles of uNK cells, endometrial gland organoids, and stromal subsets were used as "signature matrices" for computational deconvolution of bulk endometrial gene expression profiles. Although a number of computational approaches have been described (Mohammadi *et al*, 2015), CIBERSORT is considered superior as it implements a machine learning approach, called support vector regression, that improves deconvolution performance through a combination of feature selection and mathematical optimization techniques (Newman *et al*, 2015).

CIBERSORT analysis was first applied to a publicly available microarray data set consisting of endometrial biopsies obtained throughout the cycle (Gene Expression Omnibus (GEO) repository, accession number: GSE4888). Analysis was based on histologically dated endometrial biopsies obtained during the proliferative (PE; n=4), early-secretory (ESE; n=3); mid-secretory (MSE; n=8) and late-secretory (LSE; n=6) phase of the cycle (Talbi *et al*, 2006). Computational deconvolution of this data showed an increase in the relative proportion of uNK cells throughout the menstrual cycle peaking - as expected - in the late secretory phase (Figure 3.5). CIBERSORT was not able to deconvolute different stromal subsets. However, it clearly showed that the relative abundance stromal versus epithelial cells changes dynamically throughout the cycle. As shown in Figure 3.5, the abundance of stromal cells was significantly higher than the abundance of epithelial cells throughout the cycle except during the midluteal WOI.

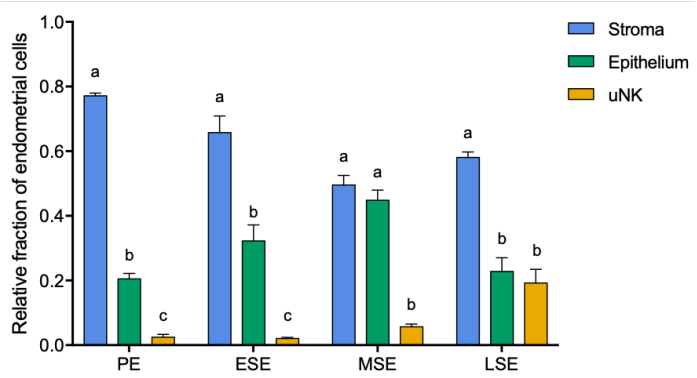

Figure 3.5. Deconvolution of microarray data of 21 endometrial biopsies collected across the menstrual cycle. PE-proliferative (n=4); ESE-early secretory (n=3); MSE-mid-secretory (n=8) and LSE-late secretory endometrium (n=6). Two-way ANOVA followed by Tukey's test was applied for multiple comparisons within each phase of the cycle, Different letters above the error bars indicate that those groups are significantly different from each other at $p < 0.05$. Data represent mean ± SEM. Data retrieved from Gene Expression Omnibus (GEO) repository, accession number: GSE4888 (Talbi *et al*, 2006)

Although CIBERSORT deconvolution yielded no information on stromal subsets, we reasoned that that the change in stromal/epithelial cell ratio during the WOI may be important for successful embryo implantation and pregnancy. To test this hypothesis, CIBERSORT deconvolution was applied to RNA-seq data of 36 endometrial biopsies obtained between LH+6 and LH+9. The data was generated by Dr. Emma Lucas in the Brosens' lab to determine if a pre-pregnancy endometrial gene expression signature could be identified as predictive of subsequent pregnancy outcome. The samples were obtained from 3 different patient groups:

- Group A (n=12): infertile patients who subsequently had a successful IVF cycle resulting in live birth.
- Group B (n=12): Recurrent miscarriage (RM) patients who subsequently had a successful pregnancy resulting in live birth.
- Group C (n=12): RM patients who subsequently suffered another pregnancy loss.

Demographic details of the 3 clinical groups are summarized in Table 3.1. The groups were matched for age, day of the biopsy relative to the preovulatory LH surge and uNK cell count.

Table 3.1. Demographic details of patients from each clinical group. Data is presented as median (range, N). Kruskal-Wallis test, Different superscript letters indicate significant difference between groups after Dunn's multiple comparison test.

	Group A	Group B	Group C	*P* value
Age	33 (25-39, 12)	33.5 (27-39,12)	32.5 (25-36, 12)	0.74
BMI	25 (21-31, 10)	23.5 (21-32, 8)	24.5 (21-34, 10)	0.9674
Cycle Day	8 (7-9, 12)	8 (6-9, 11)	7 (6-9, 12)	0.1646
Previous Losses	0^{a} (0-1, 12)	4.5^{b} (3-7, 12)	4.5^{b} (3-9, 12)	<0.0001
uNK %	3.05 (0.48-8.84, 12)	3.91 (0.88-10.73, 11)	6.22 (0.71-13.6, 12)	0.3979

PCA showed that the samples did not cluster by patient group (Figure 3.6). PC1 was accounted for by the expression of receptivity-associated genes, including those used in the commercially available endometrial receptivity array (ERA) (Díaz-Gimeno *et al*, 2011). ERA encompasses a transcriptomic signature for human endometrial receptivity based defined by 238 genes with a prediction sensitivity of 0.99758 for endometrial dating (Díaz-Gimeno *et al*, 2011).

Briefly, from right to left the samples could be classified as pre-receptive (n=4), early-receptive (n=7) and receptive (n=25). To ensure that the designation of the samples was correct, I examined the transcript levels of 6 validated receptivity marker genes (*SLC15A1, CD55, C4BPA, DPP4, GPX3* and *PAEP*), all of which are selectively expressed in glandular epithelium ((Díaz-Gimeno *et al*, 2011; Suhorutshenko *et al*, 2018). As show in Figure 3.7, all 6 marker genes were significantly induced in the receptive phase when compared to the pre-receptive phase ($P < 0.05$). The early-receptive samples show an expression pattern with levels between the pre- and receptive samples, especially for *CD55, C4BPA* and *SLC15A1* (Figure 3.7).

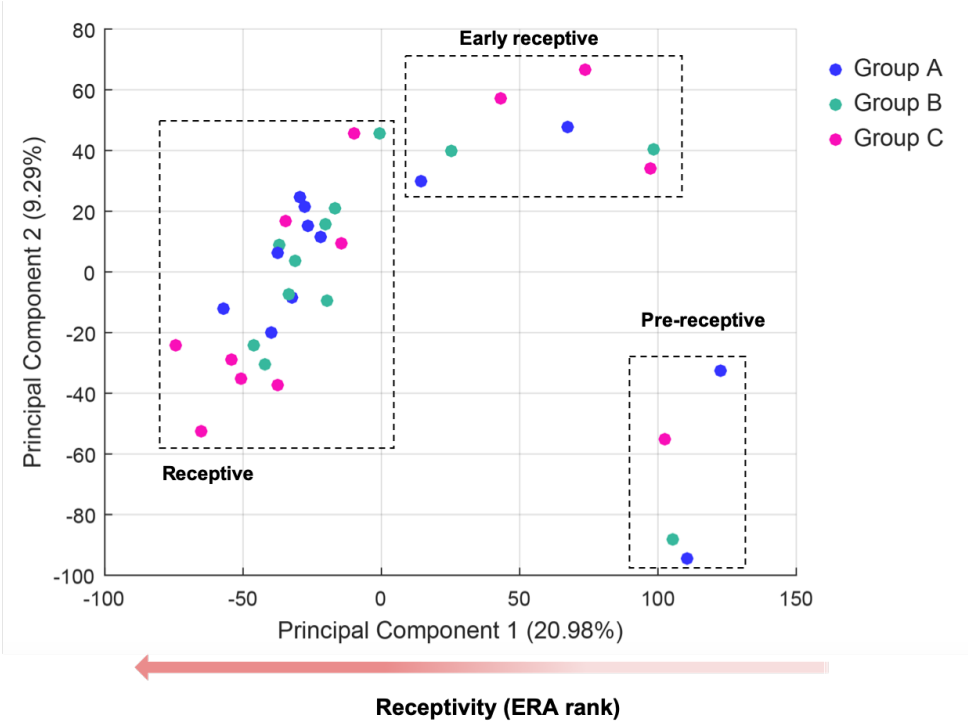

Figure 3.6. Principal component analysis of endometrial bulk RNA-Seq. Principal-component scores of RNA-seq are plotted on components 1 and 2. Patient samples were colour coded according to their original group : group A, blue – infertile followed by live birth, group B, green – RM followed by live birth and group C, pink – RM followed by miscarriage. From right to left the samples could be classified as pre-receptive, early-receptive and receptive. The RNA-seq data sets were generated previously by Dr. Emma Lucas in Professor Brosens lab.

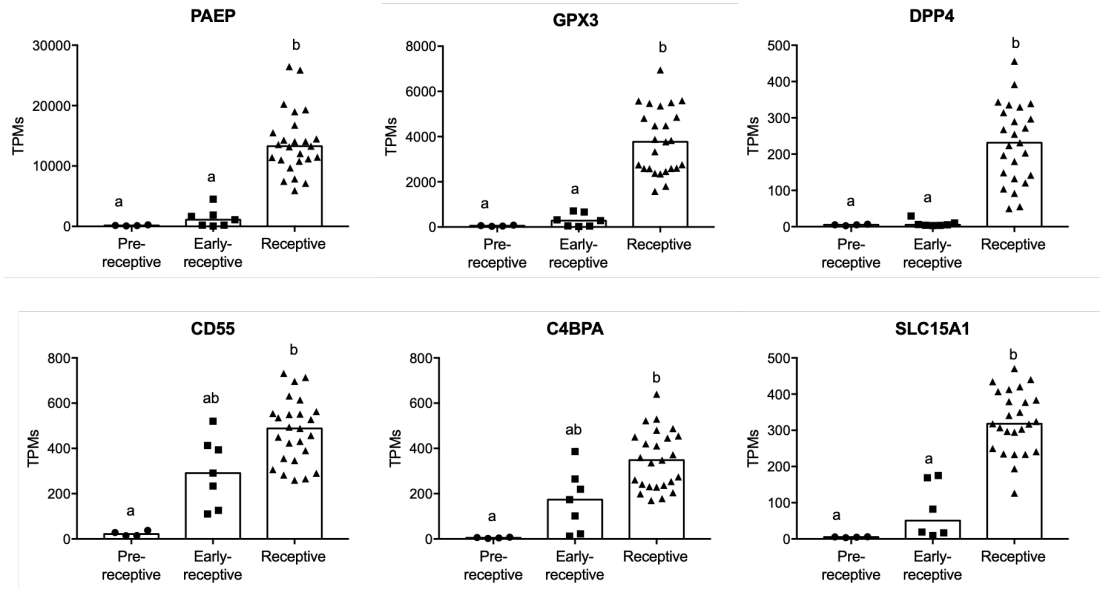

Figure 3.7. Receptivity biomarkers expression in endometrial samples. Vertical axis corresponds to transcripts per million (TPM) values from bulk RNA-seq. Group comparison by one-way ANOVA on ranks (Kruskal-Wallis) test. Different letters above bars indicate that those groups are significantly different from each other at $P < 0.05$. Data is presented as median.

All 36 biopsies were also subjected to uNK cell analysis using a clinically validated test based quantitative analysis of CD56-positive cells underlying the luminal epithelium (Brighton *et al*, 2017). The % uNK cells was calculated based on the number of CD56-positive cells per 100 CD56-negative stromal cells. Hence, to validate the CIBERSORT approach, uNK cell quantification by immunohistochemistry was compared to the proportion of uNK cells from the deconvolution analysis of whole tissue transcriptome data. As shown in Figure 3.8 A, there was a significant albeit imperfect correlation in uNK cell estimates based on these very different approaches ($r = 0.45$; $P = 0.003$)

Next I used the computational deconvolution to assess the relative abundance of stromal, epithelial, and uNK cells in endometrial biopsies from the 3 clinical groups (Figure 3.8 B). Although no statistical significant differences were observed, it was notable that the spread of data (i.e. variation in proportion of cells) was more pronounced in Group C (RM patients who experienced another miscarriage) in all 3 cell types.

Computational deconvolution analysis of the previous data set (Figure 3.5) indicated that the WOI coincided with a sudden change in stromal/epithelial cell ratio approximating 1. However, the RNA-seq data from the 36 endometrial samples enabled further classification of mid-luteal biopsies in pre-receptive, early-receptive and receptive.

Hence, computational deconvolution analysis was performed on pre-, early- and receptive samples to time the change in stromal/epithelial cell ratio more accurately. As shown in Figure 3.8 C-E, stromal cells were always more abundant to epithelial cells except in the early-receptive samples when the ratio equaled ~1. The relative increase in uNK cells from pre-receptive to receptive was as expected.

Taken together, computational deconvolution analysis of endometrial transcriptomic data suggests that the start of the WOI coincides with a dramatic and sudden change in epithelial/stromal cell ratio. Furthermore, the data suggest that the change in this ratio may be more pronounced in RM patients, although this requires further examination in a larger cohort of samples. Once again, CIBERSORT analysis failed to identify different stromal subsets.

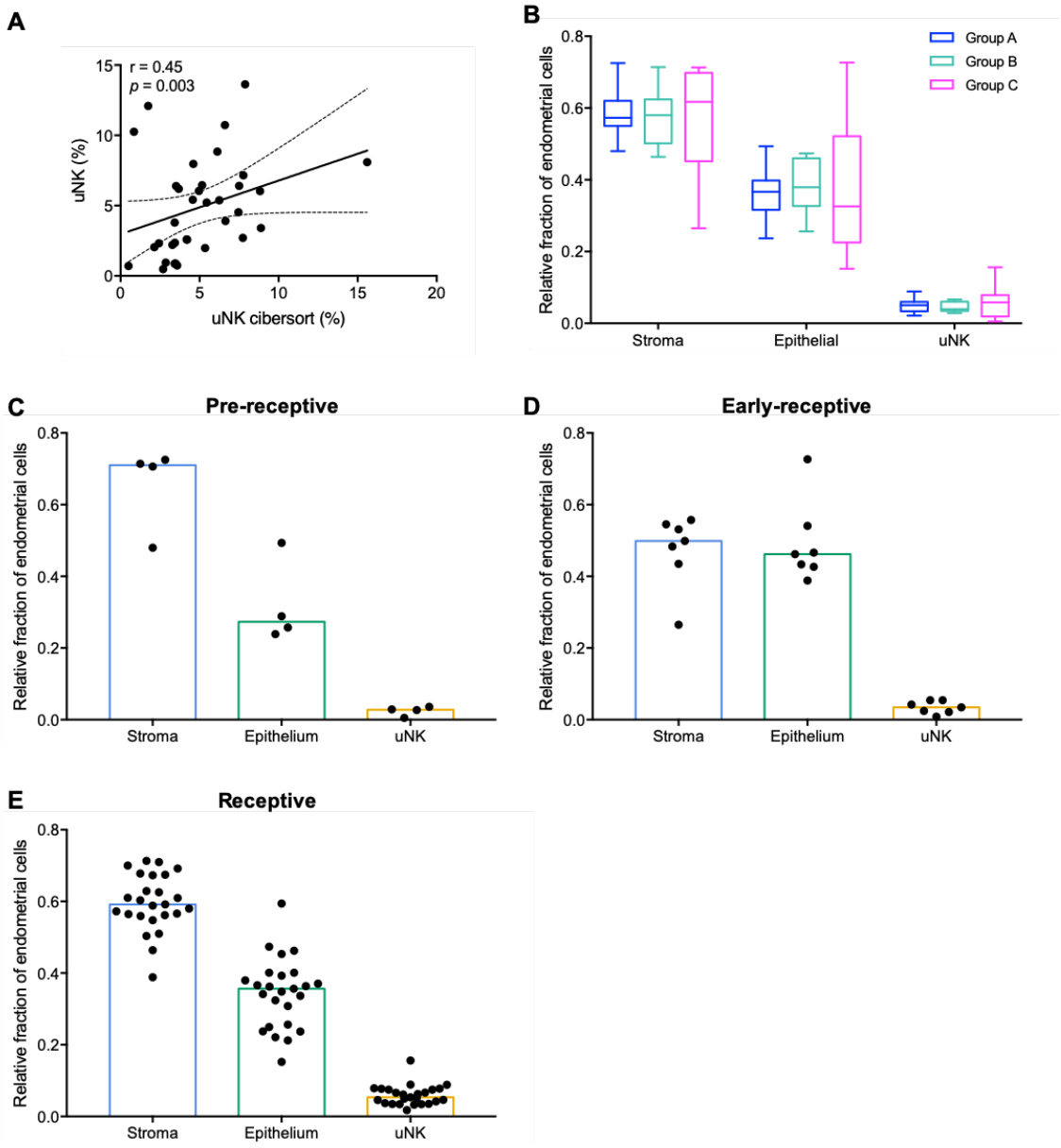

Figure 3.8 Deconvolution of in-house RNA-Seq data of endometrial samples. (A) Spearman's rank correlation between uNK quantification by immunohistochemistry and CIBERSORT uNK proportion. (B) Proportions of stromal, epithelial and uNK cells in endometrial biopsies estimated by the computational deconvolution approach per group of patients: group A, blue – infertile followed by live birth, group B, green – RM followed by live birth and group C, pink – RM followed by miscarriage. Two-way ANOVA followed by Tukey's test showed no significant difference between groups. Box plot displays the median value and the full range of variation, (n=12 per group). (C-F) Proportions of stromal, epithelial and uNK cells in endometrial biopsies timed as pre-, early- and receptive. Data is represented as median.

3.3.3 Transcriptomic analysis of cultured stem cells

The 'signature matrices' for the CIBERSORT analysis were based on RNA-seq analysis of cultured eMSC, TA, PVC and EnSC from 3 different endometrial data. A step-wise approach was taken to mine these RNA-seq data sets to identify putative markers that can be used to isolate or quantify endometrial stem cells.

Differential gene expression (DGE) between cultured PVC and EnSC

DGE were defined on basis of fold-change ≥ 2 and an adjusted (Benjamini-Hochberg) *P*-value < 0.05. When comparing cultured PVC and EnSC, 91 differently expressed genes were identified, from which 16 and 75 were enriched in PVC and EnSC, respectively (Supplemental Tables 1 and 2). The relative low number of DGE is not surprising as PVC partly de-differentiate when propagated in culture as previously described (Murakami *et al*, 2014). Nevertheless, several genes enriched in cultured PVC encode for factors that selectively expressed around the endometrial vasculature upon cross-referencing the Human Protein Atlas (http://www.proteinatlas.org/) (Supplemental Figure 1; Figure 3.9). Perivascular marker genes, *CDH13*, *ITGA7*, *MYH11*, *KCNE4* and *ESAM* are upregulated in cultured PVC. In addition, *POSTN* has been previously associated with cultured PVC (Murakami *et al*, 2014)

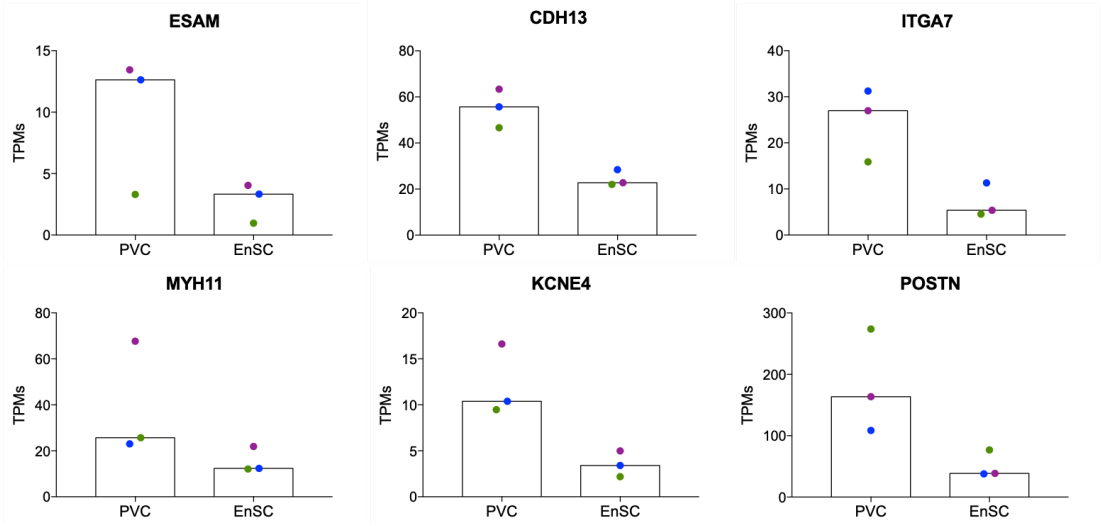

Figure 3.9. Established perivascular markers in cultured PVC. Transcripts per million (TPM) values from RNA-seq data between perivascular cells (PVC) and endometrial stromal cells (EnSC). Samples from the same patient are colour coded. Data is represented as median (n=3)

Differential gene expression between cultured eMSC and TA

Only 33 DGE were identified between the clonogenic populations, eMSC and TA, showing that endometrial stem/progenitor cells share a basal transcriptome profile, at least when cultured *in vitro* (Supplemental table 3). Out of 33 DGE, 30 were upregulated in eMSC and 3 in TA. Figure 3.10 depicts the top 6 DGE (Figure 3.10). Interestingly, the top marker gene for eMSC, *SERPINB2,* is a master regulator of sonic hedgehod (SHH) signalling that antagonizes aging process (senescence) in endometrial stem cells (Cho *et al*, 2019).

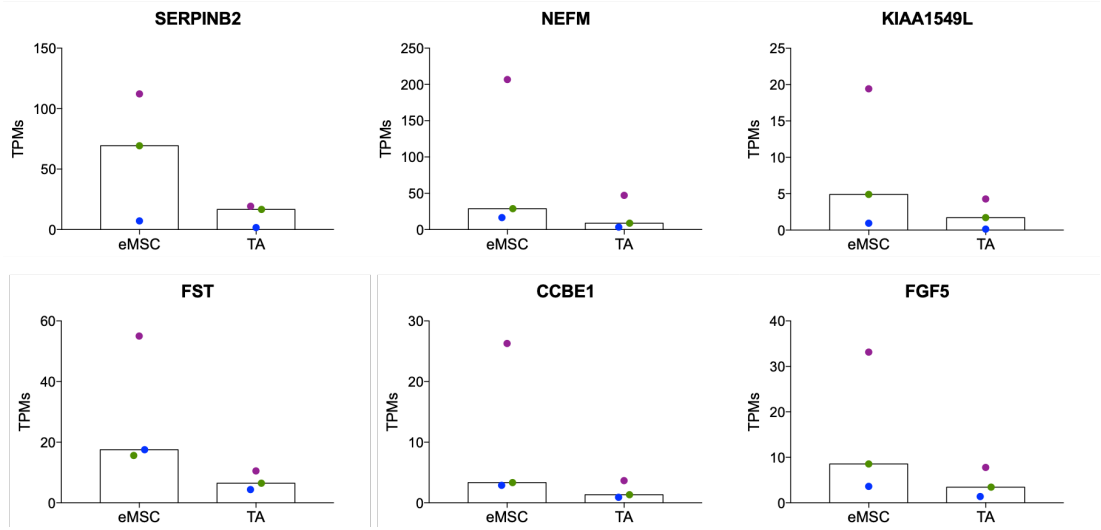

Figure 3.10. Top 6 genes enriched in eMSC, when compared to TA. Transcripts per million (TPM) values from RNA-seq data between endometrial mesenchymal stem cells (eMSC) and transit-amplifying cells (TA). Samples from the same patient are colour coded. Data is represented as median (n=3)

Differential gene expression between cultured eMSC and EnSC / PVC

Due to the similarity between eMSC and TA profiles, the following analysis was performed focusing only on the eMSC transcriptome profile. To assess which is the eMSC genetic signature that differentiates these cells from other stromal populations, the expression profile was compared with PVCs and EnSC (Figure 3.11). Between eMSC and EnSC 314 genes were upregulated, while 1423 were downregulated. When compared with PVCs, a similar pattern was observed, with 473 upregulated genes and 1334 downregulated genes. The venn-diagram shows that 258 genes were commonly upregulated in eMSC compared with PVC and EnSC. On the other hand, 1002 genes were commonly downregulated in eMSC compared with PVC and EnSC (Figure 3.11 A).

Gene ontology (GO) enrichment analysis was applied to the up and downregulated genes depicted in the venn-diagram. GO analysis showed that the extracellular environment is highly distinguished between populations with collagen deposition enriched in eMSC (Figure 3.11 B-E). On the other hand, markers of aging and apoptotic pathways are downregulated in the stem cell fraction indicative of the naïve nature of the eMSC population.

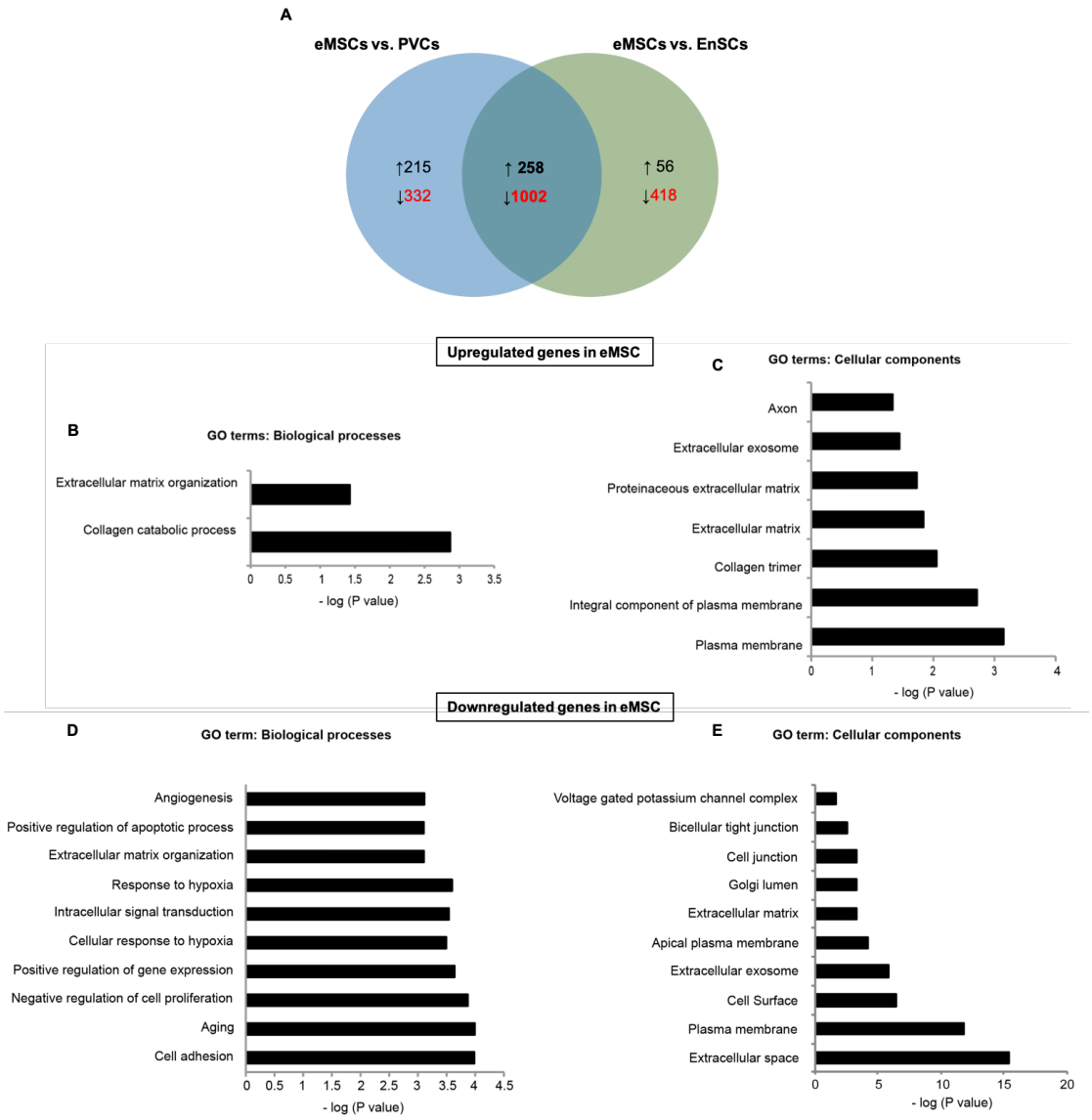

Figure 3.11. Characterization of eMSC gene signature. (A) Venn diagram showing overlap of 258 genes upregulated and 1002 genes downregulated in eMSC. Genes were selected based on fold change ≥ 2 and adjust P-value < 0.05 (B and C) GO analysis of the 258 upregulated genes from b using DAVID database. (C and D) GO analysis of the 1002 downregulated genes. GO terms associated with 'biological processes' and 'cellular components' were taken into consideration for this analysis.

From the 258 genes, the top 10 markers were identified and the correlation between their expression in bulk tissue and clonogenic efficiency was assessed. Top markers include: *ITGA8*, *CBLN2*, *PCDH9*, *COL10A1*, *CLDN11*, *KRT40*, *DPT*, *NPWBR*, *CST* and *LRRC17*. The expression of these putative marker genes was analysed in 33 biopsies. In parallel, CFU assays were performed on the same biopsy samples as depicted schematically in Figure 3.12A. For the cloning efficiency experiments, unselected stromal cells were used and cultured at low density (50 cells / cm^2) for 10 days. None of these markers showed a significant positive correlation with the clonogenic efficiency (Figure 3.12B). One possible explanation is that these genes might not be exclusive of the clonogenic cells. Even if the expression levels are lower in other cells, the results will be masked by the abundance of other cell types. One of the genes, *KRT40*, was eliminated from the analysis since it was not possible to detect the transcript during the RT-qPCR.

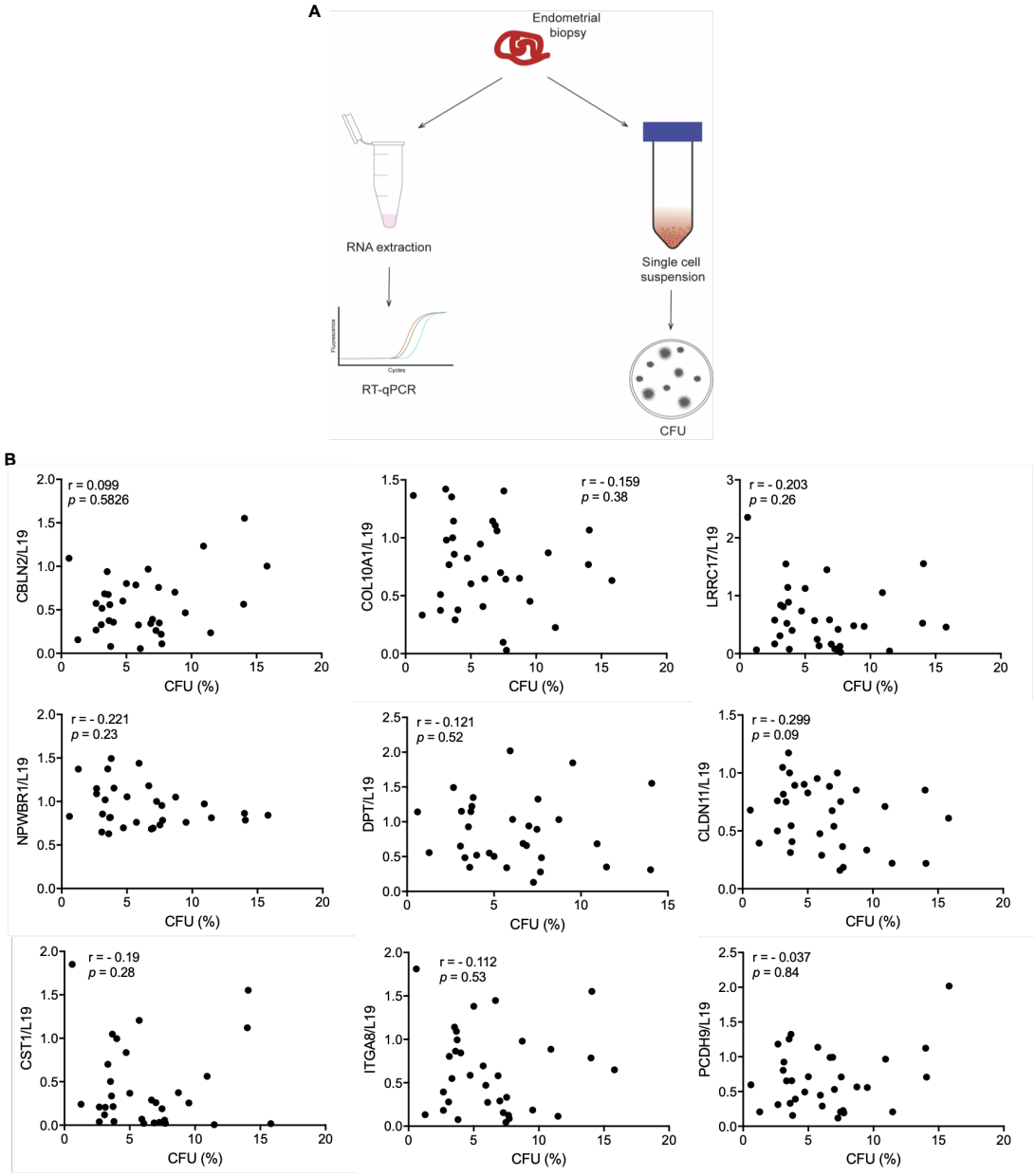

Figure 3.12. Top markers of eMSC do not correlate with clonogenic efficiency. (A) Schematic of experimental workflow. (B) Spearman's rank correlation between RT-qPCR in whole tissue and parallel CFU assays (n=34).

To characterize the phenotype and putative signalling pathways involved in eMSC identity, cell surface proteins and transcription factors were identified through *in silico* analysis using the Cell Surface Protein Atlas and the FANTOM consortium, respectively (Bausch-Fluck *et al*, 2015; Ravasi *et al*, 2010) (Supplemental table 4). From the sixteen transcription factors enriched in eMSC, *FOXF1*, *TFAP2C*, *SATB2* and *GLI3* have been implicated in stemness maintenance in different cellular systems (Sturtzel *et al*, 2018; Wang *et al*, 2018b; Zhou *et al*, 2016; Rodrigues *et al*, 2018). Although there is a lack of information in literature regarding eMSC regulation, this analysis indicates there are common transcription factors that govern the phenotype between eMSC and other ASC.

To explore specific eMSC markers, 49 cell surface proteins were initially identified and further selected following the criteria:

1) > 3 transcripts per million (TPM) in eMSC

2) Fold change > 2

3) Absence of expression in either glandular or stromal compartment (Human Protein Atlas).

Out of 49 putative cell surface markers, 21 met the pre-specified criteria (Table 3.2). Note that some genes designated as cell surface markers encode for ECM proteins (e.g. *TNC*, *COL7A1*) or signal intermediates (e.g. WNT5B). Interestingly, a multi-drug resistance gene, *ABCC4*, which is associated with SP, was amongst the marker genes. This is the first time that a list of transcription factors and cell surface proteins involved in cultured eMSC identity has been generated.

Table 3.2. Short-list of genes of cell surface proteins enriched in eMSC.

Gene	FoldChange eMSC_vs_PVC	FoldChange eMSC_vs_EnSC	eMSC_TPM	TA_TPM	PVC_TPM	EnSC_TPM
OLFML3	6.68	5.55	241.72	214.87	34.50	43.38
TNC	2.28	2.68	155.46	99.17	56.49	43.54
COL7A1	2.71	2.41	129.79	114.20	45.20	50.88
WNT5B	2.27	2.32	107.35	65.44	42.60	41.60
LRP11	2.33	2.03	48.90	61.68	19.85	22.65
ABCC4	3.80	3.07	45.15	53.89	11.13	13.61
GLT8D2	3.35	3.23	38.52	36.74	10.82	10.89
GPR126	4.22	3.68	37.27	47.93	8.06	9.29
THSD4	2.85	2.68	36.64	40.59	11.70	12.27
CD109	3.26	2.96	30.50	25.19	8.64	9.34
GPR39	8.18	3.64	25.99	11.18	3.07	8.10
TRHDE	7.68	6.53	20.30	21.84	2.87	3.04
ITGA8	15.85	14.14	19.96	26.65	1.29	1.35
SLIT2	6.52	11.80	19.48	5.23	2.52	1.57
ELTD1	4.02	5.44	13.44	7.21	3.26	2.33
PCDH9	11.37	13.10	13.27	6.54	1.09	0.93
MPZ	7.21	14.04	11.10	9.07	1.61	0.77
TMEM26	4.16	3.45	9.68	15.44	1.77	2.06
ODZ4	3.49	3.35	7.07	4.68	2.09	2.17
COLEC12	7.19	10.44	6.81	10.70	0.72	0.52
PRSS35	4.50	8.81	6.74	6.67	1.43	0.89
NCAM2	4.29	4.65	4.43	3.42	0.94	0.86

3.3.4 MRP4, a putative marker of an endometrial side population

Multidrug resistance protein 4 (MRP4), encoded by the gene *ABCC4*, is a member of the C subfamily of ATP-binding cassette (ABC) transporters. MRP4/ABCC4 has the remarkable ability to transport a range of endogenous molecules that have a key role in cellular communication and signalling, including cyclic nucleotides, ADP, eicosanoids, urate and conjugated steroid hormones (Russel *et al*, 2008). ABC transporters have been linked to the existence of SP, characterized by specific Hoechst dye efflux pattern in flow cytometry analysis. SP fraction cells are enriched in cells capable of self-renewal and differentiation with reconstitution of the original cell population (Al-Hajj and Clarke, 2004; Masuda et al, 2010). In the endometrium, immunostaining for ABCG2/Bcrp1, a characteristic cell surface transporter in SP cells, shows a distribution across both the functionalis and basalis layers with a higher incidence around small capillaries (Masuda *et al*, 2010).

To test if the endometrium harbours MRP4$^+$ cells, I performed MACS on freshly isolated stromal cells from 12 individual biopsies using a PE-conjugated antibody against MRP4. In parallel, W5C5$^+$ cells were used for comparison. As expected, PVC represent about 5% of the stroma compartment (Murakami *et al*, 2013), while MRP4$^+$ population corresponds to 0.7% (Figure 3.13 A). Due to such low percentage and to exclude that it was not just background from the MACS, a negative control without primary antibody was added showing to retain only 0.12% of “false positive” cells.

After MACS, cells from 3 samples were expanded in culture and their phenotype was validated by RT-qPCR (Figure 3.13 B). Although not statistically significant, *SUSD2* transcript levels were tendency higher in PVC (P = 0.05, Mann-Whitney test), while *MRP4* transcript levels were higher in MRP4$^+$ cells (P = 0.1, Mann-Whitney test) confirming the identity of the cells sorted by MACS. Additionally, the quiescent and activated phenotype of these cells was investigated by the expression of a quiescent fibroblast marker, fibroblast specific *FSP1* (also known as *S100A4*), and compared to *ACTA2*, a marker of activated fibroblasts (Kalluri, 2016). It was observed that the expression of *ACTA2* was equivalent between both cell subsets (Figure 3.13), which could be due to the processing of cells in culture. Although not statistically significant, the median of *S100A4* transcript levels was higher in MRP4$^+$ cells (P = 0.05, Mann-Whitney test), indicative of a quiescent phenotype.

The expression of *ABCG2* was also explored in these cell subsets. As mentioned above, *ABCG2* is an ABC transporter, with the ability to extrude lipophilic dye Hoechst

33342 and commonly associated with SP. Again, although not statistically significant, the expression of *ABCG2* was higher in MRP4$^+$ cells (P = 0.2, Mann-Whitney test) linking this cell subset to a SP phenotype. Figure 3.13C shows the percentage change between MRP4$^+$ and W5C5$^+$ cells. MRP4$^+$ cells are characterized by an increase of expression of the multi-drug resistance genes, *ABCC4* and *ABCG2*, and the quiescent fibroblast marker, *S100A4.*

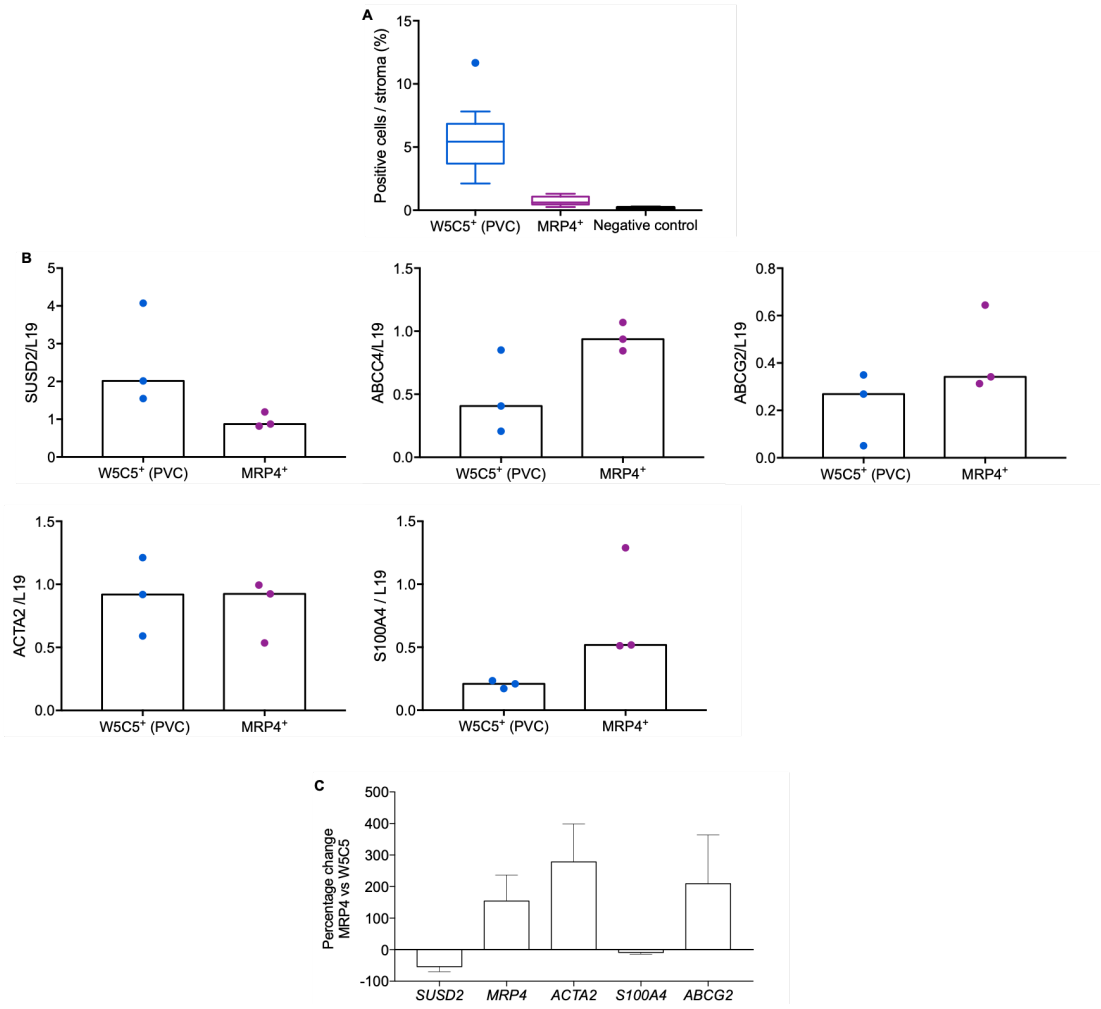

Figure 3.13. W5C5$^+$ and MRP4$^+$ cell sorting and validation. (A) Percentage of W5C5$^+$ (PVC) and MRP4$^+$ cells from fresh endometrial biopsies. Box plot displays the median value and the full range of variation. Individual dots represent outliers, (n=12). (B) RT-qPCR analysis of indicated gene expression on cultured PVC and MRP4$^+$ cells after magnetic activated cell sorting. Mann Whitney test was used. Data represent median. (C) Percentage change between MRP4+ and W5C5+ cells. PCR carried out in 3 different biological samples and in technical triplicates per sample. Data represent median.

To investigate the localization of MRP4^{+} cells on the tissue, immunohistochemistry was performed initially on endometrium tissue slides. However, this technique failed to yield any positive results, probably due to an antibody inefficiency. As an alternative, single molecule *in situ* hybridization (ISH) was performed on mid-luteal endometrial biopsies. This technique enables the visualization of single RNA molecules (red dots) per cell in tissue samples. Peptidylpropyl isomerase B (*PPIB*) and bacterial gene *DapB* were used as a positive and negative control probes, respectively. Figure 3.14 shows at the top left and right a representative image of the positive and negative probes (magnification: X40), respectively. When tested against an *MRP4/ABCC4* probe, positive cells showed to be rarely dispersed in the stroma and with higher prevalence at the perivascular sites (Figure 3.14C).

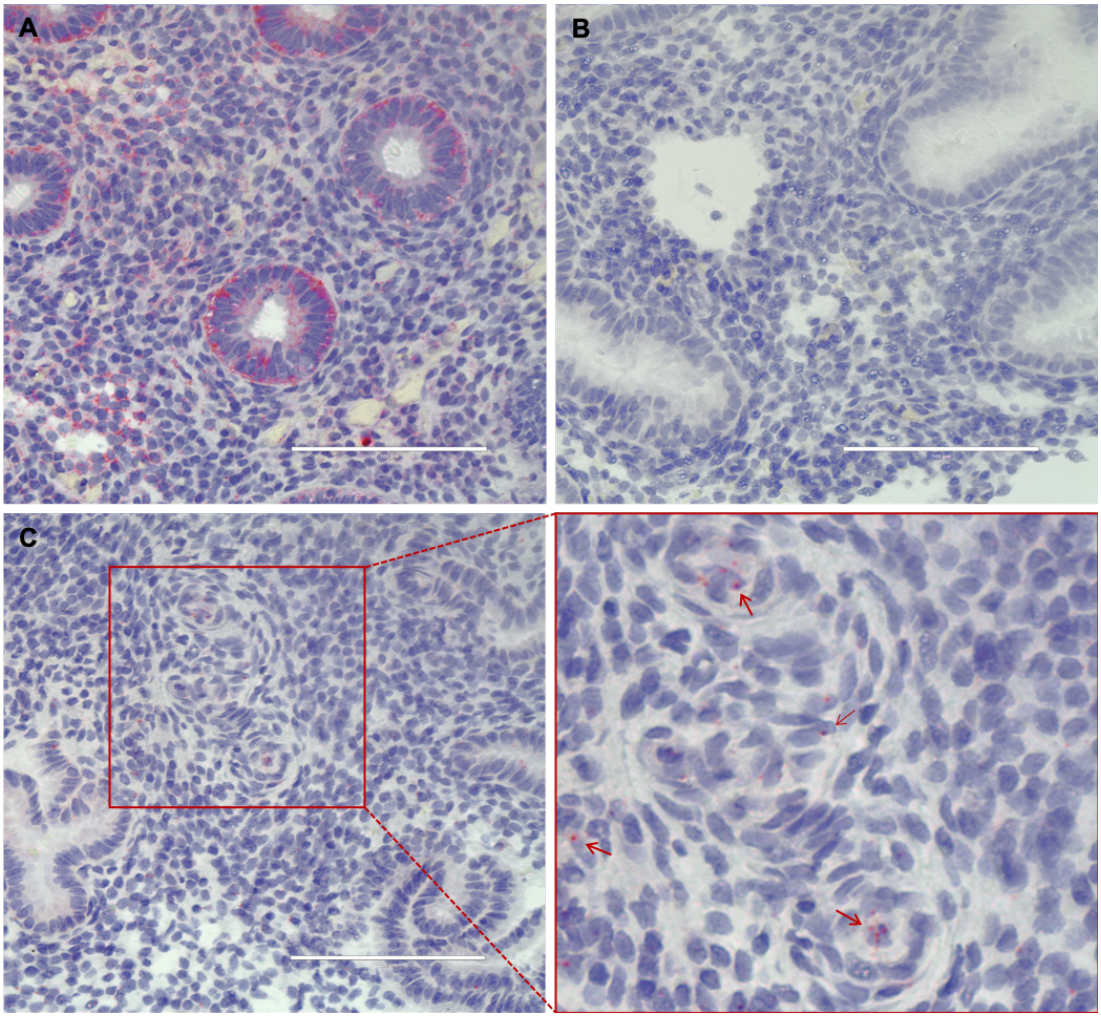

Figure 3.14. RNA *in situ* hybridization (ISH) on mid-luteal phase endometrial biopsies. (A) Positive control (*PPIB*). (B) Negative control (*DapB*). (C) MRP4^{+} probe. Right panel shows a magnification of MRP4^{+} cells (pink, arrows). Scale bar: 100 µM. Original magnification: x40.

To test the cloning efficiency, cells were subjected to a CFU assay. As described above, when freshly isolated PVC are seeded at low density, the resulting clones are designated as eMSC. Alongside the eMSC, the MRP4$^+$ population also showed the ability to form colonies (Figure 3.15 A and B). Although the efficiency value was markedly lower (0.6 $\pm$ 0.2, mean $\pm$ sem) when compared to eMSC (5.3 $\pm$ 0.8), results show that both efficiencies correlate significantly (r = 0.63, $P < 0.05$) (Figure 3.15 C and D).

Initial studies classified large CFUs as the original stem cells while small CFUs are derived from more differentiated transit-amplifying cells (Gargett *et al*, 2009). Thus, the large size of the colonies from MRP4$^+$ was indicative that they relate to an endometrial stem population.

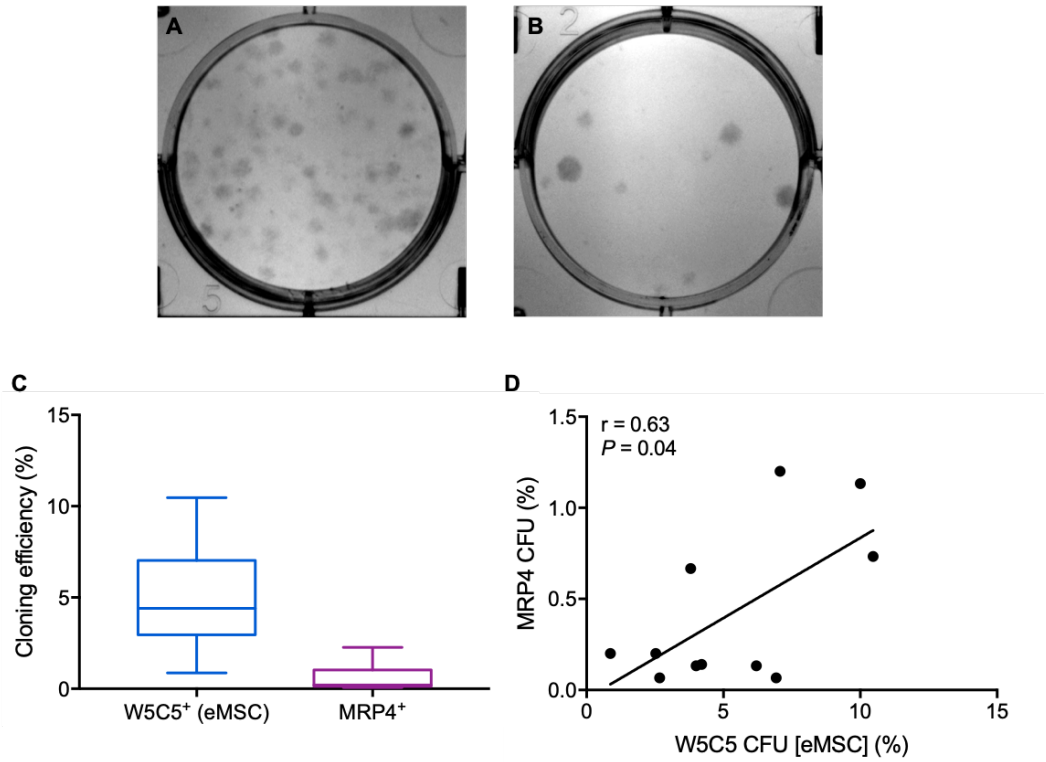

Figure 3.15. Cloning efficiency of eMSC and MRP4$^+$ cells. (A) Representative clonogenic assays established from PVC. (B) Representative clonogenic assays established from MRP4$^+$ cells. (C) Cloning efficiency from MRP4$^+$ and W5C5$^+$. Box plot displays the median value and the full range of variation. (D) Pearson correlation between MRP4$^+$ and W5C5$^+$ cloning efficiencies.

To test the self-renewal ability of both cell types, colonies were passaged until P4 (Figure 3.16A). Initially, it was observed that from P0 to P1, colonies became confluent when cells were plated at 50 cells/ cm^2 so it was necessary to reduce the number of cells for the passage. Although not statistically significant, it was observed that when $MRP4^+$ colonies were passaged, the cloning efficiency matched the eMSC for P1 and surpassed for P2 (Figure 3.16B). For later passages, cloning efficiencies tended to match between cell populations.

The initial low cloning efficiency and notable increase upon passaging suggests that $MRP4^+$ cells are in a quiescent state *in vivo* and that under culturing conditions cells become activated and proliferate with a higher ability to self-renewal than $W5C5^+$ cells, as previously demonstrated by Masuda *et al*, 2015.

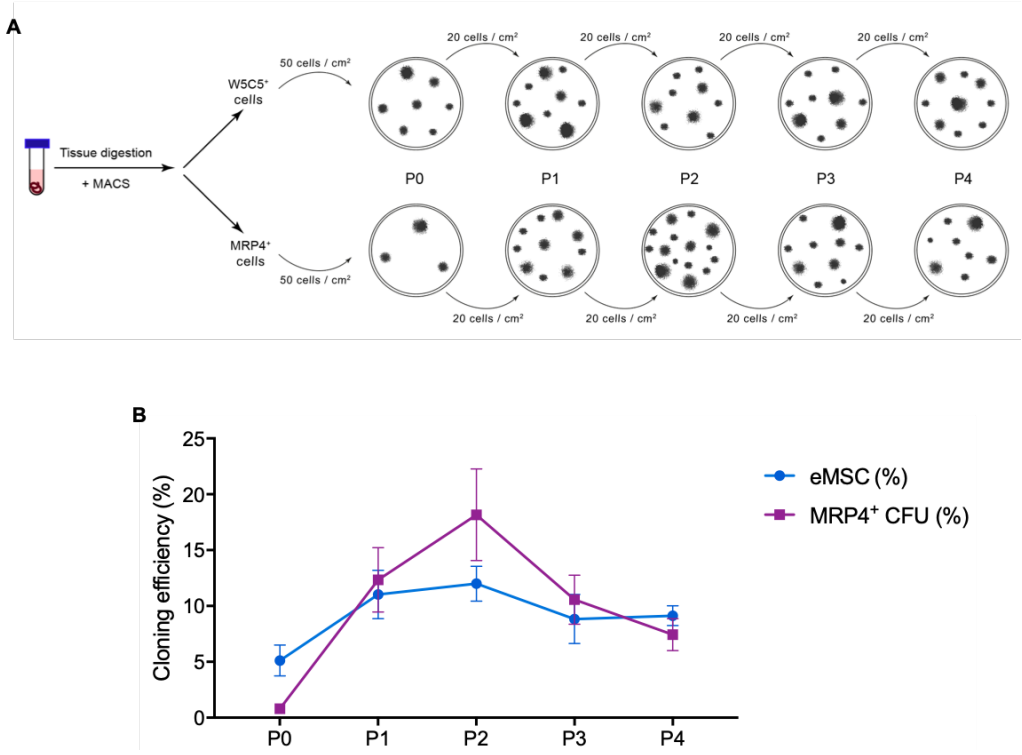

Figure 3.16. Self-renewal ability of eMSC and $MRP4^+$ cells. A) Schematic workflow of CFU passage from P0 until P4. B) Cloning efficiency of eMSC and $MRP4^+$ CFUs throughout colony passaging (n = 4).

3.3 Discussion

The first main objective of this study was to isolate the different endometrial cell types and subsets in order to create a signature matrix for each population that retrospectively could be used for different *in silico* analysis. First, this matrix was used to investigate whether the changes in gene expression levels between the different phases of the menstrual cycle might be influenced by the cellular composition of the biopsy. Through a computational deconvolution approach, it was detected that as the cycle progresses, the epithelial fraction becomes more dominant. This switch is more pronounced in the transition from early- to mid- secretory phase. Recently, another group published the deconvolution of endometrial transcriptomes from early- and mid-secretory samples. Suhorutshenko *et al* (2018) combined histological analysis to transcriptome deconvolution and showed that stromal and epithelial cells are present in a proportion of 70% and 30%, respectively in early secretory samples. As the cycle progresses, the proportion changes to 50% for each cell population. Additionally, the group identified that only 26 % of the initial differentially expressed genes remained after adjustment for biopsy cellular composition, such as *SLC15A1, CD55, HABP2, DPP4, GPX3* and *PAEP* (Suhorutshenko *et al*, 2018). In contrast, in this project the immune fraction and other stromal subpopulations were also taken into consideration. One of the biggest drawbacks of sample heterogeneity is the signal dilution, in which genes expressed in cell subsets present at low proportion may be masked by the signal coming from the same gene expressed in a prevalent cell subset (Shen-Orr and Gaujoux, 2013). Nevertheless, when different stromal subpopulations were used, the deconvolution method did not yield a specific signal. This could be due to the similarity between cultured EnSC, PVC, eMSC and TA transcriptome signatures preventing CIBERSORT to discern the proportion of each cell subtype.

The shift in the transcriptional profile of PVC after culturing has been reported before for both $CD146^{+}PDGFR\beta^{+}$ and $SUSD2/W5C5^{+}$ cells (Schwab and Gargett, 2007; Murakami *et al*, 2014). The same phenomenon was observed for eMSC and TA cells, although it is also pertinent to question if these populations share a basal transcriptome signature *in vivo*. It is critical to acknowledge that by removing these subpopulations from their niche and culturing them *in vitro* we might be inducing modifications in their expression profile. In fact, hierarchical clustering showed that the stromal subpopulations are the first to diverge from the whole tissue. However, the uNK cells, which are at a low representation in the endometrium, have a transcriptomic profile more akin to the whole tissue. Since immune cells were only

incubated overnight while other populations were propagated for longer, it could be implied that the Euclidean distance metric analysis is a visualization of the transcription adaptation to the culturing process. Additionally, the hierarchical clustering analysis showed a proximity between gland organoids and whole tissue transcriptome. Since the gland organoids were set from fresh cultures, it is possible that the initial separation of epithelial cell was not completely efficient and thus the matrigel droplets were cultured with a mix of epithelial cells and other cell types (e.g. stromal and uNK).

Although the culturing process may interfere with the transcriptome profile of each cell type , the data here shows that cultured PVC retained gene signatures of perivascular niche cells. In addition, eMSC gene expression analysis indicated that they maintained their naïve profile when compared to PVC and EnSC.

This work contributes the first description of the transcription factors and cell surface proteins enriched in *in vitro* eMSC. Cross-referencing of transcription factors between different systems suggests that the regulation mechanisms of stem cell properties might be conserved between eMSC from different sources. For example, forkhead box transcription factor FOXF1 has been reported to be selectively expressed in endothelial colony forming cells compared to mature endothelial cells and to regulate Notch2 signalling (Sturtzel *et al*, 2018). Recently, Pastor *et al* (2018) also described the role of TFAP2C as an important regulator of human naïve pluripotency during the embryo development. On the other hand, zinc-finger transcription factors of the Gli family are involved in the signal transduction of the SHH pathway, which is essential for the maintenance and response of several types of stem cells (Hui and Angers, 2011; Zhang *et al*, 2017). In the liver, the SHH/GLI3 axis regulates CD90-cancer stem cells (Zhang *et al*, 2018). In oral squamous cancer stem cells, GLI3 knockdown decreases stemness, cell proliferation and invasion (Rodrigues *et al*, 2018). For future experiments, it would be interesting to investigate the role of specific transcription factors through gene knockdown experiments followed by functional analysis.

My analysis identified MRP4 as a candidate cell surface marker for endometrial stem cells. $MRP4^+$ cloning efficiency correlates with eMSC, suggesting that MRP4 subpopulation accounts for 10% of eMSC. Due to the nature of MRP4 as an ATP-dependent unidirectional efflux transporter, it was hypothesized that $MRP4^+$ cells could be related to an endometrial SP.

Cell isolation based on flow cytometry sorting may have detrimental effects on the viability of the SP cells (Masuda *et al*, 2015), whereas MACS is a more gentle technique (Masuda *et al*, 2012). The quiescent state of magnetic bead-selected $MRP4^+$ endometrial cells evidenced by the expression of *S100A4* ties in with the previous finding that endometrial SP cells isolated directly from tissue are mainly in G0 phase (Tsuji *et al*, 2008). However, when isolated from cultured cells, SP had been recruited into G1 and showed a greater cloning efficiency (Tsuji *et al*, 2008). The same phenomenon of cell activation was observed with $MRP4^+$ selected cells, when after colony passaging, the cloning efficiency tendentially increased to higher values than eMSC to later stabilize at the same level.

Taken all together, the data here presented reinforces the concept of a hierarchy of endometrial stem / progenitor cell populations responsible for the regeneration of the tissue (Gargett *et al*, 2016). Additionally, it suggests that endometrial stem/progenitor cell populations share a naive basal transcriptomic profile. However, due to the inevitable culturing process to isolate endometrial stem cells, the access to a specific marker might be masked by transcriptome modifications. Thus, it is crucial to use alternatives to surpass the *in vitro* propagation process and the use of bulk RNA-seq, which dilutes the information from low representative populations in one sample.

Chapter 4

Single-cell analysis of peri-implantation endometrium: Identification of a putative mesenchymal progenitor population *in vivo*

4.1 Introduction

As described previously, bulk RNA-seq technology is a powerful tool to study gene expression patterns, but it is limited in decoding tissue complexity. To investigate the role and regulation of different cell types and subsets in a complex and heterogenous tissue, it is essential to map the transcriptome of individual cells. Since Tang and colleagues published the first single-cell RNA-sequencing (scRNA-seq) study in 2009 (Tang *et al*, 2009), there has been an exponential increase in the number of publications employing and improving different scRNA-seq platforms. scRNA-seq has already been used to investigate distinct tissues and organs, both during development and adulthood. These studies include various brain regions (Rosenber *et al*, 2018; Li *et al*, 2019; Sauders *et al*, 2018), lung (Guo *et al*, 2019; Zilionis *et al*, 2019, Angelidis *et al*, 2019), heart (Cui *et al*, 2019; Massaia *et al*, 2018), immune system (Papalexi and Satija, 2017), and in hematopoiesis (Pellin *et al*, 2019; Povinelli *et al*, 2018). The development of methods for high-throughput single-cell molecular profiling has been adopted rapidly by the scientific community to the point where it is now possible to access comprehensive transcriptomic maps of different cell types and subsets across many human tissues (Human Cell Atlas, https://www.humancellatlas.org), in different cancer types (CancerSEA, http://biocc.hrbmu.edu.cn/CancerSEA/), and even across different species (Single Cell Expression Atlas, https://www.ebi.ac.uk/gxa/sc/home).

The recent rapid spread of scRNA-seq methods has resulted in a large variety of experimental protocols and computational pipelines. Each scRNA-seq analysis can have different goals including differential expression (DE) analysis, classification and clustering of cells and trajectory reconstruction (Vieth *et al*, 2019). Commonly, scRNA-Seq analysis workflow encompasses single-cell dissociation, single-cell isolation, library construction and sequencing. The most popular platforms for scRNA-Seq use microfluidic technology, which requires low sample consumption, low analysis cost and enables precise fluid control. Importantly, the nanoliter-sized volumes required for this technique substantially reduce the risk of external contamination (Hwang *et al*, 2018). Several in-house (e.g. Drop-seq) and commercial (e.g 10X Chromium) microdroplet-based microfluidics protocols are available diverging in cost per experiment and capture efficiency.

Common steps required for the generation of scRNA- seq libraries include cell lysis, reverse transcription into first-strand cDNA, second-strand synthesis, and cDNA amplification. Analysis tools for scRNA-seq data are written in a variety of

programming languages—most prominently R and Python. Popular platforms such as Seurat, Scater, or Scanpy provide integrated environments to develop pipelines and contain large analysis toolboxes (Luecken and Theis, 2019). Additionally, some commercial companies provide software tools, such as 10x Genomics and Fluidigm (Hwang *et al*, 2018). After sequencing, alignment and de-duplication are performed to quantify an initial gene expression profile matrix. Next, normalization is performed with raw expression data using various statistical methods. Additional QC is performed based on three QC covariates: the number of counts per cell (count depth), the number of genes per cell, and the fraction of counts from mitochondrial genes per cell. Finally, the normalized matrix is then subjected to main analysis through clustering of cells to identify subtypes (Hwang *et al*, 2018; Luecken and Theis, 2019). The continuous improvement of analysis tools is beneficial for generating new scientific insight, although it also hinders standardization between studies.

Due to the cellular heterogeneity and cyclic transformative nature of the endometrium, scRNA-seq has become a valuable tool to investigate both static and dynamic aspects of the tissue across the menstrual cycle (Wang *et al*, 2018a), in first-trimester pregnancy (Surayawanshi *et al*, 2018; Vento-Tormo *et al*, 2018) and the end of gestation (Tsang *et al*, 2017). Six different cell types have been characterized during the menstrual cycle – stroma, endothelium, macrophages, lymphocytes, ciliated epithellium and non-ciliated epithelium (Wang *et al*, 2018a). One of the features enabled by scRNA-seq analysis is the placing of single cells along a continuous trajectory. This approach, termed pseudotime, enables visualization of progression of cells towards different fates, such as differentiation or cell death (Trapnell *et al*, 2014). This type of analysis revealed that the start of the WOI coincides with an abrupt transcriptomic transition in epithelial cells, accompanied by a more continuous transition in stromal fibroblasts (Wang *et al*, 2018a). An in-depth analysis of different stromal populations has so far only been performed in the decidua in early pregnancy, in which discrete clusters of perivascular and stromal cells were identified in distinct decidua layers (Vento-Tormo *et al*, 2018). Two clusters of perivascular cells were distinguished by different levels of *MCAM* and *MMP11*. Additionally, three clusters of stromal cells were identified in different layers of the decidua and with divergent levels of expression of the classical decidual markers prolactin (PRL) and IGFBP1 (Vento-Tormo *et al*, 2018).

High-throughput scRNA-seq has not yet been employed to identify putative stem/progenitor cell populations in cycling human endometrium. It has been reported that scRNA-seq has the unique ability to identify rare cell populations, representing <1% of cellular constituents in a given tissue (Grün *et al*, 2015; Segerstolpe *et al*, 2016; Villani *et al*, 2017). Rare cell populations are undetectable in bulk analytical approaches. Therefore, in this study, high-throughput single-cell droplet barcoding was employed to profile the transcriptome of peri-implantation endometrial biopsies. In the stroma, a rare population of highly proliferative mesenchymal cells was identified and subjected to further explorative analysis.

4.2 Results

4.2.1 Single-cell analysis of mid- luteal endometrial biopsies

To characterize the endometrial complexity *in situ*, freshly isolated cells from seven endometrial biopsies were subjected to single-cell analysis using nanoliter droplet barcoding and high throughput sequencing of RNA (Drop-Seq). Table 4.1 shows the demographic details of the samples used for this study. Three samples were LH+8 whereas the other four were LH+10. The median (range) age and BMI were 35 (31-42) and 27 (24-32), respectively. Previous losses ranged from 0 and 5 miscarriages, but only two patients had one live birth.

Table 4.1. Demographic details of patients from whom biopsies were used for scRNA-seq

Age	BMI	Cycle Day	Previous losses	Live-births
39	24	8	2	0
31	23	8	4	0
39	27	8	0	0
32	32	10	0	0
42	31	10	2	1
33	26	10	0	0
35	30	10	5	1

Figure 4.1 summarizes the workflow applied to this study. Each endometrial biopsy was enzymatically digested with collagenase type IA and DNase type I for 1 hour at 37 °C. The dissociated cells were filtered through a 40-µm cell strainer, which resulted in the underrepresentation of EpCs, as the endometrial glands are relatively resistant to the enzymatic digestion. The single cell suspension was then layered over Ficoll-Paque PLUS and centrifuged to remove red blood cells. Using a microfluidic device, each cell was co-encapsulated with a distinct barcoded microparticle (bead) in a nanoliter-scale droplet. Inside each droplet, the cell membrane was lysed and the mRNA was released and hybridized to the primers on the microparticle. Droplets were broken and the microparticles plus mRNA were collected. The mRNA was reverse transcribed into cDNA, which is then amplified, tagmented and sequenced (Macosko *et al*, 2015).

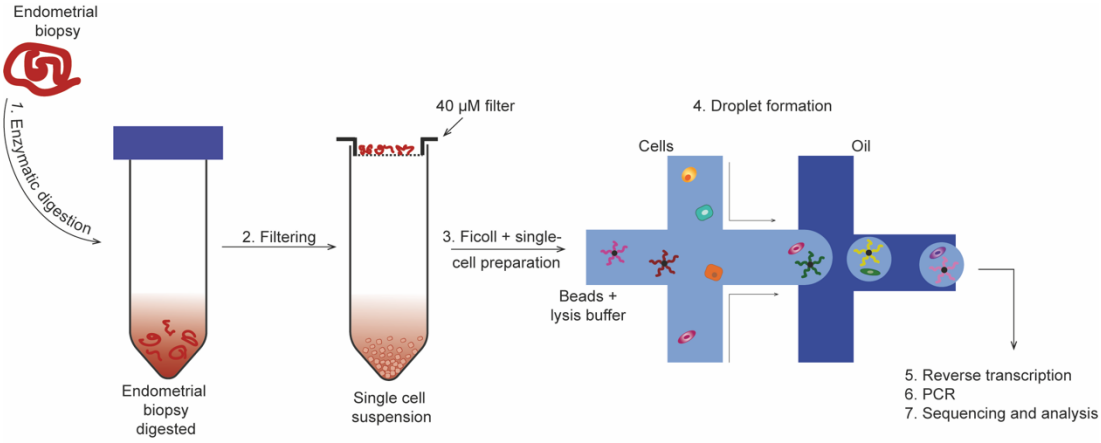

Figure 4.1. Schematic workflow of single-cell analysis of peri-implantation endometrial biopsies. A single cell suspension was obtained following tissue digestion, filtering and ficoll density gradient centrifugation. Each cell was then encapsulated with a barcoded microparticle inside a droplet, in which the mRNA was released and attached the primers on the microparticle. The mRNA was reversed-transcribed into cDNA, amplified and sequenced.

Computational dimensional reduction via *t*-distributed stochastic neighbour embedding (*t*-SNE) (Maaten and Hinton, 2008) combined with Shared Nearest Neighbor (SNN) analysis revealed segregation of 3282 cells into four main groups: endothelial (EC; n=156), epithelial (EpC; n=384), immune (IC; n=356), and stromal cells (EnSC; n=2,345) (Figure 4.2 A). Four distinct EpC populations were identified. The most abundant population, EpC1, highly expressed marker genes of secretory epithelium (e.g. *GPX3*, *PAEP*, and *DPP4*) (Figure 4.2 B). EpC2 were identified as ciliated endometrial cells, first described in human endometrium in 1894 (Benda, 1894; More and Masterton, 1976). Cross-referencing the EpC2 marker genes (e.g. *RSPH1, DNAAF1* and *CAPS)* with Protein Atlas showed that ciliated cells are localized between non-ciliated cells across endometrial glands (Supplemental Figure 2). Although EpC3 were enriched in genes highly expressed during the early- to mid-luteal phase of the cycle (e.g. *SCGB2A1* and *PDK4*), almost all cells in this population came from a single biopsy, suggesting either mistiming of the biopsy or retarded glandular maturation. Finally, EpC4 was considered an ambiguous population, characterized by expression both epithelial (e.g. *PAEP*, *CMC2*) and stromal (e.g. *DCN*, *ZEB1*) markers.

The IC were subjected to further dimension reduction (*t*-SNE) analysis (Figure 4.2 C); revealing that 89% of ICs in cycling endometrium are NCAM1/CD56^{+} uNK cells. uNK cells segregated into 3 subpopulations (NK1-3), matching the different NK populations described recently in pregnant decidua (Vento-Tormo *et al*, 2018). These uNK states

were in part defined by the relative abundance of cell cycle genes. The NK1 population represented the most proliferating uNK cells expressing genes involved in granule exocytosis (e.g. *PRF1, GNLY, GZMA* and *GZMB*). On the other hand, NK3 cells expressed low levels of cell cycle genes but were defined by *CCL5* and *CXCR4* expression. Notably, $CXCR4^{+}$ uNK cells have previously been implicated in vascular remodeling in pregnancy (Gibson *et al*, 2015). Cross-referencing with canonical markers curated from the literature identified IC1, IC2 and IC3 as naive B-cells, monocytes and macrophage/dendritic cells, respectively. The gene *CD79A* is expressed at the very early stages of B cell development (Dworzak *et al*, 1998) and maintained until the last stage of maturation before differentiation to plasma cells (Luger *et al*, 2013). On the other hand, *CD19* and *MS4A1* (also known as CD20) are lineage-restricted molecules expressed throughout B-cell differentiation prior to terminal differentiation of B cells to plasma cells (Naeim *et al*, 2013). Human blood monocytes are heterogeneous and conventionally subdivided into three subsets based on CD14 and CD16 expression. The expression of CD74 and HLA-DR are specific markers of the intermediate monocyte subset (Wong *et al*, 2012). As observed on the heatmap (Figure 4.2 D) and already described in literature, the allograft inflammatory factor-1 (AIF-1) is expressed in both monocytes and macrophages (Utans *et al*, 1995; Pawlik *et al*, 2016). Endometrial macrophages are recognized as critical players in the initiation of menstruation and repair and remodelling of the functional layer of the endometrium post-menses (Thiruchelvam *et al*, 2013; Cousins *et al* 2016). In a tissue injury situation, the angiogenic proteins, IL-8 and CXCL2, are expressed by macrophages to control neutrophil recruitment (Koch *et al*, 1992; Arici, 2002; De Filippo *et al*, 2013). Interestingly, also GPNMB, a macrophage transmembrane glycoprotein, regulates the viability, proliferation, and migration of MSCs, which are key players in the repair of injured or diseased tissues (Yu *et al*, 2016).

EnSC represented the bulk of cells captured by scRNA-seq analysis. However, the *t*-SNE analysis also identified a discrete population of proliferating cells (PC), representing 1.8% of cells in the stromal compartment. PC were distinct from both EnSC and IC. Their presence during the secretory phase, which is characterized by the suppression of proliferation and induction of cell differentiation in response to elevated progesterone levels (Strowitzki *et al*, 2006), was the focus of my further analysis.

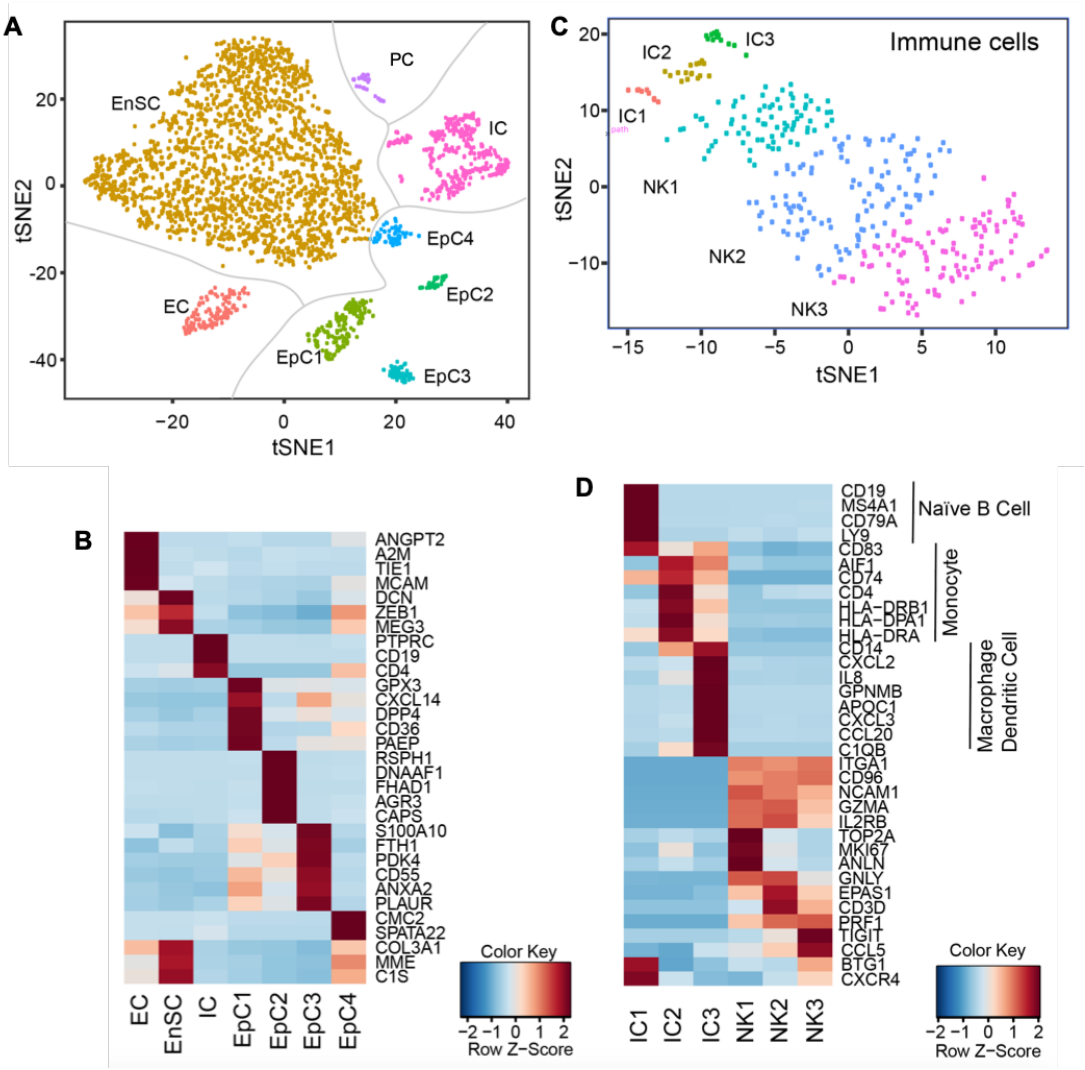

Figure 4.2. Identification of cell-types in mid-luteal endometrial samples. (A) t-SNE plot of 3283 cells isolated from 7 LH-timed biopsies captures all major endometrial cell types, including epithelial cells (EpC), immune cells (IC), endothelial cells (EC), stromal cells (EnSC) and a discrete but transcriptionally distinct proliferative (PC) stromal subpopulation. (B) Immune cells (IC) were subjected to additional t-SNE analysis, revealing three uNK cell subsets (NK1-3) and naïve B-cells (IC1), monocytes (IC2) and macrophage/dendritic cells (IC3). (C) Heatmap showing relative expression (z-score) of markers defining cell-types and EpC subpopulations. (D) Heatmap showing relative expression of markers defining endometrial IC populations during the implantation window.

4.2.2 Transcriptome profile of PC in the endometrium

To explore the nature of PC, the cell cycle status of all cell types in the 7 midluteal biopsies was first determined computationally using the Seurat package (https://satijalab.org/seurat/). Figure 4.3 A shows a schematic representation of the different phases of the cell cycle whereas Figure 4.3 B depicts the *t*-SNE plot colour-coded to indicate the various phases of the cell cycle: G1 phase, S phase (synthesis), and G2/M phase (interphase and mitosis/cytokinesis). Figure 4.3C shows the relative proportion of cells in different phases of the cell cycle for all endometrial cell types. The PC population is composed exclusively of cells in either S-phase (40%) or G2/M-phase (60%). By contrast, a majority of EnSC (55%) were found to be in G1 (Fig. 4.3 C). Likewise, most of EpC (63%) were assigned to G1 with only a minor proportion of cells in either S or G2/M phase. The abundance of EC and IC in G1-phase was 42% and 28%, respectively. Conversely, the proportion of EC or IC in either S or G2/M-phase was 58% and 72%, respectively (Figure 4.3 C). Thus, based on computational analysis of the cell cycle, the antiproliferative effects of the postovulatory rise in progesterone levels are most pronounced in EpC followed by EnSC and then EC. PC and to a lesser extend IC continue to proliferate during the progesterone-dominant luteal phase of the cycle.

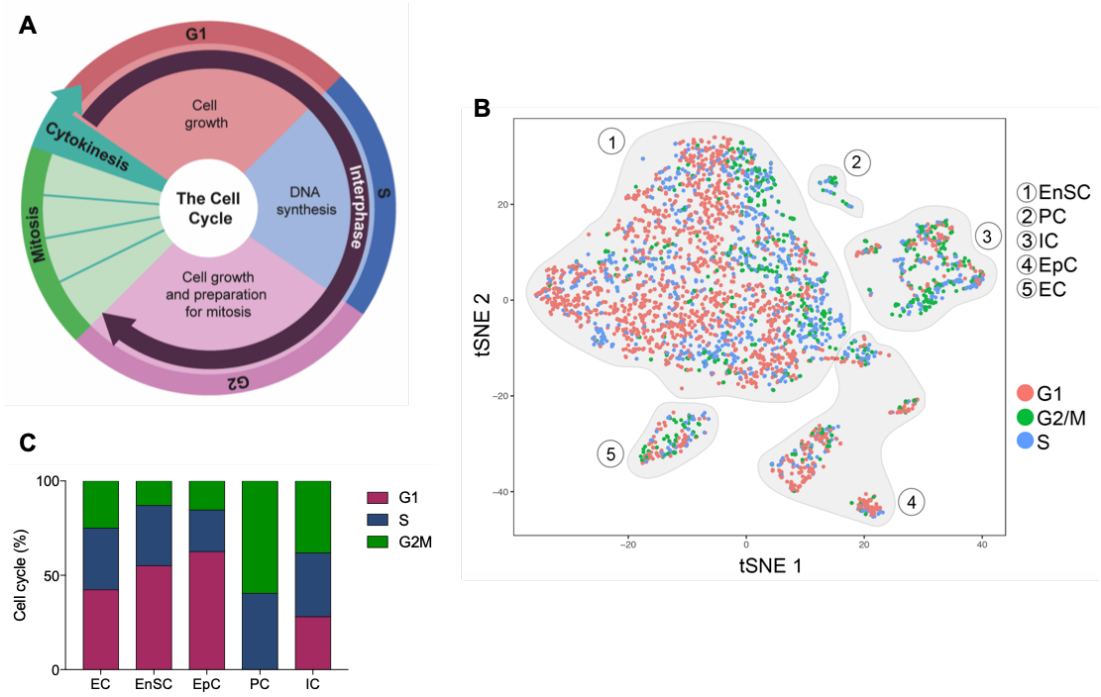

Figure 4.3. Analysis of the cell cycle in the endometrial clusters. (A) Schematic of the cell cycle phases (B) *t*-SNE projection of midluteal endometrial cell populations [epithelial (EpC), immune (IC), endothelial (EC), stromal (EnSC) and proliferative cells (PC)] colour-coded to indicate cells in different phases of the cell cycle (G1, S and G2/M). (C) Graph showing the distribution of cell in the cell cycle for each endometrial cluster.

The cell cycle phase has a profound impact on gene expression (Ma et al, 2015; Müller and Nieduszynksi, 2017). Hence, subsequent analysis was restricted to cells assigned to the same phase of the cycle: i.e. G2/M. A total of 19 DGE were identified in PC compared to all other cell types in luteal-phase endometrium (Table 4.2, Bonferroni adjusted $P < 0.05$). Cross-referencing of upregulated genes against the Cell Surface Protein Atlas (Bausch-Fluck et al, 2015) yielded no specific cell surface marker for PC. Although the analysis was restricted to cells in G2/M phase of the cell cycle, PC were conspicuously enriched in genes involved in cell cycle progression (Figure 4.4), suggesting that they are highly proliferative. One of the top DGE in PC is ANLN (Fig. 4.4), which encodes the actin-binding protein anillin involved in cytokinesis, cell growth and migration (Field and Alberts, 1995; Zhang and Maddox, 2010). Analysis of the Protein Atlas database revealed the presence of rare anillin$^+$ cells that are scattered throughout the endometrium (Supplemental Figure 3). At a glance, the abundance of anillin$^+$ cells in luteal endometrium appeared compatible with the scRNA-Seq analysis. Hence, I used anillin as a surrogate marker for PC in subsequent analyses.

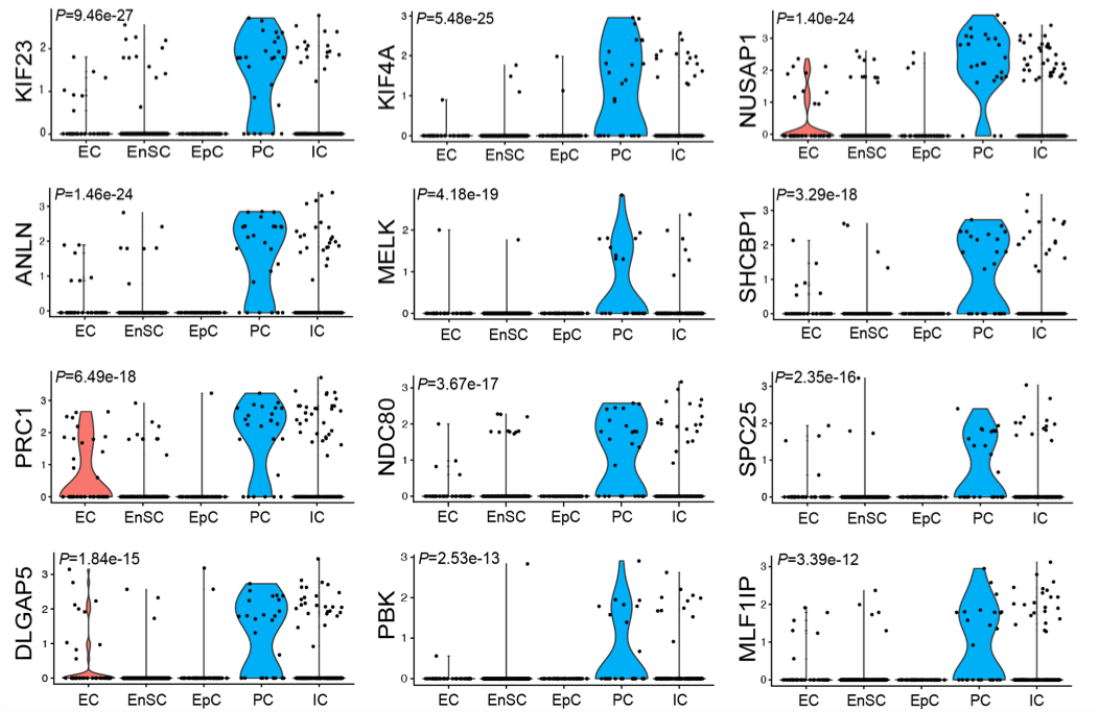

Figure 4.4. Transcriptome profile of PC in mid luteal endometrial samples. Violin plots showing log-transformed, normalized expression levels for the PC top markers in cells at G2/M across clusters. Bonferroni adjusted P-values shown on top left corner of each plot for the expression of each gene in PC when compared to the other clusters.

Table 4.2. Genes enriched in PC at G2M

Gene	Gene name	Fold Change	Adjusted P value
TOP2A	DNA Topoisomerase II Alpha	141.63	9.43E-23
MKI67	Marker of Proliferation Ki-67	82.15	4.45E-19
NUSAP1	Nucleolar and Spindle Associated Protein 1	81.63	1.40E-24
ANLN	Anillin	37.45	1.46E-24
KIF4A	Kinesin Family Member 4A	34.63	5.48E-25
PRC1	Protein Regulator of cytokinesis 1	33.46	6.49E-18
KIF23	Kinesin Family Member 23	29.55	9.46E-27
SHCBP1	SHC Binding and Spindle Associated 1	22.50	3.30E-18
NDC80	Kinetochore-Associated Protein 2	18.09	3.67E-17
DLGAP5	Disks Large-Associated Protein 5	15.46	1.84E-15
MLF1IP	Centromere protein U	12.92	3.39E-12
TYMS	Thymidylate Synthetase	12.06	2.00E-14
TK1	Thymidine Kinase 1	11.22	5.38E-15
MELK	Maternal Embryonic Leucine Zipper Kinase	10.44	4.18E-19
HJURP	Holliday Junction Recognition Protein	9.86	2.11E-16
PBK	PDZ Binding Kinase	9.77	2.53E-13
SPC25	Kinetochore Protein Spc25	8.35	2.35E-16
RRM2	Ribonucleotide Reductase Regulatory Subunit M2	5.85	1.83E-05
BRIP1	BRCA1-Associated C-Terminal Helicase	5.29	3.29E-12

4.2.3 Anillin$^+$ cells in the peri-implantation endometrium

Immunohistochemistry (IHC) was performed to assess the spatiotemporal distribution of anillin$^+$ cells in the endometrium throughout the luteal phase. A total of 61 LH-timed biopsies were analysed and divided in three groups depending on the timing of the sample: Group 1 (LH+6/7, n = 20), Group 2 (LH+8/9, n = 24), and Group 3 (LH+10/11, n = 17). The demographic characteristics of the samples are summarized in Supplementary Table 5. Initial analysis revealed that anillin$^+$ cells are present not only in the stroma but also in glandular and luminal epithelium. Thus, quantification of anillin$^+$ cells was performed separately for each of the 3 endometrial compartments. As shown in Figure 4.6, anillin-labelled cells are scarcely dispersed throughout the stroma although they appeared more abundant around the terminal spiral arteries; i.e. in the perivascular niche where eMSC also reside (Masuda *et al*, 2012) (Fig. 4.5A). Rare anillin$^+$ cells were also observed in endometrial glands and in luminal epithelial (Fig. 4.5 B and C). The average (± SEM) abundance of anillin$^+$ cells in this compartment across all timepoints was 2.06 ± 0.6 % versus 1.63 ± 0.6 % in glandular epithelium. By contrast to glandular or luminal epithelium, the abundance of anillin$^+$ cells increased significantly in the stroma upon progression of LH+6/7 to LH+10/11 (Fig. 4.5 D-F). Figure 4.6A shows the relative distribution of anillin$^+$ cells in stromal, glandular and luminal epithelium in each biopsy. Across all timepoints, the stroma compartment harboured on average significantly more (72.5 ± 3 %) when compared to either the glandular compartment (14.3 ± 2 %) or luminal epithelium (14.6 ± 1.7 %) (P < 0.05, Mann Whitney test). Additionally, figure 4.6B-D shows that the quantification of anillin$^+$ cells is significantly correlated between the three different compartments. The stroma and the luminal epithelium have the weakest correlation (r = 0.4, P = 0.002; Figure 4.6C) compared to glandular epithelium and stroma or luminal epithelium (r = 0.7, P < 0.0001; Figure 4.6 B and D).

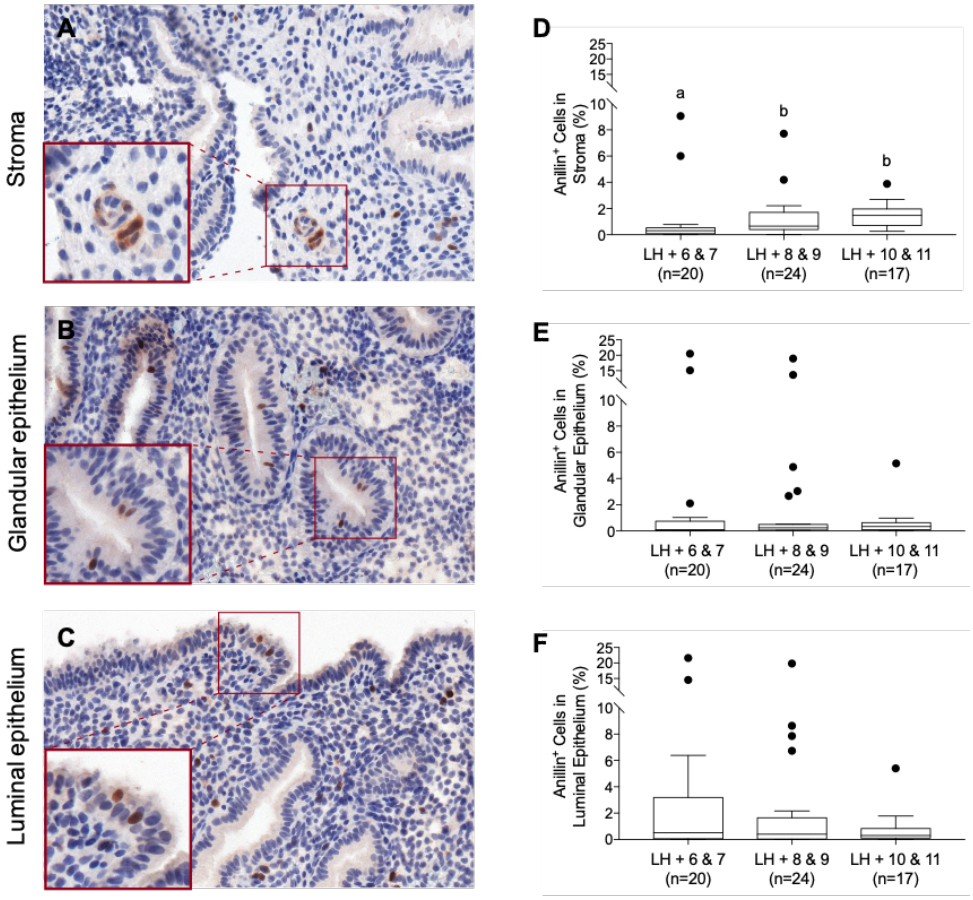

Figure 4.5. Anillin$^+$ cells in peri-implantation endometrium. (A-C) Anillin immunohistochemistry in stroma, glandular and luminal epithelium. (D-F) Quantification of Anillin$^+$ cell density in endometrial biopsies obtained from 5 to 12 days after the LH-surge. Different letters above the box plots indicate that groups are significantly different from each other at $P < 0.05$. Group comparison by one-way ANOVA on ranks (Kruskal-Wallis) test.

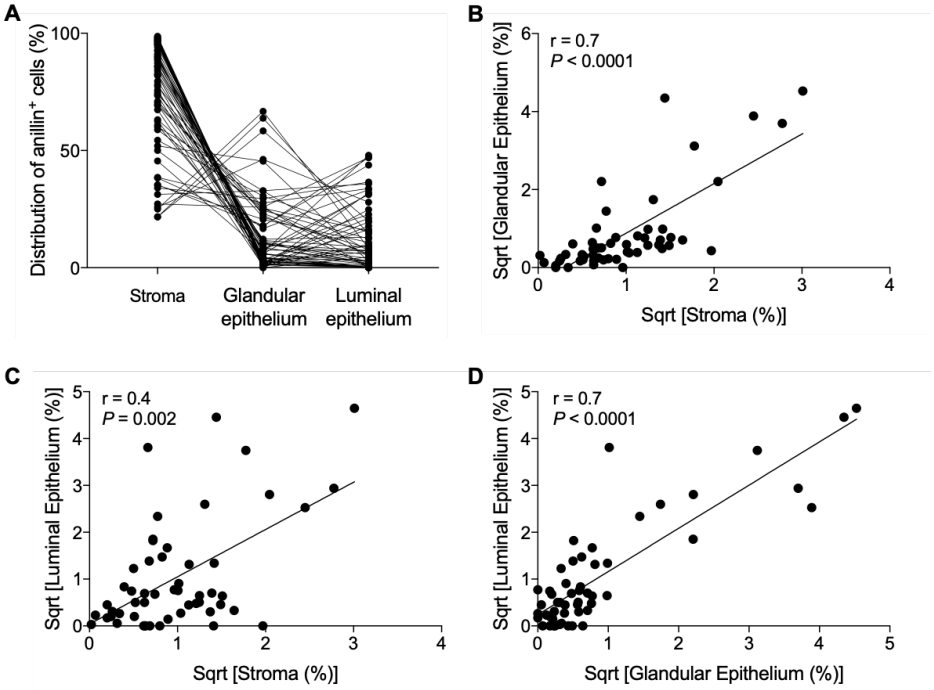

Figure 4.6. Correlation of anillin$^+$ cell between compartments. (A) Distribution of anillin$^+$ cell density quantified by IHC in different endometrial compartments. (B) Spearman's rank correlation of anillin immunohistochemistry in stroma and glandular epithelium. (C) Spearman's rank correlation of anillin immunohistochemistry in stroma and luminal epithelium. (D) Spearman's rank correlation of anillin immunohistochemistry in glandular and luminal epithelium. Raw data was square root (sqrt) transformed to reduce left skewness.

In parallel with IHC, the expression of *ANLN* was analysed in whole tissue samples by RT-qPCR. Interestingly, *ANLN* mRNA levels correlated positively with the relative abundance (%) of anillin$^+$ cells in both the stromal compartment and glandular epithelium (r = 0.33, P = 0.01, test; Fig. 4.7A and B). Further, *ANLN* gene expression also showed a positive trend with anillin$^+$ cells in luminal epithelium, although this association was not statistically significant (r = 0.25, P = 0.08, test; Fig. 4.7C).

Taken together, anillin$^+$ cells are present throughout the endometrium during the luteal phase. They are enriched around the spiral arteries and rare cells are scattered throughout the stroma, glands and luminal epithelial. The relative abundance of anillin$^+$ cells in endometrial glands and luminal epithelium does not change during the luteal phase of the cycle whereas more and more cells accumulate in the stroma in a time-dependent manner.

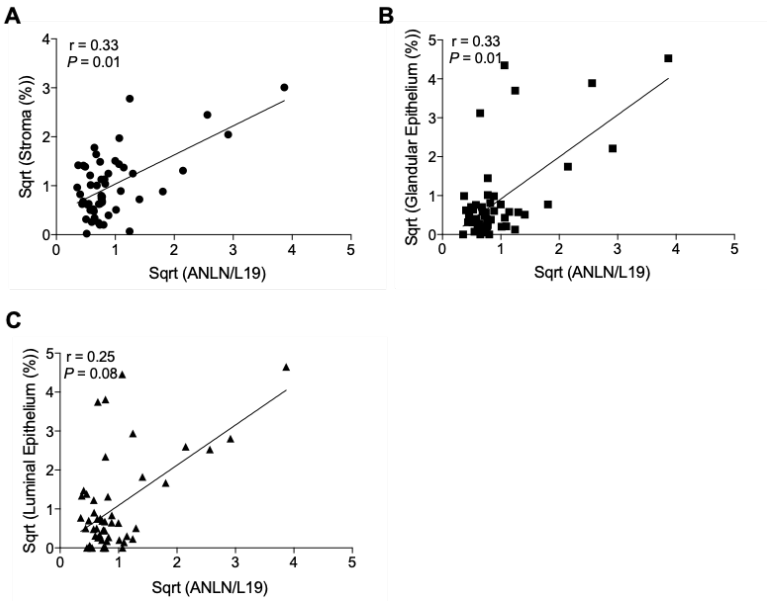

Figure 4.7. Comparison between histochemistry and RT-qPCR analysis for ANLN expression. (A) Spearman's rank correlation of *ANLN* expression in whole tissue RT-qPCR and immunohistochemistry in stroma. (B) Spearman's rank correlation of ANLN expression in whole tissue RT-qPCR and immunohistochemistry in glandular epithelium. (C) Spearman's rank correlation of ANLN expression in whole tissue RT- qPCR and immunohistochemistry in luminal epithelium. Raw data was square root (sqrt) transformed to reduce left skewness.

4.2.4 Immune cells contribute to the anillin$^+$ cell population in endometrial stroma

Anillin marks both proliferating and migratory cells (Chuang *et al*, 2014; Tian *et al*, 2015). The transition of mid- to late-luteal phase coincides with influx of proliferating uNK cells and macrophages (Pace *et al*, 1989; Starkey *et al*, 1991), which potentially accounts for the time-dependent increase in anillin$^+$ cells in the stroma. To investigate this possibility, double-labelling immunofluorescence microscopy was used to quantify co-expression of anillin with CD163 and CD56, a macrophage and uNK cell markers, respectively (Fabriek *et al*, 2005; Brighton *et al*, 2017). Also, to assess the contribution of leukocyte precursors, the abundance of anillin$^+$ cells co-expressing the common hematopoietic stem cell marker CD34 was also quantified (Berenson *et al*, 1988).

Quantitative double-labelling immuno-fluorescence microscopy was performed on a total of 18 biopsies obtained on LH+7 (n=6), LH+9 (n=6) and LH+11 (n=6), representing early-, mid-, and late-luteal phase endometrium, respectively. The

demographic characteristics of the samples are summarized in Supplementary Table 6. For each biopsy, 5 randomly chosen high-power fields were analysed. Representative images are shown in Figure 4.8A-C. On LH+7, the median proportion of anillin$^+$ cells co-expressing CD34, CD163 or CD56 was 24.9%, 12% and 0%, respectively (Fig. 4.8D-E). However, as the menstrual cycle progresses the overall abundance of anillin+ cells increases but the contribution of proliferating CD34 hematopoietic progenitor cells decreases significantly to 11.51%. In fact, the increase in anillin$^+$ cell population was entirely accounted for by the significant expansion of anillin$^+$/CD163$^+$ macrophages and anillin$^+$/CD56$^+$ uNK cells in the stroma (Fig. 4.8 E and F).

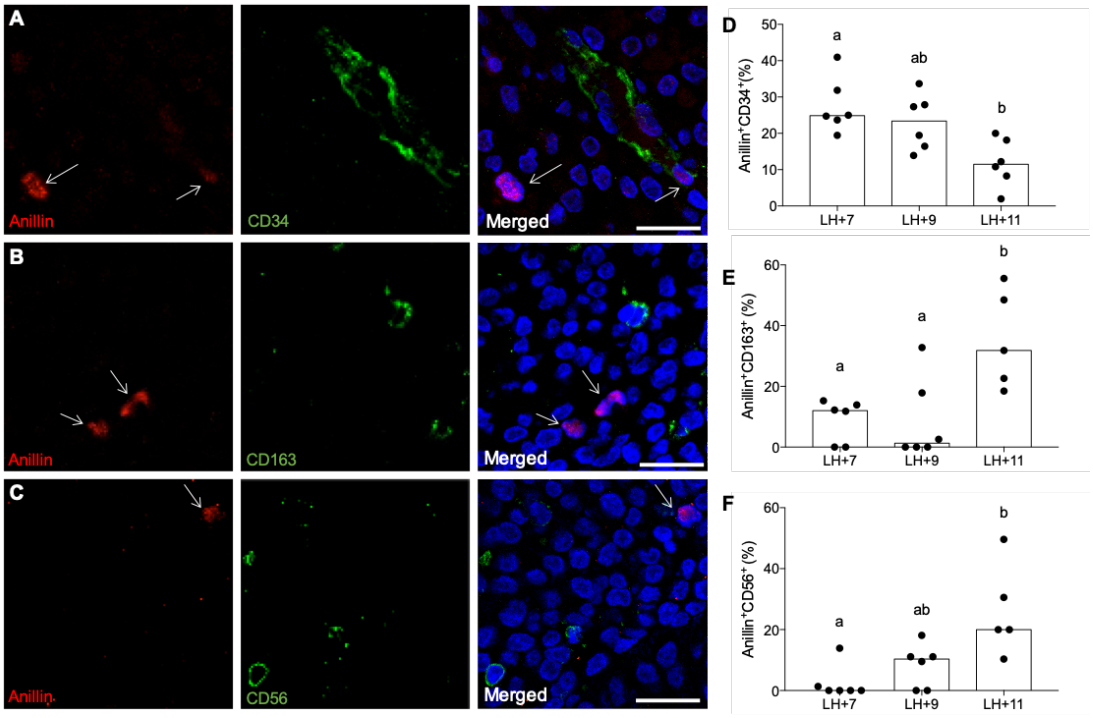

Figure 4.8. Localization analysis of anillin vs hematopoietic and immune markers. (A) Immunofluorescence of anillin vs hematopoietic stem cells (B) Immunofluorescence of anillin vs macrophages (C) Immunofluorescence of anillin vs uNK cells. Arrows indicate anillin$^+$ cells. Scale bar = 20μm. (D-F) Quantification of double stained cells for each cell surface marker in midluteal endometrial biopsies obtained 7, 9 and 11 days after the LH surge, representing the early, mid and late luteal phases, respectively (n=6 per timepoint). Bar charts show the median from six independent biopsies per timepoint. Different letters above the bars indicate that groups are significantly different from each other at $P < 0.05$. Group comparison by one-way ANOVA on ranks (Kruskal-Wallis) test.

4.2.5 The abundance of anillin$^+$ cells *in vivo* correlates with endometrial clonogenicity

To explore the possibility that anillin marks mesenchymal progenitor cells, I established paired clonal assays and standard primary EnSC cultures from 3 individual endometrial biopsies. The relative abundance of anillin$^+$ cells was quantified using immunofluorescence microscopy after 7 days in culture. As shown in Figure 4.9A, the abundance of anillin$^+$ cells in standard cultures was 1.7% (median) versus 17% in clonal assays ($P < 0.05$, Mann-Whitney test). I reasoned that culturing may lead to progressive loss of the proliferative capacity of MSC. To test this hypothesis, abundance of anillin$^+$ cells was quantified using immunofluorescence microscopy in CFU assays after 3, 6 or 9 days in culture. Notably, the abundance of anillin$^+$ MSC after 3 days was 68% (median). By day 9, this had dropped significantly to 15% (median) ($P < 0.05$, one-way ANOVA on ranks test).

Next, I examined if the abundance of anillin$^+$ cells *in vivo* is a marker of endometrial clonogenicity. To test this conjecture, CFU assays were established from 47 endometrial biopsies and, in parallel, the abundance of anillin$^+$ cells in the stromal compartment was quantified using immunohistochemistry. Figure 4.10A depicts the design of the analysis and the demographic characteristics of the samples are summarized in Supplementary Table 7. An unexpectedly strong correlation was observed between the abundance of anillin$^+$ stromal cells *in vivo* and CFU activity of isolated EnSC *in vitro* ($r = 0.5$, $P = 0.0004$, test; Fig. 4.10B).

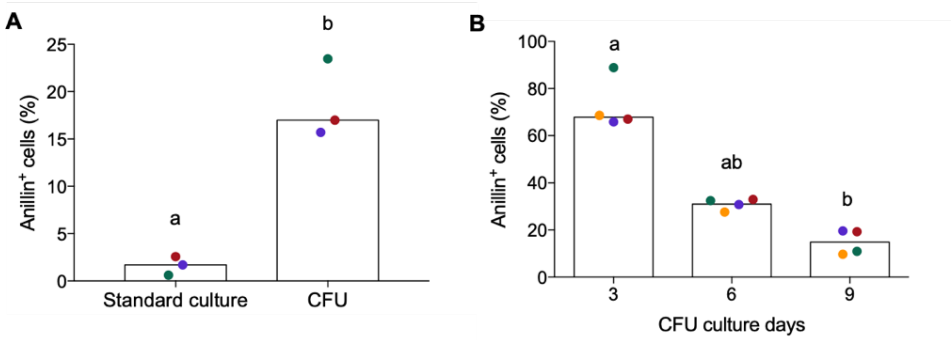

Figure 4.9. Anillin expression in clonogenic populations. (A) Percentage of anillin$^+$ cells in stromal standard cultures and CFUs after 7 days in culture. Bar charts show median in three independent primary cultures and matched CFU assay. Mann Whitney test was used. (B) Percentage of anillin$^+$ cells in colonies at day 3, 6 and 9 of culture. Bar charts show median in four independent CFU assays. Group comparison by one-way ANOVA on ranks (Kruskal-Wallis) test.

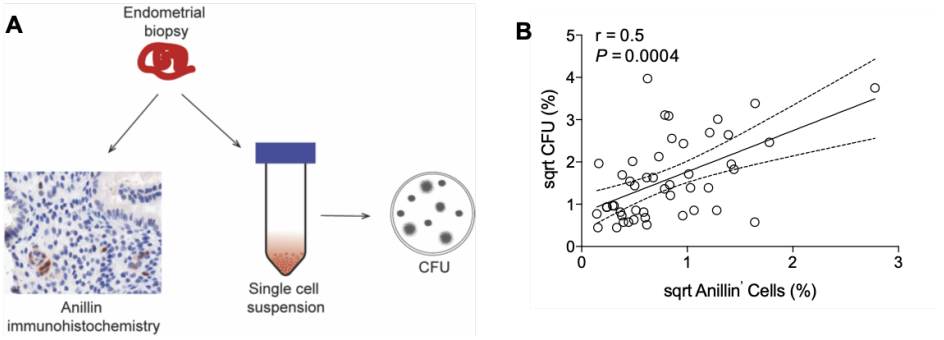

Figure 4.10 Anillin staining versus clonogenic populations. (A) Schematic workflow for anillin IHC and CFU analysis from the corresponding biopsy. (B) Spearman's rank correlation of anillin immunohistochemistry in the stroma compartment and CFUs from corresponding biopsy.

4.2.6 A shared gene signature in PC *in vivo* and clonal MSC *in vitro*

The lack a specific cell surface marker precluded isolation and direct characterization of PC. Hence, I compared the transcriptome profile of PC *in vivo* to the gene signatures obtained from different cultured stromal subpopulations (i.e. eMSC, TA, PVC and EnSC) as described in Chapter 3. The scRNA-seq profiles of EnSC and EC *in vivo* were also integrated in this analysis.

As shown in Figure 4.11, both eMSC and TA express proliferation markers that match the PC profile. This proliferation signature included multiple genes that reportedly play critical roles in cancer stem cells (e.g. *PBK*, *NUSAP1*, *MELK*, *CDC20* and *ASPM*) (Li *et al*, 2019; Dougherty *et al*, 2005; Ren *et al*, 2019, Bikeye *et al*, 2010). Apart from the proliferation markers, genes highly enriched in eMSC and TA cells were also enriched in either PC or EC *in vivo*. *ALDH1L1*, encoding aldehyde dehydrogenase 1 family member L1, and *CD109* are putative biomarkers of cancer stem-like cells (Douville *et al*, 2009; Emori *et al*, 2013) whereas profilin 2 (*PFN2*) promotes migration, invasion and stemness of HT29 human colorectal cancer stem cells (Kim *et al*, 2015). Matrix metallopeptidase 16 (*MMP16*) controls the migration of human cardiomyocyte progenitor cells (Liu *et al*, 2012). Intriguingly, eMSC, and to a lesser extend TA cells, also express a endothelial-like gene signature, although non correspond to known endothelial cell markers. Genes in this signature, such as *SKP2*, *ITGA8*, *SLIT2* and *SOX9*, have been shown to be involved in different stem/progenitor cell niches (Polisetti *et al*, 2015; Wang *et al*, 2014; Shibata *et al*, 2009; Kadaja *et al*, 2014).

In addition, PC is enriched in genes implicated in stem cells function were identified to be differentially expressed in PC (e.g. *POU2F1*, *CXCR4* and *KIT*). *POU2F1*, also known as *OCT1*, although less characterized than its paralogous gene *OCT4*, has been described as a normal and cancer stem cell determinant and a stem cell marker (Maddox *et al*, 2012). The expression of the receptors CXCR4 and c-kit by PC and their corresponding ligands, CXCL12 and stem cell factor (encoded by *KITLG*), by stromal and endothelial cells, respectively, are indicative of the presence of paracrine stem cell regulating signalling pathways. Taken together, the transcriptomic analysis provided additional evidence of the kinship between PC in vivo and eMSC/TA cells *in vitro*. Interestingly, cultured eMSC/TA cells also express marker genes of EC *in vivo*, which are silenced in PC.

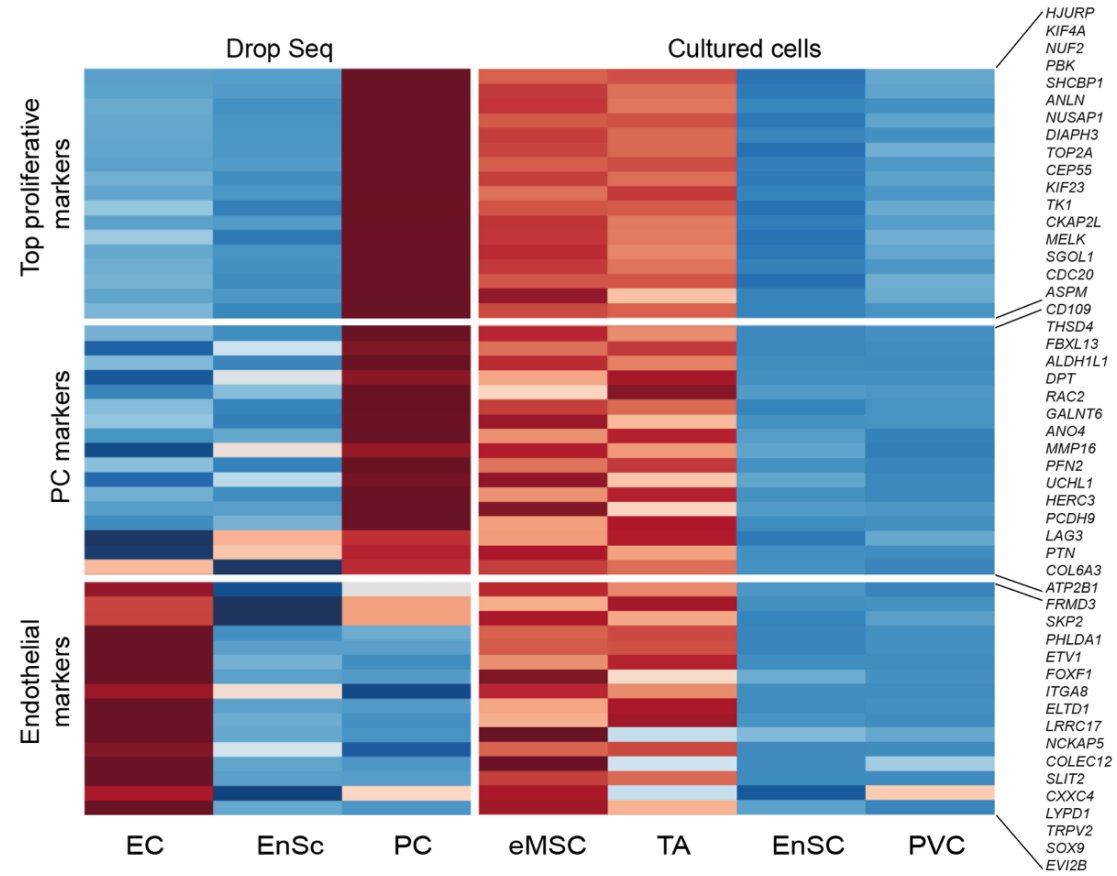

Figure 4.11. Comparison between PC and cultured stromal subpopulations. Side by side heatmap analysis of top markers previously identified through RNA-seq in cultured endometrial mesenchymal stem cells (eMSC) and transit-amplifying cells (TA) vs endometrial stromal cells (EnSC) and perivascular cells (PVC) and the gene expression levels identified through scRNA-Seq *in vivo* endothelial (EC), stromal (EnSC) and proliferative cells (PC). Expression for each gene is scaled (*z*-scored) across clusters and stromal subsets. Red and blue represent high or low expression of a given marker gene, respectively.

4.2.7 Quantification of anillin$^+$ cells in midluteal biopsies from RPL patients

Previously, it has been reported that RPL is associated with a deficiency in eMSC as assessed by CFU assays (Lucas *et al*, 2016). However, the lack of specific markers precluded *in situ* analysis of eMSC in tissue samples. Here, I demonstrated that the anillin$^+$ cells in the endometrial stroma correlate significantly with the CFU activity of freshly isolated EnSC. Hence, I examined if RPL is associated with loss of non-hematopoietic anillin$^+$ cells during the midluteal implantation window. To mitigate against interference of anillin$^+$ immune cells, the analysis was restricted to endometrial biopsies obtained on LH+7 from control (n = 15) and RPL (n = 15) patients. The demographic characteristics of the samples are summarized in Supplementary Table 8. Each tissue section was double-labelled for CD34 and anillin in order to distinguish between stromal and hematopoietic stem cells. The samples were blinded to the clinical diagnosis and abundance of anillin+ cells, anillin$^+$/CD34$^+$ cells and anillin$^+$/CD34$^-$ cells quantified in 3 randomly chosen high-power fields (magnification: 20X). As shown in Figure 4.12, RPL appeared to be associated with an overall reduction in the abundance of anillin$^+$ stromal cells, although this observation was not statistically different (P = 0.08, Mann-Whitney test). However, there was a significant reduction anillin$^+$/CD34$^-$ cells in RPL patients compared to control subjects (69% versus 84%, respectively; $P < 0.05$, Mann-Whitney test). Intriguingly, this reduction anillin$^+$/CD34$^-$ cells corresponded to a reciprocal increase in anillin$^+$/CD34$^+$ cells (31% versus 19%, respectively; $P < 0.05$, Mann-Whitney test). Taken together, the data suggest that RPL is associated with an imbalance in endometrial mesenchymal / hematopoietic progenitor populations.

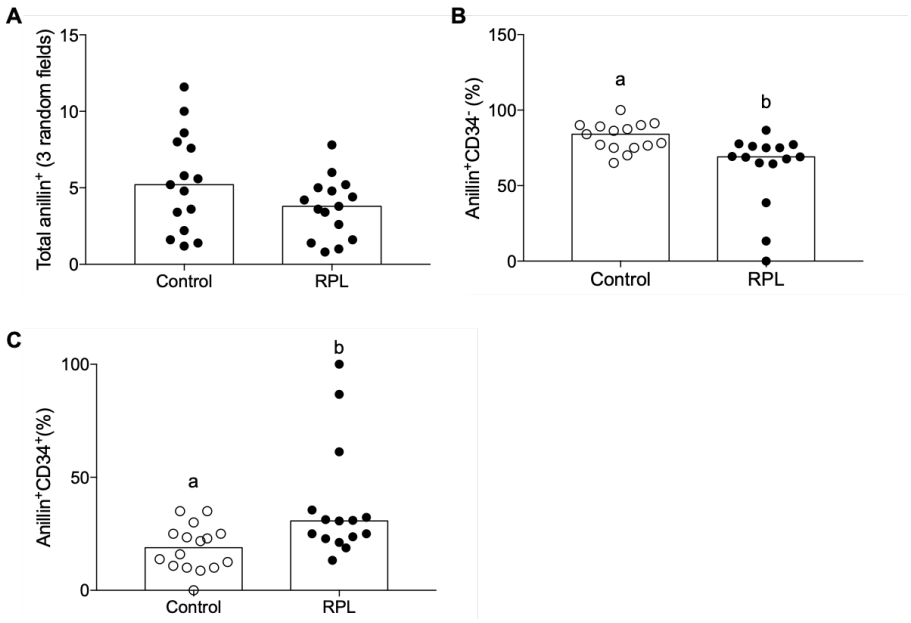

Figure 4.12 Anillin$^+$ cells in control and recurrent pregnancy loss (RPL) patients. (A) Mean of 3 random high-power fields was calculated per sample and analysed per group (control versus RPL). (B) Percentage of anillin$^+$/CD34$^-$ cells was quantified over the total number of anillin$^+$ cells in in control and recurrent pregnancy loss (RPL) patients. (C) Percentage of anillin$^+$/CD34$^+$ cells was quantified over the total number of anillin$^+$ cells in in control and recurrent pregnancy loss (RPL) patients. Mann Whitney test was used. Different letters above the bars indicate that groups are significantly different from each other at $P < 0.05$.

4.3 Discussion

Previously in Chapter 3, the interpretation of endometrial heterogeneity and characterization of stem/progenitor cell populations was tackled by the combination of cell culture, bulk RNA-seq and computation deconvolution, yielding to the identification of a switch in the cell type proportions during the luteal phase of the cycle and the description of a list of cell surface proteins and transcription factors expressed in eMSC. However, it was also demonstrated that *in vitro* cell propagation introduces modifications in the transcriptomic profile and hinders the identification of *in vivo* cell markers.

In this Chapter, single-cell transcriptomic analysis was applied to freshly isolated cells from luteal-phase endometrial biopsies. Apart from the main stromal population, the analysis also highlighted the cellular complexity of endometrial glands, including transcriptional characterization of ciliated epithelial cells. Within the immune compartment, 3 uNK cell states were identified corresponding to the different decidual NK cell subsets recently identified by single-cell analysis in early pregnancy (Vento-Tormo *et al*, 2018). Additionally, it was identified a discrete population of highly proliferative mesenchymal cells. This subpopulation, termed PC, was further investigated.

Anillin was used as a putative marker of PC in midluteal cells. I demonstrated that anillin also marks proliferating immune cells, i.e. macrophages and uNK cells, especially in the late-luteal phase. Further, a proportion of anillin^{+} cells co-expressed CD34, indicative of hematopoietic progenitor cells. Despite these shortcomings, several lines of evidence indicated that anillin also included eMSC/TA cells.

First, highly proliferating cells are widely implicated in the proliferation and self-renewal of progenitor cells of different systems (Nakano et al, 2005; Majewski et al, 2010; Dougherty et al, 2005). Adult stem cells are maintained in a quiescent state but are able to exit quiescence and rapidly expand and differentiate (Li and Bhatia, 2011). In fact, highly proliferative cells are commonly associated to progenitor cells and tissue regeneration (Ranger-Huerat and Maldonado, 2017). For example, in the human vascular system endothelial progenitor cells with high proliferative rate had the ability to form vascular tubules in vitro in a stromal supported co-culture assay (Watt *et al*, 2010). Also, recently, a proliferative trophoblast progenitor cell population was identified at the base of the cytotrophoblast in first trimester placentas

contributing to the villous cytotrophoblast and extravillous cytotrophoblast cell layer (Lee *et al*, 2018).

Unfortunately, the lack of specific cell surface markers in the PC population restricted the direct access to these cells. This absence could be due to a technical issue since even for the most sensitive scRNA-seq protocols, it is frequent that some specific transcripts cannot be detected (termed dropout events) (Haque *et al*, 2017; Chen *et al*, 2019). On the other hand, this is not the first time that it was noted a lack of specific surface markers associated to a putative stem/ progenitor population. Ishibashi and colleagues (2016) reported that when comparing chondrocytes with different proliferation rates, the cell group with the higher rate presented a higher chondrogenic ability, showed somatic stem cell-like characteristics but did not express a specific surface marker. Also, stem cells from human exfoliated deciduous teeth have high proliferation potency and present MSC characteristics but no specific surface marker (Sukarawan and Osathanon, 2017). Hence, the lack of specific surface markers might be a characteristic of the high proliferation profile of an intermediate (transit) cell population in a tissue.

As a second line of evidence, it was demonstrated that anillin$^+$ cells are present in the stroma and epithelium. Additionally, it was also observed a positive correlation between the abundance of anillin$^+$ cells in both compartments. This result supports the hypothesis that both subpopulations are originated from one common source of cells that proliferate and differentiate into various cell types (Figueira *et al*, 2011). Corroborative bone marrow transplant studies in human and mice showed the participation of bone marrow-derived stem cells in the repopulation of endometrial stroma and glands (Taylor, 2004; Taylor and Du, 2007; Ikoma *et al*, 2009).

Third, double-labelling experiments allowed to discern that at the timepoint LH+7, 63% (median) of anillin$^+$ cells correspond to mesenchymal cells. The increase of anillin$^+$ cells in the stromal compartment towards the end of the cycle was explained by the influx of proliferative immune cells, *i.e.*, macrophages and uNK cells.

Fourth, the expression of anillin was identified in clonogenic populations. Clonogenic assays showed that anillin$^+$ cells are present in 68% of cells that form a colony by day 3 of culturing. Additionally, these cells are also in higher abundance in colonies than in standard monolayer cultures. Furthermore, the quantification of anillin$^+$ cells in the stroma compartment presents a strong correlation to the cloning efficiency of

endometrial stem/progenitor cells, showing that anillin could be used as a marker of clonogenicity.

However, the identity of these endometrial mesenchymal anillin^{+} cell was still unclear. Therefore, the transcriptomic profile of PC from scRNA-seq data was compared to the transcriptome of cultured stromal populations, *i.e.,* eMSC, TA, PVC and EnSC, described in the previous chapter. Thus, as the fifth line of evidence, it was demonstrated that PC shares part of its gene signature with the clonogenic populations, eMSC and TA. Further examination of the data showed that PC is associated with stem cell function genes, such as, *POU2F1*, *CXCR4* and *KIT* (Miller *et al,* 2008; Maddox *et al*, 2012; Lennartsson and Lars Rönnstrand, 2012).

Ultimately, the aim was to find a connection to translational medicine. Anillin^{+} cells were segregated in non-hematopoietic (CD34^{-}) and hematopoietic stem cells (CD34^{+}) and quantified on LH+7 samples from control and RPL patients. Here, I showed that RPL is associated with a reduction of anillin^{+}CD34^{-}, which links with previous findings that this clinal phenotype is associated with a depletion of eMSC (Lucas *et al*, 2016).

For the first time, scRNA-seq allowed the identification of a putative endometrial progenitor cell population and corresponding candidate intracellular marker, anillin, in peri-implantation endometrial biopsies. It was demonstrated that not only anillin correlates with the cloning efficiency, as it also represents the deficiency of eMSC in the RPL group. This study brings a new insight into the endometrial stem/progenitor cell biology and the identification of a marker that in the future could be used for the analysis of clinical samples.

Chapter 5

Single-nucleus RNA-seq:

Optimization of the technique for human endometrial samples

5.1 Introduction

The field of single cell transcriptomics has become a fundamental tool in the identification of new cell types, cell states and regulatory networks between different populations. For *in* vivo samples, the success of scRNA-seq starts with dissociation of tissue into intact and viable cells (Nguyen *et al*, 2018). However, single cell suspensions must be prepared from freshly obtained tissue, which is a major hurdle to assess clinical samples, archived materials and tissues that cannot be readily dissociated (Habib *et al*, 2017). Enzymatic dissociation can be particularly problematic for certain tissues (e.g. brain and kidney) affecting the integrity of the RNA and introducing artefactual transcriptional stress responses (Habib *et al*, 2017; Wu *et al*, 2019). An alternative to these cases is to lyse and dounce homogenize the tissue in order to isolate intact nuclei for single-nucleus RNA sequencing (snRNA-seq) (Nguyen *et al*, 2018).

In contrast to scRNA-seq, snRNA-seq offers not only the possibility to handle complex tissues that cannot be dissociated, but also unique access to archived tissues such as flash-frozen and stored clinical samples (Nguyen *et al*, 2018). Comparative studies of scRNA-seq and snRNA-seq in matched cortical cell types demonstrated that although more transcripts are detected in individual whole cells than nuclei, closely related neuronal cell types can be similarly discriminated with both methods (Bakken *et al*, 2018). In adult kidney, single-cell and single-nucleus platforms presented equivalent gene detection sensitivity, but snRNA-seq captured a diversity of kidney cell types that were not represented in the scRNA-seq (Wu *et al*, 2019). This difference was due to cell-enriched genes involved in mitochondria, ribosome and heat shock response genes, while nuclei-enriched genes predominantly encoded drivers of cell identity, such as solute carriers, transcription factors, and long noncoding RNA (Wu *et al*, 2019). Single-cell and nuclei RNA sequencing of 3T3 cells detected an average of 5,134 and 3,295 genes for cells and nuclei, respectively with a high correlation (Pearson, r = 0.87) for average expression profile (Habib *et al*, 2017). Together these results suggest that the relative transcript profile between cells and nuclei is highly correlated but still dependent on tissue-type.

Different snRNA-seq methods have been developed recently (Habib *et al*, 2016, Lake *et al*, 2016) including the DroNc-seq technology, which is a modification of Drop-seq that combines the advantages of snRNA-seq and droplet microfluidics to profile nuclei at low cost and high throughput (Figure 5.1; Habib *et al*, 2017). Briefly, after tissue

dissociation and nuclei isolation, each nucleus is co-encapsulated with a distinct barcoded microparticle (bead) in a nanoliter-scale droplet. At this stage, the nuclear membrane is lysed and the mRNA binds to the primers on the microparticle. The mRNA is reverse transcribed into cDNA, which is then amplified, tagmented and sequenced (Macosko *et al*, 2015; Habib *et al*, 2017).

Previously, scRNA-seq was used to profile the transcriptome of fresh endometrial biopsies. However, due to the limitations of this technique, it is essential to investigate whether snRNA-seq can be a viable alternative for archived endometrial samples. In that case, snRNA-seq would become a valuable tool for prospective studies, in which the clinical outcome is only known months apart from the initial sample collection. Therefore, this chapter focuses on optimization of the snRNA-seq process for archived endometrial samples. All single nuclei transcriptome studies were performed using the DroNc-seq platform (Habib *et al*, 2017).

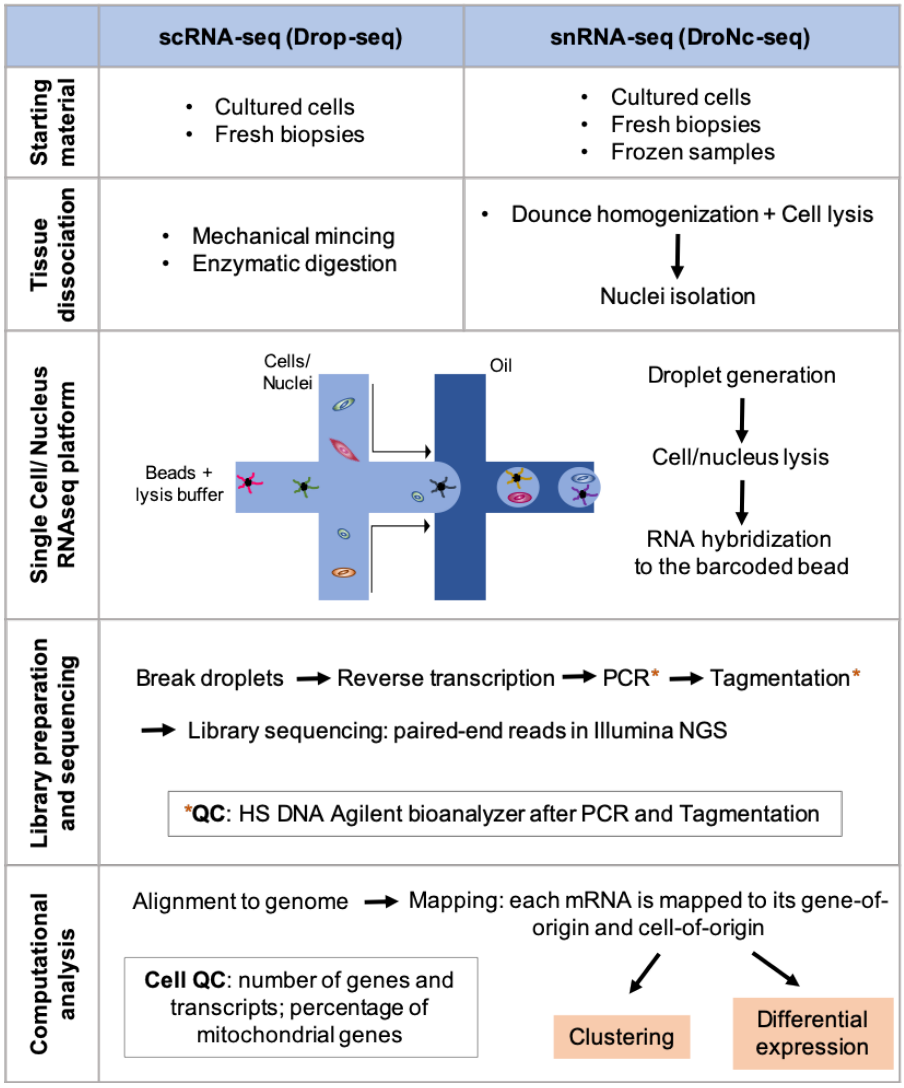

Figure 5.1. Schematic workflow of single-cell and single-nucleus analysis. Although sample preparation is different for both techniques, the following procedure is similar. A microfluidic device connects two aqueous flows (cells/nucleus and barcoded primer beads suspended in a lysis buffer) before their encapsulation into discrete droplets. The cell/nucleus is lysed and the mRNA binds to the primers on the microparticle. The droplets are broken and the microparticles collected and washed. The mRNA is reverse transcribed into cDNA, which is then amplified, tagmented and sequenced. Quality control (QC) steps are important to check library quality. For the computational analysis, the reads are first aligned to a reference genome to identify the gene-of-origin and then organized by their cell barcodes. Multiple transcriptomic analysis can be performed to inform cell heterogeneity through cell clustering and differential expression analysis.

5.2 Results

5.2.1 Nuclei isolation from snap-frozen and RNAlater preserved tissue

The biological material for snRNA-seq can either be cultured cells or tissue that was previously preserved in RNAlater or snap-frozen (Habib *et al*, 2017). The first step in this study was to compare the nuclei isolation process between snap frozen and RNA-later preserved endometrial tissue. Both methods are known to stabilize RNA, although snap-frozen tissues require rapid homogenization to avoid the fast RNA degeneration that occurs during thawing (Mutter *et al*, 2004), whereas RNAlater solution inactivates RNases and stabilizes RNA within tissues or cells, thus providing some protection during processing. The sample can then be stored indefinitely at -80°C.

In parallel, two pieces of tissue from the same patient, each preserved by a different method, were dounce homogenised in Nuclei EZ lysis buffer and the resulting nuclei were stained with DAPI. As shown in Figure 5.2, nuclei isolated from the RNAlater preserved sample presented clumps of nuclei and debris due to insufficient tissue lysis. In contrast, snap-frozen tissue was readily dissociated into a single nuclei solution (Figure 5.2). The presence of clumps makes the scRNA system more prone to clogging events during droplet generation and might interfere with data interpretation.

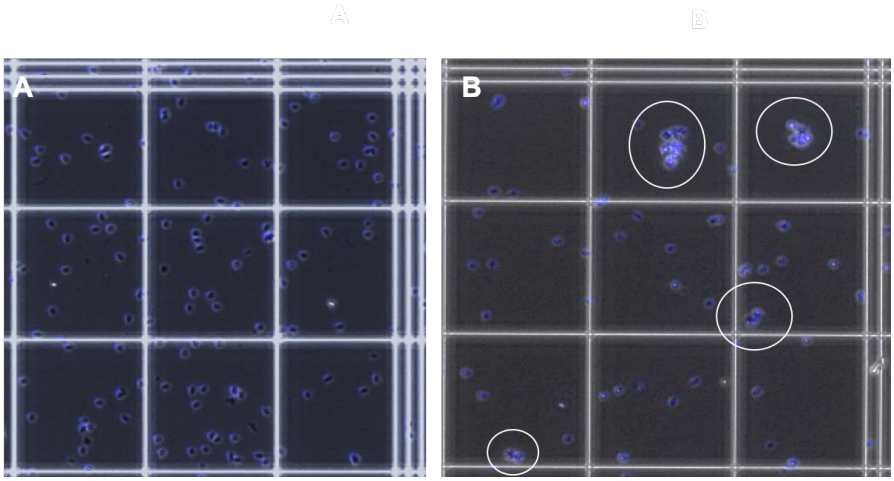

Figure 5.2. Nuclei isolation from snap-frozen and RNAlater preserved endometrial tissue. (A) Representative phase contrast image of DAPI stained nuclei isolated from snap frozen tissue. (B) Representative phase contrast image of DAPI stained nuclei isolated from RNA later preserved tissue.

Both nuclei preparations were used for droplet generation on the scRNAseq system and samples were processed until tagmentation. Figure 5.3 shows the bioanalyzer traces from an example, the RNAlater and the snap-frozen tissue. An ideal tagmented library should be fairly smooth, with an average bp size of 500-680 bp. Although none of the libraries were similar to the example, the snap-frozen sample presented the most uniform and reliable bioanalyzer trace for sequencing (Figure 5.3). Taking into consideration the tissue dissociation efficiency and the final library quality, the following experiments were performed using snap-frozen tissue.

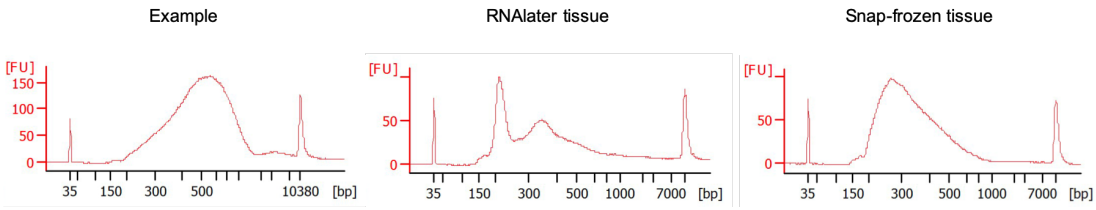

Figure 5.3. Bioanalyzer High Sensitivity DNA traces of tagmented libraries. From left to right are presented the traces for an ideal example, RNAlater and snap-frozen samples. The example trace was obtained from an in-house snRNA-seq experiment with cultured endometrial cells.

5.2.2 Modifications in lysis buffer

Tagmented library from the snap frozen tissue presented in the previous section was sequenced and analysed. As part of the data analysis workflow nuclei were filtered based on quality control (QC) metrics such as number of genes, number of transcripts and percentage of mitochondrial genes (Figure 5.4 A). While the scRNA-seq experiment from the previous chapter had an average of 1,284 genes per cell, the snRNA-seq had an average of 296 genes per nuclei. As expected, the percentage of mitochondrial genes was markedly lower when compared to whole cells. After initial quality filtering, a total of 1929 single nuclei were computationally assigned to the two main endometrial cell types, EpC and EnSC (Figure 5.4 B). Unexpectedly, the proportion between cell types was biased towards the epithelial compartment comprising 94.3% of total number of nuclei. In addition, it was not possible to identify immune or endothelial cells.

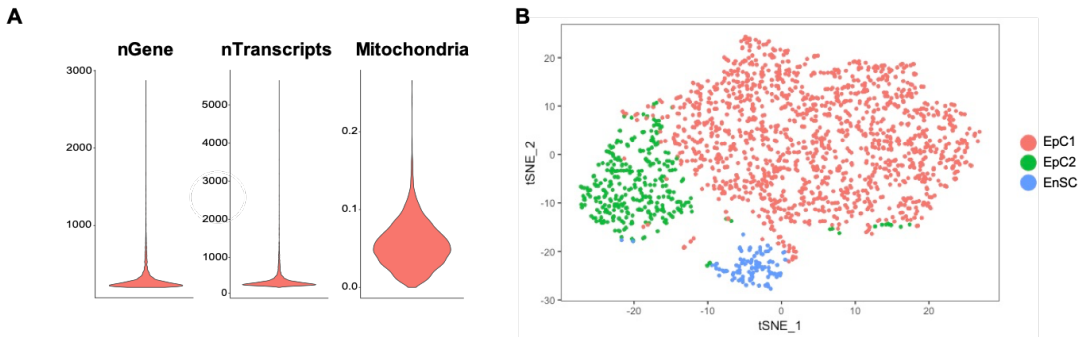

Figure 5.4. snRNA-seq with 0.2% lysis buffer. (A) Violin plots of number of genes, number of UMI and percent of mitochondrial genes per cell. Cells were included for further analysis if their number of genes ranged from 200 to 1500 and their proportion of mitochondrial genes did not exceed 5%. (B) t-SNE plot of 1928 nuclei from a mid-luteal biopsy captured the two main endometrial cell types, EpC and EnSC.

Previously, it has been described that for proper cell and nuclear membrane lysis, different buffers should be used with increasing detergent strength (Baghirova *et al*, 2015). In the original DroNc-seq protocol, the nuclei lysis buffer used during droplet generation is the same as the cell lysis buffer from the Drop-seq protocol (Macosko *et al*, 2015; Habib *et al*, 2017). However, Sathyamurthy and colleagues later modified the DroNc-seq protocol to profile spinal cord cell types, in which they used lysis buffer containing 0.7% sarkosyl instead of the original 0.2% concentration (Sathyamurthy *et al*, 2018).

To test the nuclei lysis efficiency, I isolated nuclei from three independent frozen samples, incubated with DAPI for 5 min and then used the nuclei for droplet generation with lysis buffer containing three concentrations of sarkosyl: 0, 0.2 and 0.7%. Droplets were visualized immediately after generation (0 minutes) and after an incubation period (30 minutes). Figure 5.5 and Table 5.1 summarize the results for this test showing the lysis efficiency and capture rate, which is calculated as the percentage of intact and lysed nuclei over the total number of droplets. When the nuclear membrane is lysed, the DNA is released and DAPI signal will be distributed throughout the droplet.

The lysis buffer containing 0% sarkosyl did not affect the nuclear membrane at 0 min and after the incubation only 6% of encapsulated nuclei were lysed, confirming the requirement for sarkosyl in the buffer to facilitate lysis (Table 5.1 and Figure 5.5 A). It was also observed that 7.07% of droplets contained one nucleus and that there were no nuclei doublets. At 0.2% sarkosyl, the buffer lysed 46% of the encapsulated nuclei

immediately and this efficiency increased slightly to 53% after the incubation period, indicating limited suitability of this concentration for snap-frozen endometrial samples (Figure 5.5 B). The capture rate was highly similar to the 0% sarkosyl droplets. In comparison, lysis was highly efficient with the 0.7% sarkosyl lysis buffer, with 100 % of captured nuclei lysed immediately after droplet generation and approximately the same capture rate as the previous buffers (Table 5.1). However, when observed under the microscope, the droplet sizes were not uniform throughout the emulsion (Figure 5.5 C). In order to generate uniform droplets, the flow rates for the bead and nuclei lines were reduced from 20 μl/min to 15 μl/min, which had a negative impact on the capture rate (Figure 5.5 D and Table 5.1). Since there is a correlation between droplet volume and yield of captured mRNA (Habib *et al*, 2017) it is important to maintain a uniform emulsion. Therefore, for subsequent experiments, the 0.7% sarkosyl lysis buffer was used in combination with the reduced flow rates despite the reduced capture rate.

Table 5.1. Comparison between 0.2% and 0.7% lysis buffer efficiency and capture rate. Data is presented as median (range); n=3.

	Lysis efficiency (%)	**Capture rate (%)**
	0 % Sarkosyl	
0 min	0 (0 - 0)	
30 min	6 (0 - 8.5)	7.07 (6.63 - 7.45)
	0.2 % Sarkosyl	
0 min	46 (35 - 85)	
30 min	53 (47 - 93)	7.10 (7.00 - 7.27)
	0.7 % Sarkosyl	
0 min	100 (100 - 100)	
30 min	100 (100 - 100)	6.97 (6.6 - .3)
	0.7 % Sarkosyl (reduced flow rates)	
0 min	100 (100 - 100)	
30 min	100 (100 - 100)	4.20 (4.15 - 4.24)

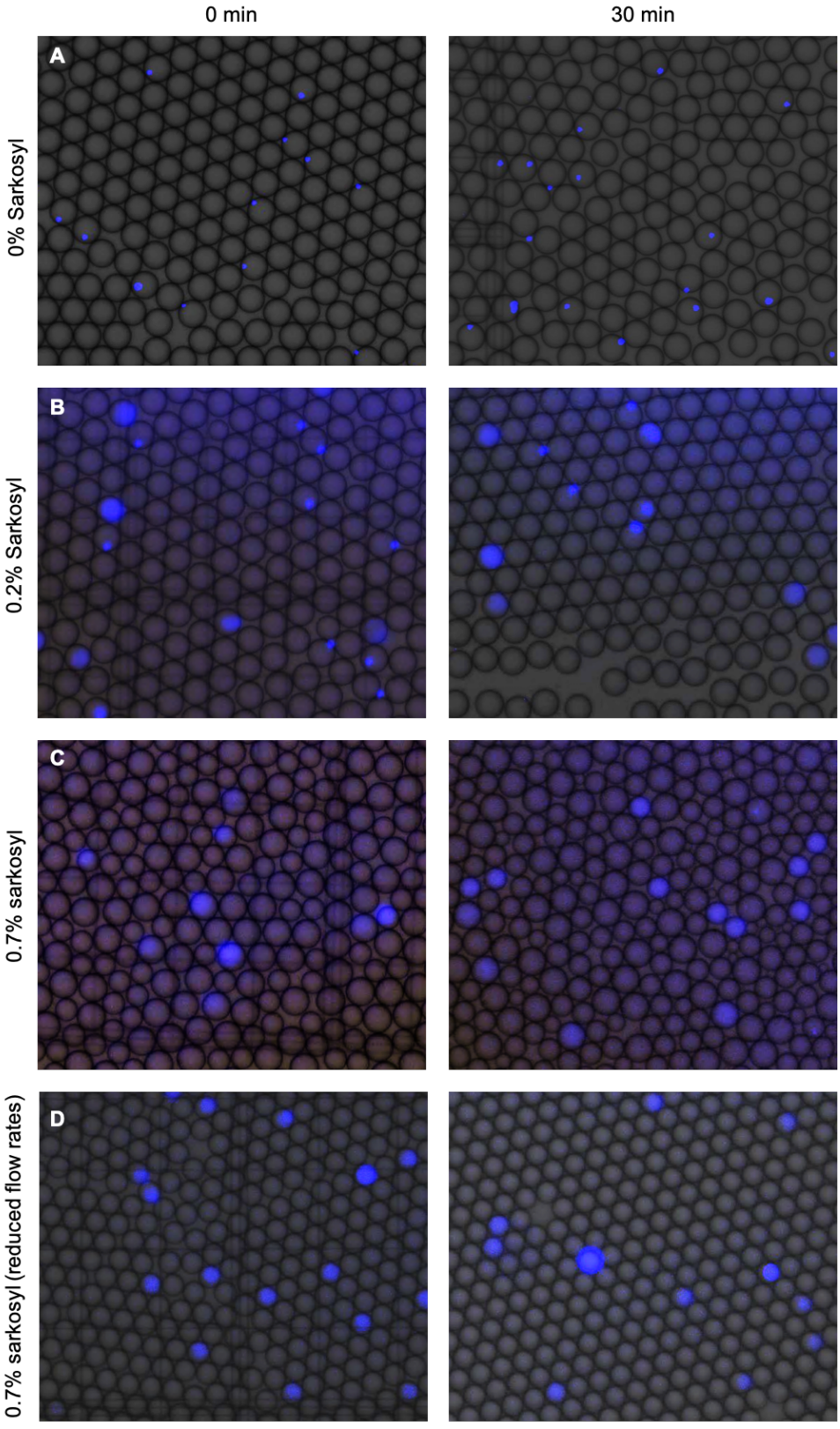

Figure 5.5. Comparison between 0, 0.2 and 0.7% lysis buffer efficiency. (A) Representative phase contrast images of DAPI stained nuclei inside droplets with 0% lysis buffer at 0 and 30 minutes. (B) Representative phase contrast images of DAPI stained nuclei inside droplets with 0.2% lysis buffer at 0 and 30 minutes. (C) Representative phase contrast images of DAPI stained nuclei inside droplets with 0.7% lysis buffer at 0 and 30 minutes. (D) Representative phase contrast images of DAPI stained nuclei inside droplets generated at reduced flow rates with 0.7% lysis buffer at 0 and 30 minutes.

Taking into account the previous observations, a new snap-frozen endometrial sample was subjected to snRNA-seq with 0.7% lysis buffer. A total of 3884 nuclei passed the initial quality filtering with an average of 925 genes per nuclei and a lower percentage of mitochondrial genes (Figure 5.6 A). Dimensional reduction analysis segregated the nuclei into 8 clusters corresponding to 4 main cell types: EpC, EnSC, EC and IC (Figure 5.6 B).

The immune population represents 1.3% of total number of cells and is segregated in two clusters, IC1 and IC2. The expression of *HLA-DRA*, *LST1* and *STAB1* has been reported in a variety of leukocytes, which hinders the accurate identification of immune subpopulations inside IC1 (Draber *et al*, 2012; Skirecki *et al*, 2016; Kondo *et al*, 2016). On the other hand, uNK cells are specifically allocated in IC2 as denoted by the expression of *GNLY* and *NCAM1*. Additionally*, ITGAX* (Integrin alpha X, CD11c) has been described to be expressed in naïve NK cells (Bezman *et al*, 2012), while *ITGA* (Integrin alpha D, CD11d) is expressed in human decidual NK cells (Koopman *et al*, 2003).

An advantage of snRNA-seq for endometrial samples is the possibility to have the complete representation of the epithelial compartment, whereas scRNA-seq is limited by insufficient enzymatic digestion of the epithelial compartment. Amidst the 4 epithelial clusters, EpC1 was characterized by the expression of receptivity-associated genes, such as, *PAEP*, *HAP1* and *AIMP1* (Bhagwat et al, 2013; Chan et al, 2013; Altmäe et al, 2017). Similarly, EpC2 showed a profile associated with receptivity, based on expression of *RXFP1* (relaxin receptor) and *PTGS1* (prostaglandin endoperoxidase synthase 1, previously known as COX-1). Once again, one of the epithelial clusters, EpC3, was characterized by an ambiguous profile with expression of epithelial (e.g. *CMC2*) and stromal (e.g. *C1S*, *ZEB1*) markers. Dimensionality reduction analysis also identified a ciliated population, EpC4, depicted by the expression of *DNAAF1* and *FHAD1*.

The EnSC population was characterized by the expression of stromal markers, *ZEB1*, *MEG3*, *C1S* and *COL3A1*, and comprised 9.1% of the total number of cells. Additionally, the presence of EC was identified by the expression of *A2M* and *MCAM*. These results show that the increase in the lysis buffer improved the quality of the analysis but still there was a discrepancy in the ratio between epithelial and stromal cells. This observation could be due to an intrinsic biological variation or a technical issue. For example, if different types of tissue have different sensitivity to the concentration of the lysis buffer, then it is also possible that the distinctive cell types from the same sample react differently to the lysis buffer.

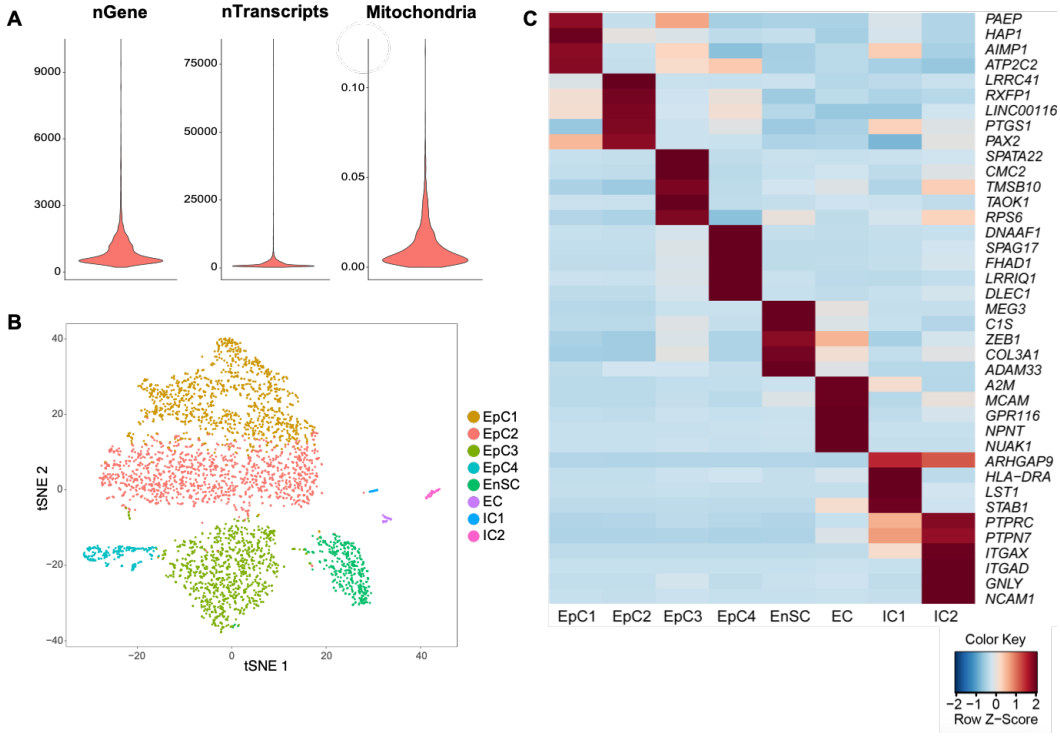

Figure 5.6. snRNA-seq with 0.7% lysis buffer. (A) Violin plots of number of genes, number of UMI and percent of mitochondrial genes per cell. Cells were included for further analysis if their number of genes ranged from 200 to 3000 and their proportion of mitochondrial genes did not exceed 5%. (B) t-SNE plot of 3729 nuclei from a mid-luteal biopsy captured epithelial (EpC), stromal (EnSC), endothelial (EC) and immune (IC) populations. (C) Heatmap showing relative expression (z-score) of markers defining cell-types.

5.2.3 Transcriptome profile of endometrial samples across the menstrual cycle

Single nucleus transcriptome analysis was then extended to frozen endometrial samples collected at specific timepoints of the menstrual cycle: proliferative phase, LH+5, LH+8 and LH+11. The libraries and sequencing were prepared in two batches (A and B), each with one sample per timepoint. Table 5.2 presents the demographic details of patient samples used on scRNA-seq.

Unexpectedly, computational analysis showed that the proliferative and LH+11 samples had low QC values and on average only 67 nuclei passed the initial filtering steps (Figure 5.7). Congruence between both batches showed that this result is biologically dependent and timepoint specific. Therefore, proliferative and LH+11 samples were excluded, and further analysis was limited to biopsies LH+5 and LH+8.

Table 5.2. Demographic details of patient samples used on snRNA-seq.

Batch	Day of Cycle	Age	Live-births	Previous losses	BMI	NK (%)
A	Proliferative	39	1	5	28	N/A
B		31	1	4	23	N/A
A	LH+5	39	1	2	24	1.15
B		35	0	1	22	1.82
A	LH+8	35	0	4	28	1.16
B		37	0	3	25	11.22
A	LH+11	38	0	4	24	6.11
B		31	0	1	N/A	17.03

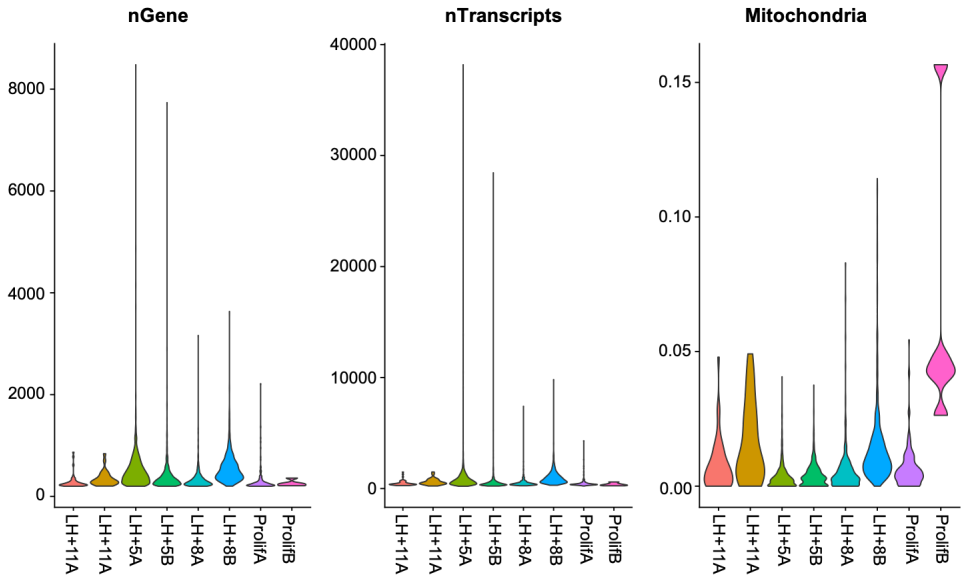

Figure 5.7. Quality control metrics of snap-frozen endometrial samples across the menstrual cycle. Violin plots of number of genes, number of UMI and percent of mitochondrial genes per cell. Cells were included for further analysis if their number of genes ranged from 200 to 2000 and their proportion of mitochondrial genes did not exceed 5%.

Dimensionality reduction analysis of LH+5 and LH+8 samples segregated the nuclei into 9 clusters corresponding to EnSC, EpC and IC populations (Figure 5.8). tSNE plots A and B from Figure 5.8 show the same nuclei colour coded according to the different clusters and to the sample of origin, respectively. Figure 5.8C shows the heatmap with the top 5 markers of each cluster as identified on Figure 5.8A.

The ciliated epithelial cluster, EpC5, had the contribution of all 4 samples, while the EpC clusters from 1 to 4 correspond to each individual sample. To further investigate these 4 main EpC clusters, the marker genes were cross-referenced with the RNA-seq data from Chapter 3, section 3.2.2, in which 36 endometrial samples were classified as pre-receptive, early-receptive and receptive (Figure 5.8 D). The expression pattern of *LRP4* and *ESR1*, suggest that the sample LH+5A (EpC1) is in an early-receptive stage, while LH+5B (EpC2) might be transitioning between pre and early-receptive, according to the expression markers, *DUOX1* and *DNAJC15*. Interestingly, LH+8A (EpC3) shares the same epithelial markers as EpC2, suggesting that this sample might be delayed and hasn't reached the receptive phenotype (Figure 5.8 D). On the other hand, the sample LH+8B (EpC4) has already transitioned into a receptive phenotype according to the expression of *KIF12* and *IRX3* (Figure 5.8 D) and the receptivity-associated genes *PAEP* and *HAP1* (Figure 5.8 C).

Contrary to the previous snRNA-seq, in this analysis 42% of the captured nuclei were identified as stromal cells. Once again, the segregation between the transcriptome profile of LH+8B (EnSC2) and the other samples (EnSC1) reinforces the suggestion that these biopsies are in different phases of the cycle. Dimensionality reduction analysis didn't identify an endothelial cluster, which could be due to the reduced number of nuclei explored per sample. On the other hand it was possible to identify uNK and other lymphocyte markers segregated into 2 clusters, IC1 and IC2. While IC2 is composed exclusively by the sample LH+8B, IC1 integrates nuclei from all four samples. According to the demographic details previously presented on table 5.2, the sample LH+8B has the highest percentage of uNK. This data suggests that the high abundance of uNK in endometrial samples might be associated to the influx of specific cell subsets, which are then represented as discrete clusters in single cell/nuclei transcriptomic studies.

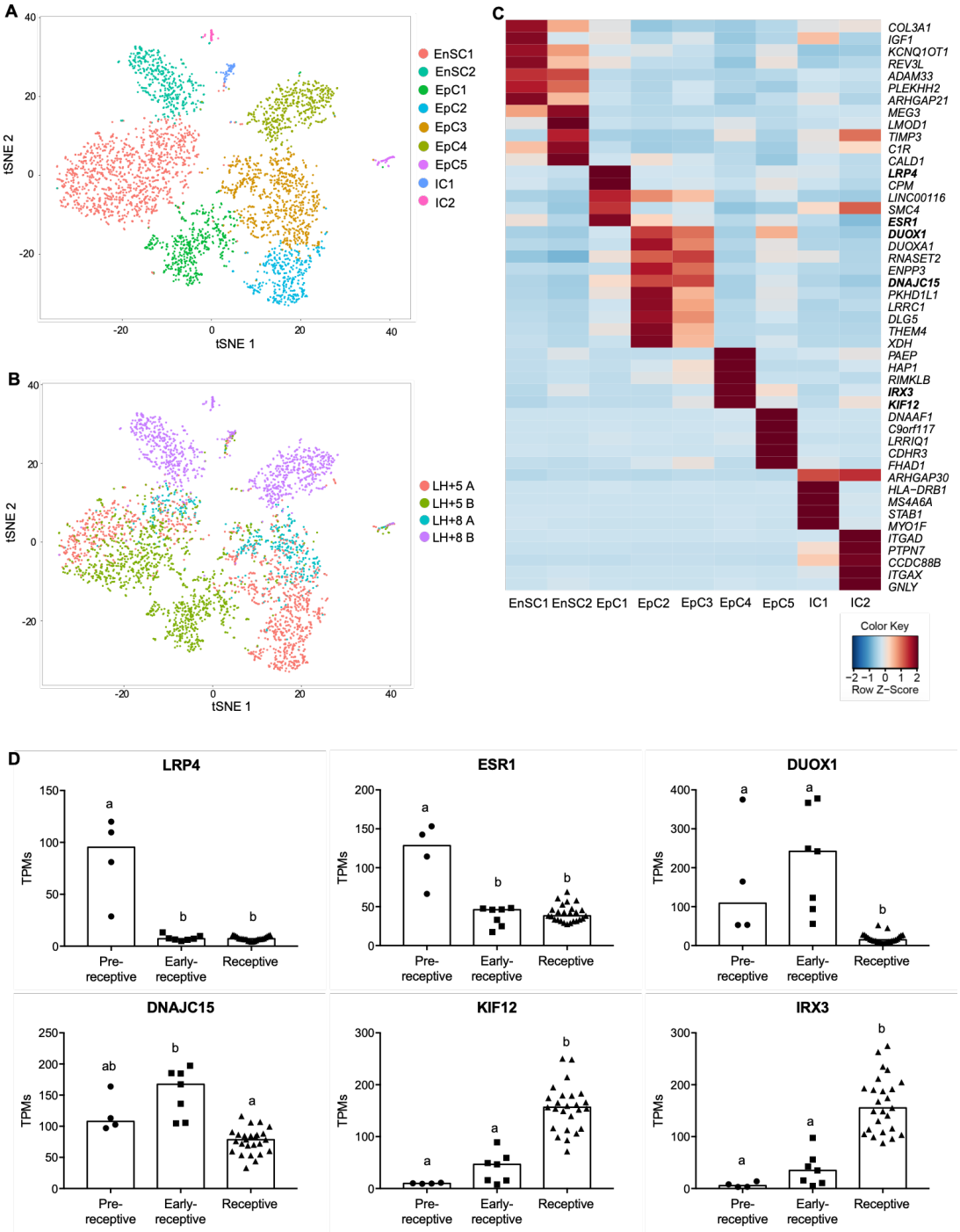

Figure 5.8. Identification of endometrial cell-types. (A) t-SNE plot of 3755 cells isolated from LH+5 and LH+8 archived biopies identified EpC, IC and EnSC. (B) t-SNE plot of the previous samples colour coded according to the sample of origin. (C) Heatmap showing relative expression (z-score) of markers defining cell-types. (D) Expression analysis of the EpC markers from snRNA-seq in pre-, early- and receptive. Vertical axis corresponds to transcripts per million (TPM) values from bulk RNA-seq. Group comparison by one-way ANOVA on ranks (Kruskal-Wallis) test. Different letters above the error bars indicate that those groups are significantly different from each other at $P < 0.05$. Data is presented as median.

5.3 Discussion

This chapter presents an alternative method to bypass the drawbacks of single cell transcriptomics and how it can be used to investigate frozen endometrial samples. scRNA-seq is restricted to freshly obtained tissues and the intrinsic process of enzymatic dissociation can affect RNA integrity and introduce artefactual transcriptional stress response (Habib *et al*, 2017; Wu *et al*, 2019). Thus, snRNA-seq, a technique that does not require any enzymatic procedure and can be employed on archived samples, has become a resourceful substitute of scRNA-seq.

The first step was to test and compare the nuclei isolation of snap-frozen and RNAlater preserved endometrial tissue. It was observed that the RNAlater preservation methodology was less efficient resulting in clumps of nuclei and cell debris. Previously, it has been reported in cochlear samples that RNAlater alters the physical properties of the tissue (Cai *et al*, 2013), which could also explain the previous results in the endometrial samples making it harder to break the tissue and lyse the cell membrane. The poor nuclei isolation from RNAlater tissue had a subsequent impact on the sequencing library quality when compared to the snap-frozen sample. Furthermore, it should be considered that the disruption of the tissue could be biased toward a specific cell type and thus the subsequent analysis would show unrealistic cell type proportions. Therefore, following experiments were performed using snap-frozen tissue.

The analysis of the first snRNA-seq fell short of expectations right at the initial QC filtering steps. The low number of genes and transcripts suggested that at the time of the nuclei lysis, a low number of mRNA molecules attached to the barcoded beads, which could be due an inefficient lysis of the nuclear membrane. To test this theory the concentration of sarkosyl in the lysis buffer was increased from 0.2% to 0.7%. Although the latter showed higher efficiency, it altered the viscosity of the fluid in the beads line, ultimately disturbing the droplet generation. In order to uniformize the droplet emulsion, the flow rates had to be reduced, which also affected the capture rate with a decrease from 6.97% to 4.20%. Curiously, the original capture rate reported by Dolomite Bio, the system manufacturer, was 5%, which is closer to the reduced values here observed. Even so, it was observed that there are no nuclei doublets at a capture rate of 7%. Therefore, for future experiments, parameters such as concentration of nuclei and beads can be adjusted in order to increase the capture rate when using a higher concentration of sarkosyl.

Although snRNA-seq often detects a lower number of RNA than scRNA-seq, as it excludes transcripts outside the nucleus, previous studies demonstrated that nuclear RNA represents a significant population of transcripts important for cell identity (Habib *et al*, 2017; Bakken *et al*, 2018; Nguyen *et al*, 2018). Thus, it was expected that snRNA-seq analysis on endometrial samples would identify the same cell populations as scRNA-seq or even to overpower it and capture a higher diversity of cell types (Wu *et al*, 2019). However, when the snRNA-seq was performed with a higher sarkosyl concentration, it was observed an improvement on data quality than the previous experiment, but still there was a lack of biological information when compared to scRNA-seq (Chapter 4). Although, the four main endometrial cell types were captured, there was a distinct bias towards the epithelial compartment reducing the information regarding the other cell clusters, specially the IC and EC. Hence, to make the snRNA-seq a promising tool for the study of endometrial heterogeneity, it is required to scale up the experiments and to analyse a higher number of nuclei.

One of the obstacles when interpreting snRNA-seq data can be driven by the differences between nuclear and cell transcriptomic profiles (Nguyen *et al*, 2018). Despite the high concordance in the nuclear and cell gene expression (Habib *et al*, 2017), nuclear transcriptome is enriched for long noncoding RNAs (lncRNA), nuclear-function genes and intronic regions (Gao *et al*, 2017, Wu *et al*, 2019). The presence of these features need to be accounted during the analysis, especially when they are markers of cell clusters, such as *MEG3* (LINC00023) and *LINC00116* are markers of endometrial stroma and epithelial clusters, respectively.

The snRNA-seq methodology used in this study is based on the capture of RNA molecules by their poly(A)-tail that hybridize to the oligo dT sequence present at the end of the barcoded beads. The failure in performing single nucleus transcriptome analysis on proliferative and LH+11 samples, whereas early and mid-secretory biopsies were successful, suggests that the capture of the nuclear RNA at both timepoints was unsuccessful. Taking into consideration that Wang and colleagues (2018) employed scRNA-seq to investigate the transcriptome profile of endometrial samples across the menstrual cycle, it is suitable to consider that the obstacle is specific to the nuclear transcriptome. The restriction to capture nuclear RNA in proliferative samples could be related with the fast turnover that endometrial cells are subjected during this phase. Proliferating cells have a higher rate of replication, transcription and therefore processing, export and protein translation to maintain cell division (Russell and Zomerdijk, 2005; Heath et al, 2016). Nuclear transport factors

are key players in RNA translocation into the cytoplasm and subsequent translation to the point that alteration of these factors affects both mRNA export and cell proliferation (Wickramasinghe *et al*, 2014; Heath *et al*, 2016). Therefore, it is suggested that the rapid turnover dependent on mRNA export limits the access to the nuclear transcriptome for snRNA-seq of proliferative phase endometrial samples. On the other hand, the late secretory phase is characterized by an increase of stressed cells followed by a peak of senescent cells and the regulation mechanisms of autophagy and apoptosis (Harada *et al*, 2004; Brighton *et al*, 2017; Yang *et al*, 2019). Studies have shown that animal cells under such cellular processes are associated with a tight posttranscriptional regulation often dependent on deadenylases (Mauxion *et al*, 2008; Thomas *et al*, 2015; Tokmakov *et al*, 2017). These enzymes are localized both in the nucleus and the cytoplasm and their role is to either modulate the length of the poly(A) tail or to decrease the mRNA levels. After the deadenylation process, some mRNAs might undergo a new round of poly(A) tail extension and translation, while others might be degraded (Zhang *et al*, 2010). Thus, mRNA deadenylation may indirectly contribute to cell turnover via translational shutdown and it might be behind the obstacle to capture nuclear poly (A) tail mRNA in late-secretory samples.

To conclude, snRNA-seq is a viable but limited tool to study the endometrial cell heterogeneity. Although it has the ability to identify all main endometrial cell types in snap-frozen sample its efficiency is highly dependent on the phase of the menstrual cycle. However, new promising and alternative methodologies are arising such as single cell ATAC seq, which measures chromatin accessibility on a single cell level allowing the unbiased discovery of cell types and regulatory elements (Lareau *et al*, 2019). Single cell ATAC seq technology overcomes the limitation of snRNA-seq, since it does not involve the analysis of transcriptome and instead directly identifies open chromatin regions that are indicative of active regulatory regions at single cell resolution.

Chapter 6

General Discussion

Discussion

The preparation of a receptive endometrium is driven by an intricate interplay between ovarian steroid hormones and the different endometrial cell populations. While the luminal epithelium undergoes apical surface specialization expressing cell adhesion molecules to permit adherence of the blastocyst, the glandular epithelial cells secrete substances that support blastocyst development (Strauss and Lessey, 2009). Meanwhile endometrial stromal cells differentiate into specialized secretory decidual cells upon the postovulatory rise in progesterone levels and increasing local cAMP production. The decidualization process and simultaneous influx and proliferation of leukocytes modulate endometrial angiogenesis and provide an immunoprivileged matrix essential for embryo implantation and placental development (Gellersen and Brosens, 2014). The combined actions of the locally acting molecules and ECM promote trophoblast attachment and, at the same time, limit the aggressive invasion by the embryonic tissue (Strauss and Lessey, 2009). In the absence of pregnancy and following progesterone withdrawal, the functional layer is shed during menstruation, and the endometrium is prepared for a new menstrual cycle.

One of the key factors behind the remarkable plasticity of the endometrium is the existence of rare stem cell populations. Typically, adult stem cells play a crucial role in tissue homeostasis and integrity by maintaining, generating and replacing terminally differentiated cells as part of the routine cellular turnover or for repair of damaged tissues (Li and Xie, 2005). Despite the extensive proliferation and remodelling that the endometrium undergoes in each cycle, studies on endometrial stem cell biology lag far behind other areas of stem cell research (Ghobadi *et al*, 2015). Only recently, N-cadherin was identified as a specific endometrial epithelial progenitor cell marker that can possibly be used for further characterization of these cells and their role in endometrial proliferative disorders, including endometriosis and Asherman's syndrome (Nguyen *et al*, 2017). On the other hand, the investigation on eMSC has benefited from sharing the same *in vitro* properties as BM-MSC. The defining features of these cells are plastic adherence, clonogenicity, multilineage differentiation (osteocytes, chondrocytes, adipocytes) *in vitro,* and a distinct phenotype ($CD73^+$, $CD90^+$, $CD105^+$, $CD14^-$, $CD34^-$, $CD45^-$) (Gargett *et al*, 2016).

$CD146^+PDGFR\beta^+$ and SUSD2/W5C5 are recognized in literature as eMSC markers (Gargett *et al*, 2016), although as previously described they should be regarded as PVC-specific cell surface proteins. For example, when Barragan and colleagues

(2016), compared the gene profiles of freshly isolated $CD146^{+}PDGFR\beta^{+}$ and $CD146^{-}PDGFR\beta^{+}$ with clonal cultures of both cell types, they labelled the freshly sorted $CD146^{+}PDGFR\beta^{+}$ as eMSC. Thus, the authors drew their conclusions on fresh eMSC versus cultured eMSC when genuinely the comparison was done between freshly isolated PVC and cultured eMSC. This inaccuracy has been propagated in literature due to the lack of specific eMSC markers.

Hence, this thesis has investigated endometrial stem cell biology through the comparison of cultured stromal subpopulations (eMSC, TA, PVC and EnSC) and employed new methods to identify *in vivo* endometrial stem/progenitor cell populations. Additionally, the potential of nucleus transcriptomics to analyze archived endometrial samples was also explored.

In summary, I provide evidence that:

i. The transition from early- to mid-secretory is followed by an adjustment in the stromal:epithelial ratio.

ii. The maintenance of eMSC stemness might be related to key transcription factors that are shared with other adult stem cell populations. Additionally, cultured eMSC is a heterogeneous population, which includes a quiescent SP.

iii. scRNA-seq can be employed to analyse endometrial cell heterogeneity. Apart from stromal, endothelial, epithelial and diverse immune cell populations, it was also identified a discrete population of highly proliferative mesenchymal cells.

iv. A putative progenitor cell population characterized by a high proliferation transcriptome signature is present in peri-implantation endometrial samples. Anillin is a candidate marker for this population and in the future could be used to screen for stem cell deficiency in RPL patients.

v. snRNA-seq is a viable but limited tool to study the endometrial cell heterogeneity. Despite its the ability to identify all main endometrial cell types in snap-frozen samples, efficiency of this technique is highly dependent on the phase of the menstrual cycle.

6.1 Interpretation of tissue complexity

The endometrial cellular heterogeneity allied to the morphological modifications that this tissue undergoes throughout the menstrual cycle become a major hurdle when interpreting bulk (whole biopsy) transcriptomic data. The expression of the same genes in varying degrees across multiple cell subsets imply that the measured abundance of any such transcript is confounded by the composition of the sample from which it is measured (Shen-Orr and Gaujoux, 2013). To address this issue, I presented three different approaches.

First, I generated a reference matrix consisting of the transcriptome profile of epithelial, uNK and stromal subsets to be used in computational deconvolution analysis of whole tissue transcriptome data. Initially, deconvolution of microarray data of proliferative, early-, mid- and late-secretory phase endometrial samples showed that the WOI coincided with a sudden change in stroma:epithelial cell ratio approximating 1. Recently, this result has been corroborated by Suhorutshenko and colleagues (2018), who combined histological analysis to transcriptome deconvolution. Further analysis of endometrial samples ranging from pre- to receptive phase demonstrated that the stromal cells were always more abundant to epithelial cells except in the early-receptive phase when the ratio equaled ~1. This modulation in the stroma:epithelial ration could be related to the fact that hypersecretory grands precedes the decidualization process (Crum *et al*, 2003). Additionally, a previous study has demonstrated that proliferation of glandular epithelial cells cease completely from day 21 onwards of the menstrual cycle, whereas proliferation of the stromal compartment is reduced postovulatory until day 20, followed by a subtle and continuous proliferation until the end of the cycle (Jürgensen *et al*, 1996), which could explain the dominance of the stromal cells in the late secretory phase. It is important to note that due to the date of the study, the authors did not question the nature of this stromal proliferation (Jürgensen *et al*, 1996), but it could be related to expansion of a progenitor cell population, proliferation of resident immune cells, or both.

Previously, it was demonstrated that RPL is associated with a disordered and prolonged pro-inflammatory decidual response, which extends the WOI, promotes out-of-phase implantation and disables embryo selection (Salker *et al*, 2010; Salker *et al*, 2012). This result was explained by an alteration in the IL-33/ST2L/sST2 axis, decreased expression of the decidual marker prolactin (PRL) and increased levels of prokineticin-1 (PROK1), a cytokine that promotes implantation, in RPL patients (Salker *et al*, 2010; Salker *et al*, 2012). Apart from the differences in the regulation of

specific genes, here I showed for the first time that the RPL might also be associated with more pronounced variation in cell types, although this observation requires further investigation with a larger number of samples.

On the other hand, endometrial cellular heterogeneity was analysed using scRNA-seq. While the deconvolution methodology is confined to the knowledge of existing cell populations in a specific type of tissue (Shen-Orr and Gaujoux, 2013), the development of scRNA-seq enabled to determine the transcriptome profile on a single-cell basis and subsequently, to identify *de novo* populations (Andrews and Hemberg, 2018). scRNA-seq analysis of mid-luteal endometrial samples identified EnSC, EC, ciliated and non-ciliated EpC, a discrete PC population and IC comprising uNK, macrophages, monocytes and B-cells. The existence of ciliated cells has been described over a century ago (Benda, 1894), but there is still no clear concept regarding their role. One of the speculated functions of cilia is to remove products discharged by the cells (Demir *et al*, 2002). Alterations in ciliogenesis and non-ciliated:ciliated cells ratio has been linked to infertility in patients with septate uterus (Fedele *et al*, 1996). Although the investigation on these cells is still limited, the identification of specific markers (*RSPH1, CAPS and DNAAF1*) can be used in future experiments to track and further elucidate the importance of endometrial ciliated cells. Resident immune cells were also captured, including three subpopulations of uNK cells, likely reflecting cell state transitions from a proliferative to a differentiated phenotype. Thus scRNA-seq superceed previous methodology by providing insightful information regarding endometrial heterogeneity. Nevertheless, it was predicted that the captured EpCs were an underrepresentation of the *in vivo* glandular compartment owing to the fact that endometrial glands are relatively refractory to mild enzymatic digestion. Therefore, I also investigated an alternative to scRNA-seq.

In contrast to scRNA-seq, single nucleus transcriptome analysis does not require any enzymatic procedure and can be employed on archived samples. However, here I showed that snRNA-seq is limited to on early- to mid-secretory samples and thus it is not a viable technique to study endometrial heterogeneity throughout the menstrual cycle. This limitation may also reflect differences in mRNA processing during the proliferative and late-secretory phase of the cycle (Tollervey and Caceres, 2000). Further investigation is required to fully understand this observation.

Taken together, computational deconvolution may be useful to reappraise RNA-seq data, but for future experiments scRNA-seq or emerging technology such as single cell ATAC-seq become a better alternative to profile endometrial transformations

across the menstrual cycle. Additionally, to improve the scRNA-seq analysis, it is important to search for new methodology that efficiently digest the endometrial glandular compartment.

6.2 Hierarchy of endometrial stem cells and their niche

ASC mediate the fine balance between quiescence, self-renewal, proliferation and differentiation through interaction with the local microenvironment (O'Brien and Bilder, 2013). The stem cell-niche unit remains one of the most challenging targets in cell biology research. More than just the physical location for stem cells, the niche is also the dynamic place where cell-to-cell and cell-to-matrix interactions, soluble molecules signalling, physical and mechanical stimuli determine cell behaviour (O'Brien and Bilder, 2013). Being able to isolate and expand ASC *in vitro* became a powerful tool to further explore stem cell biology and develop regenerative medicine applications. However, it is technically challenging, since ASC removal from their native microenvironment has negative repercussions on their sustainability (Redondo *et al*, 2017).

In humans, the endometrial stem cell niche encompasses the perivascular space around the rapidly growing spiral arterioles (Murakami *et al*, 2014). This niche promotes activation and migration of eMSC to regenerate the endometrial functional layer (Khatun *et al*, 2017). Although stem cell niches vary among tissues, they share common microenvironmental features (Redondo *et al*, 2017). One of the key components of stem cell niche is the ECM, which has a major impact on tissue homeostasis and regeneration under physiological and pathological conditions (Gattazzo *et al*, 2014). In the endometrium, the stem cell niche is still poorly defined, but in this project, I observed that the *in vitro* expansion of eMSC involved modulation of the extracellular environment with enrichment of collagen deposition. As variations of collagen-coated substrates are now more regularly used to expand stem cells (Redondo *et al*, 2017), tracing the collagen signature of the native eMSC niche may offer a significant improvement to further understand the biology of these cells. Additionally, I identified a list of transcription factors and cell surface proteins in eMSC that support the concept of a conserved regulation between different sources of ASC.

Another important feature of stem cell niches are the neighbouring cells, which may be other stem cell copies, more committed progenitors, fibroblasts, immune cells,

endothelial cells and nerves (Redondo *et al*, 2017). In the endometrium, the PVC are responsive to Notch signalling (Murakami *et al*, 2014), which is a common niche feature essential for cell-fate specification and maintenance of stem cells in a poised quiescent state (Cheung and Rando, 2013). I demonstrated that apart from the PVC and eMSC, the perivascular niche also encompasses a SP and highly proliferative progenitor cells. These observations support the concept of a hierarchy of stem cells in the endometrium that is responsible for the regeneration of this tissue (Gargett *et al*, 2016). Transversally, the presence of a differentiation hierarchy of stem cells has been identified in other systems as an important regulator of tissue homeostasis and regeneration (Hardy *et al*, 2017; Lukowski *et al*, 2019). Moreover, I showed that the isolated eMSC population is heterogeneous and comprises cells with a SP phenotype. Gradually, the assumption of MSC clonal purity is being revisited and new data is showing that in MSC cultures there is variation within single-cell-derived colonies (Rennerfeldt and Vliet, 2016). Nevertheless, one question that remains is the purpose of this identified hierarchy in endometrial samples from the secretory phase.

6.3 Stem/progenitor cells in preparation for pregnancy

The origin and recruitment mechanism of eMSC are still controversial aspects of the endometrial regeneration process. Several studies have demonstrated that endometrial repair after menstruation involves the activation of epithelial progenitor cells and eMSC residing in the basal layer (Masuda *et al*, 2010; Gargett *et al*, 2016). Simultaneously, bone marrow-derived cells (BMDC) are recruited to the endometrium and differentiate into non-hematopoietic endometrial lineages, including endothelial, stromal and epithelial cells (Taylor, 2004; Aghajanova *et al*, 2010; Gil-Sanchis *et al*, 2015).

Steroid hormone withdrawal during the late secretory phase triggers the menstruation process characterized by a pro-inflammatory production of several cytokines and chemokines (Evans and Salamonsen, 2012), such as SDF-1 (CXCL12), which is considered a potential mediator of BMDC recruitment and homing to the endometrium (Hu *et al*, 2013; Wang *et al,* 2015). SDF-1 is proteolytically inactivated by dipeptidyl-peptidase IV (DPP4). Subsequently, it has been demonstrated that DPP4 inhibitors recruit stem cells and mediate regeneration of ischaemia-reperfusion injury in mouse lung (Jungraithmayr *et al*, 2012). Recently, a preclinical trial hypothesised that sitagliptin, which is a DPP4 inhibitor, would enhance the abundance of eMSC in RPL

patients (Tewary *et al*, 2020). The authors observed that the CFU count increased 1.68-fold in the sitagliptin group and 1.08-fold in the placebo group. This result supports the hypothesis that BMDC are recruited to the endometrial niches by a SDF-1-dependent mechanism, where they differentiate into eMSC and thereby contribute to endometrial renewal (Khatun *et al*, 2017). Here, following the identification of a putative highly proliferative progenitor population, it was also observed a correlation in the abundance of anillin^{+} cells between the stroma and glandular compartment. Again, this result suggests a common origin for both stromal and glandular stem cells (Taylor, 2004; Aghajanova *et al*, 2010).

Moreover, the identification of a putative progenitor population with a high proliferative transcriptomic signature in mid-secretory biopsies suggests that there is a second signalling mechanism in the menstrual cycle to activate endometrial stem/progenitor cell population. At the time of submitting this thesis, a new study reported the recruitment of BMDC to the decidua of pregnant mice (Tal *et al*, 2019). Initially, the authors traced GFP-expressing bone marrow cells transplanted in immunocompromised mice and showed that during pregnancy proliferating nonhematopoietic BMDC are recruited into the decidua and differentiate into stromal decidual cells. To explore the role of BMDC to implantation and pregnancy, the following experiments were performed on *Hoxa11* genetic knockout (KO) mice models, which are associated with pregnancy loss in heterozygous (+/−) mice and decidualization failure and lack of pregnancy in homozygous (−/−) mice. Transplantation of BM from wild type (WT) donor into Hoxa11+/− mice resulted in normalization of uterine expression of decidualization-related genes and rescued pregnancy loss. BM transplantation into Hoxa11-/− mice induced endometrial stromal expansion, gland formation, and decidualization. Thus, the authors demonstrated that BMDC have a nonhematopoietic physiologic contribution to the decidual stroma and play an important role in implantation and pregnancy maintenance.

In parallel, the identification of a putative proliferating progenitor cell population in endometrial samples during the WOI, suggests that these cells might be important for the decidua expansion during pregnancy. Over the course of pregnancy, the human uterus undergoes a 500–1000-fold increase in volume. Subsequentially, the decidua increases noticeably too (Guo *et al*, 2010). In contrast to decidualization in mice that only occurs after blastocyst attachment (Dey *et al*, 2004), in humans this process is spontaneous and embryo independent (Gellersen and Brosens, 2014). As previously described *in vitro* decidualization is associated with a modest but significant increase

in colony-forming cells suggesting that decidualization also contributes to increases tissue plasticity prior to pregnancy (Brighton *et al*, 2017). Taken together, I postulate that in each cycle the decidualization, also characterized by a transient pro-inflammatory period, will recruit and lead to the activation and proliferation of stem/progenitor cells important for decidual remodelling. In the absence of implantation the PC population will be shed with menstruation and thus create a pool of MenSC, which are characterized by a high proliferation rate (Chen *et al*, 2019).

The deficiency of eMSC in RPL (Lucas *et al*, 2016) was once again corroborated by the decrease of anillin^{+} cells in mid-luteal samples of this clinical group. As previously described, this deficiency can be modulated by pharmacological approaches that induce the recruitment of BMDC to the endometrium (Tewary *et al*, 2020). Until recently, the research on endometrial stem cells and their impact on reproductive disorders has been mainly focused on their role in the cyclic tissue regeneration (Gargett *et al*, 2016). However, here I present a paradigm shift whereby this population is also recruited and activated in the secretory phase of the cycle to possibly support the decidua expansion and pregnancy maintenance. Thus, alterations in the recruitment and proliferation of endometrial stem cells during the WOI might directly impact on the remodelling of the maternal tissues and pregnancy outcome.

6.4 Future work

The transcriptome analysis of endometrial stem/ progenitor cells provided information regarding the biology of these cells and led to the identification of a progenitor cell population that might be related to the remodelling of the decidua during pregnancy.

The RNA-seq performed on cultured endometrial cell populations generated a list of upregulated genes in cultured eMSC that requires further data mining. Additionally, it would be interesting to investigate the role of the identified transcription factors through gene knockdown experiments followed by functional analysis.

It is also important to profile the single-cell transcriptome of endometrial samples across the menstrual cycle. Here I performed the analysis of LH+8 and +10 endometrial samples and identified EnSC, EpC, EC, various IC and PC. Thus, this is a valuable technique to trace the modulation and transformation of these populations

throughout the cycle. For this, a cohort of proliferative to late secretory phase samples should be used. It would be particularly interesting to follow the activation of the PC population and possibly compare it to stem/progenitor cell populations identified in the proliferative phase. Moreover, knowing that the hallmarks of RPL are the alteration in the transient pro-inflammatory process during decidualization and a deficiency of stem cells, it would be crucial to compare the regulation between endometrial cell populations in RPL and control groups.

Lastly, the optimization of snRNA-seq for archived endometrial samples opened the doors to new questions regarding the mRNA processing in proliferative and late secretory phase. It would be interesting to study the processes of mRNA nuclear export and deadenylation through the western blot analysis of nucleo-cytoplasmic transporting factors and PCR-based analysis of the poly(A) tail length.

Supplementary Information

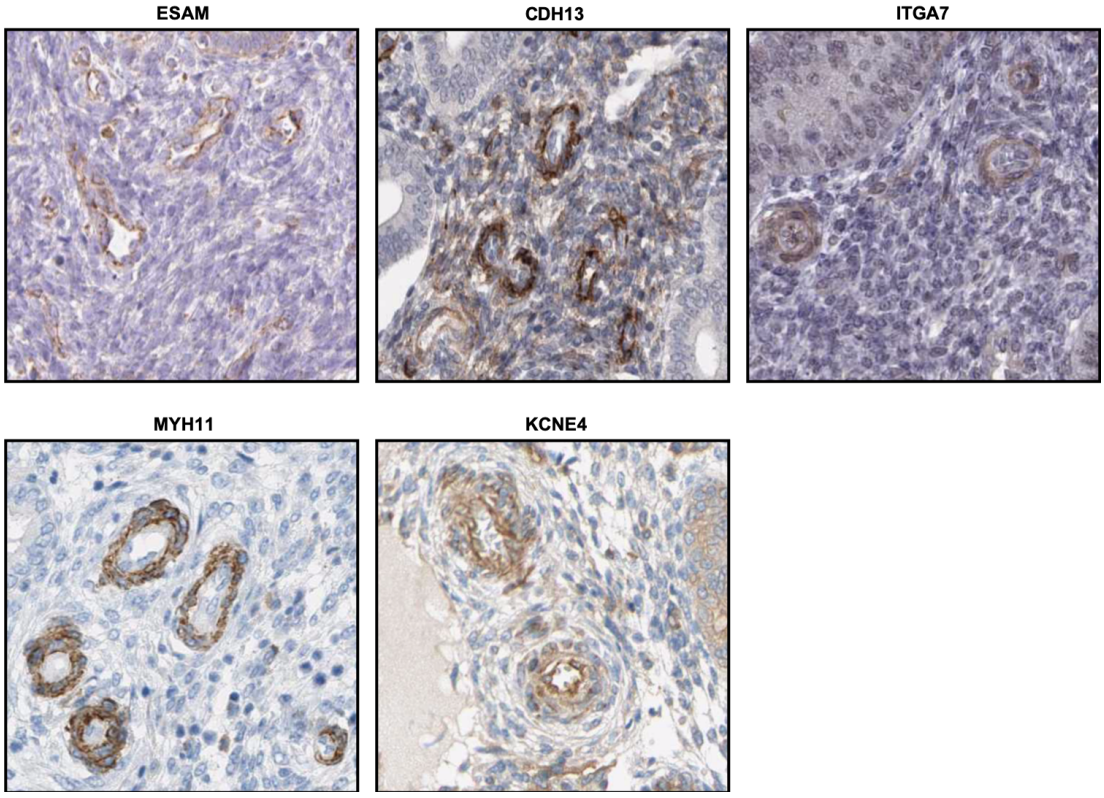

Supplemental Figure 1. Tissue distribution of perivascular marker genes enriched in cultured PVC. The micrographs were obtained from The Human Protein Atlas (http://www.proteinatlas.org/).

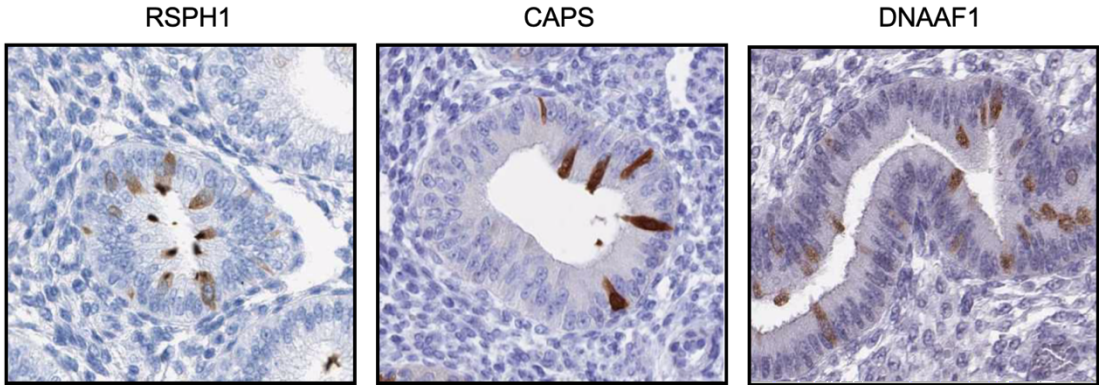

Supplemental Figure 2. Ciliated cell marker genes. The micrographs were obtained from The Human Protein Atlas (http://www.proteinatlas.org/).

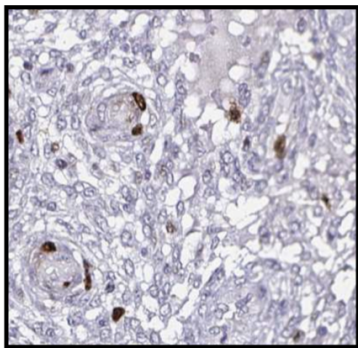

Supplemental Figure 3. Anillin expression on endometrial tissue. Micrographs was obtained from The Human Protein Atlas (http://www.proteinatlas.org/).

Supplemental Table 10. Genes enriched in cultured PVC

Gene	Description	Fold Change
GPR116	G protein-coupled receptor 116	4.10
POSTN	periostin, osteoblast specific factor	3.00
NDUFA4L2	NADH dehydrogenase 1 alpha subcomplex, 4-like 2	2.83
ITGA7	integrin, alpha 7	2.67
SGCD	sarcoglycan, delta	2.42
ANKRD1	ankyrin repeat domain 1	2.35
KCNE4	potassium voltage-gated channel, member 4	2.34
GDF6	growth differentiation factor 6	2.32
COL15A1	collagen, type XV, alpha 1	2.21
ACTG2	actin, gamma 2, smooth muscle, enteric	2.14
ESAM	endothelial cell adhesion molecule	2.09
COL16A1	collagen, type XVI, alpha 1	2.07
MYH11	myosin, heavy chain 11, smooth muscle	2.02
ITGBL1	integrin, beta-like 1	2.02
CDH13	cadherin 13	2.02
LTBP1	latent transforming growth factor beta binding protein 1	2.00

Supplemental Table 11. Genes enriched in cultured EnSC

Gene	Description	Fold Change
AIM1L	absent in melanoma 1-like	2.04
KRTAP2-3	keratin associated protein 2-3	2.04
B4GALNT3	beta-1,4-N-acetyl-galactosaminyl transferase 3	2.05
TRIM16	tripartite motif containing 16	2.06
CLIC5	chloride intracellular channel 5	2.06
FAM83H	family with sequence similarity 83, member H	2.08
SOX9	SRY (sex determining region Y)-box 9	2.08
IFI27	interferon, alpha-inducible protein 27	2.08
CXCL5	chemokine (C-X-C motif) ligand 5	2.10

AIM1	absent in melanoma 1	2.12
BSPRY	B-box and SPRY domain containing	2.14
ZBED2	zinc finger, BED-type containing 2	2.14
ARL4C	ADP-ribosylation factor-like 4C	2.14
RAB25	RAB25, member RAS oncogene family	2.17
ESRP1	epithelial splicing regulatory protein 1	2.17
MBP	myelin basic protein	2.18
MISP	mitotic spindle positioning	2.22
CDCP1	CUB domain containing protein 1	2.24
CD74	CD74 molecule	2.25
DSC2	desmocollin 2	2.26
SCNN1A	sodium channel, non-voltage-gated 1 alpha subunit	2.28
EPS8L1	EPS8-like 1	2.30
LSR	lipolysis stimulated lipoprotein receptor	2.30
CDC42BPG	CDC42 binding protein kinase gamma	2.30
SLC44A4	solute carrier family 44, member 4	2.31
LIF	leukemia inhibitory factor	2.31
ELF3	E74-like factor 3	2.32
GJB3	gap junction protein, beta 3, 31kDa	2.32
AP1M2	adaptor-related protein complex 1, mu 2 subunit	2.32
LRRN1	leucine rich repeat neuronal 1	2.33
CGN	cingulin	2.35
IL18	interleukin 18 (interferon-gamma-inducing factor)	2.36
SLC4A11	solute carrier family 4, member 11	2.39
EVPL	envoplakin	2.40
XDH	xanthine dehydrogenase	2.46
FAM107A	family with sequence similarity 107, member A	2.48
LCN2	lipocalin 2	2.48
DSG2	desmoglein 2	2.48
JUP	junction plakoglobin	2.48
CXCL16	chemokine (C-X-C motif) ligand 16	2.49
UNC5A	unc-5 homolog A (C. elegans)	2.51
GPR110	G protein-coupled receptor 110	2.52
EDN2	endothelin 2	2.53
PLCB4	phospholipase C, beta 4	2.54
EHF	ets homologous factor	2.54
LLGL2	lethal giant larvae homolog 2 (Drosophila)	2.57
COBL	cordon-bleu WH2 repeat protein	2.57
CLDN3	claudin 3	2.58
GCNT3	glucosaminyl (N-acetyl) transferase 3, mucin type	2.60
C10orf55	chromosome 10 open reading frame 55	2.62
TUBA4A	tubulin, alpha 4a	2.62
CLDN7	claudin 7	2.68
PLAU	plasminogen activator, urokinase	2.70
SPNS2	spinster homolog 2	2.74
C3	complement component 3	2.77
KRT23	keratin 23	2.79
PLLP	plasmolipin	2.80
MYO5B	myosin VB	2.81
CST6	cystatin E/M	2.83
SGPP2	sphingosine-1-phosphate phosphatase 2	2.85
ANXA3	annexin A3	2.86
CLDN4	claudin 4	2.91

TGFA	transforming growth factor, alpha	2.94
PRSS8	protease, serine, 8	3.03
PDZK1IP1	PDZK1 interacting protein 1	3.05
SOX17	SRY (sex determining region Y)-box 17	3.06
C1orf116	chromosome 1 open reading frame 116	3.09
MSLN	mesothelin	3.12
L1CAM	L1 cell adhesion molecule	3.24
WWC1	WW and C2 domain containing 1	3.30
SERPINA1	serpin peptidase inhibitor, clade A, member 1	3.36
MUC16	mucin 16, cell surface associated	3.55
ITGB4	integrin, beta 4	3.59
MYH14	myosin, heavy chain 14, non-muscle	3.63
LAMB3	laminin, beta 3	4.00

Supplemental Table 12. DGE between eMSC and TA

Gene	Description	Fold Change
SERPINB2	serpin peptidase inhibitor, clade B, member 2	3.52
NEFM	neurofilament, medium polypeptide	3.38
KIAA1549L	KIAA1549-like	2.70
FST	follistatin	2.59
CCBE1	collagen and calcium binding EGF domains 1	2.43
FGF5	fibroblast growth factor 5	2.35
SERPINE1	serpin peptidase inhibitor, clade E, member 1	2.32
SERPINB7	serpin peptidase inhibitor, clade B, member 7	2.30
FAM167A	family with sequence similarity 167, member A	2.29
MSC	musculin	2.26
NRG1	neuregulin 1	2.25
SPHK1	sphingosine kinase 1	2.25
LYPD1	LY6/PLAUR domain containing 1	2.19
COL15A1	collagen, type XV, alpha 1	2.19
POU2F2	POU class 2 homeobox 2	2.18
PDGFA	platelet-derived growth factor alpha polypeptide	2.15
LTBP1	latent transforming growth factor beta binding protein 1	2.14
STC1	stanniocalcin 1	2.09
HMGA2	high mobility group AT-hook 2	2.08
IL11	interleukin 11	2.07
NNMT	nicotinamide N-methyltransferase	2.07
TNFAIP6	tumor necrosis factor, alpha-induced protein 6	2.05
ITGBL1	integrin, beta-like 1	2.05
STMN3	stathmin-like 3	2.03
SLC22A23	solute carrier family 22, member 23	2.03
TMEM158	transmembrane protein 158	2.03
DOCK10	dedicator of cytokinesis 10	2.03
RGMB-AS1	RGMB antisense RNA 1	2.02
COL10A1	collagen, type X, alpha 1	2.02
GPR39	G protein-coupled receptor 39	2.00
BRINP1	bone morphogenetic protein/retinoic acid inducible neural-specific 1	-2.31
COCH	cochlin	-2.12
ACKR3	atypical chemokine receptor 3	-2.04

Supplemental Table 13. Genes enriched in eMSC when compared to PVC and EnSC. Genes were classified in transcription factors (green), cell surface proteins (blue), and 10 top markers (purple).

Gene	FoldChange MSC_vs_PVC	FoldChange MSC_vs_EnSC	Classification
CBLN2	255.26	140.71	
COL10A1	63.04	70.30	
LRRC17	57.29	64.19	
AL121963.1	128.63	46.40	
NPBWR1	83.56	45.62	
CLEC1B	76.38	39.51	
CDK15	15.37	38.45	
KRT40	159.51	33.63	
EVI2B	11.49	30.68	
TMEM119	8.50	27.25	
GREM2	33.22	22.45	
SLITRK5	14.05	21.39	
DPT	20.24	21.09	
SLC38A4	13.80	20.88	
CLDN11	25.16	18.80	
BAI3	11.79	18.17	
FBXL13	15.34	17.42	
AKR1C1	9.01	16.99	
CST1	23.76	16.20	
ALDH1L1	22.07	16.15	
HGF	39.95	15.41	
ITGA8	15.85	14.14	
MPZ	7.21	14.04	
ITPRIPL1	11.09	14.01	
PCDH9	11.37	13.10	
AKR1C2	11.28	12.30	
CXXC4	11.01	12.20	
SLIT2	6.52	11.80	
AK5	12.14	11.38	
COLEC12	7.19	10.44	
TRPV2	9.81	9.87	
CST4	13.18	9.69	
CNIH3	14.84	9.63	
LINC00942	4.17	9.44	
BNC1	13.56	9.13	
NQO1	10.03	9.06	
RP11-138I1.2	10.44	9.00	
RP11-3L21.2	14.30	8.94	
EDARADD	6.19	8.91	
ETV1	13.47	8.84	
PRSS35	4.50	8.81	
TRPA1	5.42	8.71	
FOXF1	12.49	8.58	
DACH1	6.04	8.55	
CD163L1	9.21	8.54	
TOX	9.69	8.51	
FST	4.94	8.15	
SLC14A1	26.02	8.11	
ISM1	7.68	7.96	
PRSS3	6.18	7.90	
VEPH1	4.51	7.85	
S100A4	9.06	7.78	
LRP1B	13.74	7.67	

CTD-2033A16.1	7.32	7.65	
FAM180A	4.37	7.54	
LPAR3	14.90	7.48	
ST8SIA4	5.34	7.44	
SCN9A	3.37	7.19	
LAG3	8.49	7.04	
NCKAP5	9.53	7.02	
GALNT6	7.25	6.96	
MMP1	13.01	6.56	
TRHDE	7.68	6.53	
GSG1	4.98	6.40	
ENOX1	4.46	6.39	
VAT1L	8.36	6.28	
HTR1B	4.23	6.23	
NHSL2	3.05	6.20	
WTAPP1	11.71	6.13	
SLC7A11	6.82	6.10	
RAC2	9.45	5.89	
HSD17B2	6.13	5.88	
SERPINF1	5.50	5.88	
DOCK10	3.35	5.73	
BFSP1	7.24	5.71	
LRRC8C	6.43	5.65	
PLA2G4A	19.99	5.62	
OLFML3	6.68	5.55	
GABRA2	5.88	5.51	
HMCN1	7.33	5.48	
TRHDE-AS1	5.33	5.47	
ELTD1	4.02	5.44	
ENAM	8.90	5.40	
PTGER4	11.19	5.37	
PIR	9.57	5.28	
ST6GAL2	6.31	5.19	
SLC4A4	9.05	5.18	
SYTL5	8.18	5.16	
SLC7A11-AS1	5.67	5.13	
RP11-342D11.2	3.80	5.13	
STEAP3	6.17	5.07	
ADAMTS17	9.45	5.02	
CAMK1G	9.03	4.87	
AL121578.2	8.62	4.86	
STEAP3-AS1	5.20	4.84	
RP11-133O22.6	6.01	4.79	
E2F7	4.81	4.76	
RP11-25K19.1	5.62	4.75	
PLEK2	7.37	4.74	
AKR1C3	15.46	4.67	
NCAM2	4.29	4.65	
CPNE7	2.71	4.61	
POPDC3	4.95	4.60	
G6PD	5.90	4.59	
NRP1	3.62	4.47	
FRMD3	3.48	4.46	
LIN7A	3.49	4.45	
METTL7A	4.60	4.44	
ITGA10	5.14	4.41	

F2RL2	4.27	4.36
SNCG	4.06	4.35
ANO4	3.18	4.29
ADIRF	3.22	4.19
RASGRF2	7.46	4.17
AC098617.1	3.52	4.07
ARHGAP18	3.88	4.03
ABI3BP	2.60	4.00
TNFSF15	6.17	4.00
ATP2B1	3.49	3.98
RP11-34A14.3	3.28	3.93
LYPD1	10.08	3.90
COL6A3	3.77	3.88
SEMA3D	4.56	3.82
TFAP2C	5.26	3.78
SPRY2	4.78	3.74
TNFRSF19	5.41	3.69
GPR126	4.22	3.68
LOXL4	3.41	3.68
GPR39	8.18	3.64
CHN1	3.47	3.63
CROT	3.72	3.47
TMEM26	4.16	3.45
HS3ST3A1	4.50	3.44
LINC00883	3.89	3.42
PCDHGA10	3.12	3.40
NR2F1	3.75	3.39
ADAM23	3.02	3.38
TENM4	3.49	3.35
FRMD4A	3.01	3.29
DPYD	2.47	3.27
EHD3	3.41	3.27
PREX1	5.67	3.26
MMP16	2.56	3.25
GLT8D2	3.35	3.23
SECTM1	5.66	3.22
RP11-879F14.2	3.24	3.19
RPS6KA5	4.15	3.18
SEMA6A	4.49	3.17
TKT	4.23	3.17
NRGN	4.19	3.16
GLI3	3.48	3.15
AOX1	3.21	3.10
ABCC4	3.80	3.07
TMEM200A	2.32	3.06
SH2B3	3.00	3.05
CARD16	4.46	3.03
SCPEP1	3.09	3.02
CD109	3.26	2.96
ADRA1D	4.39	2.96
MAP1A	2.48	2.89
COL6A1	2.14	2.89
SCN1B	3.58	2.88
ITGA2	3.40	2.88
B4GALNT1	2.90	2.86
DOCK4	4.00	2.85
AHRR	2.66	2.85
SLC20A1	2.66	2.84

SERPINB7	5.43	2.81	
BEND6	2.69	2.80	
PRDM8	3.15	2.80	
F2RL1	5.12	2.73	
TBC1D4	2.40	2.73	
SRPX	2.44	2.70	
SLC4A8	2.69	2.69	
THSD4	2.85	2.68	
GPER1	2.76	2.68	
TNC	2.28	2.68	
WLS	3.02	2.67	
PTGR1	3.18	2.66	
TBC1D8	3.41	2.66	
LRP8	3.07	2.65	
MLLT11	2.88	2.64	
MUM1L1	2.99	2.63	
PCDHGA11	2.25	2.63	
TLE3	2.73	2.62	
EMILIN1	2.66	2.61	
AEBP1	2.45	2.61	
SLC6A6	2.75	2.60	
RGL1	2.75	2.59	
MXRA5	3.41	2.56	
MAP3K7CL	2.34	2.55	
PHKA1	2.82	2.54	
HS3ST3B1	3.33	2.54	
COL4A5	2.25	2.51	
CPT1A	2.82	2.49	
SKP2	2.57	2.49	
DUSP6	2.98	2.48	
NR2F1-AS1	2.64	2.48	
GSTM2	2.43	2.47	
PGD	3.41	2.46	
LRRN4CL	3.08	2.45	
SAMD12	3.24	2.45	
PVRL3	2.43	2.44	
BMP2K	2.49	2.44	
ME1	2.48	2.43	
SPRY4	2.68	2.41	
RP11-290L1.3	3.28	2.41	
COL7A1	2.71	2.41	
MMP14	2.54	2.39	
TXNRD1	2.58	2.37	
TMEM164	2.90	2.37	
PRNP	2.27	2.35	
RP11-867G23.12	2.65	2.34	
PHLDA1	2.76	2.32	
WNT5B	2.27	2.32	
SDPR	2.82	2.32	
TRERF1	2.36	2.32	
DNM1	2.67	2.31	
ACAT2	2.60	2.29	
PFN2	2.13	2.28	
UCHL1	2.01	2.28	
NLRC5	2.29	2.27	
NXPE3	2.31	2.26	
TMEM51	3.89	2.26	

RIN1	2.77	2.25	
IDH1	2.90	2.24	
IQGAP2	2.40	2.23	
MMP17	2.07	2.23	
CPED1	2.61	2.23	
MELK	2.62	2.22	
CDC20	2.85	2.21	
SRPX2	2.61	2.20	
PDIA4	2.86	2.20	
PLAU	6.70	2.18	
ARRB1	2.53	2.17	
FTL	2.25	2.15	
GNG11	2.12	2.15	
COL13A1	2.99	2.15	
SATB2	2.43	2.14	
HERC3	2.04	2.14	
AGPAT9	4.47	2.13	
PTPLAD2	2.27	2.13	
CDC25B	2.41	2.11	
RP11-529K1.4	2.23	2.11	
ARHGAP19	2.67	2.11	
RUNX2	2.84	2.09	
CTSL	2.19	2.09	
KIAA0101	2.09	2.09	
SSTR1	2.59	2.08	
FAH	2.28	2.08	
FHOD1	2.12	2.08	
PPT1	2.12	2.07	
IKBKG	2.32	2.07	
ZDHHC2	2.03	2.04	
ASPM	2.28	2.03	
LRP11	2.33	2.03	
SH3BP1	2.05	2.01	
C6orf201	2.12	2.00	

Supplemental Table 14. Summary of demographic details of patient samples used on section 4.2.3. Data is represented as median (range).

	Day of Cycle	Age	Live-births	Previous losses	BMI
Group 1	LH+6/7	35.5 (25-41)	0 (0-2)	5 (0-18)	25 (20-43)
Group 2	LH+8/9	36.5 (31-40)	0 (0-1)	1.5 (0-9)	25.5 (20-34)
Group 3	LH+10/11	36 (30-41)	0 (0-1)	1.5 (0-7)	24 (20-41)

Supplemental Table 15. Summary of demographic details of patient samples used on section 4.2.4. Data is represented as median (range).

Day of Cycle	Age	live-births	Previous losses	BMI
7	38 (31-41)	0 (0-1)	5 (1-7)	26.5 (21-50)
9	38 (31-46)	0 (0-1)	3.5 (2-6)	24 (22-32)
11	34.5 (30-40)	0 (0-1)	5 (0-6)	23 (21-29)

Supplemental Table 16. Summary of demographic details of patient samples used on section 4.2.5. Data is represented as median (range).

Day of the Cycle	Previous losses	n
7	5 (3-14)	14
8	5 (0-9)	13
9	7 (1-14)	11
10	1 (1-5)	3
11	7 (2-8)	4

Supplemental Table 17. Summary of demographic details of patient samples used on section 4.2.7. Data is represented as median (range).

Group	Age	Live Births	Previuos losses	BMI
Control	34 (31-40)	0 (0-0)	0 (0-1)	22 (20-29)
RPL	35.5 (31-39)	0 (0-1)	5.5 (3-18)	24.5 (21-58)

References

Abomaray, F. M., Abumaree, M. H., Alshehri, N. A., Almutairi, A., Alaskar, A. S., Kalionis, B. & Al Jumah, M. A. (2016) Phenotypic and Functional Characterization of Mesenchymal Stem/Multipotent Stromal Cells from Decidua Parietalis of Human Term Placenta. Reproductive Sciences, 23 (9): 1193-1207.

Achache, H. & Revel, A. (2006) Endometrial receptivity markers, the journey to successful embryo implantation. Human Reproduction Update, 12 (6): 731-746.

Aghajanova, L., Hamilton, A. E. & Giudice, L. C. (2008) Uterine Receptivity to Human Embryonic Implantation: Histology, Biomarkers, and Transcriptomics. Seminars in Cell and Developmental Biology, 19 (2): 204-211.

Aghajanova, L., Horcajadas, J. A., Esteban, F. J. & Giudice, L. C. (2010) The Bone Marrow-Derived Human Mesenchymal Stem Cell: Potential Progenitor of the Endometrial Stromal Fibroblast1. Biology of Reproduction, 82 (6): 1076-1087.

Alawadhi, F., Du, H., Cakmak, H. & Taylor, H. S. (2014) Bone Marrow-Derived Stem Cell (BMDSC) transplantation improves fertility in a murine model of asherman's syndrome. PLoS ONE, 9 (5): 1-6.

Alcayaga-Miranda, F., Cuenca, J., Luz-Crawford, P., Aguila-Díaz, C., Fernandez, A., Figueroa, F. E. & Khoury, M. (2015) Characterization of menstrual stem cells: angiogenic effect, migration and hematopoietic stem cell support in comparison with bone marrow mesenchymal stem cells. Stem cell research & therapy, 6 (1): 32-32.

Alexandris, E., Milingos, S., Kollios, G., Seferiadis, K., Lolis, D. & Messinis, I. E. (1997) Changes in gonadotrophin response to gonadotrophin releasing hormone in normal women following bilateral ovariectomy. Clinical Endocrinology, 47 721-726.

Allickson, J. G., Sanchez, A., Yefimenko, N., Borlongan, C. V. & Sanberg, P. R. (2011) Recent Studies Assessing the Proliferative Capability of a Novel Adult Stem Cell Identified in Menstrual Blood. The open stem cell journal, 3 (2011): 4-10.

Altmäe, S., Koel, M., Vösa, U., Adler, P., Suhorutsenko, M., Laisk-Podar, T., Kukushkina, V., Saare, M., Velthut-Meikas, A., Krjutskov, K., Aghajanova, L., Lalitkumar, P. G., Gemzell-Danielsson, K., Giudice, L., Simón, C. & Salumets, A. (2017) Meta-signature of human endometrial receptivity: A meta-analysis and validation study of transcriptomic biomarkers. Scientific Reports, 7 (1): 1-15.

Andrews, T. S. & Hemberg, M. (2018) Identifying cell populations with scRNASeq. Molecular Aspects of Medicine, 59 114-122.

Angelidis, I., Simon, L. M., Fernandez, I. E., Strunz, M., Mayr, C. H., Greiffo, F. R., Tsitsiridis, G., Ansari, M., Graf, E., Strom, T. M., Nagendran, M., Desai, T., Eickelberg, O., Mann, M., Theis, F. J. & Schiller, H. B. (2019) An atlas of the aging lung mapped by single cell transcriptomics and deep tissue proteomics. Nature communications, 10 (1): 963-963.

Aplin, J. D., Charlton, A. K. & Ayad, S. (1988) An immunohistochemical study of human endometrial extracellular matrix during the menstrual cycle and first trimester of pregnancy. Cell tissue research, 253 231-240.

Arici, A. (2002) Local Cytokines in Endometrial Tissue: The Role of Interleukin-8 in the Pathogenesis of Endometriosis. Annals of the New York Academy of Sciences, 955 (1): 101-109.

Baghirova, S., Hughes, B. G., Hendzel, M. J. & Schulz, R. (2015) Sequential fractionation and isolation of subcellular proteins from tissue or cultured cells. MethodsX, 2 440-445.

Bakken, T. E., Hodge, R. D., Miller, J. A., Yao, Z., Nguyen, T. N., Aevermann, B., Barkan, E., Bertagnolli, D., Casper, T., Dee, N., Garren, E., Goldy, J., Graybuck, L. T., Kroll, M., Lasken, R. S., Lathia, K., Parry, S., Rimorin, C., Scheuermann, R. H., Schork, N. J., Shehata, S. I., Tieu, M., Phillips, J. W., Bernard, A., Smith, K. A., Zeng, H., Lein, E. S. & Tasic, B. (2018) Single-nucleus and single-cell transcriptomes compared in matched cortical cell types. PLOS ONE, 13 (12): 1-24.

Barragan, F., Irwin, J. C., Balayan, S., Erikson, D. W., Chen, J. C., Houshdaran, S., Piltonen, T. T., Spitzer, T. L. B., George, A., Rabban, J. T., Nezhat, C. & Giudice, L. C. (2016) Human Endometrial Fibroblasts Derived from Mesenchymal Progenitors Inherit Progesterone Resistance and Acquire an Inflammatory Phenotype in the Endometrial Niche in Endometriosis. Biology of Reproduction, 94 (5): 118-118.

Barros, F. (2017). Characterization of human endometrial glandular epithelium in vitro and in vivo.

Barros, F., Brosens, J. & Brighton, P. (2016) Isolation and Primary Culture of Various Cell Types from Whole Human Endometrial Biopsies. Bio-Protocol, 6 (22): 1-13.

Bartsch, G., Yoo, J. J., Coppi, P. D., Siddiqui, M. M., Schuch, G., Pohl, H. G., Fuhr, J. & Perin, L. (2005) Propagation, Expansion, and Multilineage Differentiation of Human Somatic Stem Cells from Dermal Progenitors. Stem Cells and Development, 14 (3):

Battula, V. L., Treml, S., Abele, H. & Bühring, H.-J. (2008) Prospective isolation and characterization of mesenchymal stem cells from human placenta using a frizzled-9-specific monoclonal antibody. Differentiation, 76 (4): 326-336.

Baum, C. M., Weissman, I. L., Tsukamoto, A. S., Buckle, A. M. & Peault, B. (1992) Isolation of a candidate human hematopoietic stem-cell population. Proceedings of the National Academy of Sciences of the United States of America, 89 (7): 2804-2808.

Bausch-Fluck, D., Hofmann, A., Bock, T., Frei, A. P. & Cerciello, F. (2015) A Mass Spectrometric-Derived Cell Surface Protein Atlas. PloS one, 10 e0121314-e0121314.

Benda (1894) Klinisches Handbuch der Harn und Sexualorgane. Leipzig. p71

Berenson, R. J., Andrews, R. G., Bensinger, W. I., Kalamasz, D., Knitter, G., Buckner, C. D. & Bernstein, I. D. (1988) Antigen CD34+ marrow cells engraft lethally irradiated baboons. The Journal of clinical investigation, 81 (3): 951-955.

Bezman, N. A., Kim, C. C., Sun, J. C., Min-Oo, G., Hendricks, D. W., Kamimura, Y., Best, J. A., Goldrath, A. W. & Lanier, L. L. (2012) ImmGen Report: Molecular definition of Natural Killer cell identity and activation. Nat Imm, 13 (10): 1000-1009.

Bhagwat, S. R., Chandrashekar, D. S., Kakar, R., Davuluri, S., Bajpai, A. K., Nayak, S., Bhutada, S., Acharya, K. & Sachdeva, G. (2013) Endometrial Receptivity: A Revisit to Functional Genomics Studies on Human Endometrium and Creation of HGEx-ERdb. PLoS ONE, 8 (3):

Bikeye, S. N. N., Colin, C., Marie, Y., Vampouille, R., Ravassard, P., Rousseau, A., Boisselier, B., Idbaih, A., Calvo, C. F., Leuraud, P., Lassalle, M., El Hallani, S., Delattre, J. Y. & Sanson, M. (2010) ASPM-associated stem cell proliferation is involved in malignant progression of gliomas and constitutes an attractive therapeutic target. Cancer Cell International, 10 1-9.

Bindu A, H. & B, S. (2011) Potency of Various Types of Stem Cells and their Transplantation. Journal of Stem Cell Research & Therapy, 01 (03): 1-6.

Brighton, P. J., Maruyama, Y., Fishwick, K., Vrljicak, P., Tewary, S., Fujihara, R., Muter, J., Lucas, E. S., Yamada, T., Woods, L., Lucciola, R., Hou Lee, Y., Takeda, S., Ott, S., Hemberger, M., Quenby, S. & Brosens, J. J. (2017) Clearance of senescent decidual cells by uterine natural killer cells in cycling human endometrium. eLife, 6 1-23.

Brosens, I. & Benagiano, G. (2013) Is neonatal uterine bleeding involved in the pathogenesis of endometriosis as a source of stem cells? Fertility and Sterility, 100 (3): 622-623.

Brosens, J. J., Pijnenborg, R. & Brosens, I. a. (2002) The myometrial junctional zone spiral arteries in normal and abnormal pregnancies. American Journal of Obstetrics and Gynecology, 187 (5): 1416-1423.

Brosens, J. J., Salker, M. S., Teklenburg, G., Nautiyal, J., Salter, S., Lucas, E. S., Steel, J. H., Christian, M., Chan, Y.-W., Boomsma, C. M., Moore, J. D., Hartshorne, G. M., Su$f$áurovi$f$á, S., Mulac-Jericevic, B., Heijnen, C. J., Quenby, S., Koerkamp, M. J. G., Holstege, F. C. P., Shmygol, A. & Macklon, N. S. (2014) Uterine selection of human embryos at implantation. Scientific reports, 4 3894-3894.

Bryder, D., Rossi, D. J. & Weissman, I. L. (2006) Hematopoietic stem cells: The paradigmatic tissue-specific stem cell. American Journal of Pathology, 169 (2): 338-346.

Bu, S., Wang, Q., Zhang, Q., Sun, J., He, B., Xiang, C., Liu, Z. & Lai, D. (2016) Human endometrial mesenchymal stem cells exhibit intrinsic anti-tumor properties on human epithelial ovarian cancer cells. Scientific Reports, 6 (October): 1-14.

Bulmer, D., Morrison, J.N., Longfellow, L., Ritson, M., Pace, A., (1991) Granulated lymphocytes in human endometrium: histochemical and immunohistochemical studies. Human reproduction, 6 791-798.

BüHring, H.J., Battula, V. L., Treml, S., Schewe, B., Kanz, L. & Vogel, W. (2007) Novel Markers for the Prospective Isolation of Human MSC. Annals of the New York Academy of Sciences, 1106 (1): 262-271.

Caglayan, S., Ahrens, T. D., Cieslar-Pobuda, A. & Staerk, J. (2019) Chapter 3 - Modern Ways of Obtaining Stem Cells. In: Stem Cells and Biomaterials for Regenerative Medicine. Academic Press: 17-36.

Cai, Q., Wang, B., Patel, M., Yang, S. M. & Hu, B. H. (2013) RNAlater facilitates microdissection of sensory cell-enriched samples from the mouse cochlea for transcriptional analyses. Journal of Neuroscience Methods, 219 (2): 1-7.

Caplan, A. I. (1991) Mesenchymal stem cells. Journal of Orthopaedic Research, 9 (5): 641-650.

Caplan, A. I. (2015) Are All Adult Stem Cells The Same? Regenerative Engineering and Translational Medicine, 1 (1-4): 4-10.

Carolina, N. (2007) TISSUE-SPECIFIC STEM CELLS Concise Review: Hematopoietic Stem Cells and Tissue Stem Cells. Access, 1135-1141.

Castrechini, N. M., Murthi, P., Qin, S., Kusuma, G. D., Wilton, L., Abumaree, M., Gronthos, S., Zannettino, A., Gude, N. M., Brennecke, S. P. & Kalionis, B. (2012) Decidua Parietalis-Derived Mesenchymal Stromal Cells Reside in a Vascular Niche Within the Choriodecidua. Reproductive Sciences, 19 (12): 1302-1314.

Chaffkin, L. M., Luciano, A. A. & Peluso, J. J. (1992) Progesterone as an autocrine/paracrine regulator of human granulosa cell proliferation. The Journal of Clinical Endocrinology & Metabolism, 75 (6): 1404-1408.

Chan, C., Virtanen, C., Winegarden, N. A., Colgan, T. J., Brown, T. J. & Greenblatt, E. M. (2013) Discovery of biomarkers of endometrial receptivity through a minimally invasive approach: A validation study with implications for assisted reproduction. Fertility and Sterility, 100 (3): 810-817.e818.

Chan, R. W. S., Schwab, K. E. & Gargett, C. E. (2004) Clonogenicity of Human Endometrial Epithelial and Stromal Cells1. Biology of Reproduction, 70 (6): 1738-1750.

Chen, L., Qu, J. & Xiang, C. (2019) The multi-functional roles of menstrual blood-derived stem cells in regenerative medicine. Stem Cell Research & Therapy, 10 (1): 1-10.

Chen, L., Xiang, B., Wang, X. & Xiang, C. (2017) Exosomes derived from human menstrual blood-derived stem cells alleviate fulminant hepatic failure. Stem Cell Research & Therapy, 8 (1): 9-9.

Chen, B., Khodadoust, M.S., Liu, C.L., Newman, A.M. & Alizadeh, A.A. (2018) Profiling Tumor Infiltrating Immune Cells with CIBERSORT. Methods in molecular biology (Clifton, N.J.). 1711, pp.243–259.

Cheung, T. & Rando, T. (2013) Molecular regulation of stem cell quiescence. Nature Reviews Molecular Cellular Biology, 14 (6):

Cho, A., Park, S. R., Kim, S. R., Nam, S., Lim, S., Park, C. H., Lee, H. Y. & Hong, I. S. (2019) An Endogenous Anti-aging Factor, Sonic Hedgehog, Suppresses Endometrial Stem Cell Aging through SERPINB2. Molecular Therapy, 27 (7): 1-13.

Chuang, H. Y. & Ou, Y. H. (2014) Overexpression of anillin in colorectal cancer promotes the cell proliferation, cell mobility and cell invasion. Cancer Research, 74 (19 Supplement): 4068-4068.

Conti, M., Hsieh, M., Zamah, a. M. & Oh, J. S. (2012) Novel signaling mechanisms in the ovary during oocyte maturation and ovulation. Molecular and cellular endocrinology, 356 (1-2): 65-73.

Cousins, F. L., Murray, A., Esnal, A., Gibson, D. A., Critchley, H. O. D. & Saunders, P. T. K. (2014) Evidence from a mouse model that epithelial cell migration and mesenchymal-epithelial transition contribute to rapid restoration of uterine tissue integrity during menstruation. PLoS ONE, 9 (1): 1-12.

Craig, W., Kay, R., Cutler, R. L. & Lansdorp, P. M. (1993) Expression of Thy-1 on human hematopoietic progenitor cells. Journal of Experimental Medicine, 177 (5): 1331-1342.

Crisan, M., Yap, S., Casteilla, L., Chen, C. W., Corselli, M., Park, T. S., Andriolo, G., Sun, B., Zheng, B., Zhang, L., Norotte, C., Teng, P. N., Traas, J., Schugar, R., Deasy, B. M., Badylak, S., Buhring, H. J., Giacobino, J. P., Lazzari, L., Huard, J. & P√©ault, B. (2008) A Perivascular Origin for Mesenchymal Stem Cells in Multiple Human Organs. Cell Stem Cell, 3 (3): 301-313.

Crum, C. P., Hornstein, M. D., Nucci, M. R. & Mutter, G. L. (2003) Hertig and beyond: A systematic and practical approach to, the endometrial biopsy. Advances in Anatomic Pathology, 10 (6): 301-318.

Cui, C.-H., Uyama, A., Miyado, K., Terai, M., Kyo, S., Kiyono, T. & Umezawa, A. (2007) Menstrual Blood derived cells confer dystrophin expression in the murine

model of Duchene muscular dystrophy via cell fusion and myogenic transdifferentiation. Molecular biology of the cell, 18 1586-1594.

Cui, Y., Zheng, Y., Liu, X., Yan, L., Fan, X., Yong, J., Hu, Y., Dong, J., Li, Q., Wu, X., Gao, S., Li, J., Wen, L., Qiao, J. & Tang, F. (2019) Single-Cell Transcriptome Analysis Maps the Developmental Track of the Human Heart. Cell Reports, 26 (7): 1934-1950.e1935.

Davidson, L. M. & Coward, K. (2016) Molecular mechanisms of membrane interaction at implantation. Birth Defects Research Part C - Embryo Today: Reviews, 108 (1): 19-32.

De Filippo, K., Dudeck, A., Hasenberg, M., Nye, E., Van Rooijen, N., Hartmann, K., Gunzer, M., Roers, A. & Hogg, N. (2013) Mast cell and macrophage chemokines CXCL1/CXCL2 control the early stage of neutrophil recruitment during tissue inflammation. Blood, 121 (24): 4930-4937.

Demir, R., Kayisli, U. A., Celik-Ozenci, C., Korgun, E. T., Demir-Weusten, A. Y. & Arici, A. (2002) Structural differentiation of human uterine luminal and glandular epithelium during early pregnancy: An ultrastructural and immunohistochemical study. Placenta, 23 (8-9): 672-684.

Deng, C., Xu, Y., Fu, J., Zhu, X., Chen, H., Xu, H., Wang, G., Song, Y., Song, G., Lu, J., Liu, R., Tang, Q., Huang, W. & Wang, J. 2020. Reprograming the tumor immunologic microenvironment by neoadjuvant chemotherapy in osteosarcoma. Accepted in Cancer Science.

Dey, S. K., Lim, H., Das, S. K., Reese, J., Paria, B. C., Daikoku, T. & Wang, H. (2004) Molecular cues to implantation. Endocrine reviews, 25 (3): 341-373.

Dimitrov, R., Kyurkchiev, D., Timeva, T., Yunakova, M., Stamenova, M., Shterev, A. & Kyurkchiev, S. (2010) First-trimester human decidua contains a population of mesenchymal stem cells. Fertility and Sterility, 93 (1): 210-219.

Dominici, M., Le Blanc, K., Mueller, I., Slaper-Cortenbach, I., Marini, F. C., Krause, D. S., Deans, R. J., Keating, A., Prockop, D. J. & Horwitz, E. M. (2006) Minimal criteria for defining multipotent mesenchymal stromal cells. The International Society for Cellular Therapy position statement. Cytotherapy, 8 (4): 315-317.

Dougherty, J. D., Garcia, A. D. R., Nakano, I., Livingstone, M., Norris, B., Polakiewicz, R., Wexler, E. M., Sofroniew, M. V., Kornblum, H. I. & Geschwind, D. H. (2005) PBK/TOPK, a Proliferating Neural Progenitor-Specific Mitogen-Activated Protein Kinase Kinase. Journal of Neuroscience, 25 (46): 10773-10785.

Douville, J., Beaulieu, R. & Balicki, D. (2009) ALDH1 as a Functional Marker of Cancer Stem and Progenitor Cells. Stem cells and Development, 18 (1):

Draber, P., Stepanek, O., Hrdinka, M., Drobek, A., Chmatal, L., Mala, L., Ormsby, T., Angelisova, P., Horejsi, V. & Brdicka, T. (2012) LST1/A is a myeloid leukocyte-specific

transmembrane adaptor protein recruiting protein tyrosine phosphatases SHP-1 and SHP-2 to the plasma membrane. Journal of Biological Chemistry, 287 (27): 22812-22821.

Drury, J. A., Tang, A. W., Turner, M. A. & Quenby, S. (2013) A rapid, reliable method for uNK cell density estimation. Journal of Reproductive Immunology, 97 183-185.

Du, H. & Taylor, H. S. (2007) Contribution of Bone Marrow-Derived Stem Cells to Endometrium and Endometriosis. Stem Cells, 25 (8): 2082-2086.

Dworzak, M. N., Fritsch, G., Fr√∂schl, G., Printz, D. & Gadner, H. (1998) Four-color flow cytometric investigation of terminal deoxynucleotidyl transferase-positive lymphoid precursors in pediatric bone marrow: CD79a expression precedes CD19 in early B-cell ontogeny. Blood, 92 (9): 3203-3209.

Díaz-Gimeno, P., Horcajadas, J. A., Martinez-Conejero, J. A., Esteban, F. J., Alama, P., Pellicer, A. & Simon, C. (2010) A genomic diagnostic tool for human endometrial receptivity based on the transcriptomic signature. Revista Iberoamericana de Fertilidad y Reproduccion Humana, 27 (4): 337-351.

Elahi, K. C., Klein, G., Avci-Adali, M., Sievert, K. D., Macneil, S. & Aicher, W. K. (2016) Human mesenchymal stromal cells from different sources diverge in their expression of cell surface proteins and display distinct differentiation patterns. Stem Cells International, 2016 (Figure 1):

Embryology, E. S. o. H. R. a. (2017) Recurrent pregnancy loss. Guideline of the European Society of Human Reproduction and Embryology. European Society of Human Reproduction and Embryology, (November): 0-153.

Emori, M., Tsukahara, T., Murase, M., Kano, M., Murata, K., Takahashi, A., Kubo, T., Asanuma, H., Yasuda, K., Kochin, V., Kaya, M., Nagoya, S., Nishio, J., Iwasaki, H., Sonoda, T., Hasegawa, T., Torigoe, T., Wada, T., Yamashita, T. & Sato, N. (2013) High expression of CD109 antigen regulates the phenotype of cancer stem-like cells/cancer-initiating cells in the novel epithelioid sarcoma cell line ESX and is related to poor prognosis of soft tissue sarcoma. PLoS ONE, 8 (12): 1-17.

Eskenazi, B. & Warner, M. L. (1997) EPIDEMIOLOGY OF ENDOMETRIOSIS. Obstetrics and Gynecology Clinics of North America, 24 (2): 235-258.

Evans, G. E., Martinez-Conejero, J. A., Phillipson, G. T. M., Simón, C., McNoe, L. A., Sykes, P. H., Horcajadas, J. A., Lam, E. Y. N., Print, C. G., Sin, I. L. & Evans, J. J. (2012) Gene and protein expression signature of endometrial glandular and stromal compartments during the window of implantation. Fertility and Sterility, 97 (6):

Evans, J., Kaitu'u-Lino, T. & Salamonsen, L. A. (2011) Extracellular Matrix Dynamics in Scar-Free Endometrial Repair: Perspectives from Mouse In Vivo and Human In Vitro Studies. Biology of Reproduction, 85 (3): 511-523.

Evans, J. & Salamonsen, L. a. (2012) Inflammation, leukocytes and menstruation. Reviews in endocrine & metabolic disorders, 13 (4): 277-288.

Evans, J., Salamonsen, L. A., Winship, A., Menkhorst, E., Nie, G., Gargett, C. E. & Dimitriadis, E. (2016) Fertile ground: Human endometrial programming and lessons in health and disease. Nature Reviews Endocrinology, 12 (11): 654-667.

Fabriek, B. O., Dijkstra, C. D. & van den Berg, T. K. (2005) The macrophage scavenger receptor CD163. Immunobiology, 210 (2): 153-160.

Farrer-Brown, G., Beilby, J. O. W. & Tarbit, M. H. (1970) The Blood Supply of the Uterus. BJOG: An International Journal of Obstetrics & Gynaecology, 77 (8): 673-681.

Fedele, L., Bianchi, S., Marchini, M., Franchi, D., Tozzi, L. & Dorta, M. (1996) Ultrastructural aspects of endometrium in infertile women with septate uterus. Fertility and Sterility, 65 (4): 750-752.

Field, C. M. & Alberts, B. M. (1995) Anillin, a contractile ring protein that cycles from the nucleus to the cell cortex. The Journal of cell biology, 131 (1): 165-178.

Figueira, P. G. M., Abrão, M. S., Krikun, G. & Taylor, H. (2012) Stem Cells in endometrium and their role in the pathogenesis of endometriosis. Annals of the New York Academy of Sciences, 1221 (1): 10-17.

Filant, J. & Spencer, T. E. (2014) Uterine glands: biological roles in conceptus implantation, uterine receptivity and decidualization. The International journal of developmental biology, 58 (2-4): 107-116.

Gang, E. J., Bosnakovski, D., Figueiredo, C. A., Visser, J. W. & Perlingeiro, R. C. R. (2007) SSEA-4 identifies mesenchymal stem cells from bone marrow. Blood, 109 (4): 1743-1751.

Gao, R., Kim, C., Sei, E., Foukakis, T., Crosetto, N., Chan, L. K., Srinivasan, M., Zhang, H., Meric-Bernstam, F. & Navin, N. (2017) Nanogrid single-nucleus RNA sequencing reveals phenotypic diversity in breast cancer. Nature Communications, 8 (1):

Gargett, C. & Rogers, P. A. W. (2001) Human endometrial angiogenes. Reproduction, 121 181-186.

Gargett, C. E., Chan, R. W. S. & Schwab, K. E. (2008) Hormone and growth factor signaling in endometrial renewal: Role of stem/progenitor cells. Molecular and Cellular Endocrinology, 288 (1-2): 22-29.

Gargett, C. E. & Masuda, H. (2010) Adult stem cells in the endometrium. Molecular Human Reproduction, 16 (11): 818-834.

Gargett, C. E., Nguyen, H. P. T. & Ye, L. (2012) Endometrial regeneration and endometrial stem/progenitor cells. Reviews in endocrine & metabolic disorders, 13 (4): 235-251.

Gargett, C. E., Schwab, K. E. & Deane, J. A. (2016) Endometrial stem/progenitor cells: The first 10 years. Human Reproduction Update, 22 (2): 137-163.

Gargett, C. E., Schwab, K. E., Zillwood, R. M., Nguyen, H. P. T. & Wu, D. (2009) Isolation and Culture of Epithelial Progenitors and Mesenchymal Stem Cells from Human Endometrium1. Biology of Reproduction, 80 (6): 1136-1145.

Gargett, C. E. & Ye, L. (2012) Endometrial reconstruction from stem cells. Fertility and Sterility, 98 (1): 11-20.

Garry, R., Hart, R., Karthigasu, K. a. & Burke, C. (2009) A re-appraisal of the morphological changes within the endometrium during menstruation: a hysteroscopic, histological and scanning electron microscopic study. Human reproduction (Oxford, England), 24 (6): 1393-1401.

Gattazzo, F., Urciuolo, A. & Bonaldo, P. (2014) Extracellular matrix: a dynamic microenvironment for stem cell niche. Biochimica et biophysica acta, 1840 (8): 2506-2519.

Gazit, Z., Aslan, H., Gafni, Y., Kimelman, N., Pelled, G. & Gazit, D. (2008) 19 - Mesenchymal Stem Cells. In: Atala, A., Lanza, R., Thomson, J. A. & Nerem, R. M. B. T. P. o. R. M., eds. San Diego: Academic Press: 318-343.

Gellersen, B. & Brosens, J. J. (2014) Cyclic decidualization of the human endometrium in reproductive health and failure. Endocrine Reviews, 35 (6): 851-905.

Gentles, A.J., Newman, A.M., Liu, C.L., Bratman, S. V, Feng, W., Kim, D., Nair, V.S., Xu, Y., Khuong, A., Hoang, C.D., Diehn, M., West, R.B., Plevritis, S.K. & Alizadeh, A.A. (2015) The prognostic landscape of genes and infiltrating immune cells across human cancers. Nature medicine. 21(8), pp.938–945.

Ghobadi, F., Mehrabani, D. & Mehrabani, G. (2015) Regenerative potential of endometrial stem cells: a mini review. World journal of plastic surgery, 4 (1): 3-8.

Gil-Sanchis, C., Cervell√≥, I., Khurana, S., Faus, A., Verfaillie, C. & Sim√≥n, C. (2015) Contribution of different bone marrow-derived cell types in endometrial regeneration using an irradiated murine model. Fertility and Sterility, 103 (6): 1596-1605.e1591.

Giudice, L. C. (2004) Microarray Expression Profiling Reveals Candidate Genes for Human Uterine Receptivity. American Journal of Pharmacogenomics, 4 (5): 299-312.

Gómez-López, S., Lerner, R. G. & Petritsch, C. (2014) Asymmetric cell division of stem and progenitor cells during homeostasis and cancer. Cellular and Molecular Life Sciences, 71 (4): 575-597.

Groome, N., Illingworth, P., Brien, M., Pai, R., Rodger, F., Mather, J. & McNeilly, A. (1996) Measurement of Dimeric Ihnibin B throughout the Human Menstrual Cycle. Journal of Clinical Endocrinology and Metabolism, 81 (4): 1401-1405.

Grün, D., Lyubimova, A., Kester, L., Wiebrands, K., Basak, O., Sasaki, N., Clevers, H. & Van Oudenaarden, A. (2015) Single-cell messenger RNA sequencing reveals rare intestinal cell types. Nature, 525 (7568): 251-255.

Guimarães-Camboa, N., Cattaneo, P., Sun, Y., Moore-morris, T., Dalton, N.D., Rockenstein, E., Masliah, E., Peterson, K.L., Stallcup, B., Chen, J. & Evans, S.M. (2017) Pericytes of multiple organs do not behave as mesenchymal stem cells in vivo. Cell Stem Cell. **20**(3), pp.345–359.

Guo, C., Zhu, H., Huang, W., Li, S., Qu, W., Liu, Y. & Tan, A. (2010) Side population cells in the human decidua of early pregnancy exhibit stem/progenitor cell-like characteristics. Reproductive BioMedicine Online, 21 (6): 783-793.

Guo, M., Du, Y., Gokey, J. J., Ray, S., Bell, S. M., Adam, M., Sudha, P., Perl, A. K., Deshmukh, H., Potter, S. S., Whitsett, J. A. & Xu, Y. (2019) Single cell RNA analysis identifies cellular heterogeneity and adaptive responses of the lung at birth. Nature Communications, 10 (1):

Gurung, S., Werkmeister, J. A. & Gargett, C. E. (2015) Inhibition of Transforming Growth Factor-β Receptor signaling promotes culture expansion of undifferentiated human Endometrial Mesenchymal Stem/stromal Cells. Scientific Reports, 5 (June): 15042-15042.

Gurusamy, N., Alsayari, A., Rajasingh, S. & Rajasingh, J. (2018) Chapter One - Adult Stem Cells for Regenerative Therapy. In: Progress in Molecular Biology and Translational Science. Academic Press: 1-22.

Habib, N., Li, Y., Heidenreich, M., Swiech, L., Trombetta, J. J., Zhang, F. & Regev, A. (2016) Div-Seq: A single nucleus RNA-Seq method reveals dynamics of rare adult newborn neurons in the CNS. bioRxiv, 7 (August): 1-20.

Haque, A., Engel, J., Teichmann, S. A. & Lönnberg, T. (2017) A practical guide to single-cell RNA-sequencing for biomedical research and clinical applications. Genome Medicine, 9 (1): 1-12.

Harada, T., Kaponis, A., Iwabe, T., Taniguchi, F., Makrydimas, G., Sofikitis, N., Paschopoulos, M., Paraskevaidis, E. & Terakawa, N. (2004) Apoptosis in human endometrium and endometriosis. Human Reproduction Update, 10 (1): 29-38.

Hardy, W. R., Moldovan, N. I., Moldovan, L., Livak, K. J., Datta, K., Goswami, C., Corselli, M., Traktuev, D. O., Murray, I. R., Péault, B. & March, K. (2017) Transcriptional Networks in Single Perivascular Cells Sorted from Human Adipose

Tissue Reveal a Hierarchy of Mesenchymal Stem Cells. Stem Cells, 35 (5): 1273-1289.

Heath, C. G., Viphakone, N. & Wilson, S. A. (2016) The role of TREX in gene expression and disease. Biochemical Journal, 473 (19): 2911-2935.

Hempstock, J., Cindrova-Davies, T., Jauniaux, E. & Burton, G. J. (2004) Endometrial glands as a source of nutrients, growth factors and cytokines during the first trimester of human pregnancy: a morphological and immunohistochemical study. Reproductive biology and endocrinology : RB&E, 2 58-58.

Herzyk, P. (2014) Chapter 8 - Next-Generation Sequencing In: Clinical Applications for Next-Generation Sequencinged. San Diego: Academic Press, pp.125–145.

Hickey, M., Fraser, I. S., Rogers, P. & Salamonsen, L. (2000) The structure of endometrial microvessels. Human Reproduction, 15 (SUPPL. 3): 57-66.

Hombach-Klonisch, S., Kehlen, A., Fowler, P. A., Huppertz, B., Jugert, J. F., Bischoff, G., Schlüter, E., Buchmann, J. & Klonisch, T. (2005) Regulation of functional steroid receptors and ligand-induced responses in telomerase-immortalized human endometrial epithelial cells. Journal of Molecular Endocrinology, 34 (2): 517-534.

Hu, C., Yong, X., Li, C., Lü, M., Liu, D., Chen, L., Hu, J., Teng, M., Zhang, D., Fan, Y. & Liang, G. (2013) CXCL12/CXCR4 axis promotes mesenchymal stem cell mobilization to burn wounds and contributes to wound repair. Journal of Surgical Research, 183 (1): 427-434.

Huang, G. T. J., Gronthos, S. & Shi, S. (2009) Mesenchymal stem cells derived from dental tissues vs. those from other sources: their biology and role in regenerative medicine. Journal of dental research, 88 (9): 792-806.

Hwang, B., Lee, J.H. & Bang, D. (2018) Single-cell RNA sequencing technologies and bioinformatics pipelines. Experimental and Molecular Medicine. 50(8).

Ikoma, T., Kyo, S., Maida, Y., Ozaki, S., Takakura, M., Nakao, S. & Inoue, M. (2009) Bone marrow-derived cells from male donors can compose endometrial glands in female transplant recipients. American Journal of Obstetrics and Gynecology, 201 (6): 608.e601-608.e608.

Jiang, Z., Hu, X., Yu, H., Xu, Y., Wang, L., Chen, H., Chen, H., Wu, R., Zhang, Z., Xiang, C., Webster, K. A. & Wang, J.-a. (2013) Human endometrial stem cells confer enhanced myocardial salvage and regeneration by paracrine mechanisms. Journal of cellular and molecular medicine, 17 (10): 1247-1260.

Jiménez-Ayala, M. & Jiménez-Ayala Portillo, B. (2008) Cytology of the Normal Endometrium ‚Äì Cycling and Postmenopausal. In: 32-39.

Jones, R. L., Kelly, R. W. & Critchley, H. O. D. (1997) Chemokine and cyclooxygenase-2 expression in human endometrium coincides with leukocyte accumulation. Human Reproduction, 12 (6): 1300-1306.

Jungraithmayr, W., De Meester, I., Matheeussen, V., Baerts, L., Arni, S. & Weder, W. (2012) CD26/DPP-4 inhibition recruits regenerative stem cells via stromal cell-derived factor-1 and beneficially influences ischaemiareperfusion injury in mouse lung transplantation. European Journal of Cardio-thoracic Surgery, 41 (5): 1166-1173.

Jurgensen, A., Mettler, L., Volkov, N. I. & Parwaresch, R. (1996) Proliferative activity of the endometrium throughout the menstrual cycle in infertile women with and without endometriosis. Fertility and Sterility, 66 (3): 369-375.

Kadaja, M., Keyes, B. E., Lin, M., Amalia Pasolli, H., Genander, M., Polak, L., Stokes, N., Zheng, D. & Fuchs, E. (2014) SOX9: A stem cell transcriptional regulator of secreted niche signaling factors. Genes and Development, 28 (4): 328-341.

Kalluri, R. (2016) The biology and function of fibroblasts in cancer. Nature Reviews Cancer, 16 (9): 582-598.

Kamat, B. R. & Isaacson, P. G. (1987) The immunocytochemical distribution of leukocytic subpopulations in human endometrium. The American journal of pathology, 127 (1): 66-73.

Kao, A.-P., Wang, K.-H., Chang, C.-C., Lee, J.-N., Long, C.-Y., Chen, H.-S., Tsai, C.-F., Hsieh, T.-H. & Tsai, E.-M. (2011) Comparative study of human eutopic and ectopic endometrial mesenchymal stem cells and the development of an in vivo endometriotic invasion model. Fertility and Sterility, 95 (4): 1308-1315.e1301.

Kato, K., Yoshimoto, M., Kato, K., Adachi, S., Yamayoshi, A., Arima, T., Asanoma, K., Kyo, S., Nakahata, T. & Wake, N. (2007) Characterization of side-population cells in human normal endometrium. Human Reproduction, 22 (5): 1214-1223.

Khanmohammadi, M., Khanjani, S., Edalatkhah, H., Zarnani, A. H., Heidari,ÄêVala, H., Soleimani, M., Alimoghaddam, K. & Kazemnejad, S. (2014) Modified protocol for improvement of differentiation potential of menstrual blood,Äêderived stem cells into adipogenic lineage. Cell Proliferation, 47 (6): 615-623.

Khatun, M., Sorjamaa, A., Kangasniemi, M., Sutinen, M., Salo, T., Liakka, A., Lehenkari, P., Tapanainen, J. S., Vuolteenaho, O., Chen, J. C., Lehtonen, S. & Piltonen, T. T. (2017) Niche matters: The comparison between bone marrow stem cells and endometrial stem cells and stromal fibroblasts reveal distinct migration and cytokine profiles in response to inflammatory stimulus. PLoS ONE, 12 (4): 1-21.

Khoury, M., Alcayaga-Miranda, F., Illanes, S. E. & Figueroa, F. E. (2014) The promising potential of menstrual stem cells for antenatal diagnosis and cell therapy. Frontiers in Immunology, 5 (MAY): 1-8.

Kim, M. J., Lee, Y. S., Han, G. Y., Lee, H. N., Ahn, C. & Kim, C. W. (2015) Profilin 2 promotes migration, invasion, and stemness of HT29 human colorectal cancer stem cells. Bioscience, Biotechnology and Biochemistry, 79 (9): 1438-1446.

King, A. E. & Critchley, H. O. D. (2010) Oestrogen and progesterone regulation of inflammatory processes in the human endometrium. The Journal of steroid biochemistry and molecular biology, 120 (2-3): 116-126.

Koch, A. E., Polverini, P. J., Kunkel, S. L., Harlow, L. A., DiPietro, L. A., Elner, V. M., Elner, S. G. & Strieter, R. M. (1992) Interleukin-8 as a macrophage-derived mediator of angiogenesis. Science, 258 (5089): 1798-1801.

Kohli, N., Al-Delfi, I. R. T., Snow, M., Sakamoto, T., Miyazaki, T., Nakajima, H., Uchida, K. & Johnson, W. E. B. (2019) CD271-selected mesenchymal stem cells from adipose tissue enhance cartilage repair and are less angiogenic than plastic adherent mesenchymal stem cells. Scientific Reports, 9 (1): 3194-3194.

Kondo, M., Tanaka, Y., Kuwabara, T., Naito, T., Kohwi-Shigematsu, T. & Watanabe, A. (2016) SATB1 Plays a Critical Role in Establishment of Immune Tolerance. The Journal of Immunology, 196 (8): 3495-3495.

Kondo, M., Wagers, A. J., Manz, M. G., Prohaska, S. S., Scherer, D. C., Beilhack, G. F., Shizuru, J. A. & Weissman, I. L. (2003) BIOLOGY OF HEMATOPOIETIC STEM CELLS AND PROGENITORS: Implications for Clinical Application. Annual Review of Immunology, 21 (1): 759-806.

Koopman, L. A., Kopcow, H. D., Rybalov, B., Boyson, J. E., Orange, J. S., Schatz, F., Masch, R., Lockwood, C. J., Schachter, A. D., Park, P. J. & Strominger, J. L. (2003) Human Decidual Natural Killer Cells Are a Unique NK Cell Subset with Immunomodulatory Potential. Journal of Experimental Medicine, 198 (8): 1201-1212.

Kuroda, Y., Kitada, M., Wakao, S., Nishikawa, K., Tanimura, Y., Makinoshima, H., Goda, M., Akashi, H., Inutsuka, A., Niwa, A., Shigemoto, T., Nabeshima, Y., Nakahata, T., Nabeshima, Y.-I., Fujiyoshi, Y. & Dezawa, M. (2010) Unique multipotent cells in adult human mesenchymal cell populations. Proceedings of the National Academy of Sciences of the United States of America, 107 (19): 8639-8643.

Laird, S. M., Widdowson, R., El-Sheikhi, M., Hall, A. J. & Li, T. C. (2011) Expression of CXCL12 and CXCR4 in human endometrium; Effects of CXCL12 on MMP production by human endometrial cells. Human Reproduction, 26 (5): 1144-1152.

Lake, B. B., Liu, R., Gao, D., Fung, H.-L., Chen, S., Zhang, K., Ai, R., Wildberg, A., Wang, W., Kaeser, G. E., Yung, Y. C., Wong, J., Chen, A., Sheng, X., Chun, J., Salathia, N. S., Vijayaraghavan, R., Kaper, F., Shen, R., Ronaghi, M. & Fan, J.-B. (2016) Neuronal subtypes and diversity revealed by single-nucleus RNA sequencing of the human brain. Science, 352 (6293): 1586-1590.

Laplane, L. & Solary, E. (2019) Towards a classification of stem cells. eLife, 8 (e46563): 2010-2010.

Lee, C. Q. E., Turco, M., Gardner, L., Simons, B., Hemberger, M. & Moffett, A. (2018) A niche of trophoblast progenitor cells identified by integrin Œ±2 is present in first trimester human placentas. Development, dev.162305-dev.162305.

Lee, S. K., Kim, C. J., Kim, D.-J. & Kang, J.-h. (2015) Immune Cells in the Female Reproductive Tract. Immune Network, 15 (1): 16-16.

Lennartsson, J. & Rönnstrand, L. (2012) Stem cell factor receptor/c-Kit: From basic Science to clinical implications. Physiological Reviews, 92 (4): 1619-1649.

Leyendecker, G., Herbertz, M., Kunz, G. & Mall, G. (2002) Endometriosis results from the dislocation of basal endometrium. Human Reproduction, 17 (10): 2725-2736.

Li, H., Zhang, W., Yan, M., Qiu, J., Chen, J., Sun, X., Chen, X., Song, L. & Zhang, Y. (2019a) Nucleolar and spindle associated protein 1 promotes metastasis of cervical carcinoma cells by activating Wnt/β-catenin signaling. Journal of Experimental and Clinical Cancer Research, 38 (1): 1-18.

Li, L. & Bhatia, R. (2011) Stem cell quiescence. Clinical cancer research: an official journal of the American Association for Cancer Research, 17 (15): 4936-4941.

Li, L. & Xie, T. (2005) STEM CELL NICHE: Structure and Function. Annual Review of Cell and Developmental Biology, 21 (1): 605-631.

Li, Q., Cheng, Z., Zhou, L., Darmanis, S., Neff, N. F., Okamoto, J., Gulati, G., Bennett, M. L., Sun, L. O., Clarke, L. E., Marschallinger, J., Yu, G., Quake, S. R., Wyss-Coray, T. & Barres, B. A. (2019b) Developmental Heterogeneity of Microglia and Brain Myeloid Cells Revealed by Deep Single-Cell RNA Sequencing. Neuron, 101 (2): 207-223.e210.

Li, Y. & Xie, X. (2013) A mixture model for expression deconvolution from RNA-seq in heterogeneous tissues From RECOMB-seq: Third Annual Recomb Satellite Workshop on Massively Parallel Sequencing. BMC Bioinformatics, 14 (Suppl 5): S11-S11.

Logan, P. C., Steiner, M., Ponnampalam, A. P. & Mitchell, M. D. (2012) Cell Cycle Regulation of Human Endometrial Stromal Cells During Decidualization. Reproductive Sciences, 19 (8): 883-894.

Love, M. I., Anders, S., Kim, V. & Huber, W. (2016) RNA-Seq workflow: gene-level exploratory analysis and differential expression. F1000Research, 4 1070-1070.

Lucas, E. S., Dyer, N. P., Murakami, K., Lee, Y. H., Chan, Y.-W., Grimaldi, G., Muter, J., Brighton, P. J., Moore, J., Patel, G., Chan, J. K. Y., Takeda, S., Lam, E. W. F.,

Quenby, S., Ott, S. & Brosens, J. (2016) Loss of Endometrial Plasticity in Recurrent Pregnancy Loss. Stem Cells, 34 346-356.

Lucas, E. S., Vrljicak, P., Muter, J., Diniz-da-Costa, M. M., Brighton, P. J., Kong, C. S., Lipecki, J., Fishwick, K., Odendaal, J., Ewington, L. J., Quenby, S., Ott, S. & Brosens, J. J. (2020) Recurrent pregnancy loss is associated with a pro-senescent decidual response during the peri-implantation window. Communications Biology, 3 (37)

Luecken, M.D. & Theis, F.J. (2019) Current best practices in single-cell RNA-seq analysis: a tutorial. Molecular Systems Biology. 15(6).

Luger, D., Yang, Y. a., Raviv, A., Weinberg, D., Banerjee, S., Lee, M. J., Trepel, J., Yang, L. & Wakefield, L. M. (2013) Expression of the B-Cell Receptor Component CD79a on Immature Myeloid Cells Contributes to Their Tumor Promoting Effects. PLoS ONE, 8 (10):

Luisi, S., Florio, P., Reis, F. M. & Petraglia, F. (2005) Inhibins in female and male reproductive physiology: role in gametogenesis, conception, implantation and early pregnancy. Human reproduction update, 11 (2): 123-135.

Lukowski, S. W., Patel, J., Andersen, S. B., Sim, S. L., Wong, H. Y., Tay, J., Winkler, I., Powell, J. E. & Khosrotehrani, K. (2019) Single-Cell Transcriptional Profiling of Aortic Endothelium Identifies a Hierarchy from Endovascular Progenitors to Differentiated Cells. Cell Reports, 27 (9): 2748-2758.e2743.

Ma, Y., Kanakousaki, K. & Buttitta, L. (2015) How the cell cycle impacts chromatin architecture and influences cell fate. Frontiers in Genetics, 6 19-19.

Maaten, L. v. d. & Hinton, G. (2008) Visualizing Data using t-SNE. Journal of Machine Learning Research, 9 2579-2605.

Macosko, E. Z., Basu, A., Satija, R., Nemesh, J., Shekhar, K., Goldman, M., Tirosh, I., Bialas, A. R., Kamitaki, N., Martersteck, E. M., Trombetta, J. J., Weitz, D. A., Sanes, J. R., Shalek, A. K., Regev, A. & McCarroll, S. A. (2015) Highly parallel genome-wide expression profiling of individual cells using nanoliter droplets. Cell, 161 (5): 1202-1214.

Maddox, J., Shakya, A., South, S., Shelton, D., Andersen, J. N., Chidester, S., Kang, J., Gligorich, K. M., Jones, D. A., Spangrude, G. J., Welm, B. E. & Tantin, D. (2012) Transcription factor Oct1 is a somatic and cancer stem cell determinant. PLoS genetics, 8 (11): e1003048-e1003048.

Majeti, R., Park, C. Y. & Weissman, I. L. (2007) Identification of a Hierarchy of Multipotent Hematopoietic Progenitors in Human Cord Blood. Cell stem cell, 1 (6): 635-645.

Majewski, I. J., Ritchie, M. E., Phipson, B., Corbin, J., Pakusch, M., Ebert, A., Busslinger, M., Koseki, H., Hu, Y., Smyth, G. K., Alexander, W. S., Hilton, D. J. & Blewitt, M. E. (2010) Opposing roles of polycomb repressive complexes in hematopoietic stem and progenitor cells. Blood, 116 (5): 731-739.

Martin, R. D. (2007) The Evolution of Human Reproduction: A Primatological Perspective. Yearbook of physical anthropology, 84 59-84.

Martinez, C., Hofmann, T. J., Marino, R., Dominici, M. & Horwitz, E. M. (2007) Human bone marrow mesenchymal stromal cells express the neural ganglioside GD2: a novel surface marker for the identification of MSCs. Blood, 109 (10): 4245-4248.

Massaia, A., Chaves, P., Samari, S., Miragaia, R. J., Meyer, K., Teichmann, S. A. & Noseda, M. (2018) Single Cell Gene Expression to Understand the Dynamic Architecture of the Heart. Frontiers in Cardiovascular Medicine, 5 (November): 1-19.

Masuda, H., Anwar, S. S., B√ºhring, H.-J., Rao, J. R. & Gargett, C. E. (2012) A Novel Marker of Human Endometrial Mesenchymal Stem-Like Cells. Cell Transplantation, 21 (10): 2201-2214.

Masuda, H., Maruyama, T., Gargett, C. E., Miyazaki, K., Matsuzaki, Y., Okano, H. & Tanaka, M. (2015) Endometrial Side Population Cells: Potential Adult Stem/Progenitor Cells in Endometrium1. Biology of Reproduction, 93 (4): 1-8.

Masuda, H., Matsuzaki, Y., Hiratsu, E., Ono, M., Nagashima, T., Kajitani, T., Arase, T., Oda, H., Uchida, H., Asada, H., Ito, M., Yoshimura, Y., Maruyama, T. & Okano, H. (2010) Stem Cell-Like Properties of the Endometrial Side Population: Implication in Endometrial Regeneration. PLOS ONE, 5 (4): e10387-e10387.

Mauxion, F., Faux, C. & Séraphin, B. (2008) The BTG2 protein is a general activator of mRNA deadenylation. EMBO Journal, 27 (7): 1039-1048.

Max, K. E. A., Tuschl, T., Kustagi, M., Straus, A., Sahasrabudhe, N., Suryawanshi, H., Williams, Z., Garzia, A. & Morozov, P. (2018) A single-cell survey of the human first-trimester placenta and decidua. Science Advances, 4 (10)

Maybin, J. a. & Critchley, H. O. D. (2012) Steroid regulation of menstrual bleeding and endometrial repair. Reviews in endocrine & metabolic disorders, 13 (4): 253-263.

Maybin, J. A., Hirani, N., Brown, P., Jabbour, H. N. & Critchley, H. O. D. (2011) The regulation of vascular endothelial growth factor by hypoxia and prostaglandin $F_2\alpha$ during human endometrial repair. The Journal of clinical endocrinology and metabolism, 96 (8): 2475-2483.

Meng, X., Ichim, T. E., Zhong, J., Rogers, A., Yin, Z., Jackson, J., Wang, H., Ge, W., Bogin, V., Chan, K. W., Thébaud, B. & Riordan, N. H. (2007) Endometrial regenerative cells: A novel stem cell population. Journal of Translational Medicine, 5 1-10.

Messinis, I. E. (2006) Ovarian feedback, mechanism of action and possible clinical implications. Human reproduction update, 12 (5): 557-571.

Messinis, I. E., Messini, C. I. & Dafopoulos, K. (2010) The role of gonadotropins in the follicular phase. Annals of the New York Academy of Sciences, 1205 5-11.

Messinis, I. E., Messini, C. I. & Dafopoulos, K. (2014) Novel aspects of the endocrinology of the menstrual cycle. Reproductive biomedicine online, 28 (6): 714-722.

Miller, R. J., Banisadr, G. & Bhattacharyya, B. J. (2008) CXCR4 signaling in the regulation of stem cell migration and development. Journal of neuroimmunology, 198 (1-2): 31-38.

Milne, S. A., Critchley, H. O. D., Drudy, T. A., Kelly, R. W. & Baird, D. T. (1999) Perivascular interleukin-8 messenger ribonucleic acid expression in human endometrium varies across the menstrual cycle and in early pregnancy decidua. Journal of Clinical Endocrinology and Metabolism, 84 (7): 2563-2567.

Moffett, A. & Colucci, F. (2014) Uterine NK cells: active regulators at the maternal-fetal interface. The Journal of clinical investigation, 124 (5): 1872-1879.

Mohammadi, S., Zuckerman, N., Goldsmith, A. & Grama, A. (2017) A Critical Survey of Deconvolution Methods for Separating Cell Types in Complex Tissues. Proceedings of the IEEE, 105 (2): 340-366.

More, I. A. R. & Masterton, R. G. (1976) The role of oestrogen in the control of ciliated cells of the human endometrium. Journal of Reproductive Fertility, 47 19-24.

Mou, X.-z., Lin, J., Chen, J.-y., Li, Y.-f., Wu, X.-x., Xiang, B.-y., Li, C.-y., Ma, J.-m. & Xiang, C. (2013) Menstrual blood-derived mesenchymal stem cells differentiate into functional hepatocyte-like cells. Journal of Zhejiang University. Science. B, 14 (11): 961-972.

Murakami, K., Bhandari, H., Lucas, E. S., Takeda, S., Gargett, C. E., Quenby, S., Brosens, J. J. & Tan, B. K. (2013) Deficiency in clonogenic endometrial mesenchymal stem cells in obese women with reproductive failure - A pilot study. PLoS ONE, 8 (12): 1-7.

Murakami, K., Lee, Y. H., Lucas, E. S., Chan, Y. W., Durairaj, R. P., Takeda, S., Moore, J. D., Tan, B. K., Quenby, S., Chan, J. K. Y., Gargett, C. E. & Brosens, J. J. (2014) Decidualization induces a secretome switch in perivascular niche cells of the human endometrium. Endocrinology, 155 (11): 4542-4553.

Murphy, C. R. (2004) Uterine receptivity and the plasma membrane transformation. Cell Research, 14 (4): 259-267.

Musina, R. A., Belyavski, A. V., Tarusova, O. V., Solovyova, E. V. & Sukhikh, G. T. (2008) Endometrial mesenchymal stem cells isolated from the menstrual blood. Bulletin of Experimental Biology and Medicine, 145 (4): 539-543.

Mutter, G. L., Zahrieh, D., Liu, C., Neuberg, D., Finkelstein, D., Baker, H. E. & Warrington, J. A. (2004) Comparison of frozen and RNALater solid tissue storage methods for use in RNA expression microarrays. BMC Genomics, 5 (1): 88-88.

Muttukrishna, S., Sharma, S., Barlow, D. H., Ledger, W., Groome, N. & Sathanandan, M. (2002) Serum inhibins, estradiol, progesterone and FSH in surgical menopause: a demonstration of ovarian pituitary feedback loop in women. Human reproduction, 17 (10): 2535-2539.

Müller, C. A. & Nieduszynski, C. A. (2017) DNA replication timing influences gene expression level. The Journal of cell biology, 216 (7): 1907-1914.

Naeim, F., Rao, P. N., X.Song, S. & W.Grody, W. (2008) Principles of Immunophenotyping. In: 27-55.

Nakano, I., Paucar, A. A., Bajpai, R., Dougherty, J. D., Zewail, A., Kelly, T. K., Kim, K. J., Ou, J., Groszer, M., Imura, T., Freije, W. A., Nelson, S. F., Sofroniew, M. V., Wu, H., Liu, X., Terskikh, A. V., Geschwind, D. H. & Kornblum, H. I. (2005) Maternal embryonic leucine zipper kinase (MELK) regulates multipotent neural progenitor proliferation. Journal of Cell Biology, 170 (3): 413-427.

Nazarov, I., Lee, J. W., Soupene, E., Etemad, S., Knapik, D., Green, W., Bashkirova, E., Fang, X., Matthay, M. A., Kuypers, F. A. & Serikov, V. B. (2012) Multipotent stromal stem cells from human placenta demonstrate high therapeutic potential. Stem cells translational medicine, 1 (5): 359-372.

Newman, A. M., Liu, C. L., Green, M. R., Gentles, A. J., Feng, W., Xu, Y., Hoang, C. D., Diehn, M. & Alizadeh, A. A. (2015) Robust enumeration of cell subsets from tissue expression profiles. Nature methods, 12 (5): 453-457.

Ng, A. P. & Alexander, W. S. (2017) Haematopoietic stem cells: Past, present and future. Cell Death Discovery, 3 (December 2016): 2-5.

Nguyen, H. P. T., Xiao, L., Deane, J. A., Tan, K. S., Cousins, F. L., Masuda, H., Sprung, C. N., Rosamilia, A. & Gargett, C. E. (2017) N-cadherin identifies human endometrial epithelial progenitor cells by in vitro stem cell assays. Human Reproduction, 32 (11): 2254-2268.

Ning, H., Lin, G., Lue, T. F. & Lin, C.-S. (2011) Mesenchymal stem cell marker Stro-1 is a 75 kd endothelial antigen. Biochemical and biophysical research communications, 413 (2): 353-357.

Nishigaki, A., Okada, H., Okamoto, R., Sugiyama, S., Miyazaki, K., Yasuda, K. & Kanzaki, H. (2011) Concentrations of stromal cell-derived factor-1 and vascular

endothelial growth factor in relation to the diameter of human follicles. Fertility and Sterility, 95 (2): 742-746.

Niswender, G. D., Juengel, J. L., Silva, P. J., Rollyson, M. K. & Intush, E. W. M. C. (2000) Mechanisms Controlling the Function and Life Span of the Corpus Luteum. Physiological reviews, 80 (1): 1-31.

Nystedt, J., Anderson, H., Tikkanen, J., Pietil√§, M., Hirvonen, T., Takalo, R., Heiskanen, A., Satomaa, T., Natunen, S., Lehtonen, S., Hakkarainen, T., Korhonen, M., Laitinen, S., Valmu, L. & Lehenkari, P. (2013) Cell Surface Structures Influence Lung Clearance Rate of Systemically Infused Mesenchymal Stromal Cells. STEM CELLS, 31 (2): 317-326.

O'Brien, L. E. & Bilder, D. (2013) Beyond the Niche: Tissue-Level Coordination of Stem Cell Dynamics. Annual Review of Cell and Developmental Biology, 29 (1): 107-136.

Ogasawara, M., Aoki, K., Okada, S. & Suzumori, K. (2000) Embryonic karyotype of abortuses in relation to the number of previous miscarriages. Fertility and Sterility, 73 (2): 300-304.

Oreshkova, T., Dimitrov, R. & Mourdjeva, M. (2012) A Cross-Talk of Decidual Stromal Cells, Trophoblast, and Immune Cells: A Prerequisite for the Success of Pregnancy. American Journal of Reproductive Immunology, 68 (5): 366-373.

Owen, M. & Friedenstein, A. J. (1988) Stromal stem cells: marrow-derived osteogenic precursors. Ciba Foundation Symposium, 136 42-60.

Pace, D., Morrison, L. & Bulmer, J. N. (1989) Proliferative activity in endometrial stromal granulocytes throughout menstrual cycle and early pregnancy. Journal of Clinical Pathology, 42 (1): 35-39.

Papalexi, E. & Satija, R. (2017) Single-cell RNA sequencing to explore immune cell heterogeneity. Nature Reviews Immunology, 18 35-35.

Parasar, P., Ozcan, P. & Terry, K. L. (2017) Endometriosis: Epidemiology, Diagnosis and Clinical Management. Current obstetrics and gynecology reports, 6 (1): 34-41.

Pastor, W. A., Liu, W., Chen, D., Ho, J., Kim, R., Hunt, T. J., Lukianchikov, A., Liu, X., Polo, J. M., Jacobsen, S. E. & Clark, A. T. (2018) TFAP2C regulates transcription in human naive pluripotency by opening enhancers. Nature Cell Biology, 20 (5): 553-564.

Patel, A. N., Park, E., Kuzman, M., Benetti, F., Silva, F. J. & Allickson, J. G. (2008) Multipotent Menstrual Blood Stromal Stem Cells: Isolation, Characterization, and Differentiation. Cell Transplantation, 17 (3): 303-311.

Pawlik, A., Kotrych, D., Paczkowska, E., Roginska, D., Dziedziejko, V., Safranow, K. & Machalinski, B. (2016) Expression of allograft inflammatory factor-1 in peripheral blood monocytes and synovial membranes in patients with rheumatoid arthritis. Human Immunology, 77 (1): 131-136.

Pellin, D., Loperfido, M., Baricordi, C., Wolock, S. L., Montepeloso, A., Weinberg, O. K., Biffi, A., Klein, A. M. & Biasco, L. (2019) A comprehensive single cell transcriptional landscape of human hematopoietic progenitors. Nature Communications, 10 (1): 2395-2395.

Pfaffl, M. W. (2004) Quantification strategies in real-time PCR. In: Bustin SA (ed), A,ÄìZ of Quantitative PCR. La Jolla, CA: IUL Biotechnology Series, International University Line.

Pfeifer, S., Fritz, M., Goldberg, J., McClure, R., Thomas, M., Widra, E., Schattman, G., Licht, M., Collins, J., Cedars, M., Racowsk, C., Davis, O., Barnhart, K., Gracia, C., Catherino, W., Rebar, R. & La Barbera, A. (2012) Evaluation and treatment of recurrent pregnancy loss: a committee opinion. Fertility and Sterility, 98 (5): 1103-1111.

Pisaturo, V., Gatti, M., L√≥pez-P√©rez, N., Bottazzi, C., Barbieri, F., Cervell√≥, I., Florio, T. & Costa, M. (2017) Endometrial stem cells and human reproductive failure. Current Trends in Clinical Embriology, 3 (3): 90-97.

Polisetti, N., Zenkel, M., Menzel-Severing, J., Kruse, F. E. & Schl√∂tzer-Schrehardt, U. (2016) T ISSUE -S PECIFIC S TEM C ELLS Cell Adhesion Molecules and Stem Cell-Niche- Interactions in the Limbal Stem Cell Niche. Stem Cells, 34 203-219.

Polo, J. M., Liu, S., Figueroa, M. E., Kulalert, W., Eminli, S., Tan, K. Y., Apostolou, E., Stadtfeld, M., Li, Y., Shioda, T., Natesan, S., Wagers, A. J., Melnick, A., Evans, T. & Hochedlinger, K. (2011) Cell type of origin influences the molecular and functional properties of mouse induced pluripotent stem cells. Nature biotechnology, 28 (8): 848-855.

Pontikoglou, C., Langonn√©, A., Ba, M. A., Varin, A., Rosset, P., Charbord, P., Sensébé, L. & Deschaseaux, F. (2016) CD200 expression in human cultured bone marrow mesenchymal stem cells is induced by pro-osteogenic and pro-inflammatory cues. Journal of Cellular and Molecular Medicine, 20 (4): 655-665.

Popovici, R., Kao, L.-C. & Giudice, L. C. (2000) Discovery of New Inducible genes in In Vitro Decidualized Human Endometrial Stromal Cells Using Microarray technology. Endocrinology, 141 (9): 3510-3513.

Povinelli, B., Rodriguez-Meira, A. & Meada, A. J. (2018) Single cell analysis of normal and leukemic hematopoiesis. Molecular Aspects of Medicine, 59 85-94.

Psaltis, P. J., Paton, S., See, F., Arthur, A., Martin, S., Itescu, S., Worthley, S. G., Gronthos, S. & Zannettino, A. C. W. (2010) Enrichment for STRO-1 expression

enhances the cardiovascular paracrine activity of human bone marrow-derived mesenchymal cell populations. Journal of Cellular Physiology, 223 (2): 530-540.

Ramalho-Santos, M. & Willenbring, H. (2007) On the Origin of the Term "Stem Cell". Cell Stem Cell, 1 (1): 35-38.

Rangel-Huerta, E. & Maldonado, E. (2017) Transit-Amplifying Cells in the Fast Lane from Stem Cells towards Differentiation. Stem Cells International, 2017 1-10.

Rasweiler, J. J. & de Bonilla, H. (1992) Menstruation in short-tailed fruit bats (Carollia spp.). Journal of Reproductive Fertility, 95 (1):

Ravasi, T., Suzuki, H., Cannistraci, C. V., Katayama, S., Bajic, V. B., Tan, K., Akalin, A., Schmeier, S., Kanamori-Katayama, M., Bertin, N., Carninci, P., Daub, C. O., Forrest, A. R., Gough, J., Grimmond, S., Han, J. H., Hashimoto, T., Hide, W., Hofmann, O., Kamburov, A., Kaur, M., Kawaji, H., Kubosaki, A., Lassmann, T., van Nimwegen, E., MacPherson, C. R., Ogawa, C., Radovanovic, A., Schwartz, A., Teasdale, R. D., Tegn√©r, J., Lenhard, B., Teichmann, S. A., Arakawa, T., Ninomiya, N., Murakami, K., Tagami, M., Fukuda, S., Imamura, K., Kai, C., Ishihara, R., Kitazume, Y., Kawai, J., Hum, D. A., Ideker, T. & Hayashizaki, Y. (2010) An atlas of combinatorial transcriptional regulation in mouse and man. Cell, 140 (5): 744-752.

Raynaud, C. M., Maleki, M., Lis, R., Ahmed, B., Al-Azwani, I., Malek, J., Safadi, F. F. & Rafii, A. (2012) Comprehensive characterization of mesenchymal stem cells from human placenta and fetal membrane and their response to osteoactivin stimulation. Stem cells international, 2012 658356-658356.

Redondo, P. A., Pavlou, M., Loizidou, M. & Cheema, U. (2017) Elements of the niche for adult stem cell expansion. Journal of Tissue Engineering, 8

Ren, L., Deng, B., Park, V., Jae‚ÄëHyun, S. & Nakamura, Y. (2109) MELK inhibition targets cancer stem cells through downregulation of SOX2 expression in head and neck cancer cells. Oncology reports, 41 (4): 2540-2548.

Rendi, M. H., Muehlenbachs, A., Garcia, R. L. & Boyd, K. L. (2012) 17 - Female Reproductive System. In: Treuting, P. M. & Dintzis, S. M., eds. San Diego: Academic Press: 253-284.

Rennerfeldt, D. A. & Vliet, K. J. V. (2016) Concise Review: When Colonies Are Not Clones: Evidence and Implications of Intracolony Heterogeneity in Mesenchymal Stem Cells. Stem Cells, 34 1135-1141.

Ritschka, B., Storer, M., Mas, A., Heinzmann, F., Ortells, M. C., Morton, J. P., Sansom, O. J., Zender, L. & Keyes, W. M. (2017) The senescence-associated secretory phenotype induces cellular plasticity and tissue regeneration. Genes and Development, 31 (2): 172-183.

Rogers, P. A. W. (1996) Structure and function of endometrial blood vessels. Human Reproduction Update, 2 (1): 57-62.

Romito, A. & Cobellis, G. (2016) Pluripotent stem cells: Current understanding and future directions. Stem Cells International, 2016 (Icm):

Rosenberg, Rosenberg, A. B., Roco, C. M., Muscat, R. A., Kuchina, A., Sample, P., Yao, Z., Gray, L., Peeler, D. J., Mukherjee, S., Chen, W., Pun, S. H., Sellers, D. L., Tasic, B. & Seelig, G. (2018) Single-cell profiling of the developing mouse brain and spinal cord with split-pool barcoding. Science, 360 (6385): 176-182.

Rossignoli, F., Caselli, A., Grisendi, G., Piccinno, S., Burns, J. S., Murgia, A., Veronesi, E., Loschi, P., Masini, C., Conte, P., Paolucci, P., Horwiz, E. M. & Dominici, M. (2013) Isolation, characterization, and transduction of endometrial decidual tissue multipotent mesenchymal stromal/stem cells from menstrual blood. BioMed Research International, 2013

Ruifroka, A. C. & Johnston, D. A. (2001) Quantification of histochemical staining by color deconvolution. Analytical and Quantitative Cytology and Histology, 23 291-299.

Russel, F. G. M., Koenderink, J. B. & Masereeuw, R. (2008) Multidrug resistance protein 4 (MRP4/ABCC4): a versatile efflux transporter for drugs and signalling molecules. Trends in Pharmacological Sciences, 29 (4): 200-207.

Russell, J. & Zomerdijk, J. C. B. M. (2005) RNA-polymerase-I-directed rDNA transcription, life and works. Trends in biochemical sciences, 30 (2):

Rätsep, M. T., Felker, A. M., Kay, V. R., Tolusso, L., Hofmann, A. P. & Croy, B. A. (2015) Uterine natural killer cells: Supervisors of vasculature construction in early decidua basalis. Reproduction, 149 (2): R91-R102.

Salamonsen, L. A. (2003) Tissue injury and repair in the female human reproductive tract. Reproduction, 125 301-311.

Salcedo, R., Wasserman, K., Young, H. A., Grimm, M. C., Howard, O. M., Anver, M. R., Kleinman, H. K., Murphy, W. J. & Oppenheim, J. J. (1999) Vascular endothelial growth factor and basic fibroblast growth factor induce expression of CXCR4 on human endothelial cells: In vivo neovascularization induced by stromal-derived factor-1alpha. The American journal of pathology, 154 (4): 1125-1135.

Salker, M., Teklenburg, G., Molokhia, M., Lavery, S., Trew, G., Aojanepong, T., Mardon, H. J., Lokugamage, A. U., Rai, R., Landles, C., Roelen, B. A. J., Quenby, S., Kuijk, E. W., Kavelaars, A., Heijnen, C. J., Regan, L., Macklon, N. S. & Brosens, J. J. (2010) Natural selection of human embryos: Impaired decidualization of endometrium disables embryo-maternal interactions and causes recurrent pregnancy loss. PLoS ONE, 5 (4):

Salker, M. S., Nautiyal, J., Steel, J. H., Webster, Z., ≈†uƒáuroviƒá, S., Nicou, M., Singh, Y., Lucas, E. S., Murakami, K., Chan, Y. W., James, S., Abdallah, Y., Christian, M., Croy, B. A., Mulac-Jericevic, B., Quenby, S. & Brosens, J. J. (2012) Disordered IL-33/ST2 Activation in Decidualizing Stromal Cells Prolongs Uterine Receptivity in Women with Recurrent Pregnancy Loss. PLoS ONE, 7 (12):

Sampson, J. A. (1922) Ovarian Hematomas of Endometrial Type (Perforating Hemorrhagic Cysts of the Ovary) and Implantation Adenomas of Endometrial Type. The Boston Medical and Surgical Journal, 186 (14): 445-456.

Santamaria, X., Cabanillas, S., Cervell√≥, I., Arbona, C., Raga, F., Ferro, J., Palmero, J., Remoh√≠, J., Pellicer, A. & Sim√≥n, C. (2016) Autologous cell therapy with CD133+ bone marrow-derived stem cells for refractory Asherman's syndrome and endometrial atrophy: a pilot cohort study. Human Reproduction, 31 (5): 1087-1096.

Santamaria, X., Mas, A., Cervell√≥, I., Taylor, H. & Simon, C. (2018) Uterine stem cells: From basic research to advanced cell therapies. Human Reproduction Update, 24 (6): 673-693.

Sathyamurthy, A., Johnson, K. R., Matson, K. J. E., Dobrott, C. I., Li, L., Ryba, A. R., Bergman, T. B., Kelly, M. C., Kelley, M. W. & Levine, A. J. (2018) Massively Parallel Single Nucleus Transcriptional Profiling Defines Spinal Cord Neurons and Their Activity during Behavior. Cell Reports, 22 (8): 2216-2225.

Satija, R., Farrell, J. A., Gennert, D., Schier, A. F. & Regev, A. (2015) Spatial reconstruction of single-cell gene expression data. Nature Biotechnology, 33 (5): 495-502.

Saunders, A., Macosko, E. Z., Wysoker, A., Goldman, M., Krienen, F. M., de Rivera, H., Bien, E., Baum, M., Bortolin, L., Wang, S., Goeva, A., Nemesh, J., Kamitaki, N., Brumbaugh, S., Kulp, D. & McCarroll, S. A. (2018) Molecular Diversity and Specializations among the Cells of the Adult Mouse Brain. Cell, 174 (4): 1015-1030.e1016.

Schwab, K. E. & Gargett, C. E. (2007) Co-expression of two perivascular cell markers isolates mesenchymal stem-like cells from human endometrium. Human Reproduction, 22 (11): 2903-2911.

Seita, J. & Weissman, I. L. (2010) Published in final edited form as: Hematopoietic Stem Cell: Self-renewal versus Differentiation. Wiley Interdiscip Rev.Syst. Biol.Med., 2 (5): 1-20.

Shen-Orr, S. S. & Gaujoux, R. (2013) Computational deconvolution: extracting cell type-specific information from heterogeneous samples. Current Opinion in Immunology, 25 (5): 571-578.

Shi, S. & Gronthos, S. (2003) Perivascular Niche of Postnatal Mesenchymal Stem Cells in Human Bone Marrow and Dental Pulp. Journal of Bone and Mineral Research, 18 (4): 696-704.

Shibata, F., Goto-Koshino, Y., Morikawa, Y., Komori, T., Ito, M., Fukuchi, Y., Houchins, J. P., Tsang, M., Li, D. Y., Kitamura, T. & Nakajima, H. (2013) Roundabout 4 Is Expressed on Hematopoietic Stem Cells and Potentially Involved in the Niche-Mediated Regulation of the Side Population Phenotype. Stem Cells, 71 (2): 233-236.

Silberstein, S. D. & Merriam, G. R. (2000) Physiology of the menstrual cycle. Cephalalgia : an international journal of headache, 20 (3): 148-154.

Skirecki, T., Mikaszewska-Sokolewicz, M., Hoser, G. & Zieli≈Ñska-Borkowska, U. (2016) The early expression of HLA-DR and CD64 myeloid markers is specifically compartmentalized in the blood and lungs of patients with septic shock. Mediators of Inflammation, 2016

Smith, S. D., Dunk, C. E., Aplin, J. D., Harris, L. K. & Jones, R. L. (2009) Evidence for immune cell involvement in decidual spiral arteriole remodeling in early human pregnancy. American Journal of Pathology, 174 (5): 1959-1971.

Smith, S. K. (2001) Regulation of angiogenesis in the endometrium. Trends in endocrinology and metabolism, 12 (4): 147-151.

Sobiesiak, M., Sivasubramaniyan, K., Hermann, C., Tan, C., Örgel, M., Treml, S., Cerabona, F., de Zwart, P., Ochs, U., Müller, C. A., Gargett, C. E., Kalbacher, H. & Bühring, H.-J. (2010) The Mesenchymal Stem Cell Antigen MSCA-1 is Identical to Tissue Non-specific Alkaline Phosphatase. Stem Cells and Development, 19 (5): 669-677.

Song, Y., Xiao, L., Fu, J., Huang, W., Wang, Q., Zhang, X. & Yang, S. (2014) Increased expression of the pluripotency markers sex-determining region Y-box 2 and Nanog homeobox in ovarian endometriosis. Reproductive biology and endocrinology : RB&E, 12 42-42.

Sorrentino, A., Ferracin, M., Castelli, G., Biffoni, M., Tomaselli, G., Baiocchi, M., Fatica, A., Negrini, M., Peschle, C. & Valtieri, M. (2008) Isolation and characterization of CD146+ multipotent mesenchymal stromal cells. Experimental Hematology, 36 (8): 1035-1046.

Spencer, T. E., Dunlap, K. A. & Filant, J. (2012) Comparative developmental biology of the uterus: Insights into mechanisms and developmental disruption. Molecular and Cellular Endocrinology, 354 (1-2): 34-53.

Spitzer, T. L. B., Rojas, A., Zelenko, Z., Aghajanova, L., Erikson, D. W., Barragan, F., Meyer, M., Tamaresis, J. S., Hamilton, A. E., Irwin, J. C. & Giudice, L. C. (2012) Perivascular Human Endometrial Mesenchymal Stem Cells Express Pathways

Relevant to Self-Renewal, Lineage Specification, and Functional Phenotype. Biology of Reproduction, 86 (2): 58-58.

Spornitz, U. M. (1992) The functional morphology of the human endometrium and decidua. Advances in Anatomy, Embryology and Cell Biology, 124

Starkey, P. M., Clover, L. M. & Rees, M. C. P. (1991) Variation during the menstrual cycle of immune cell populations in human endometrium. European Journal of Obstetrics and Gynecology and Reproductive Biology, 39 (3): 203-207.

Strauss, J. F. & Lessey, B. A. (2009) CHAPTER 9 - The Structure, Function, and Evaluation of the Female Reproductive Tract. In: Strauss, J. F., Barbieri, R. L. B. T. Y. & Jaffe's Reproductive, E., eds. Philadelphia: W.B. Saunders: 191-233.

Sturtzel, C., Lipnik, K., Hofer-Warbinek, R., Testori, J., Ebner, B., Seigner, J., Qiu, P., Bilban, M., Jandrositz, A., Preisegger, K.-H., Untergasser, G., Gunsilius, E., de Martin, R., Kroll, J. & Hofer, E. (2018) FOXF1 Mediates Endothelial Progenitor Functions and Regulates Vascular Sprouting. Frontiers in Bioengineering and Biotechnology, 6 (June):

Sugawara, K., Hamatani, T., Yamada, M., Ogawa, S., Kamijo, S., Kuji, N., Akutsu, H., Miyado, K., Yoshimura, Y. & Umezawa, A. (2014) Derivation of human decidua-like cells from amnion and menstrual blood. Scientific Reports, 3 1-9.

Suhorutshenko, M., Kukushkina, V., Velthut-Meikas, A., Altmäe, S., Peters, M., Mägi, R., Krjut≈°kov, K., Koel, M., Codoñer, F. M., Martinez-Blanch, J. F., Vilella, F., Simón, C., Salumets, A. & Laisk, T. (2018) Endometrial receptivity revisited: Endometrial transcriptome adjusted for tissue cellular heterogeneity. Human Reproduction, 33 (11): 2074-2086.

Sukarawan, W. & Osathanon, T. (2017) Mesenchymal stem cells - isolation, characterization and applications. InTech.

Takahashi, K. & Yamanaka, S. (2006) Induction of Pluripotent Stem Cells from Mouse Embryonic and Adult Fibroblast Cultures by Defined Factors. Cell, 126 (4): 663-676.

Tal, R., Shaikh, S., Pallavi, P., Tal, A., López-Giráldez, F., Lyu, F., Fang, Y.-Y., Chinchanikar, S., Liu, Y., Kliman, H. J., Alderman, M., Pluchino, N., Kayani, J., Mamillapalli, R., Krause, D. S. & Taylor, H. S. (2019) Adult bone marrow progenitors become decidual cells and contribute to embryo implantation and pregnancy.

Talbi, S., Hamilton, A. E., Vo, K. C., Tulac, S., Overgaard, M. T., Dosiou, C., Le Shay, N., Nezhat, C. N., Kempson, R., Lessey, B. A., Nayak, N. R. & Giudice, L. C. (2006) Molecular phenotyping of human endometrium distinguishes menstrual cycle phases and underlying biological processes in normo-ovulatory women. Endocrinology, 147 (3): 1097-1121.

Tan, J., Li, P., Wang, Q., Li, Y., Li, X., Zhao, D., Xu, X. & Kong, L. (2016) Autologous menstrual blood-derived stromal cells transplantation for severe Asherman's syndrome. Human Reproduction, 31 (12): 2723-2729.

Tang, F., Barbacioru, C., Wang, Y., Nordman, E., Lee, C., Xu, N., Wang, X., Bodeau, J., Tuch, B. B., Siddiqui, A., Lao, K. & Surani, M. A. (2009) mRNA-Seq whole-transcriptome analysis of a single cell. Nature methods, 6 (5): 377-382.

Taylor, H. S. (2004) Endometrial cells derived from donor stem cells in bone marrow transplant recipients. Journal of the American Medical Association, 292 (1): 81-85.

Terstappen, L. W., Huang, S., Safford, M., Lansdorp, P. M. & Loken, M. R. (1991) Sequential generations of hematopoietic colonies derived from single nonlineage-committed CD34+CD38- progenitor cells. Blood, 77 (6): 1218 LP-1227.

Testart, J. & Frydman, R. (1982) Minimum time lapse between luteinizing hormone surge or human chorionic gonadotropin administration and follicular rupture. Fertility and Sterility, 37 (1): 50-53.

Tewary, S., Lucas, E. S., Fujiharaa, R., Kimanid, P. K., Polanco, A., Brighton, P. J., Muter, J., Fishwick, K. J., Diniz-Da-Costa, M. J. M., Ewington, L. J., Lacey, L., Takeda, S., Brosens, J. J. & Quenbya, S. (2020) Impact of sitagliptin on endometrial mesenchymal stem-like progenitor cells: A randomised, double-blind placebo-controlled feasibility trial - Submitted. EBioMedicine, 51

Thiruchelvam, U., Dransfield, I., Saunders, P. T. K. & Critchley, H. O. D. (2013) The importance of the macrophage within the human endometrium. Journal of Leukocyte Biology, 93 (2): 217-225.

Thomas, M. P., Liu, X., Whangb, J., McCrossan, G., Sanborn, K. B. B. E., Walch, M. & Lieberman, J. (2015) Apoptosis Triggers Specific, Rapid, and Global mRNA Decay with 3' Uridylated Intermediates Degraded by DIS3L2. Cell Reports, 11 (7): 1079-1089.

Tian, D., Diao, M., Jiang, Y., Sun, L., Zhang, Y., Chen, Z., Huang, S. & Ou, G. (2015) Anillin regulates neuronal migration and neurite growth by linking RhoG to the actin cytoskeleton. Current Biology, 25 (9): 1135-1145.

Till, J. E. & McCulloch, E. A. (1961) A Direct Measurement of the Radiation Sensitivity of Normal Mouse Bone Marrow Cells. Radiation Research, 14 (2): 213-222.

Tokmakov, A. A., Iguchi, S., Iwasaki, T., Fukami, Y. & Sato, K. I. (2017) Global decay of mRNA is a hallmark of apoptosis in aging Xenopus eggs. RNA Biology, 14 (3): 339-346.

Tollervey, D. & Caceres, J. F. (2000) RNA Processing Marches on. Cell, 103 (5): 703-709.

Trapnell, C., Cacchiarelli, D., Grimsby, J., Pokharel, P., Li, S., Morse, M., Lennon, N. J., Livak, K. J., Mikkelsen, T. S. & Rinn, J. L. (2014) The dynamics and regulators of cell fate decisions are revealed by pseudotemporal ordering of single cells. Nature biotechnology, 32 (4): 381-386.

Trundley, A. & Moffett, A. (2004) Human uterine leukocytes and pregnancy. Tissue Antigens, 63 (1): 1-12.

Tsang, J. C. H., Vong, J. S. L., Ji, L., Poon, L. C. Y., Jiang, P., Lui, K. O., Ni, Y.-B., To, K. F., Cheng, Y. K. Y., Chiu, R. W. K. & Lo, Y. M. D. (2017) Integrative single-cell and cell-free plasma RNA transcriptomics elucidates placental cellular dynamics. Proceedings of the National Academy of Sciences, 114 (37): E7786-E7795.

Tsuji, S., Yoshimoto, M., Takahashi, K., Noda, Y., Nakahata, T. & Heike, T. (2008) Side population cells contribute to the genesis of human endometrium. Fertility and Sterility, 90 (4 SUPPL.): 1528-1537.

Turco, M. Y., Gardner, L., Hughes, J., Cindrova-Davies, T., Gomez, M. J., Farrell, L., Hollinshead, M., Marsh, S. G. E., Brosens, J. J., Critchley, H. O., Simons, Benjamin¬†D., Hemberger, M., Koo, B.-K., Moffett, A. & Burton, Graham¬†J. (2017) Long-term, hormone-responsive organoid cultures of human endometrium in a chemically defined medium. Nature Cell Biology, 19 (5):

Tuuli, M. G., Shanks, A., Bernhard, L., Odibo, A. O., MacOnes, G. A. & Cahill, A. (2012) Uterine synechiae and pregnancy complications. Obstetrics and Gynecology, 119 (4): 810-814.

Ullah, I., Subbarao, R. B. & Rho, G. J. (2015) Human mesenchymal stem cells - Current trends and future prospective. Bioscience Reports, 35

Ulrich, D., Tan, K. S., Deane, J., Schwab, K., Cheong, A., Rosamilia, A. & Gargett, C. E. (2014) Mesenchymal stem/stromal cells in post-menopausal endometrium. Human Reproduction, 29 (9): 1895-1905.

Utans, U., Arceci, R. J., Yamashita, Y. & Russell, M. E. (1995) Cloning and characterization of allograft inflammatory factor-1: A novel macrophage factor identified in rat cardiac allografts with chronic rejection. Journal of Clinical Investigation, 95 (6): 2954-2962.

Valentijn, A. J., Palial, K., Al-Lamee, H., Tempest, N., Drury, J., Von Zglinicki, T., Saretzki, G., Murray, P., Gargett, C. E. & Hapangama, D. K. (2013) SSEA-1 isolates human endometrial basal glandular epithelial cells: Phenotypic and functional characterization and implications in the pathogenesis of endometriosis. Human Reproduction, 28 (10): 2695-2708.

Vento-Tormo, R., Efremova, M., Botting, R. A., Turco, M. Y., Vento-Tormo, M., Meyer, K. B., Park, J. E., Stephenson, E., Pola≈Ñski, K., Goncalves, A., Gardner, L., Holmqvist, S., Henriksson, J., Zou, A., Sharkey, A. M., Millar, B., Innes, B., Wood, L.,

Wilbrey-Clark, A., Payne, R. P., Ivarsson, M. A., Lisgo, S., Filby, A., Rowitch, D. H., Bulmer, J. N., Wright, G. J., Stubbington, M. J. T., Haniffa, M., Moffett, A. & Teichmann, S. A. (2018) Single-cell reconstruction of the early maternal‚ÄìÀìfetal interface in humans. Nature, 563 (7731): 347-353.

Vieth, B., Parekh, S., Ziegenhain, C., Enard, W. & Hellmann, I. (2019) A systematic evaluation of single cell RNA-seq analysis pipelines. Nature Communications. 10(1): p.1–11.

Villani, A.-C., Satija, R., Reynolds, G., Sarkizova, S., Shekhar, K., Fletcher, J., Griesbeck, M., Butler, A., Zheng, S., Lazo, S., Jardine, L., Dixon, D., Stephenson, E., Nilsson, E., Grundberg, I., McDonald, D., Filby, A., Li, W., De Jager, P. L., Rozenblatt-Rosen, O., Lane, A. A., Haniffa, M., Regev, A. & Hacohen, N. (2017) Single-cell RNA-seq reveals new types of human blood dendritic cells, monocytes, and progenitors. Science, 356 (6335): eaah4573-eaah4573.

Wagner, W., Wein, F., Seckinger, A., Frankhauser, M., Wirkner, U., Krause, U., Blake, J., Schwager, C., Eckstein, V., Ansorge, W. & Ho, A. D. (2005) Comparative characteristics of mesenchymal stem cells from human bone marrow, adipose tissue, and umbilical cord blood. Experimental Hematology, 33 (11): 1402-1416.

Wallach, E. E., Root, A. W. & Garcia, C.-R. (1970) Serum Gonadotropin Responses to Estrogen and Progestogen in Recently Castrated Human Females. The Journal of Clinical Endocrinology & Metabolism, 31 (4): 376-381.

Wang, J., Han, F., Lee, S. W., Wu, J., Chan, C. H., Zhang, X., Gao, Y., Su, H. K., Feng, Z. z., Xu, D. z. & Lin, H. K. (2014) E3-ligase skp2 regulates β-catenin expression and maintains hematopoietic stem cell homing. Biochemical and Biophysical Research Communications, 445 (3): 566-571.

Wang, Q., Shen, L., Huang, W., Song, Y., Xiao, L., Xu, W. & Liu, Y. (2013) Vasculogenesis of decidua side population cells of first-trimester pregnancy. Stem Cell Research and Therapy, 4 (3): 1-1.

Wang, W., Vilella, F., Moreno, I., Pan, W., Quake, S. & Simon, C. (2018a) Single cell RNAseq provides a molecular and cellular cartography of changes to the human endometrium through the menstrual cycle. Fertility and Sterility, 110 (4): e2-e2.

Wang, X., Mamillapalli, R., Mutlu, L., Du, H. & Taylor, H. S. (2015) Chemoattraction of bone marrow-derived stem cells towards human endometrial stromal cells is mediated by estradiol regulated CXCL12 and CXCR4 expression. Stem Cell Research, 15 (1): 14-22.

Wang, X., Sun, D., Tai, J., Chen, S., Yu, M., Ren, D. & Wang, L. (2018b) TFAP2C promotes stemness and chemotherapeutic resistance in colorectal cancer via inactivating hippo signaling pathway. Journal of Experimental and Clinical Cancer Research, 37 (1): 1-16.

Watt, S. M., Athanassopoulos, A., Harris, A. L. & Tsaknakis, G. (2010) Human endothelial stem/progenitor cells, angiogenic factors and vascular repair. Journal of the Royal Society Interface, 7 (SUPPL. 6):

Wickramasinghe, V. O., Andrews, R., Ellis, P., Langford, C., Gurdon, J. B., Stewart, M., Venkitaraman, A. R. & Laskey, R. A. (2014) Selective nuclear export of specific classes of mRNA from mammalian nuclei is promoted by GANP. Nucleic Acids Research, 42 (8): 5059-5071.

Williams, P. J., Searle, R. F., Robson, S. C., Innes, B. A. & Bulmer, J. N. (2009) Decidual leucocyte populations in early to late gestation normal human pregnancy. Journal of Reproductive Immunology, 82 (1): 24-31.

Wu, H., Kirita, Y., Donnelly, E. L. & Humphreys, B. D. (2019) Advantages of Single-Nucleus over Single-Cell RNA Sequencing of Adult Kidney: Rare Cell Types and Novel Cell States Revealed in Fibrosis. Journal of the American Society of Nephrology, 30 (1): 23 LP-32.

Wu, X., Luo, Y., Chen, J., Pan, R., Xiang, B., Du, X., Xiang, L., Shao, J. & Xiang, C. (2014) Transplantation of human menstrual blood progenitor cells improves hyperglycemia by promoting endogenous progenitor differentiation in type 1 diabetic mice. Stem cells and development, 23 (11): 1245-1257.

Xiang, B., Chen, L., Wang, X., Zhao, Y., Wang, Y. & Xiang, C. (2017) Transplantation of Menstrual Blood-Derived Mesenchymal Stem Cells Promotes the Repair of LPS-Induced Acute Lung Injury. International journal of molecular sciences, 18 (4): 689-689.

Yang, S., Wang, H., Li, D. & Li, M. (2019) Role of Endometrial Autophagy in Physiological and Pathophysiological Processes. Journal of Cancer, 10 (15): 3459-3471.

Yu, B., Sondag, G. R., Malcuit, C., Kim, M.-H. & Safadi, F. F. (2016) Macrophage-Associated Osteoactivin/GPNMB Mediates Mesenchymal Stem Cell Survival, Proliferation, and Migration Via a CD44-Dependent Mechanism. Journal of Cellular Biochemistry, 117 (7): 1511-1521.

Yu, D., Wong, Y. M., Cheong, Y., Xia, E. & Li, T. C. (2008) Asherman syndrome-one century later. Fertility and Sterility, 89 (4): 759-779.

Yu, K.-R., Yang, S.-R., Jung, J.-W., Kim, H., Ko, K., Han, D. W., Park, S.-B., Choi, S. W., Kang, S.-K., Schöler, H. & Kang, K.-S. (2012) CD49f Enhances Multipotency and Maintains Stemness Through the Direct Regulation of OCT4 and SOX2. STEM CELLS, 30 (5): 876-887.

Zhang, L. & Maddox, A. S. (2010) Anillin. Current biology, 20 (4): 135-136.

Zhang, Y., Ou, D.-H., Zhuang, D.-W., Zheng, Z.-F. & Lin, M.-E. (2020) In silico analysis of the immune microenvironment in bladder cancer. BMC cancer. 20(1), p.265.

Zhao, Y., Chen, X., Wu, Y., Wang, Y., Li, Y. & Xiang, C. (2018) Transplantation of Human Menstrual Blood-Derived Mesenchymal Stem Cells Alleviates Alzheimer's Disease-Like Pathology in APP/PS1 Transgenic Mice. Frontiers in molecular neuroscience, 11 140-140.

Zhong, Y., Wan, Y.-W., Pang, K., Chow, L. M. L. & Liu, Z. (2013) Digital sorting of complex tissues for cell type-specific gene expression profiles. BMC Bioinformatics, 14 (1): 89-89.

Zhou, P., Wu, G., Zhang, P., Xu, R., Ge, J., Fu, Y., Zhang, Y., Du, Y., Ye, J., Cheng, J. & Jiang, H. (2016) SATB2-Nanog axis links age-related intrinsic changes of mesenchymal stem cells from craniofacial bone. Aging, 8 (9): 2006-2011.

Zilionis, R., Engblom, C., Pfirschke, C., Savova, V., Zemmour, D., Saatcioglu, H. D., Krishnan, I., Maroni, G., Meyerovitz, C. V., Kerwin, C. M., Choi, S., Richards, W. G., De Rienzo, A., Tenen, D. G., Bueno, R., Levantini, E., Pittet, M. J. & Klein, A. M. (2019) Single-Cell Transcriptomics of Human and Mouse Lung Cancers Reveals Conserved Myeloid Populations across Individuals and Species. Immunity, 50 (5): 1317-1334.e1310.